UNIVERSITY OF IOANNINA
SCHOOL OF SCIENCES
PHYSICS DEPARTMENT

ΛCDM and the Implications of the Hubble Tension

George Alestas

PhD THESIS

IOANNINA 2022

ΠΑΝΕΠΙΣΤΗΜΙΟ ΙΩΑΝΝΙΝΩΝ
ΣΧΟΛΗ ΘΕΤΙΚΩΝ ΕΠΙΣΤΗΜΩΝ
ΤΜΗΜΑ ΦΥΣΙΚΗΣ

ΛCDM και οι Επιπτώσεις του Προβλήματος της Σταθεράς Hubble

Γεώργιος Αλέστας

ΔΙΔΑΚΤΟΡΙΚΗ ΔΙΑΤΡΙΒΗ

ΙΩΑΝΝΙΝΑ 2022

Three-member PhD advisory committee:

- L. Perivolaropoulos (Supervisor), Professor, Physics Department, University of Ioannina, Greece.
- G. Leontaris, Professor Emeritus, Physics Department, University of Ioannina, Greece.
- G. Tsagas, Professor, Physics Department, Aristotle University of Thessaloniki, Greece.

Seven-member PhD thesis examination committee:

- L. Perivolaropoulos (Supervisor), Professor, Physics Department, University of Ioannina, Greece.
- P. Kanti [1], Professor, Physics Department, University of Ioannina, Greece.
- C. Tsagas, Professor, Physics Department, Aristotle University of Thessaloniki, Greece.
- N. Stergioulas, Professor, Physics Department, Aristotle University of Thessaloniki, Greece.
- P. E. Christopoulou, Asst. Professor, Physics Department, University of Patras, Greece.
- S. Nesseris, Assoc. Professor, Instituto de Fisica Teorica (IFT), Autonomous University of Madrid, Spain.
- E. Saridakis, Senior Researcher (Researcher Grade B), Institute for Astronomy, Astrophysics, Space Applications and Remote Sensing (IAASARS), National Observatory of Athens, Greece.

[1] Professor G. Leontaris has retired and is unable to be a part of the seven-member examination committee, therefore Prof. P. Kanti has taken his place according to section 2 in article 41 of the 4485/2017 law.

But I, being poor, have only my dreams;
I have spread my dreams under your feet;
Tread softly because you tread on my dreams.

He Wishes for the Cloths of Heaven, W.B. Yeats

Acknowledgements

First and foremost, I would like to express my deep gratitude to my supervisor Professor Leandros Perivolaropoulos. He taught me what it means to conduct research at the highest level and gave me an amazing opportunity to study on the latest challenges of modern Cosmology. This thesis would have not been completed if it were not for his patience, guidance and the fact that he created an all around excellent environment that gave me confidence in myself and my research during this early stage of my career. Moreover, I would like to thank Professor Valerio Marra, Dr. Eleonora Di Valentino, Dr. George Kraniotis, Dr. Ioannis Antoniou as well as David Camarena for our exceptional collaboration in our joint projects during my PhD studies. A big thank you goes out to Associate Professor Savvas Nesseris for providing me with an enormous amount of help regarding a lot of aspects of my research, as well as for his useful guidance in all academic matters. Moreover, I would also like to thank Assistant Professor Panagiota E. Christopoulou for nurturing my interest in Astronomy during my undergraduate years, as well as all the department's theoretical division faculty members for their help and support throughout my PhD years.

I am also very grateful for the company of my friends and fellow PhD students Lavrentios Kazantzidis and Zinovia Eleme. In addition, I would like to extend a special thank you to Frideriki Tsika for putting up with me and providing me with love and motivation all these years. More than anything I am grateful for my family and my uncle John, that always stood behind my choices and supported me financially and emotionally throughout my academic endeavours. Last but not least I would like to thank the Greek State and the European Union for financially supporting me during the majority of my PhD studies.

Contents

List of Publications

During my PhD studies, I have co-authored eight peer-reviewed articles, one N-author review and two articles published in conference proceedings. Starting with the peer-reviewed articles, all of them are listed in descending chronological order:

1. **Constraining a late time transition of $G_{\rm eff}$ using low-z galaxy survey data**,
   G. Alestas, L. Perivolaropoulos and K. Tanidis,
   ArXiv: 2201.05846 (currently awaiting peer-review)
   The code used in the analysis can be found in the G_Constraints GitHub repository.

2. **Late Transition vs Smooth $H(z)$ Deformation Models for the Resolution of the Hubble Crisis**,
   G. Alestas, D. Camarena, E. Di Valentino, L. Kazantzidis, V. Marra, S. Nesseris and L. Perivolaropoulos,
   Published in Phys.Rev.D 105 (2022) 063538,
   DOI: 10.1103/PhysRevD.105.063538
   Report number: IFT-UAM/CSIC-21-98
   The code used in the analysis can be found in the H0_Model_Comparison GitHub repository.

3. **Hints for a gravitational constant transition in Tully-Fisher data**,
   G. Alestas, I. Antoniou and L. Perivolaropoulos,
   Published in Universe 7 (2021) 366,
   DOI: 10.3390/universe7100366
   The code used in the analysis can be found in the Tully_Fisher_Transition GitHub repository.

4. **Late time approaches to the Hubble tension deforming H(z), worsen the growth tension**,
   G. Alestas, L. Perivolaropoulos,
   Published in Mon.Not.Roy.Astron.Soc. 504 (2021) 3, 3956-3962,
   DOI: 10.1093/mnras/stab1070
   The code used in the analysis can be found in the Growth-Hubble_Tension GitHub repository.

5. **A $w - M$ phantom transition at $z_t < 0.1$ as a resolution of the Hubble tension**,
   G. Alestas, L. Kazantzidis, L. Perivolaropoulos,
   Published in Phys.Rev.D 103 (2021) 8, 083517,
   DOI: 10.1103/PhysRevD.103.083517
   The code used in the analysis can be found in the LwMPT GitHub repository.

6. **Existence and Stability of Static Spherical Fluid Shells in a Schwarzschild-Rindler anti-de Sitter Metric**,
   G. Alestas, G.V. Kraniotis, L. Perivolaropoulos,
   Published in Phys.Rev.D 102 (2020) 104015,
   DOI: 10.1103/PhysRevD.102.104015
   The code used in the analysis can be found in the Fluid_Shell_Stability GitHub repository.

7. **H_0 tension, phantom dark energy, and cosmological parameter degeneracies**,
   G. Alestas, L. Kazantzidis, L. Perivolaropoulos,
   Published in Phys.Rev.D 101 (2020) 12, 123516,
   DOI: 10.1103/PhysRevD.101.123516
   The code used in the analysis can be found in the H0_Tension_Data GitHub repository.

8. **Evading Derrick's theorem in curved space: Static metastable spherical domain wall**,
   G. Alestas, L. Perivolaropoulos,
   Published in Phys.Rev. D99 (2019) no.6, 064026,
   DOI: 10.1103/PhysRevD.99.064026
   The code used in the analysis can be found in the Derricks_Theorem-Curved_Space _Solutions GitHub repository.

As a member of the SNOWMASS collaboration I have contributed to the following:

1. **Cosmology Intertwined: A Review of the Particle Physics, Astrophysics, and Cosmology Associated with the Cosmological Tensions and Anomalies,**
   SNOWMASS Collaboration: Eleonora Di Valentino et al.
   Published in JHEAp 34 (2022) 49-211
   DOI: 10.1016/j.jheap.2022.04.002
   Report number: FERMILAB-CONF-22-192-SCD

The articles that have been published in conference proceedings are the following:

1. **Stable, Spherical and Thin Fluid Shells,**
   G. Alestas, G. V. Kraniotis, L. Perivolaropoulos,
   Published in Phys.Sci.Forum 2021, 2, 24,
   DOI: 10.3390/ECU2021-09332

2. **An Overview of Nonstandard Signals in Cosmological Data,**
   G. Alestas, G. V. Kraniotis, L. Perivolaropoulos,
   Published in Phys.Sci.Forum 2021, 2, 28,
   DOI: 10.3390/ECU2021-09333

Σύνοψη

Η διατριβή αυτή επικεντρώνεται γύρω από την διερεύνηση των επιπτώσεων των προβλημάτων της σταθεράς του Hubble και του S_8 στο κοσμολογικό μοντέλο Λ - Cold Dark Matter (ΛCDM) και προτείνει έναν πιθανό τρόπο επίλυσής τους. Ξεκινάμε εκτελώντας μια ανασκόπηση μερικών από των πιο βασικών και απαραίτητων πτυχών της σύγχρονης ΛCDM Κοσμολογίας, καθώς επίσης και των προαναφερθέντων προβλημάτων και συνεχίζουμε στα επόμενα κεφάλαια προτείνοντας ενα νέο μοντέλο μετάβασης ως πιθανή λύση τους. Δείχνουμε ότι είναι δυνατή η χρήση ενός εγγενούς εκφυλισμού του H_0 και της παραμέτρου κατάστασης w της καταστατικής εξίσωσης της σκοτεινής ενέργειας που υπάρχει στο πλαίσιο του φάσματος ισχύος CMB, προκειμένου να κατασκευαστεί μια παραμετροποίηση w(z) που μπορεί να αντιμετωπίσει επιφανειακά το πρόβλημα H_0 αυξάνοντας την τιμή του H_0. Στη συνέχεια προτείνουμε ένα Late w-M Transition $LwMT$ μοντέλο που βασίζεται σε μια μετάβαση της παραμέτρου w, καθώς και της παραμέτρου απόλυτου μεγέθους M για την ταυτόχρονη επίλυση των προβλημάτων Hubble και S_8. Έπειτα, μελετάμε μοντέλα που χρησιμοποιούν ομαλή παραμόρφωση του ρυθμού διαστολής Hubble $H(z)$ στα πλαίσια των best-fit του Planck18/ΛCDM για να αυξήσουν την τιμή του H_0 διατηρώντας παράλληλα τη συνέπεια με τις CMB μετρήσεις του Planck. Ανακαλύπτουμε ότι αυτα τα μοντέλα όχι μόνο δεν μπορούν να επιλύσουν το πρόβλημα S_8, αλλά το χειροτερεύουν. Ολοκληρώνουμε αναζητώντας στοιχεία μιας βαρυτικής μετάβασης η οποία μπορεί να συσχετιστεί με τη μετάβαση M που προβλέπεται από το μοντέλο $LwMT$. Για να το πετύχουμε αυτό εξετάζουμε την εξέλιξη των δεδομένων Tully-Fisher και επιχειρούμε να περιορίσουμε την βαρυτική μετάβαση με χαμηλής ερυθρής μετατόπισης δεδομένα γαλαξιών. Διαπιστώνουμε ότι και στις δύο περιπτώσεις υπάρχουν ενδείξεις για μια βαρυτική μετάβαση με το αναμενόμενο μέγεθος και στην σωστή ερυθρή μετατόπιση, αν και δεν καταφέρνουμε να εξάγουμε κάποιους σαφείς περιορισμούς για αυτή.

Abstract

This thesis is centered around the ideas of exploring the impact of the Hubble and S_8 tensions on the Λ - Cold Dark Matter (ΛCDM) cosmological model and suggesting a possible resolution to both of them. We start by performing a review of some of the most basic and necessary aspects of modern ΛCDM Cosmology as well as the aforementioned tensions, and in the following chapters we proceed by proposing a novel transition model as their possible solution. We show that it is possible to exploit an inherent degeneracy of H_0 and the dark energy equation of state parameter w that exists in the context of the CMB power spectrum, in order to construct a $w(z)$ parametrization that can superficially address the H_0 tension by raising the value of H_0. We then propose a Late w-M Transition $LwMT$ model that relies on a transition of the w parameter, as well as the absolute magnitude M parameter to resolve both the Hubble and S_8 tensions simultaneously. Next, we study models that use smooth deformation of the Hubble expansion rate $H(z)$ of the Planck18/ΛCDM best fit to raise the value of H_0 while keeping consistency with the Planck CMB measurements. In doing so we discover that not only they are unable to resolve the S_8, they in fact worsen it. We conclude by searching for hints of the gravitational transition that can be associated with the M transition predicted by the $LwMT$ model. We do that by considering the evolution of Tully-Fisher data and by attempting to constrain the gravitational transition with low-z galaxy data. We find that in both cases hints for a transition of the expected magnitude and redshift appear, although no effective constraints can be derived.

Πρόλογος

Η σύγχρονη Κοσμολογία είναι συνυφασμένη με την έννοια του κοσμολογικού μοντέλου Λ Cold Dark Matter (ΛCDM). Αυτό το μοντέλο βασίζεται σε δύο βασικές ιδέες που κυριαρχούν στη σύγχρονη αστροφυσική, τις έννοιες της Σκοτεινής Ενέργειας και της Σκοτεινής Ύλης. Σκοτεινές είναι το επίθετο που περιγράφει και τις δύο για δύο καλούς λόγους, πρώτον επειδή δεν αλληλεπιδρούν ηλεκτρομαγνητικά και δεύτερον επειδή δεν έχουμε ιδέα τι είναι στην πραγματικότητα. Τα ονόματα επινοήθηκαν από τον Fritz Zwicky (Σκοτεινή Ύλη) και τον Michael Turner (Σκοτεινή Ενέργεια), την δεκαετία του 1930 και το 1998 αντίστοιχα. Κατά μία έννοια θα μπορούσε να ειπωθεί ότι η Σκοτεινή Ύλη και η Σκοτεινή Ενέργεια μας θυμίζουν τον Αιθέρα, καθώς είναι εξαιρετικά εξωτικές έννοιες που έχουν δημιουργηθεί από την ανάγκη να εξηγηθούν ορισμένα παρατηρούμενα φαινόμενα και διαθέτουν μοναδικές ιδιοτητες και χαρακτηριστικά ιδανικά για την εξήγηση των εν λόγω φαινομένων, ενώ διαφεύγουν κάθε ανίχνευσης.

Ενώ η έννοια του Αιθέρα επινοήθηκε κατά την προ της Σχετικότητας εποχή της Κοσμολογίας από την ανάγκη να εξηγηθεί η φαινομενική ικανότητα του φωτός να διαδίδεται διαμέσω των τεράστιων κενών εκτάσεων του διάστηματος, η Σκοτεινή Ύλη και η Σκοτεινή Ενέργεια διατυπώθηκαν για να εξηγήσουν αναμφισβήτητα πιο θεμελιώδη κοσμολογικά ζητήματα. Το πρώτο τέτοιο ζήτημα ήταν αυτό του ελλείματος ύλης και γέννησε τη Σκοτεινή Ύλη. Πιο συγκεκριμένα, έγινε φανερό μέσω διαφόρων παρατηρήσεων ότι πολλοί γαλαξίες στο Σύμπαν μας δεν θα έπρεπε να συμπεριφέρονται όπως παρατηρούμε λαμβάνοντας υπόψη την ποσότητα της ορατής/παρατηρήσιμης ύλης τους, αυτή η διαφορά μερικές φορές είναι τόσο μεγάλη που πολλοί από τους γαλαξίες που έχουμε παρατηρήσει δεν θα έπρεπε καν να έχουν σχηματιστεί. Μετά από μια ποικιλία άλλων παρατηρήσεων όπως τα φαινόμενα βαρυτικών φακών και το Κοσμικό Υπόβαθρο Μικροκυμάτων (CMB) καταλήξαμε στο συμπέρασμα ότι η πλειονότητα της ύλης στο Σύμπαν αλληλεπιδρά μόνο βαρυτικά και επομένως είναι αόρατη. Για να είμαστε πιο ακριβείς, υπολογίζεται ότι η Σκοτεινή Ύλη αποτελεί 85% της συνολικής μάζας του Σύμπαντος.

Στη συνέχεια έχουμε την έννοια της Σκοτεινής Ενέργειας, η οποία γεννήθηκε από την ανάγκη να εξηγηθεί η παρατηρούμενη επιταχυνόμενη διαστολή του Σύμπαντος. Στο πλαίσιο του μοντέλου ΛCDM παρουσιάζεται με τη μορφή της κοσμολογικής σταθεράς Λ. Ο όρος της κοσμολογικής σταθεράς προτάθηκε για πρώτη φορά από τον Άλμπερτ Αϊνστάιν ως ένας μηχανισμός που θα μπορούσε να δημιουργήσει ένα στατικό σύμπαν μέσω της εξομοίωσης αρνητικών μαζών ομοιογενώς κατανεμημένων στον διαστρικό χώρο. Ωστόσο, δεδομένου ότι ένα τέτοιο στατικό σύμπαν τελικά αποδείχθηκε ασταθές και σε συνδυασμό με το γεγονός ότι ο Edwin Hubble έκανε την ιστορική παρατήρηση της διαστολής του Σύμπαντος, η έννοια της κοσμολογικής σταθεράς καταργήθηκε προσωρινά. Επανήλθε στην επικαιρότητα κατά τη διάρκεια της δεκαετίας του '90, όταν ανακαλύφθηκε η επιταχυνόμενη διαστολή του Σύμπαντος μέσω παρατηρήσεων τύπου Supernova Ia (SnIa), το Λ έγινε λοιπόν για άλλη μια φορά απαραίτητο για την εξήγηση αυτής της μνημειώδους παρατήρησης. Αυτή η υποθετική Σκοτεινή Ενέργεια εκτιμάται ότι αποτελεί το 68% της ενέργειας του σημερινού Σύμπαντος.

Ενώ το ΛCDM παραμένει το πιο ακριβές και απλό κοσμολογικό μοντέλο που περιγράφει το Σύμπαν μας μαστίζεται από πολλά ζητήματα που απειλούν την κυριαρχία του. Σε αυτή τη διατριβή επιλέγουμε να ασχοληθούμε με τα δύο πιο σημαντικά "αγκάθια στα πλευρά" του ΛCDM , τα προβλήματα της σταθεράς Hubble και του S_8. Το πρώτο αφορά την ασυμφωνία μεταξύ των τιμών της σταθεράς Hubble που δίνονται από τις μετρήσεις του "Πρόσφατου" και του "Πρώιμου" Σύμπαντος και σύμφωνα με τις τελευταίες παρατηρήσεις έχει φτάσει στο πολύ σημαντικό επίπεδο των 5σ. Το πρόβλημα του S_8, είναι ένα λιγότερο εμφανές ζήτημα του ΛCDM που αφορά την διαφορά σε επίπεδο 2-3σ μεταξύ των περιορισμών στην ισχύ της ομαδοποίησης της ύλης, όπως αυτές ορίζονται από τις ανισοτροπίες του CMB και των ανιχνευτών μετατόπισης προς το ερυθρό, όπως ο βαρυτικός φακός. Εστιάζουμε σε μια προτεινόμενη λύση και για τα δύο αυτά προβλήματα με βάση μια πολύ πρόσφατη μετάβαση του απόλυτου μεγέθους SnIa M.

Ξεκινάμε διερευνώντας μια μέθοδο για την αύξηση της τιμής της σταθεράς Hubble μέσω ενός εκφυλισμού μεταξύ της παραμέτρου w της εξίσωσης κατάστασης της σκοτεινής ενέργειας και του H_0 που υπάρχει εγγενώς στο φάσμα ισχύος του CMB. Δείχνουμε ότι παρόλο που αυτή η μεθοδολογία είναι καλά τεκμηριωμένη και επιτρέπει μια φαινομενική επίλυση του προβλήματος της σταθεράς του Hubble επικαλώντας απλώς ένα μοντέλο σκοτεινής ενέργειας wCDM , αποτυγχάνει να αντιμετωπίσει το πρόβλημα S_8 και στην πραγματικότητα το επιδεινώνει. Για την ακρίβεια, αποδεικνύουμε αργότερα ότι οποιοδήποτε τέτοιο μοντέλο προσπαθεί να επιλύσει το πρόβλημα της σταθεράς του Hubble αυξάνοντας απλώς την τιμή H_0, πάντα επιδεινώνει το ζήτημα S_8.

Μετά από αυτό, παρουσιάζουμε το μοντέλο Late w-M Transition ($LwMT$), το οποίο βασίζεται στο γεγονός ότι στην καρδιά του προβλήματος της σταθεράς του Hubble βρίσκεται η απόκλιση μεταξύ των τιμών των απόλυτων μεγεθών SnIa όπως υπολογίζονται από το CMB και τους Κειφήδες που παίζουν τον ρόλο τοπικών βαθμονομητών (Κρίση M). Αυτό, σε συνδυασμό με το γεγονός ότι η χαρακτηριστική "πρόσφατη" μέτρηση του H_0 από τη συνεργασία SH0ES δεν μετρά στην πραγματικότητα την παράμετρο Hubble στο παρόν, αλλά συνάγει την τιμή της παρεκτείνοντας από τη μέτρηση $0,023 < z < 0,15$ του $H(z)$, μας επιτρέπει να εξερευνήσουμε τη δυνατότητα ύπαρξης νέας φυσικής στην εποχή $z < 0,023$. Αυτή η νέα φυσική θα μπορούσε να έχει ως αποτέλεσμα τη μετάβαση του απόλυτου μεγέθους M που είναι ικανή να επιλύσει την προαναφερθείσα κρίση M. Η ύπαρξη μιας μετάβασης στο $G_{\rm eff}$ θα μπορούσε να έχει αυτό το επιθυμητό αποτέλεσμα, ενώ ταυτόχρονα θα μείωνε και το επίπεδο του προβλήματος S_8. Επομένως, αναζητούμε και βρίσκουμε ενδείξεις μιας τέτοιας βαρυτικής μετάβασης στην εξέλιξη της Βαρυονικής Tully-Fisher σχέσης, ενώ προσπαθούμε επίσης να περιορίσουμε την επίδρασή της χρησιμοποιώντας συλλογές δεδομένων γαλαξιών χαμηλής ερυθρής μετατόπισης 6dFGS και 2MRS.

Ενώ το μοντέλο $LwMT$ παρουσιάζει από κατασκευής μια πολύ καλή προσαρμογή σε διάφορα κοσμολογικά δεδομένα και είναι, τουλάχιστον κατ' αρχήν, ικανό να επιλύσει τόσο το πρόβλημα της σταθεράς του Hubble όσο και του S_8, μαστίζεται από θέματα fine-tuning. Η αίσθηση ότι αυτές οι κοσμολογικές εντάσεις θα είναι μαζί μας για καιρό ακόμα παραμένει. Δεν δείχνουν σημάδια βελτίωσης και ξεφεύγουν όλο και περισσότερο από την πεποίθηση ότι είναι αποτελέσματα συστηματικών σφαλμάτων που δεν έχουν ληφθεί υπόψιν εως τώρα. Μπορεί κάλλιστα να είναι καιρός για το ΛCDM να παραδώσει τη θέση του σε ένα νέο και πιο ικανό κοσμολογικό μοντέλο. Ό,τι και αν σκοπεύει να φέρει το μέλλον για την Κοσμολογία το μόνο βέβαιο είναι ότι θα είναι συναρπαστικό.

Preface

Modern Cosmology is intertwined with the concept of the standard cosmological Λ Cold Dark Matter (ΛCDM) model. This cosmological concordance model is based on two core ideas that dominate modern astrophysics, the concepts of Dark Energy and Dark Matter. Dark being the adjective that describes both of them for two good reasons, firstly because they do not interact electromagnetically and secondly because we have no idea what what they actually are. The names were coined by Fritz Zwicky (Dark Matter) and Michael Turner (Dark Energy), in the 1930s and 1998 respectively. In a sense it could be said that Dark Matter and Dark Energy remind us of luminiferous Aether, since they are extremely exotic concepts conceived out of the need to explain certain observed phenomena and they possess unique capabilities and characteristics ideal for the explanation of said phenomena, whilst they elude any and all observational detection.

While the concept of luminiferous Aether was conceived during the pre-Relativity era of Cosmology out of the need to explain the apparent ability of light to propagate through the vast stretches of vacuum in space, Dark Matter and Dark Energy were formulated in order to explain arguably more fundamental cosmological issues. The first such issue was that of the missing matter and it gave birth to Dark Matter. More specifically, it became apparent via various observations that many galaxies in our Universe should behave the way they do considering the amount of their visible/observable matter, this difference could sometimes be so great that many of the galaxies we have observed should not even have formed. After a variety of other types of observations such as gravitational lensing phenomena and the Cosmic Microwave Background (CMB) we have reached the conclusion that majority of the matter in the Universe interacts only gravitationaly and is therefore invisible. To be more precise it is calculated that dark matter constitutes 85% of the total mass of the Universe.

Next we have the concept of Dark Energy, which was born out of the necessity to explain the observed accelerated expansion of the Universe. In the context of the ΛCDM model it is presented in the form of the cosmological constant Λ. The cosmological constant term was first proposed by Albert Einstein as a fine-tuning mechanism that could create a static universe via the emulation of gravitating negative masses homogeneously distributed in interstellar space. However, since such a static universe ultimately proved to be unstable combined with the fact that Edwin Hubble made the historic observation of the expansion of the Universe the concept of the cosmological constant was scrapped for a time. It resurfaced during the 90s when the accelerated expansion of the Universe was reported via Supernova type Ia (SnIa) observations, Λ became once more essential in explaining this monumental observation. This hypothetical Dark Energy is estimated that constitutes 68% of the energy of the present-day Universe.

While ΛCDM remains the most accurate and simple cosmological models that describes our Universe is plagued by many tensions and issues that threaten its dominance. In this

thesis we choose to concern ourselves with the two most prominent thorns in ΛCDM 's side, the Hubble and S_8 tensions. The first concerns the discrepancy between the values of the Hubble constant given by "Late" and "Early" Universe measurements and according to the latest observations it has reached an incredible 5σ level. The S_8 or growth tension as it is more plainly known, is a less prominent issue of ΛCDM that concerns the 2-3σ level discrepancy between the constraints on the matter clustering strength as they are set by the primary anisotropies of the CMB and the lower redshift probes such as gravitational lensing. We focus on proposing a solution for both these tensions based on very late time transition of the SnIa absolute magnitude M.

We start by exploring a method to raise the value of the Hubble constant via a degeneracy between the equation of state parameter w and H_0 which is inherently present in the CMB power spectrum. We show that although this methodology is well documented and allows for an apparent resolution of the Hubble tension simply by invoking a phantom dark energy wCDM model, it fails to address the S_8 tension and in fact it actually worsens it. As a matter of fact, we prove later on that any such model that tries to resolve the Hubble tension by simply elevating the H_0 value, always worsens the S_8 tension.

Following that, we present the Late w-M Transition ($LwMT$) model, which is based on the fact that at the heart of the Hubble tension lies a discrepancy between the values of the SnIa absolute magnitudes as they are calculated by the CMB and the local Cepheid calibrators (M crisis). This, combined with the fact that the quintessential "late" Universe measurement of H_0 by the SH0ES collaboration does not actually measure the Hubble parameter in the present, rather infer its value by extrapolating from the $0.023 < z < 0.15$ measurement of $H(z)$, allows us to explore the possibility of new physics in the $z < 0.023$ era. This new physics could have as a result the absolute magnitude transition that is able to resolve the aforementioned M crisis. The existence of a transition in the $G_{\rm eff}$ could have this desired effect, while at the same time easing the S_8 tension as well. We therefore search and find hints of such a gravitational transition in the evolution of the Baryonic Tully-Fisher relation, while we also attempt to constrain its effect using compilations of low-z 6dFGS and 2MRS galaxy data.

While the $LwMT$ model presents by construction a very good fit to various cosmological data and is, at least in principle, able to resolve both the Hubble and S_8 tensions is itself plagued by fine-tuning issues. The feeling that these cosmological tensions will be with us for some time still remains. They show no signs of improvement and they are straying further and further from the belief that they are results of unaccounted for systematic errors. It might very well be the case that it is time for ΛCDM to relinquish its position to a new and more capable concordance model. Whatever the future may bring for Cosmology only the certainty that it will be exciting exists.

CHAPTER 1

Introduction

1.1 Modern Cosmology

Only but a handful of theories in Physics have had such an impact on the way we view the world, as the theory of General Relativity [1] formulated by Albert Einstein in the beginning of the 20^{th} century. Einstein stepped on the shoulders of such giants as the likes of Sir Isaac Newton [2] and James C. Maxwell [3], shaping our understanding of the Universe. He did that by giving us a unique theory of Gravity, one that weaves time and space into a single entity and succeeds at making accurate and precise predictions that have been tested time and time again in the span of a century.

The theory of General Relativity is essential in the study of Cosmology. Among other reasons, that is because it provides the necessary tools for the construction of the standard cosmological model Λ Cold Dark Matter (ΛCDM). In the following sections we will start by providing some important mathematical formulation necessary for understanding ΛCDM, we will talk about the most important challenges it faces and last but not least we will attempt to make a few small predictions about the future of Cosmology as a whole.

1.1.1 The Cosmological Principle

At any particular time our Universe looks the same from all positions in space, thus all directions at any point are equivalent. This principle has been the cornerstone of modern Cosmology and to put it plainly it states that we are not special. More so than that, it states that no point in our Universe, at any time since its creation till now, has been more special than any other.

The above statement is one that drives us somewhat against the layman's understanding of our world. After all if one travels to a rural area, away from the pollution of the city lights, one can clearly observe during the night sky that most of the stars are concentrated in a large group that we call the Milky Way Galaxy. So clearly this place must be more special than any other. That would be the layman's logical conclusion and has been for many millennia, from the moment that our species begun observing the night sky until the previous century. However, for better or worst, when viewed on a sufficiently large scale the properties of our Universe are the same for all observers. Going back to the Milky Way example, if we were to observe it from a large enough distance we would see that it belongs to a small galaxy group

called the Local Group, which in turn when viewed from far enough reveals that it is a part of the Virgo constellation of galaxies. Increasing the scale of our observations, significantly increases the uniformity.

This cosmological principle is essential since if it was not correct, we would not be able to extend our physics beyond our immediate surroundings and our mathematical formulas could never hope to map the workings of the entire Universe. Thankfully, we have very good evidence that our Universe is the same (*isotropic*) on large scales, mainly by the constancy of the Cosmic Microwave Background (CMB) in different directions on the sky. Therefore, we also characterize it as *homogeneous*, since it has no preferred center. At this point, we should note that even though isotropy implies homogeneity, the reverse is not always the case. We could *i.e.* consider of a universe filled with an homogeneous large-scale magnetic field pointed in a single direction that would obviously not be be isotropic.

1.1.2 The Friedmann-Lemaître-Robertson-Walker Metric

If we take into account the *homogeneity* and *isotropy* of the Universe we are left with some constraints on the nature of the three-dimensional, spacelike hypersurfaces that replace the ambiguity of the "moment in time" in General Relativity terms. The introduction of these hypersurfaces allow us to accurately define a globally valid time parameter t. This parameter enables us to define a universal time by considering that each hypersurface exists at a particular $t = const.$ time.

The isotropy postulate demands that all points on a particular hypersurface are equivalent, while the homogeneity one demands that they are equivalent considering fundamental observers. A metric constrained in this way can only take the form,

$$ds^2 = c^2dt^2 - S^2(t)h_{ij}dx^i dx^j \tag{1.1}$$

where h_{ij} are functions of the spatial coordinates (x^1, x^2, x^3) and $S(t)$ is a time-dependent scale factor. We proceed by considering that the 3 dimensional space we will concern ourselves with is maximally symmetric and therefore requires the least amount of functions in order to describe its geometric properties.

More specifically, in our case the Riemann curvature tensor R_{ijkl} has only 6 independent elements. Since we consider our space to be maximally symmetric, a single scalar is enough to characterize its constant curvature. We call it K, and it is of course coordinate independent. The simplest way to define the Riemann tensor with regards to K is,

$$R_{ijkl} = K(g_{ik}g_{jl} - g_{il}g_{jk}) \tag{1.2}$$

where g_{ij} is the metric tensor. Applying simple tensor contractions we arrive at the forms for the Ricci tensor,

$$R_{jk} = -2Kg_{jk} \tag{1.3}$$

and the curvature scalar

$$R = -6K \tag{1.4}$$

with the latter, of course, only depending on K.

In spherical polar coordinates (r, θ, ϕ) the line element of this space takes the form of the spatial part of a general, static and isotropic metric,

$$d\sigma^2 = B(r)dr^2 + r^2d\theta^2 + r^2\sin^2 d\phi^2 \tag{1.5}$$

where $B(r)$ is arbitrary and will be defined with the help of the Ricci tensor. If we consider the general definition of the Ricci tensor in terms of Christoffel symbols,

$$R_{ij} = \partial_j \Gamma^k_{ik} - \partial_k \Gamma^k_{ij} + \Gamma^l_{ik}\Gamma^k_{lj} - \Gamma^l_{ij}\Gamma^k_{lk} \tag{1.6}$$

and calculate the non-zero connection coefficients with regard to Eq. (1.5) as [4, 5],

$$\Gamma^\theta_{r\theta} = \Gamma^\phi_{r\phi} = \frac{1}{r}, \qquad \Gamma^\theta_{\phi\phi} = -\sin\theta\cos\theta, \qquad \Gamma^\phi_{\phi\theta} = \cot\theta\,,$$
$$\Gamma^r_{rr} = \frac{1}{2B(r)}\frac{dB(r)}{dr}, \qquad \Gamma^r_{\phi\phi} = -\frac{r\sin^2\theta}{B(r)}, \qquad \Gamma^r_{\theta\theta} = -\frac{r}{B(r)}\,,$$

we find that,

$$R_{rr} = -\frac{1}{rB(r)}\frac{dB(r)}{dr} \tag{1.7}$$
$$R_{rr} = -\frac{1}{B(r)} - 1 - \frac{r}{2B(r)^2}\frac{dB(r)}{dr} \tag{1.8}$$
$$R_{rr} = -R_{\theta\theta}\sin^2\theta. \tag{1.9}$$

These results, in tandem with Eq. (1.3) allow us to obtain,

$$B(r) = \frac{1}{1 - Kr^2} \tag{1.10}$$

using simple algebra. Therefore, we see that $B(r)$ is dependent upon the spatial curvature scalar K and the spatial line element (1.5) takes the form

$$d\sigma^2 = \frac{dr^2}{1 - Kr^2} + r^2 d\theta^2 + r^2\sin^2 d\phi^2. \tag{1.11}$$

There are two main take-away points from Eq. (1.11). Firstly, the fact that if we consider scales on which the spatial curvature plays a small role then it regresses back to the well-known, equivalent Euclidean one. Secondly, that this line element describes a 3-sphere embedded in a four-dimensional Euclidean space with no real center.

In essence, we have succeeded in defining the spatial part of the general metric given by Eq. (1.1) obtaining

$$ds^2 = c^2dt^2 - S^2(t)\left[\frac{dr^2}{1 - Kr^2} + r^2(d\theta^2 + \sin^2 d\phi^2)\right]. \tag{1.12}$$

Now with a simple rescaling of the scale factor $S(t)$ to $\alpha(t)$, we have,

$$ds^2 = c^2dt^2 - \alpha^2(t)\left[\frac{dr^2}{1 - kr^2} + r^2(d\theta^2 + \sin^2 d\phi^2)\right] \tag{1.13}$$

where $k = K/|K|$ supposing that $K \neq 0$ and takes the values $-1, 0, 1$ depending on the type of spatial curvature we concern ourselves with. This the standard form of the Friedmann-Lemaître-Robertson-Walker (FLRW) metric and as we have shown it has deep cosmological roots, since it is derived from the geometric properties of homogeneity and isotropy of the Universe.

1.1.3 Hubble Law

The main part of this thesis revolves around the cosmological issue of the present day value of the Hubble parameter. But what is the Hubble parameter? In the context of the FLRW metric given by Eq. (1.13) it is naturally defined as [4, 5],

$$H(t) \equiv \frac{\dot{\alpha}(t)}{\alpha(t)}. \tag{1.14}$$

where the dot denotes differentiation with regard to the cosmic time t, and its present day value is denoted as $H(t_0) \equiv H_0$.

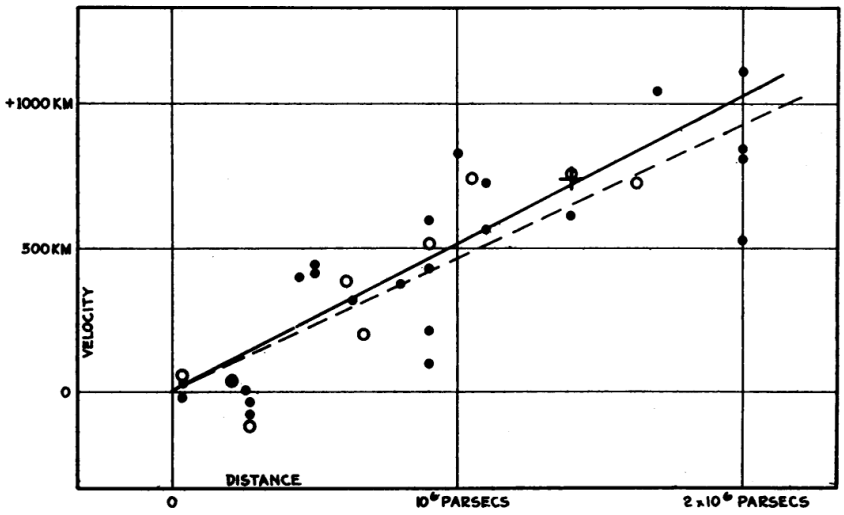

Figure 1.1: This plot shows the velocity-distance relation among extra-galactic nebulae, and served as the first observational recording of the Hubble law. Adopted from the historic Ref. [6].

The logic leading to the above definition becomes apparent if we consider a galaxy emitting a photon at a time t, then a standard power series expansion of the scale factor $\alpha(t)$ around the present cosmic time t_0 when we receive this photon will take the form

$$\begin{aligned}\alpha(t) &= \alpha[t_0 - (t_0 - t)] \\ &= \alpha(t_0) - \dot{\alpha}(t_0)(t_0 - t) + \frac{\ddot{\alpha}(t_0)}{2}(t_0 - t)^2 - ... \\ &= \alpha(t_0)\left[1 - H_0(t_0 - t) - H_0^2\frac{\ddot{\alpha}(t_0)\alpha(t_0)}{2\dot{\alpha}^2(t_0)}(t_0 - t)^2 - ...\right].\end{aligned} \tag{1.15}$$

Therefore, it is obvious from Eq. (1.14) that the Hubble parameter $H(t)$ provides us with the ratio of the rate of the scale factor's α change with regard to cosmic time, over its current value. The quantity $t_0 - t$ is defined as the look-back time and for $z << 1$ it is given by

$$t_0 - t = H_0^{-1}z - H_0^{-1}(1 + \frac{1}{2}q_0)z^2 + ... \tag{1.16}$$

In a similar fashion we can define the quantity [4, 5]

$$q(t) \equiv -\frac{\ddot{\alpha}(t)\alpha(t)}{\dot{\alpha}^2(t)} \tag{1.17}$$

which appears in Eq. (1.15), as the deceleration parameter. If we write the redshift z in regards to the look-back time $t - t_0$ we will then have

$$\begin{aligned} z &= \frac{\alpha(t_0)}{\alpha(t)} - 1 \\ &= \left[1 - (t_0 - t)H_0 - \frac{q_0}{2}(t_0 - t)^2 H_0^2 - ...\right]^{-1} - 1. \end{aligned} \tag{1.18}$$

If we combine Eqs. (1.14) (1.15) and (1.16) we will find that for small redshift the Hubble parameter $H(z)$ varies as

$$H(z) = H_0 \left[1 + (1 + q_0)z - ...\right]. \tag{1.19}$$

Now considering that for the FLRW metric the proper distance d of a nearby galaxy emitting photons at an epoch t_0 is $d \approx c(t_0 - t)$, and that Eq. (1.18) reduces to $z \approx (t_0 - t)H_0$ for small z, we get

$$v = cz = H_0 d. \tag{1.20}$$

The above equation is the well-known Hubble law and connects the recession velocity v of a nearby galaxy emitting photons towards us, with the cosmological redshift z, allowing us to interpret the latter as a Doppler shift. It therefore, allows us to deduce that all galaxies move away from us with a speed that is relative to their distance. This law implies a linearity in the relation of the galaxies recession velocities and their distances, as is also apparent in Fig. (1.1), and characterizes the dimensionality of the Hubble parameter as inverse time. This inverse time dimensionality hints towards the fact that the quantity $1/H_0$ is the approximate age of our Universe.

Edwin Hubble's calculation for the parameter H_0 which characterizes this law was approximately $500\ \mathrm{km\ s^{-1}\ Mpc^{-1}}$. A number of subsequent estimations were made in the following decades, with the most prominent one reported by R. Brent Tully [7] in late 80s. His estimation placed the value of H_0 between 50 and $100\ \mathrm{km\ s^{-1}\ Mpc^{-1}}$, a far cry from the $\approx 70\ \mathrm{km\ s^{-1}\ Mpc^{-1}}$ value reported in modern surveys. The ambiguity that still exists regarding the exact value of this constant will be one of the major points of interest of this thesis.

1.1.4 Luminosity and Angular Diameter Distances

Since we have established that our Universe is expanding we must now consider a way to appropriately define the measurement of distance inside it, at large redshifts. It is well-known [4, 8] that the apparent luminosity of a source is given in relation to its absolute one by the expression,

$$l = \frac{L}{4\pi d^2} \tag{1.21}$$

where d is its distance from the observer. However, this formula is not correct when considering large distances. If we consider a luminous object that acts as a source at a coordinate distance r_1 from us, then by t_0 when its light will have reached us it will have also reached a spherical area $4\pi r_1^2 \alpha^2(t_0)$ (supposing an FLRW metric). This means that our telescope, which will be observing, will receive a $A/4\pi r_1^2 \alpha^2(t_0)$ fraction of the source's light, supposing that A is its aperture. Therefore, l should be proportional to $1/r_1^2 \alpha^2(t_0)$ instead of $1/d^2$. Furthermore, due to the expansion of the universe the rate of the photon's emission from the source is

larger that their rate of arrival at the observer. The same is true, of course, for the energy of the photons. The photon emission/arrival rates and their energies differ by the same exact redshift factor $1/(1+z)$.

These differences allow us to define a new expression for the apparent luminosity of a source,

$$l = \frac{L}{4\pi d_L^2} \tag{1.22}$$

where d_L is the luminosity distance, given by

$$d_L = \alpha(t_0) r_1 (1+z). \tag{1.23}$$

For objects with $z << 1$ the luminosity distance can be re-written as a power series, relating it with the Hubble constant as

$$d_L = H_0^{-1} \left[z + \frac{1}{2}(1-q_0)z^2 + ... \right] \tag{1.24}$$

which enables the possibility of estimating H_0 and q_0 diretly from the measurement of d_L.

Among the other distances that are of value to Cosmology we will discuss about the angular diameter distance d_A, since it plays a very important role when comparing the angular sizes of objects. For a source located at a co-moving radial coordinate r_1 that emits light at time t_1, it is defined as

$$d_A = \alpha(t_1) r_1. \tag{1.25}$$

This means that for the case of the FLRW metric, the ratio of the angular diameter distance over the luminosity distance is given by the Etherington distance-duality relation

$$\frac{d_A}{d_L} = (1+z)^{-2}, \tag{1.26}$$

which is dependent only on redshift.

1.1.5 The Friedmann-Lemaître Equations

Moving on, we will define the two characteristic differential cosmological equations that determine the evolution of the scale factor $\alpha(t)$ within the context of the cosmic time t. In order to do so we will start from the gravitational field equations,

$$R_{\mu\nu} = -k(T_{\mu\nu} - \frac{1}{2} T g_{\mu\nu}) + \Lambda g_{\mu\nu} \tag{1.27}$$

where Λ is the non-zero cosmological constant, $T = T^{\mu}_{\mu}$ and $k = 8\pi G/c^4$. We assume that the matter in the toy universe we are studying is described by the energy-momentum tensor belonging to a perfect fluid

$$T^{\mu\nu} = (\rho + \frac{p}{c^2}) u^{\mu} u^{\nu} - p g^{\mu\nu} \tag{1.28}$$

where p, ρ are its pressure and proper density in the instantaneous rest frame and v^{μ} is its 4-velocity. Therefore, we proceed by calculating the non-zero Christoffel symbols of the FLRW metric given by Eq. (1.13). In order to calculate the surviving coefficients we use the relation

$$\Gamma^{\sigma}_{\mu\nu} = \frac{1}{2} g^{\sigma\rho} (\partial_{\nu} g_{\rho\mu} + \partial_{\mu} g_{\rho\nu} - \partial_{\rho} g_{\mu\nu}) \tag{1.29}$$

and find [4, 5],

$$\Gamma^t_{rr} = \frac{\alpha\dot{\alpha}}{c^2(1-kr^2)}, \qquad \Gamma^t_{\theta\theta} = \alpha\dot{\alpha}r^2/c^2, \quad \Gamma^t_{\phi\phi} = \alpha\dot{\alpha}r^2\sin^2\theta/c^2, \quad \Gamma^r_{rr} = \frac{kr}{1-kr^2},$$
$$\Gamma^r_{\theta\theta} = -r(1-kr^2), \quad \Gamma^r_{\phi\phi} = -r\sin^2\theta(1-kr^2), \quad \Gamma^r_{tr} = \Gamma^\theta_{t\theta} = \Gamma^\phi_{t\phi} = \frac{\dot{\alpha}}{\alpha}, \qquad \Gamma^\phi_{\theta\phi} = \cot\theta,$$
$$\Gamma^\theta_{r\theta} = \Gamma^\phi_{r\phi} = \frac{1}{r} \qquad \Gamma^\theta_{\phi\phi} = -\sin\theta\cos\theta,$$

where of course the dot symbolizes differentiation with respect to t. We are now ready to calculate the elements of the Ricci tensor which are given by the Eq. (1.6). The only Ricci elements that are non-zero are the diagonal ones [4, 5],

$$\begin{aligned}
R_{tt} &= 3\ddot{\alpha}/\alpha, \\
R_{rr} &= -(\alpha\ddot{\alpha} + 2\dot{\alpha}^2 + 2c^2k)c^{-2}/(1-kr^2), \\
R_{\theta\theta} &= -(\alpha\ddot{\alpha} + 2\dot{\alpha}^2 + 2c^2k)c^{-2}r^2, \\
R_{\phi\phi} &= -(\alpha\ddot{\alpha} + 2\dot{\alpha}^2 + 2c^2k)c^{-2}r^2\sin^2\theta.
\end{aligned}$$

We have now calculated the left-hand side terms of Eqs. (1.27). In order to proceed with the right-hand side we have to consider that the covariant components of the 4-velocity in our coordinate system are $v_\mu = c^2\delta^t_\mu$ and $v^\mu v_\mu = c^2$. It is now easy to show that the energy-momentum tensor takes the form,

$$T_{\mu\nu} = (\rho c^2 + p)c^2\delta^t_\mu\delta^t_\nu - pg_{\mu\nu} \tag{1.30}$$

and that its contraction T is equal to,

$$T = \rho c^2 - 3p. \tag{1.31}$$

Therefore, we can show that the surviving right-hand elements of Eqs. (1.27) take the forms,

$$\begin{aligned}
-k(T_{tt} - \frac{1}{2}Tg_{tt}) + \Lambda g_{tt} &= -\frac{1}{2}k(\rho c^2 + 3p)c^2 + \Lambda c^2, \\
-k(T_{rr} - \frac{1}{2}Tg_{rr}) + \Lambda g_{rr} &= -\left[\frac{1}{2}k(\rho c^2 - p) + \Lambda\right]\alpha^2/(1-kr^2), \\
-k(T_{\theta\theta} - \frac{1}{2}Tg_{\theta\theta}) + \Lambda g_{\theta\theta} &= -\left[\frac{1}{2}k(\rho c^2 - p) + \Lambda\right]\alpha^2 r^2, \\
-k(T_{\phi\phi} - \frac{1}{2}Tg_{\phi\phi}) + \Lambda g_{\phi\phi} &= -\left[\frac{1}{2}k(\rho c^2 - p) + \Lambda\right]\alpha^2 r^2\sin^2\theta.
\end{aligned}$$

It is straightforward to combine the equations above with those of the Ricci tensor components, to arrive at two independent equations that act as analytic solutions to the gravitational field Eqs. (1.27) [4, 5],

$$\ddot{\alpha} = -\frac{4\pi G}{3}(\rho + \frac{3p}{c^2})\alpha + \frac{1}{3}\Lambda c^2\alpha, \tag{1.32}$$
$$\dot{\alpha}^2 = \frac{8\pi G}{3}\rho\alpha^2 + \frac{1}{3}\Lambda c^2\alpha^2 - c^2k. \tag{1.33}$$

These are the famous Friedmann-Lemaître cosmological field differential equations. With the help of the previously defined (see Eq. (1.14)) Hubble parameter H and by assuming $c = 1$ we re-write the above equations as,

$$\ddot{H} + H^2 = -\frac{4\pi G}{3}(\rho + 3p) + \frac{1}{3}\Lambda, \tag{1.34}$$

$$H^2 = \frac{8\pi G}{3}\rho + \frac{1}{3}\Lambda - \frac{k}{\alpha^2}, \tag{1.35}$$

which is their most usual form. Until now we have used the cosmological term Λ without giving much thought into its importance. The next subsection is devoted to doing exactly that.

1.1.6 The Standard Cosmological Model ΛCDM

In order to better explain the importance of the cosmological constant Λ in modern Cosmology, we must dive into a historical recounting of the reason that lead to its original insertion in the equations of GR. It all started with the hypothesis that *our Universe is static and eternal*. Even though we know now that this proposition is false, that was not the consensus of the scientific community around the time when Einstein formulated the theory of General Relativity. Originally his theory did not account for such a static universe and that becomes quite obvious if someone takes a look at the first iteration of the gravitational field equations

$$G_{\mu\nu} = 8\pi G T_{\mu\nu}. \tag{1.36}$$

These equations do not account for a static universe and cannot lead to any such solutions. That is because they offer no "antidote" for the constant gravitational attraction of matter and would, no-doubt, eventually lead to a collapse of the universe. This problem was counteracted by Einstein with the strategic inclusion of a constant Λ in Eqs. (1.36) coupled with the metric tensor giving them the form [4, 5],

$$G_{\mu\nu} - \Lambda g_{\mu\nu} = 8\pi G T_{\mu\nu}. \tag{1.37}$$

This small inclusion managed to both preserve the invariance and symmetry of the theory, and simultaneously account for a static universe. The latter was accomplished by showing that a constant like Λ was enough to counter the attractive gravitational force of matter in the universe. However, what Einstein had no way of knowing was that almost a decade after his theory was published, Edwin Hubble was going to shatter the static universe hypothesis with an observation of great importance. More specifically Hubble discovered that the redshift of the galaxies he managed to observe was directly proportional to their distance from Earth. This observation of an expanding universe was subsequently named the Hubble law and it was quantified using Eq. (1.20), described in greater detail in the relevant previous subsection.

For many decades the scientific community, and Einstein himself, championed the idea of the expanding universe. A fact that rendered the notion of a cosmological constant irrelevant and useless. That was about to change in 1998, when observations of Type Ia Supernovae (SnIa) from the High-Redshift Supernova Research Team and the Supernova Cosmology Project showed that our universe is not only expanding, but it is expanding with

an accelerated rate [9]. This accelerated expansion was attributed to an elusive quantity aptly named Dark Energy, that seems to act as a sort of "anti-gravity", opposing the attraction of matter in the universe.

Up to the point of the 1998 SnIa observations, Cosmology was dominated by various iterations of Cold Dark Matter (CDM) models [10–12]. Dark Matter is a hypothetical, unseen form of matter that seems to comprise the majority of matter in our universe. Its inclusion in Cosmology became essential due to the fact that various astrophysical observations showed that the matter in our universe in very large scales did not seem to behave as it should have, according to GR. That would mean that either GR is incomplete, or that the amount of matter that we observe and account for in our calculations for gravitational effects due to GR is wrong. After observing Einstein's theory triumphing over experimental tests again and again, while making astounding predictions, the scientific community (mostly) opted for the latter option. Specifically, they included a type of non-baryonic matter that interacts only gravitationaly and not electromagnetically, making it invisible. Cold Dark Matter, especially, represents a flavour of Dark Matter comprising of particles with non-relativistic energies.

With the observation of the accelerated expansion came the return of the cosmological constant and its addition to the CDM model. The new standard cosmological model of our universe was named ΛCDM and it quickly became accepted in the scientific community as the "best-fit CDM model". The energy density and pressure of the cosmological constant in the context of ΛCDM are related via the equation $\rho_\Lambda = -p_\Lambda$, making the model obey a constant equation of state $w = -1$. ΛCDM assumes the existence of Dark Energy, Dark Matter, GR at cosmological scales and the existence of an inflation phase that is essential to overcome the horizon, flatness and magnetic monopole problems [4, 13–17]; while it has the extremely important advantage of remaining very successful in fitting a variety of cosmological data [18–36].

Parameter	Name	Value
$\Omega_{\mathrm{b},0}\,h^2$	Baryon Density	0.02237 ± 0.00015
$\Omega_{\mathrm{c},0}\,h^2$	Cold Dark Matter Density	0.1200 ± 0.0012
n_s	Spectral Index	0.9649 ± 0.0042
τ	Optical Depth	0.0544 ± 0.0073
$100\,\theta_{MC}$	Angular Size of the Sound Horizon at Recombination	1.04092 ± 0.00031
$ln(10^{10}\,A_s)$	Amplitude of Curvature Primordial Perturbations	3.044 ± 0.014

Table 1.1: The values of the six independent parameters of ΛCDM as they are constrained by the Planck 2018 mission [20] using the TT,TE,EE+lowE+lensing likelihood data.

The inviting simplicity of ΛCDM is further apparent if one considers the fact that it is depended only on six essential parameters. These are presented in table 1.1, along with their Planck 2018 [20] values. Using these six basic parameters in the context of ΛCDM one can indirectly obtain every other cosmological parameter. However, despite the fact that ΛCDM has been the standard cosmological model for more than two decades and that it has been lauded for its observational success, having predicted among others the properties of the power spectrum of the Cosmic Microwave Background (CMB) [18, 20], it faces a large number of challenges in the form of theoretical and observational tensions. These tensions are causing serious cracks in the model and the theories that underpin it. The following two sections are dedicated to discussing arguably the two most important such tensions.

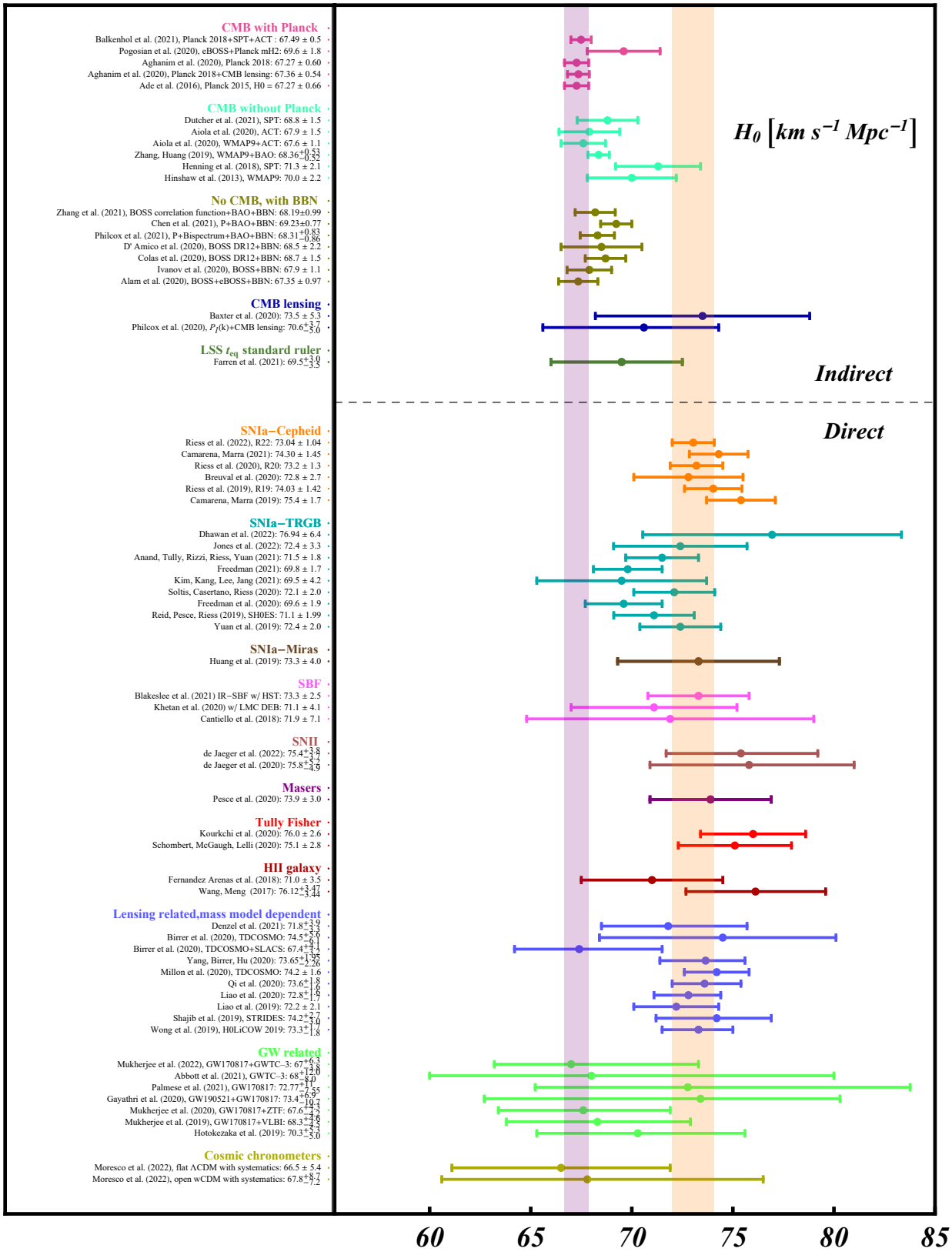

Figure 1.2: Various cosmological probes and their 68% CL constraint on H_0 (based on Refs. [37, 38] and adopted from Ref. [39]).

1.2 The Hubble Tension

More so than others, a spectre is haunting the standard cosmological model-the spectre of the so called Hubble tension. Even though almost all the powers of observational and theoretical Cosmology have entered into a holy alliance to exorcise this spectre, it still persists. It predominantly involves the 5σ level disagreement between the values of the Hubble constant H_0, as they are reported by the Planck and SH0ES collaborations. Specifically, the Planck collaboration obtained their $H_0 = 67.27 \pm 0.60$ km s^{-1} Mpc^{-1} [40] model dependent measurement using CMB data while assuming a ΛCDM cosmological background, in contrast to the direct local distance ladder methodology followed by the SH0ES group that produces an $H_0 = 73.04 \pm 1.04$ km s^{-1} Mpc^{-1} [41] value. Along with the two aforementioned key measurements there is a multitude of other, direct and indirect, cosmological probes [42–54] that stand on various levels of confidence in regards to their H_0 best-fit values. The majority of them are illustrated in Fig. 1.2.

In what follows we present the distance ladder methodology that was used by the SH0ES collaboration in order to derive their value of the H_0 parameter and we also present a variety of other measurements that contribute to the tension. We separate them into two groups, model-dependent (early time) and model-independent (late time) measurements, judging mainly whether they are depended on the standard ΛCDM scenario.

1.2.1 Distance Ladder Methodology

The direct distance ladder methodology that was used by the SH0ES collaboration is based on Type Ia Supernovae (SnIa) data, as they are calibrated using Cepheid variables [41]. More specifically the present value of the Hubble parameter H_0 is measured by the Hubble law using a complicated process that involves calculating and optimizing a χ^2 fit that constrains the values of the relevant parameters. These are the fiducial luminosity of the SnIa and Cepheids, two parameters standardizing Cepheid luminosities, H_0 and the host galaxies distances. This fit is calculated simultaneously among geometric distance measurements to standardized Cepheid variables, Cepheid variables and SnIa in nearby galaxies and lastly SnIa in the Hubble flow region.

Assuming that a correction for the effect of the interstellar dust has been made then the form of the distance modulus μ of a source is given by,

$$\mu = m - M = 5 \log d_L + 25 \tag{1.38}$$

where m is the apparent magnitude, M is the absolute magnitude and d_L is the luminosity distance of the source. When a Cepheid and a SnIa calibrator belong to the same i-th host galaxy they are connected via the equation,

$$m^0_{B,i} = \mu_{0,i} + M^0_B \tag{1.39}$$

where M^0_B is the fiducial luminosity of the SnIa and $m^0_{B,i}$ is their standardized maximum-light apparent magnitude. In order to estimate the H_0 parameter, one should consider the intercept α_B of the Hubble law (see Fig. 1.3) which takes the form

$$\alpha_B = \log cz \left[1 + \frac{1}{2}(1 - q_0)z - \frac{1}{6}(1 - q_0 - 3q_0^2 + j_0)z^2 + O(z^3)\right] - 0.2m^0_B \tag{1.40}$$

for $z > 0$ regardless of the expansion history assumed, q_0 is the deceleration parameter that we defined in subsection 1.1.3 and j_0 is the jerk parameter. After the α_B value is acquired one is able to calculate the H_0 using the equation

$$\log H_0 = 0.2M_B^0 + \alpha_B + 5. \tag{1.41}$$

In order to avoid systematic errors as much as possible it is imperative that the optimization of Eq. (1.40) is done simultaneously with that of Eq. (1.39), since the covariance of SnIa data is non-trivial.

In this approach it is assumed that the Cepheid Wesenheit magnitudes which describe their dependence on a variety of observed characteristics are described by the relation [55],

$$m_{Hij}^W = \mu_i + M_{H1}^W + b_W(\log P_{ij} - 1) + Z_W[O/H]_{ij} \tag{1.42}$$

where the j index identifies the Cepheid magnitude and the i characterizes the host. Therefore, P_{ij} is the source's period in days and $[O/H]_{ij}$ is their metallicity. Furthermore, M_{H1}^W is the fiducial absolute magnitude of a Cepheid with solar metallicity, $\log P = 10$ days, and the γ parameters b_W and Z_W define the empirical relation between Cepheid period, metallicity, and luminosity.

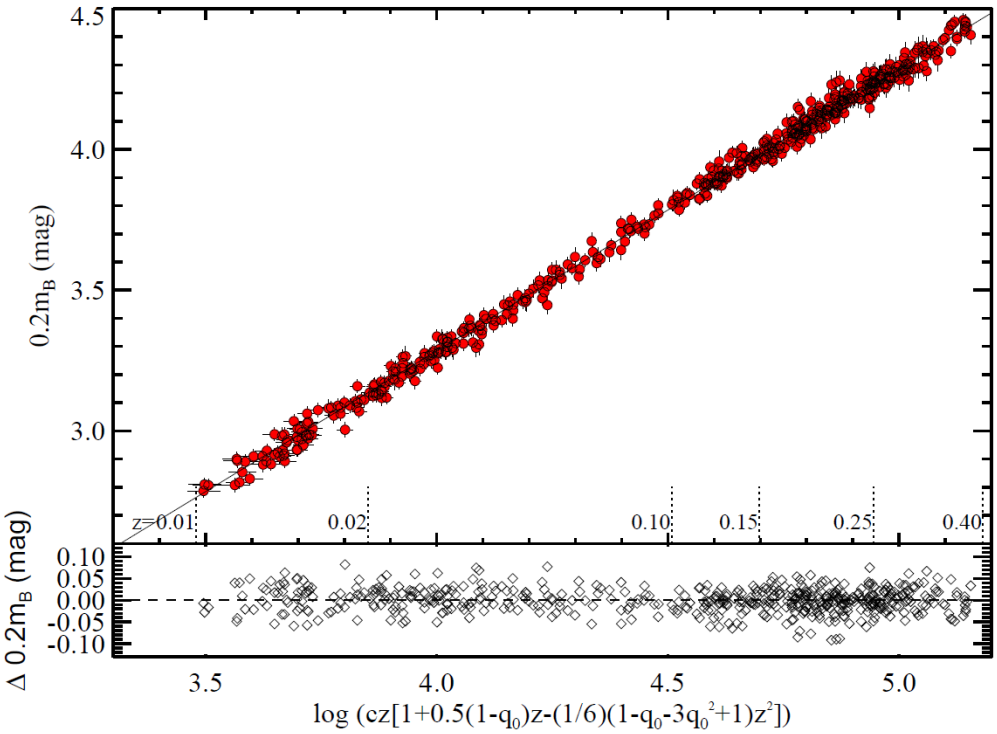

Figure 1.3: The Hubble diagram of the data [56] used in the determination of the intercept α_B, which in turn allows for the estimation of the Hubble constant. Th α_B parameter was measured using data within the $0.023 < z < 0.15$ redshift range. Adopted from Ref. [57]).

The distance ladder methodology with the implementation of SnIa and Cepheid data, has become the most precise tool of measuring the Hubble constant. This is highlighted by the fact that its certainty has now reached the 1% level [41]. Until the arrival of new data from

gravitational waves observations or from new facilities such as the JWST [58], it is very likely that this precision will not be surpassed. However, we have to mention that this methodology has a blind-spot that we will take advantage of in the next chapters. Specifically, this blind-spot is embedded on the fact that the value of H_0 this methodology reports, is not calculated at $z = 0$ as it should, rather it is inferred from an extrapolation of the Hubble diagram. Therefore, it can be argued that this method does not provide the "true" value of H_0 in the event that a change in physics has happened during the extrapolated behaviour. Such change in physics is at the heart of the model that will be thoroughly discussed in Chapter 3.

1.2.2 Model-Dependent H_0 Probes

As model-depended measurements of H_0 we consider those that depend on some basic assumptions that come with the fact that most of them are based on ΛCDM cosmology. This means that these probes are susceptible to various elements, such as the existence of inflation, the properties of Dark Matter and Dark Energy, *etc.*.

This type of measurements of H_0 generally produce lower values, which are in agreement with the Planck18/ΛCDM one. In what follows we will catalogue some of these measurements. First of all, we have ground based telescope data such as the Atacama Cosmology Telescope (ACT-DR4) which give an $H_0 = 67.9 \pm 1.5$ km s^{-1} Mpc^{-1} [44] value and the South Pole Telescope (SPT-3G) with $H_0 = 68.8 \pm 1.5$ km s^{-1} Mpc^{-1} [54]. Combining these ground based measurements with the well-known Wilkinson Microwave Anisotropy Probe (WMAP) space based one we have $H_0 = 67.6 \pm 1.1$ km s^{-1} Mpc^{-1} [44]. Another important model-depended probe of the H_0 constant are the Baryon Acoustic Oscillations (BAO) data. These are the fluctuations in the density of the visible, normal baryonic matter of the Universe and are caused by acoustic density waves of the primordial plasma at early times. A compilation of BAO measurements from various sources produces an $H_0 = 67.35 \pm 0.97$ km s^{-1} Mpc^{-1} [59] value.

Using an inverse distance ladder methodology via the radiation matter equality horizon, as it is calibrated by the CMB power spectrum, one can also employ galaxy power spectra in order to derive H_0. In this regard, the combined Baryon Oscillation Spectroscopic Survey (BOSS) full-shape data along with the Big Bang Nucleosynthesis (BBN) constraint derived from the measurements of the primordial deuterium and the BAO data gives an $H_0 = 68.6 \pm 1.1$ km s^{-1} Mpc^{-1} [60] value.

1.2.3 Model-Independent H_0 Probes

In contrast to the model-depended measurements of H_0 mentioned in the previous subsection here we present some of the measurements that disregard the ΛCDM cosmological model in their assumptions. In doing so these measurements are effectively model-independent and as such generally produce values of H_0 that are in tension with the one reported by Planck18/ΛCDM.

In general the most well-known representative of the measurements which belong in this category is the one by the SH0ES collaboration mentioned above. As we have already said, this is the characteristic measurement on which the H_0 tension was built upon. It was based on the direct distance ladder geometric process which was described with some detail

in subsection 1.2.1, and at the moment this thesis was written reports a 5σ discrepancy with the equivalent CMB model-dependent measurement. Even though there has been a lot of talk about possible systematic errors that could plague the SH0ES measurement, through thorough re-examination of the results the possible effect of these errors has been constrained to very low levels ($\approx 1\%$). Combining this with the fact that all the studies which independently tried to re-analyze the SH0ES result concluded similar H_0 values, as shown in Table 1.2, we have almost irrefutable evidence that the SH0ES methodology and subsequent result is robust.

Methodologies	H_0 (km s^{-1} Mpc^{-1})	References
Bayesian hyper-parameters	73.75 ± 2.11	[61]
Cosmographic Expansion of the Luminosity Distance	74.30 ± 1.45	[62]
Near-Infrared (NIR) Standard Candles	72.8 ± 2.7	[63]
Bayesian Hierarchical Model of the Distance Ladder	73.15 ± 1.78	[64]
Second Gaia Data Release (GDR2) Cepheids	73.0 ± 1.9	[65]

Table 1.2: The values of H_0 as reported by selected studies that tried to repeat the SH0ES collaboration analysis, using some variations in their methodologies.

Other model-independent methodologies that can be used to measure the Hubble constant include the Surface Brightness Fluctuations (SBF) method. This methodology is based on the fact that the variance in a galaxy's light distribution is analogous to the luminosities and numbers fluctuations of its individual stars, per resolution element. Using the Cepheids from the GW170817 host galaxy to calibrate this SBF methodology, one can find an $H_0 = 71.9 \pm 7.1$ km s^{-1} Mpc^{-1} [66] value.

Furthermore, the Tip of the Red Giant Branch (TRGB), which uses the luminosity of th brightest red giant star in a galaxy as a primary distance indicator, has also been used to calibrate SnIa producing various H_0 values. Among them are $H_0 = 69.8 \pm 1.6$ km s^{-1} Mpc^{-1} [67] and $H_0 = 72.4 \pm 3.3$ km s^{-1} Mpc^{-1} [68] *etc.*. If we calibrate the previously mentioned SBF using TRGB data we get an $H_0 = 73.3 \pm 2.4$ km s^{-1} Mpc^{-1} [51] value. There have also been observations of water Megamasers, found in the accretion disks of supermassive black holes residing in active galactic nuclei (AGN). These observations can be used to measure galactic distances. Specifically, one can obtain the Hubble constant from Megamaser data by using the angular diameter distance measurements, which are independent of the distance ladder methodology or the CMB. The leading collaboration in this field called the Megamaser Cosmology Project (MCP) [69] have predicted an $H_0 = 73.9 \pm 3.0$ km s^{-1} Mpc^{-1} [49] value.

1.3 The S_8 Tension

With the term S_8 tension we refer to the fact that the Planck18/ΛCDM parameter values in the context of General Relativity prefer stronger a growth of the cosmological perturbations than that indicated by the cosmological data [44, 70–78]. The S_8 parameter is a combination of the parameters σ_8 and Ω_{0m} given by the relation $S_8 \equiv (\Omega_{0m}/0.3)^n$, where in the literature n is given usually the value $1/2$. In what follows we will assume this value as well.

Data	S_8	Ω_{0m}	σ_8	Refs.
CMB Planck TT,TE,EE+lowE	0.834 ± 0.016	0.3166 ± 0.0084	0.812 ± 0.007	[20]
CMB Planck TT,TE,EE+lowE+lens.	0.832 ± 0.013	0.3153 ± 0.0073	0.811 ± 0.006	[20]
CMB ACT+WMAP	0.832 ± 0.013	0.3153 ± 0.0073	0.840 ± 0.030	[44]
WL KiDS-1000	$0.759^{+0.024}_{-0.021}$	-	-	[70]
WL KiDS + VIKING + DES-Y1	$0.755^{+0.019}_{-0.021}$	-	-	[79]
WL KiDS + VIKING + DES-Y1	$0.762^{+0.025}_{-0.024}$	-	-	[73]
WL KiDS+VIKING-450	$0.716^{+0.043}_{-0.038}$	-	-	[80]
WL KiDS+VIKING-450	$0.737^{+0.040}_{-0.036}$	-	-	[81]
WL KiDS-450	0.651 ± 0.058	-	-	[82]
WL KiDS-450	0.745 ± 0.039	-	-	[71]
WL DES-Y3	$0.759^{+0.025}_{-0.023}$	$0.290^{+0.039}_{-0.063}$	$0.783^{+0.073}_{-0.092}$	[83, 84]
WL DES-Y1	$0.782^{+0.027}_{-0.027}$	-	-	[85]
WL HSC-TPCF	$0.804^{+0.032}_{-0.029}$	$0.346^{+0.052}_{-0.100}$	$0.766^{+0.110}_{-0.098}$	[86]
WL KiDS-1000 pseudo-C_l	$0.754^{+0.027}_{-0.029}$	-	-	[87]
WL HSC-pseudo-C_l	$0.780^{+0.030}_{-0.033}$	-	-	[88]
WL CFHTLenS	$0.740^{+0.033}_{-0.038}$	-	-	[89]
WL+CMB lensing DES-Y3+SPT+Planck	$0.73^{+0.04}_{-0.03}$	$0.25^{+0.03}_{-0.04}$	$0.82^{+0.08}_{-0.07}$	[90]
WL+GC[a]	$0.795^{+0.049}_{-0.042}$	$0.383^{+0.028}_{-0.053}$	$0.718^{+0.044}_{-0.031}$	[91]
WL+GC+CMB lensing[b]	0.7781 ± 0.0094	$0.305^{+0.021}_{-0.025}$	0.774 ± 0.033	[92]
WL+GC KiDS-1000 3×2pt	$0.766^{+0.020}_{-0.014}$	$0.305^{+0.010}_{-0.015}$	$0.76^{+0.025}_{-0.020}$	[93]
WL+GC KiDS-450 3×2pt	0.742 ± 0.035	$0.243^{+0.026}_{-0.045}$	$0.832^{+0.080}_{-0.079}$	[94]
WL+GC KiDS+GAMA 3×2pt	$0.800^{+0.029}_{-0.027}$	$0.33^{+0.05}_{-0.06}$	$0.78^{+0.06}_{-0.08}$	[95]
WL+GC DES-Y3 3×2pt	$0.776^{+0.017}_{-0.017}$	$0.339^{+0.032}_{-0.031}$	$0.733^{+0.039}_{-0.049}$	[96]
WL+GC DES-Y1 3×2pt	$0.773^{+0.026}_{-0.020}$	$0.267^{+0.030}_{-0.017}$	$0.817^{+0.045}_{-0.056}$	[97]
WL+GC KiDS+VIKING-450+BOSS	0.728 ± 0.026	$0.323^{+0.014}_{-0.017}$	0.702 ± 0.029	[98]
GC BOSS DR12 bispectrum	0.751 ± 0.039	$0.32^{+0.01}_{-0.01}$	$0.722^{+0.032}_{-0.036}$	[99]
GC BOSS+eBOSS	0.72 ± 0.042	-	-	[100]
GC BOSS galaxy power spectrum	0.703 ± 0.045	0.293 ± 0.012	0.713 ± 0.045	[60]
GC BOSS power spectra	0.736 ± 0.051	0.303 ± 0.0082	0.733 ± 0.047	[101]
GC BOSS DR12	0.729 ± 0.048	$0.317^{+0.015}_{-0.019}$	0.710 ± 0.049	[98]
GC+CMB lensing DESI+Plank	0.73 ± 0.03	-	-	[102]
GC+CMB lensing unWISE+Plank	0.784 ± 0.015	0.307 ± 0.018	0.775 ± 0.029	[103]
CC AMICO KiDS-DR3	0.78 ± 0.04	$0.24^{+0.03}_{-0.04}$	0.86 ± 0.07	[104]
CC SDSS-DR8	$0.79^{+0.05}_{-0.04}$	$0.22^{+0.05}_{-0.04}$	$0.91^{+0.11}_{-0.10}$	[36]
CC ROSAT (WtG)	0.77 ± 0.05	0.26 ± 0.03	0.83 ± 0.04	[105]
CC DES-Y1	$0.65^{+0.04}_{-0.04}$	$0.179^{+0.031}_{-0.038}$	$0.85^{+0.04}_{-0.06}$	[106]
CC XMM-XXL	0.83 ± 0.11	0.40 ± 0.09	0.72 ± 0.07	[107]
CC SPT-tSZ	0.749 ± 0.055	0.276 ± 0.047	0.781 ± 0.037	[108]
CC Planck tSZ	0.785 ± 0.038	0.32 ± 0.02	0.76 ± 0.03	[35]
CC Planck tSZ	0.792 ± 0.056	0.31 ± 0.04	0.78 ± 0.04	[34]
RSD+BAO+Pantheon+CC	$0.777^{+0.026}_{-0.027}$	0.288 ± 0.008	$0.793^{+0.018}_{-0.020}$	[109]
RSD+BAO+Pantheon	$0.762^{+0.030}_{-0.025}$	0.286 ± 0.008	$0.7808^{+0.021}_{-0.019}$	[109]
RSD	$0.739^{+0.036}_{-0.040}$	$0.254^{+0.038}_{-0.058}$	$0.804^{+0.048}_{-0.071}$	[109]
RSD	$0.700^{+0.038}_{-0.037}$	$0.201^{+0.036}_{-0.033}$	$0.857^{+0.044}_{-0.042}$	[110]
RSD	0.747 ± 0.029	0.279 ± 0.028	0.775 ± 0.018	[111]

Table 1.3: The value of the growth parameter combination S_8, the matter density parameter Ω_{0m} and the the power spectrum amplitude σ_8 at 68% CL through direct and indirect measurements. The first three are separated from the rest because they are calculated via CMB data. Adopted from Ref. [38].

[a] HSC-Y1+SDSSS-III/BOSS DR11

[b] KiDS+DES+eBOSS+Planck

Most of the observations seem to indicate a value of S_8 that is at a $2-3\sigma$ level smaller than the $S_8 = 0.834 \pm 0.016$ value given by the Planck CMB measurement of Ref. [78]. Although this tension does not reach the level of the Hubble tension mentioned in the previous section, it still constitutes a very important cosmological challenge to ΛCDM. In the following subsection we will talk briefly about some of the more characteristic measurements.

1.3.1 CMB and Weak Gravitational Lensing Measurements

We include the values of the S_8 and Ω_{0m} parameters in the context of various data combinations in Table 1.3, however there are two types of measurements worth discussing further. One of the most important S_8 measurement is derived from the amplitude CMB Power Spectrum and the CMB lensing data. Even though these CMB estimates are model depended and vary with regards to the data compilation used, with each generation of observations they converge more and more on some central values for the parameters S_8 and Ω_{0m}.

The fact that the CMB S_8 measurements are model-depended carries some weight in the possibility of the existence of systematic errors. More specifically, they are based upon the hypothesis of ΛCDM Cosmology as the background. In this context the fact that the S_8 measurements are depended on the τ parameter, which symbolizes the optical depth to the reionization, is a very likely source of systematics. That is because the value of the τ parameter is estimated with great uncertainty in the case of the ΛCDM model, in fact larger than any other parameter. Furthermore, we should consider the fact that the Planck18/ΛCDM data show indications of a higher amount of matter clustering than other analyses [44, 112]. This lensing amplitude anomaly that is displayed in the Planck data could be a systematic error that leads to an overestimation of the S_8 value.

The next important source of S_8 measurements we are going to discuss is the weak gravitational lensing data. Weak gravitational lensing is the phenomenon of image distortion of Large Scale Structures (LSS), due to the numerous deflections of the light-path as it travels from its source to the observer. Ever since the first S_8 measurement from the Canada-France-Hawaii Telescope Wide Synoptic Legacy Survey (CFHTWLenS) [113] which set the tension level with the then Planck/CMB one at 2σ, there have been a plethora of others such as the Kilo Degree Survey (KiDS) [87], the Dark Energy Survey (DES) [36], the VISTA Kilo-degree Infrared Galaxy (VIKING) Survey [114] and the Subaru Hyper Suprime Cam (HSC) [88] Survey to name a few. The joint characteristic of all these measurements performed by independent groups, was that all of them predicted smaller S_8 values at early times than those reported by the CMB estimates.

1.4 A Forecast on the Future of Cosmology

When it comes to the field of Cosmology it is fair to say that we are entering in an exciting decade. It is becoming more and more clear that the emergence of tensions in the standard cosmological model ΛCDM will lead to its eventual demise, much as the discovery of the accelerated expansion of the Universe lead to the demise of the flat sCDM model. We have discussed about the Hubble and S_8 tensions that are arguably in the spearhead of the revolution against ΛCDMhowever there are a plethora of other, perhaps lesser known ones posing a threat as well. For example we have the lensing anomaly [115, 116], the quadrupole-octopole alignement [117–122], the CMB cold spot [123–126], the hints for an open Universe

from the BAO in contrast to those for a closed one by the CMB data (CMB vs BAO) [127–129], the Lithium problem [130–132] *etc.*

In the next decade there will be a plethora of new data from long awaited scientific missions. For example we will see the deployment of both the third generation ground and space based gravitational wave interferometers [133–136]. This will have a tremendous impact on Cosmology in general and especially the Hubble tension, since GWs are an extremely direct and precise cosmological probe for the determination of the H_0 parameter. That is because their amplitudes are inversely related to the luminosity distance from their sources, allowing for a model-independent determination of H_0 from the Hubble law, without any distance ladder techniques.

Furthermore, we will also have the deployment of the Euclid satellite [137, 138], an ESA mission operating from the L2 Lagrange point for a minimum of six years, which will have the goal of understanding the physical origin of the accelerated expansion of the Universe. As such, it will provide us with detailed maps of the Universe which will help us measure its expansion and growth history from the evolution of large scale cosmic structures. It will do so with the help of a 1.2m telescope and three imaging/spectroscopic instruments working in the visible and near-infrared wavelength domains. Specifically it is expected to perform a reconstruction of the pattern of light distortion from weak lensing to $z = 3$ and the clustering of galaxies out to $z = 2$.

However, even though there is a lot to be expected from new data and scientific missions that aim to enrich our understanding of the Universe via a better understanding of Dark Matter and Dark Energy, there are still those in the scientific community that look towards a different path. They consider the possibility that the assumptions of Dark Energy and Dark Matter which lie at the heart of ΛCDM are wrong, and that the observations that lead to their establishment could be indications of a much needed modification to GR. Modified Gravity theories have always been a part of modern Cosmology, albeit a small one, and now with the much anticipated fall of ΛCDM around the corner they are here once again. Significant examples of such theories include the $f(R)$ [139–163], $f(T)$ [164–173] and scalar-tensor theories [174–185]. Although it is true that GR has been proven correct time and time again it still has weaknesses that the modifications proposed in the above theories attempt to eradicate. Moving on and breaking new ground in Cosmology with the help of General Relativity never fails to leave us pondering the following question "*Sir Isaac Newton forged his Universe out of order via divine intervention and it held true for a little more than two centuries, how long will Einstein's Universe survive?*".

CHAPTER 2

Phantom Dark Energy and Cosmological Parameter Degeneracies

This chapter is dedicated to the analytical and numerical exploration of the degeneracies that arise when we consider different cosmological parameter combinations, and are inherent in the CMB power spectrum. In doing so, we study the consequences of varying the dark energy equation of state parameter $w(z)$ on various cosmological parameters. In particular we focus on the Hubble parameter H_0, that is associated with the Hubble tension, and the matter density parameter $\Omega_{0\mathrm{m}}$. It is becoming clear that the consideration of new dark energy properties plays a significant role both in the case of the resolution of the Hubble and S_8 tensions. In particular, if one considers the key to solving the Hubble tension to be a higher value of the Hubble parameter H_0 within the context of the CMB data, then it can be shown [186–191, 191, 192] that a mildly phantom dark energy with an equation of state parameter evolving slightly below $w = -1$ has the power to achieve that.

The usual approaches followed by most of the previous works in the literature utilize evolving equation of state parameters with sophisticated functional forms. This methodology suffers from, at least, two major issues. The first is that the forms of $w(z)$ that are most commonly used exhibit a worse fit to various cosmological data and the Planck CMB TT power spectrum than ΛCDM ($\Delta\chi^2 > 0$) and the second is that they are most of the times very complex employing a multitude of extra parameters, a fact that goes against the notion that a good physical theory should strive to beauty via simplicity. It is therefore plain for everyone to see that these parametrizations would be heavily penalised and disfavored [193] in the event that they would be judged using an information criterion like the Akaike one against the ΛCDM . Therefore, following this logic it is obvious that by constructing a model with no new parameters that can potentially resolve both the Hubble and growth tensions just by modifying the dark energy properties would be akin to finding the holy grail.

In the context of the analysis that will be presented in this chapter we will attempt to address the following questions:

- What are the properties of the new phantom degree of freedom required in order to increase the best fit value of H_0, in the context of the CMB data, to the level required for consistency with local measurements and the apparent resolution of the H_0 tension?

- What are the corresponding best fit values of cosmological parameters that emerge in

the context this type of phantom dark energy and can they lead to the improvement or the resolution of the growth tension?

- What is the quality of fit of these extended models to the CMB Planck and other cosmological data and how does it compare with the corresponding quality of fit of ΛCDM?

This will be done in part by using an approximate analytical method that will make use of the degeneracies that are present within the cosmological parameters when considering the CMB power spectrum. Furthermore, we will utilize accurate numerical estimates of best fit cosmological parameters using Markov Chain Monte Carlo (MCMC) and Boltzmann codes.

2.1 CMB Spectrum Degeneracies and the $H_0(w)$ Dependence

It has been shown [194, 195] that one can uniquely describe the CMB temperature power spectrum by fixing a number of parameter combinations. Specifically, these parameter combinations are the matter density parameter combination $\omega_{\rm m} \equiv \Omega_{0\rm m}h^2$, the baryon density parameter combination $\omega_b \equiv \Omega_{0\rm b}h^2$, the radiation density parameter combination $\omega_{\rm r} \equiv \Omega_{0\rm r}h^2$, the primordial fluctuation spectrum and the curvature parameter $\omega_{\rm k} = \Omega_{0\rm k}h^2$ where $h = \frac{H_0}{100}\ km\ sec^{-1}\ Mpc^{-1}$, $\Omega_{0\rm b}$ is the present day baryon density parameter and $\Omega_{0\rm r}$ is the present day radiation density parameter. Considering also that the flat universe co-moving angular diameter distance to the recombination surface

$$d_A(\omega_m, \omega_r, \omega_b, h, w(z)) = \int_0^{z_r} \frac{dz}{H(z)} \tag{2.1}$$

where $z_r \simeq 1100$ is the redshift of recombination provided to better accuracy as [196]

$$\begin{aligned} z_{\rm r} &= 1048(1 + 0.00124\omega_{\rm b}^{-0.738})(1 + g_1\omega_{\rm m}^{g_2}) \\ g_1 &= 0.0783\omega_{\rm b}^{-0.238}/(1 + 39.5\omega_{\rm b}^{0.763}) \\ g_2 &= 0.560/(1 + 21.1\omega_{\rm b}^{1.81}). \end{aligned} \tag{2.2}$$

and $H(z)$ is the Hubble parameter at redshift z. We see that the Hubble parameter can be written as

$$H(z, \omega_m, \omega_r, \omega_b, h, w(z)) = H_0\sqrt{\Omega_{0m}(1+z)^3 + \Omega_{0\rm r}(1+z)^4 + \Omega_{0\rm de}e^{3\int_0^z dz'\ (1+w(z'))/(1+z')}} \tag{2.3}$$

where $w(z)$ is the dark energy equation of state parameter at redshift z and $\Omega_{0\rm de} = 1 - \Omega_{0\rm m} - \Omega_{0\rm r}$ is the present day value of the dark energy density parameter. The product $\sqrt{\omega_m} \cdot d_A$ is independent of H_0 and constitutes the well known shift parameter defined as [194, 197]

$$R = \sqrt{\omega_m}\int_0^{z_r} \frac{dz}{H(z)} \tag{2.4}$$

The observed values of the above parameter combinations as determined by the Planck18/ΛCDM CMB temperature power spectrum are the following [40]

$$\bar{\omega}_m = 0.1430 \pm 0.0011 \tag{2.5}$$
$$\bar{\omega}_b = 0.02237 \pm 0.00015 \tag{2.6}$$
$$\bar{\omega}_r = (4.64 \pm 0.3)\ 10^{-5} \tag{2.7}$$
$$\bar{\omega}_k = -0.0047 \pm 0.0029 \tag{2.8}$$
$$\bar{d}_A = (100\ km\ sec^{-1}\ Mpc^{-1})^{-1}(4.62 \pm 0.08) \tag{2.9}$$

where for the radiation density we have assumed three relativistic neutrino species.

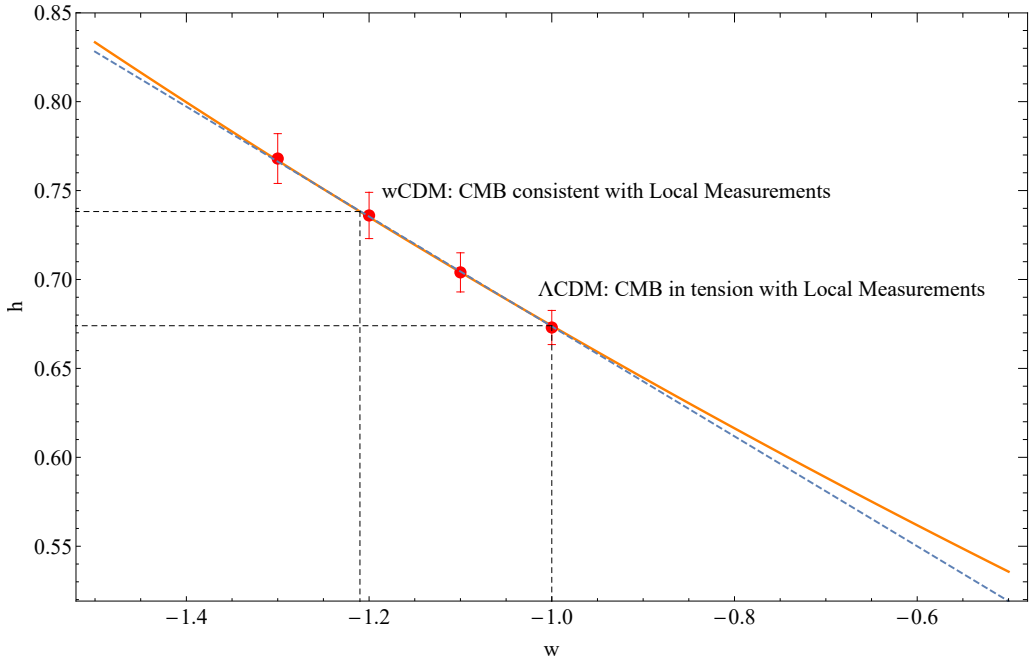

Figure 2.1: The predicted value of h as a function of the fixed w for the one parameter dark energy (wCDM) model. The orange line corresponds to the theoretically predicted best fit values of h for different values of w in the case of the wCDM model, whereas the dashed blue line corresponds to the linear fitting that has been made. The red points display the actual best fit values, including the errorbars, of h for specific values of w obtained by fitting these models to the CMB TT anisotropy via the MGCosmoMC (see Table 2.2). Adopted from Ref. [198].

We use the above combinations in order to express and exploit the degeneracy of the CMB with respect to various specific cosmological parameters. By exploiting this degeneracy it is straightforward to create an $h(w_0, w_1, ...)$ function that gives, semi-analytically, the predicted best fit value of h given a specific form of the dark energy equation of state $w(z)$. This is done by using Eqs. (2.1), (2.3), (2.5) and (2.9). To show an example of how one could analytically predict the best fit value of the Hubble parameter given the dark energy equation of state parameter $w(w_0, w_1, ..., z)$ where $w_0, w_1, ...$ are the parameters entering the $w(z)$ parametrization[1], all we have to do is consider the fact that if we fix the first four parameter combinations

[1]In the present analysis we assume a flat universe and fix $\bar{\omega}_k = 0$.

to the values given by Eqs. (2.5) - (2.8), then the fifth given by Eq. (2.9) would allow us to constrain H_0. The predicted $h(w_0, w_1, ...)$ function is derived by solving the following equation with respect to h

$$d_A(\bar{\omega}_m, \bar{\omega}_r, \bar{\omega}_b, h = 0.674, w = -1) = d_A(\bar{\omega}_m, \bar{\omega}_r, \bar{\omega}_b, h, w(z)) \tag{2.10}$$

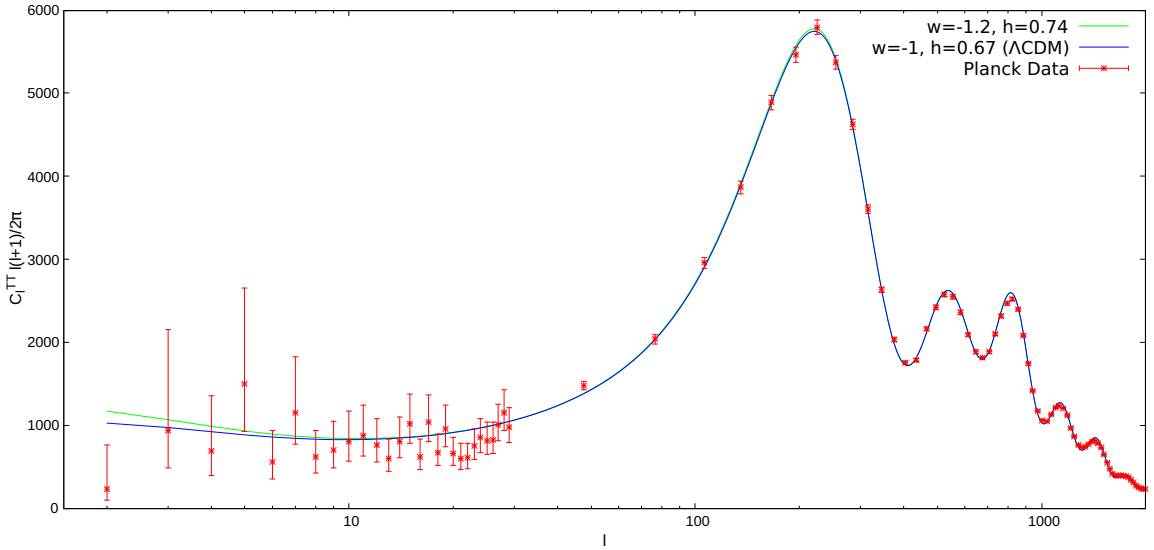

Figure 2.2: The CMB power spectrum for ΛCDM (blue line) and $w = -1.2$ (green line). We also show the binned high-l and low-l Planck data (red points). Adopted from Ref. [198].

Following this approach for the case of a one parameter parametrization where $w(z)$ remains constant in time and redshift (wCDM model), it is simple enough to derive the degeneracy function $h(w)$ shown in Fig. 2.1 (continuous orange line) by solving Eq. (2.10) considering that Eq. (2.3) takes the form

$$H(z, \omega_m, \omega_r, \omega_b, h, w(z)) = H_0 \sqrt{\Omega_{0\mathrm{m}}(1+z)^3 + \Omega_{0\mathrm{r}}(1+z)^4 + (1 - \Omega_{0\mathrm{m}} - \Omega_{0\mathrm{r}})\,(1+z)^{3(1+w)}} \tag{2.11}$$

We can show then, with the help of Fig. 2.1, that the degeneracy function can be approximated as a straight line (dashed blue line) in the range $w \in [-1.5, -1]$

$$h(w) \approx -0.3093w + 0.3647. \tag{2.12}$$

The points with the errorbars were obtained by numerical fitting to the Planck/CMB power spectrum using the corresponding wCDM models with fixed w. This analysis is discussed in more detail in the next section. Next we show in Fig. 2.2 the predicted form of the CMB TT anisotropy spectrum for the parameter values $w = -1$ ($h = 0.67$, $\Omega_{0m} = 0.314$) (ΛCDM) and $w = -1.2$ ($h = 0.74$, $\Omega_{0m} = 0.263$). This effectively demonstrates the invariance of the CMB power spectrum as the cosmological parameters are allowed to vary with consideration to the above described degeneracy.

According to Eq. (2.12) the value of w that is required in order to achieve a $h(w) = 0.74$ is $w \approx -1.217$, a fact that is very consistent with previous studies in the literature [186, 187]. In Ref. [186], in particular, the author attempts a similar analysis where he reports that fixing the dark energy equation of state $w \approx -1.3$ or the effective number of relativistic

species $N_{eff} \approx 3.95$ may ease of the H_0 tension. However the novelty of the methodology presented here lies on the fact that it uses analytical methods to identify the qualitative features required for any form of $w(z)$ to attempt to relax the H_0 tension.

The use of this methodology for the derivation of the predicted dark energy properties required to seemingly resolve the H_0 tension is not confined simply on the case of the wCDM model, on the contrary it may be extended to more parametrizations of $w(z)$. For example it can be used in the case of the two parameter CPL parametrization [199, 200] expansion of $w(z)$

$$w = w_0 + w_1(1-a) = w_0 + w_1 z/(1+z) \tag{2.13}$$

where Eq. (2.3) is written as

$$H(z) = H_0\sqrt{\Omega_{0\mathrm{m}}(1+z)^3 + \Omega_{0\mathrm{r}}(1+z)^4 + (1-\Omega_{0\mathrm{m}}-\Omega_{0\mathrm{r}})\,(1+z)^{3(1+w_0+w_1)}e^{-3\frac{w_1 z}{1+z}}} \tag{2.14}$$

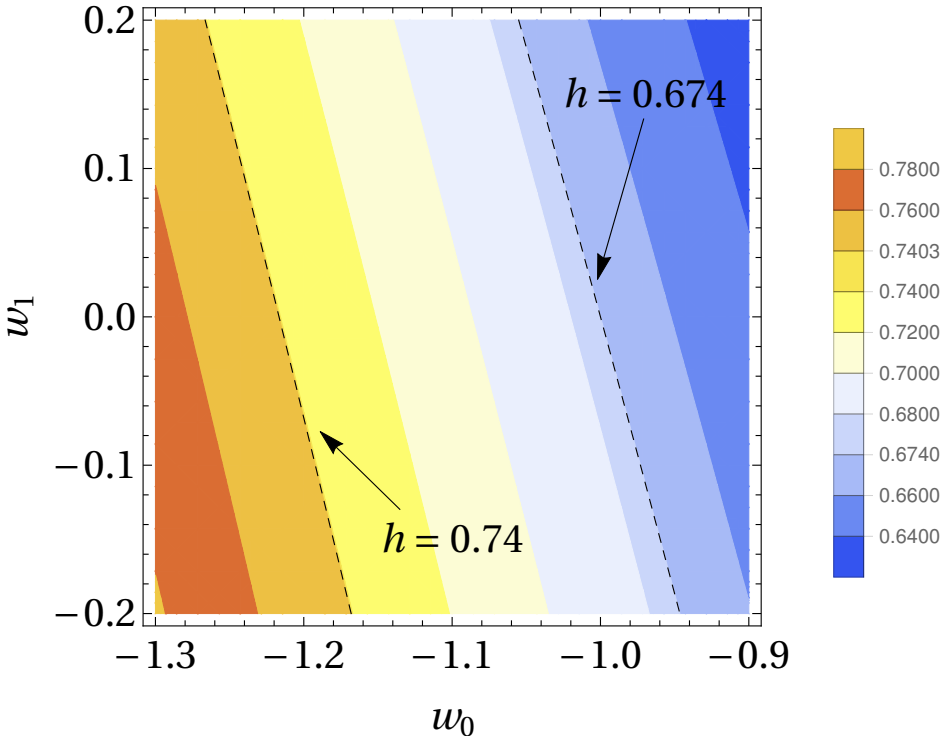

Figure 2.3: The degeneracy with respect to the CMB spectrum in the parameter space $(w_0 - w_1)$. The dashed lines correspond to $h = 0.674$ (ΛCDM value) and to $h = 0.74$ (the value of Ref. [201]). Adopted from Ref. [198].

Using now Eqs. (2.1), (2.5), (2.9) and (2.12) and the above described methodology in the context of the CPL parametrization, the derivation of the relevant degeneracy function $h(w_0, w_1)$, by solving Eq. (2.10) is quite simple. Similarly to Fig. 2.1 for wCDM we can construct Fig. 2.3, where the dashed lines correspond to the parameter values that satisfy both $h(w_0, w_1) = 0.674$, with the ΛCDM value going through the point $(w_0, w_1) = (-1, 0)$ as expected, and the local distance ladder measurements value $h(w_0, w_1) = 0.74$. The constant h contour lines shown in Fig. 2.3 are approximately straight in the range of the $w_0 - w_1$ parameter space shown. In particular, for the case of the value $h = 0.74$, which attempts to

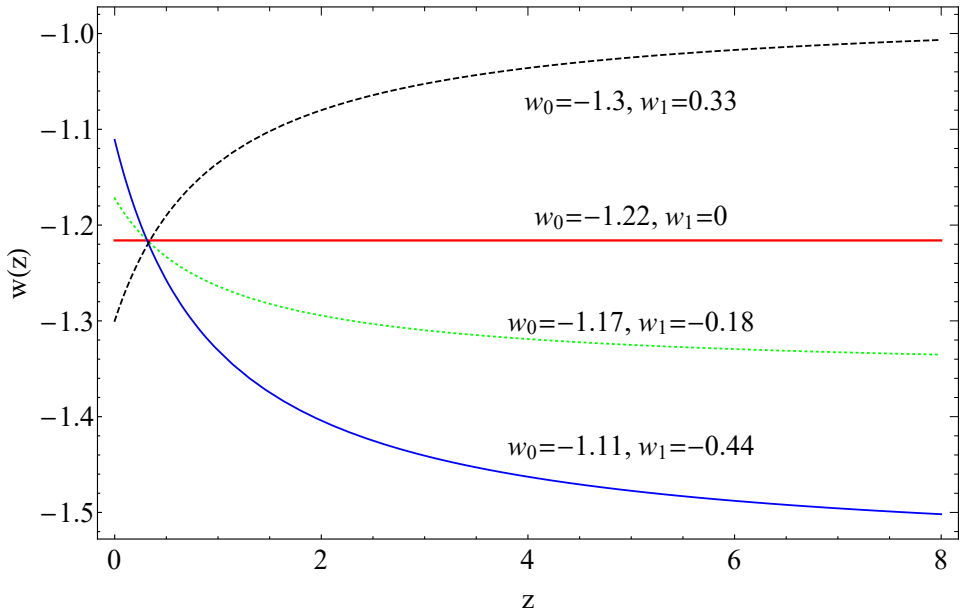

Figure 2.4: The evolution of $w(z)$ for various values of (w_0, w_1) along the degeneracy $h = 0.74$ line of Fig. 2.3. All these parameter values lead to a best fit value $h = 0.74$ in the context of the CMB power spectrum. However, they do not have the same quality of fit to other cosmological data which can be used to break this model degeneracy. The common (z, w) point of intersection of all the $w(z)$ plots is $(0.31, -1.22)$. Adopted from Ref. [198].

ease the H_0 tension, we can approximate the relevant line by the equation,

$$w_1 \approx -4.17 w_0 - 5.08 \tag{2.15}$$

The preference for a phantom-like behaviour in some redshift ranges is apparent in Fig. 2.3 when we attempt to approach the local measurement of h. This is also demonstrated in Fig. 2.4 where we show four forms of $w(z)$ based on the CPL parametrization that can resolve the H_0 tension by providing a best fit value of $h = 0.74$ from the CMB data. The corresponding wCDM value of $w = -1.22$ is also shown. Clearly all degenerate forms of CPL $w(z)$ that relax the H_0 tension go through the same point at $z = 0.31$ crossing the $w = -1.22$ line. This type of degeneracy in particular redshifts for cosmological parameters has been discussed in Ref. [202]. Also degenerate $w(z)$ curves with $w_0 < 1.22$ are increasing functions of z, while those with $w_0 > 1.22$ are decreasing functions of z. This appears to be a general feature of all $w(z)$ parametrizations that can relax the H_0 tension. For example the PEDE parametrization [191] and the late dark energy transition hypothesis [203] with $w(z \simeq 0) > -1.22$ are decreasing functions of the redshift z as predicted by the above degeneracy analysis. The identification of these properties opens up the possibility of a very late type phase transition at $z \simeq 0.01$ from a phantom phase to a ΛCDM phase with a sharply increasing rather than decreasing function of $w(z)$.

It is expected that even in the case of some $w(z)$ parametrization that has the potential to lead to an apparent alleviation of the H_0 tension we would also have to consider its quality of fit to the actual CMB spectrum and to other cosmological data is significantly with regards to ΛCDM ($w = -1$). Therefore, it is of the out-most importance that we consider the quality of fit of the preferred degenerate forms of $w(z)$ to other cosmological data like SnIa, BAO and

growth of perturbations data (Redshift Space Distortion $f\sigma_8(z)$ and weak lensing data) as well as to actual CMB power spectrum data which may not fully respect the above exploited approximate degeneracy (especially at low l). Thus, we set the following questions for the next section:

- What is the quality of fit of the forms of $w(z)$ that are predicted to resolve the H_0 tension, on cosmological data involving SnIa, BAO, growth Redshift Space Distortion data and the actual Planck CMB TT power spectrum data? Is this quality of fit (χ^2) similar to the corresponding quality for ΛCDM?
- Is the H_0 tension actually alleviated when the full CMB spectrum data are used in the context of a model with fixed $w(z)$ to its predicted form (*e.g.* $w = -1.22$ in the context of a constant w)?
- Is the growth tension partially relaxed in the context of the above preferred $w(z)$ found?

These questions will be addressed mainly in the context of a redshift independent w (wCDM) but it is straightforward to generalize the analysis for more general forms of $w(z)$.

2.2 Numerical Analysis of Dark Energy Models

We use the numerical package MGCosmoMC [204–206] (see Appendix B.2 for the modified MGCAMB core files) in order to test the quality of the semi-analytic results that were presented in the previous section against the CMB and other cosmological data. Specifically, we use the *Planck* TT and lowP dataset, *i.e.* the TT likelihood for high-l multipoles $(l > 30)$ as well as the Planck temperature and polarization data for low multipoles $(l < 30)$. The priors that have been used as input can be seen in Table 2.1.

Parameters	Priors
$\Omega_b h^2$	$[0.005, 0.1]$
$\Omega_c h^2$	$[0.001, 0.99]$
$100\theta_{MC}$	$[0.5, 10]$
τ	$[0.06, 0.8]$
$ln\,(10^{10} A_s)$	$[1.61, 3.91]$
n_s	$[0.8, 1.2]$

Table 2.1: The MGCosmoMC priors that have been used in Figs. 2.5 and 2.7. We also set $A_{lens} = 1$ and $\Omega_k = 0$.

By fixing w to the values of the points shown in Fig. 2.1 ($w = -1.0, -1.1, -1.2, -1.3$) and subsequently constructing the likelihood contours (Fig. 2.5) for the cosmological parameters for each case, we find the best fit values of h which are shown in Table 2.2 (see also Fig. 2.1). We therefore conclude that they are in excellent agreement with the expectations based on our previous degeneracy analysis (see orange continuous line of Fig. 2.1). It is once again clear that the likelihood contours for the Hubble parameter shift to higher best fit values as

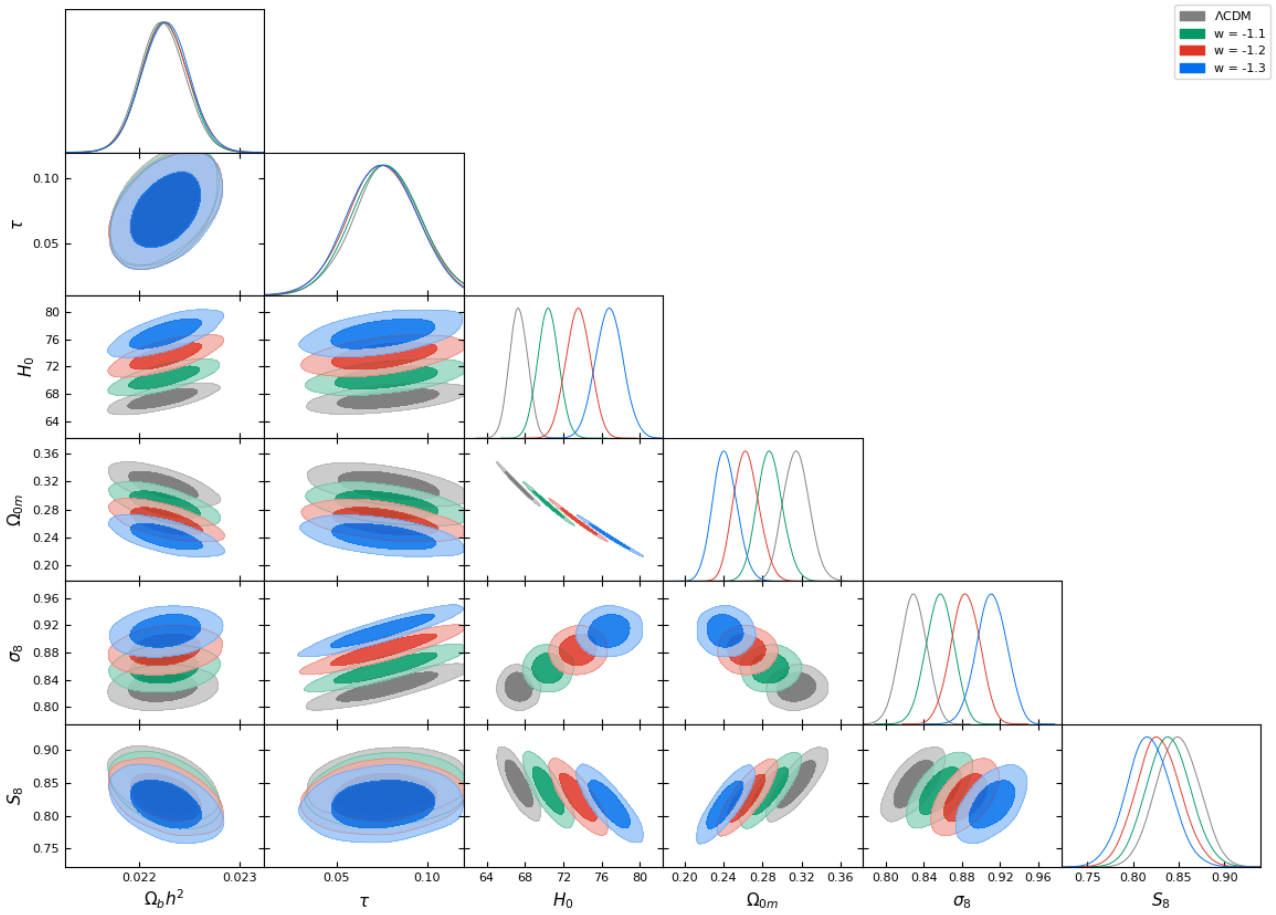

Figure 2.5: The contour plots constructed with MGCosmoMC using the *Planck*TT and lowP likelihoods for ΛCDM and wCDM models. The gray contours correspond to the ΛCDM model. The green contours correspond to $w = -1.1$, the red ones to $w = -1.2$, while the blue to $w = -1.3$. For $w = -1.1$, the best fit value of H_0 is close to that of the Planck18/ΛCDM measurement [72], while the $w = -1.2$ and $w = -1.3$ values shift h closer to the local distance ladder measurements [201]. Adopted from Ref. [198].

w decreases in the phantom regime ($w < -1$) and that at the same time the best fit values of the matter density parameter $\Omega_{0\mathrm{m}}$ decrease in accordance with the degenerate parameter combination $\Omega_{0\mathrm{m}}h^2$.

w	Ω_{0m}^{th}	h_{th}	Ω_{0m}^{obs}	h_{obs}	χ^2_{CMB}	$\Delta\chi^2_{CMB}$
-1.0	0.316	0.674	0.315 ± 0.013	0.673 ± 0.010	11266.516	–
-1.1	0.289	0.704	0.288 ± 0.013	0.704 ± 0.011	11266.530	0.014
-1.2	0.265	0.735	$0.263^{+0.012}_{-0.014}$	0.736 ± 0.013	11267.132	0.616
-1.3	0.244	0.766	$0.242^{+0.012}_{-0.013}$	0.768 ± 0.014	11266.520	0.004

Table 2.2: The analytically predicted CMB best fit values of h and Ω_{0m} for fixed w, obtained by using the CMB parameter degeneracy arguments, as well as the ones obtained by the actual fit of the corresponding w model to the Planck TT CMB anisotropy power spectrum. The quality of fit for each model compared to ΛCDM is also indicated by the value of $\Delta\chi^2$.

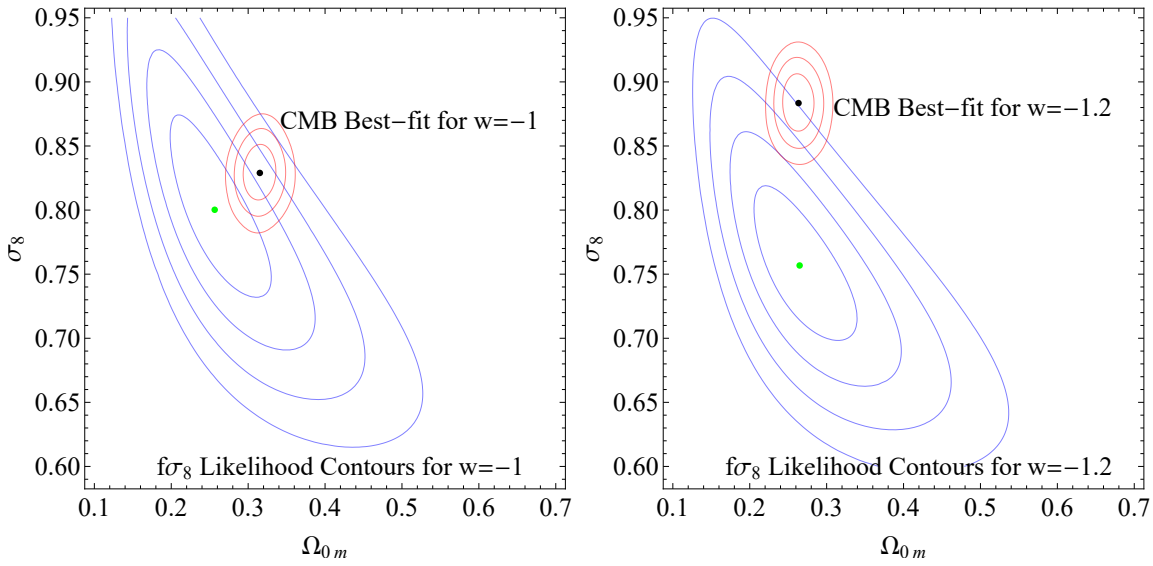

Figure 2.6: The $1\sigma - 4\sigma$ contours in the parametric space $\Omega_{0\mathrm{m}} - \sigma_8$. The blue contours correspond to the best fit growth compilation of Ref. [207], while the red to the $1\sigma - 4\sigma$ confidence contours for $w = -1$ (left panel) and $w = -1.2$ (right panel) obtained from the Planck data. Adopted from Ref. [198].

This reduced value of the best fit $\Omega_{0\mathrm{m}}$ would naively imply reduced growth of cosmological perturbations and thus resolution of the growth tension. However, the reduced best fit value of the matter density parameter $\Omega_{0\mathrm{m}}$ matter density is not enough to soften the growth tension, since the best fit value of the parameter σ_8 (the present day rms matter fluctuations variance on scales of $8h^{-1}\mathrm{Mpc}$) appears to increase more rapidly, as w decreases in the phantom regime. Since this parameter is proportional to the initial amplitude of the matter perturbations power spectrum, its increase amplifies the growth of perturbations and tends to cancel the effect of the decrease of the best fit $\Omega_{0\mathrm{m}}$ in the context of perturbations growth. This is demonstrated in Fig. 2.6 where we show the σ_8 likelihood contours obtained by fitting the models $w = -1$ (ΛCDM) and $w = -1.2$ to the growth $f\sigma_8$ data (we have used the conservative robust dataset of Table 2 of Ref. [207], a subset of an up to date compilation presented in [208]). Superimposed we also show the corresponding likelihood contours obtained from the Planck CMB TT power spectrum obtained for each value of fixed w. Clearly, the tension between the RSD $f\sigma_8$ data and the Planck data increases in the context of the phantom model $w = -1.2$ compared to ΛCDM ($w = -1$).

In addition to the growth data we also fit the models $w = -1$ and $w = -1.2$ to a cosmological data combination including the Pantheon SnIa [22], BAO data [209–211], CMB data [72], as well as the prior of the Hubble constant published by Riess et al. [201] and obtain for ΛCDM $\chi^2 = 12319.2$, while for $w = -1.2$ we obtain $\chi^2 = 12332.7$. We thus find $\Delta\chi^2 = 13.5$. This difference of $\Delta\chi^2 = 13.5$ for the phantom model, indicates a significantly reduced quality of fit compared to ΛCDM in agreement with previous studies [212]. The corresponding likelihood contours are shown in Fig. 2.7. It is therefore clear that the particular fixed w models considered here lead to an apparent resolution of the Hubble tension since they increase the best fit value of H_0 in the context of the CMB data but the resolution is not viable since the growth tension gets worse while the quality of fit of these models to the SnIa and BAO data

is not as good as for ΛCDM. This result is consistent with previous studies [187], where it has been demonstrated that non-CMB data, such as BAO and SNIa favour lower values of H_0 which are more consistent with the CMB value, while also disfavouring $w < -1$ in the context of flat and non-flat untilted inflation models [213]. It is, however, worth mentioning that for the combination of the CMB Planck data and the Riess Hubble constant prior the quality of the fit improves drastically for $w = -1.2$, with $\Delta\chi^2 = -10.7$ in respect to $w = -1$. The exploitation of the CMB spectrum degeneracy of more complicated forms of $w(z)$ however may lead to better fits to growth, SnIa and BAO cosmological data.

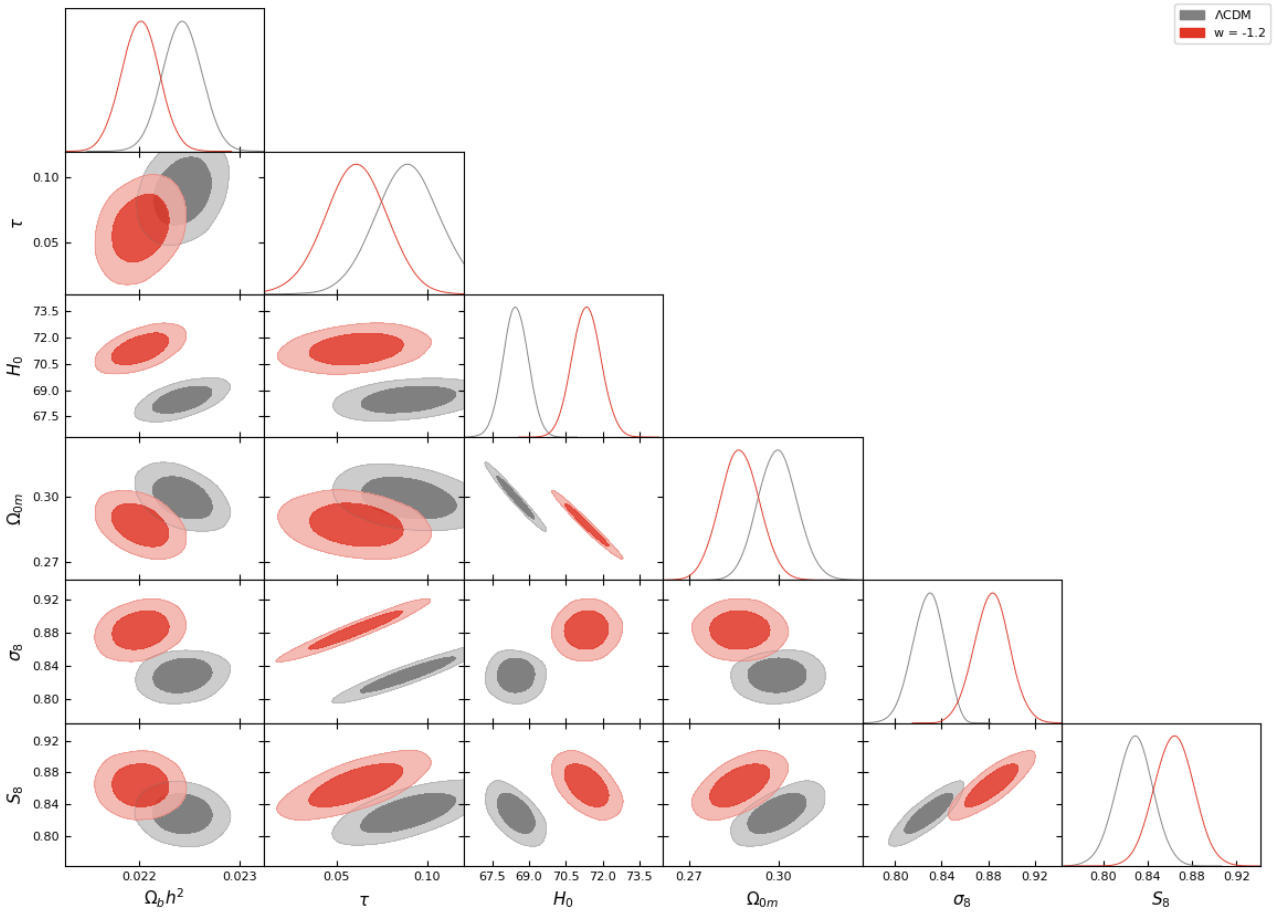

Figure 2.7: The likelihood contours constructed with MGCosmoMC using the cosmological data combination of Pantheon SnIa [22], BAO data [209–211], CMB data [72], as well as the prior of the Hubble constant [201] for ΛCDM (gray contours) and wCDM with $w = -1.2$ (red contours). Adopted from Ref. [198].

2.3 In Brief

Summing-up, in this chapter we have shown how one can use inherent analytical degeneracy relations among cosmological parameters and numerical fits to cosmological data, in order to identify the qualitative and quantitative features of dark energy models that have the potential to relax the H_0 tension of the ΛCDM model. We have found that mildly phantom models with mean equation of state parameter $w \simeq -1.2$ can show signs of easing this

tension. The models may be constructed in such a way that there are no extra parameters compared to ΛCDM by using fixed parametrizations of $w(z)$. In practice however they involve more fine tuning compared to ΛCDM and are clearly less natural. In addition the quality of fit of the simplest of such models to cosmological data beyond the CMB is not as good as the corresponding quality of fit of ΛCDM. However, it is straightforward to construct physical models involving either phantom scalar field with non-canonical kinetic terms or modified gravity models that naturally produce the required phantom behavior of dark energy. Despite the usual stability issues of such models it can be shown that it is possible to construct ghost free versions [183]. For example, physical models described by scalar field Lagrangians can reproduce an effective dark energy with a constant equation of state parameter w in the context of both quintessence ($w > -1$) [214–216] and phantom dark energy $w < -1$ [217].

In particular, a dynamical dark energy scalar field with an inverse power law potential of the form $V(\phi) = M^{(4+\alpha)}\,\phi^{-\alpha}$ (where M and $\alpha > 0$ are free parameters), corresponds to a physically interesting model where the dark energy equation of state parameter w is constant and takes the form [216],

$$w = \frac{\frac{\alpha}{2} w_B - 1}{1 + \frac{\alpha}{2}} \tag{2.16}$$

where w_B is the equation of state parameter of the dominant background. Clearly, for a matter dominated epoch ($w_B = 0$), and $\alpha > 0$, we can obtain a constant w and a quintessence like behaviour ($w > -1$).

Similarly, a phantom like behaviour ($w < -1$) with constant w, may be obtained [217] in the context of a scalar field with non-canonical kinetic terms with an action of the form

$$S = \int d^4x\sqrt{-g}\left(\frac{1}{2\kappa^2}R + p(\phi, \nabla\phi)\right) + S_B \tag{2.17}$$

where $\kappa^2 = 8\pi G$ and S_B is the action of the background. The Lagrangian may be assumed to depend only on the scalar field ϕ and its derivative squared $X = -\frac{1}{2}\nabla^\mu\phi\nabla_\mu\phi$. In the case of a slowly varying field X the pressure p and energy density ρ of the field take the form [217]

$$p = f(\phi)(-X + X^2), \tag{2.18}$$

$$\rho = 2X\frac{\partial p}{\partial X} - p = f(\phi)(-X + 3X^2) \tag{2.19}$$

For $f(\phi) \propto \phi^{-\alpha}$, Eqs. (2.18) and (2.19) lead to an equation of state parameter of the form

$$w = \frac{(1 + w_B)\alpha}{2} - 1. \tag{2.20}$$

For a matter dominated epoch ($w_B = 0$) an appropriate value of α can lead to either a quintessence or a phantom behavior. In particular for $\alpha < 2$ we obtain $w > -1$ (quintessence behavior), while for $a < 0$ we obtain a physical model with $w < -1$ (phantom equation of state).

However, the constant w behavior of both of the above physical models described by Eqs. (2.16) and (2.20) is a good approximation only in the context of a dominant background fluid with constant equation of state w_B. In our universe this would occur for example only well in the matter dominated epoch. These equation of state parameters would cease to have a constant form near the end of the matter era and in the present transition cosmological era.

Thus, the constancy of w in the context of these physical models is a good approximation only on high redshifts ($z > 2$).

The analytical approach for the H_0-$w(z)$ degeneracy pointed out in this chapter offers a new method to systematically search and design $w(z)$ forms that can combine some of the proper features that are seemingly required to relax the Hubble tension while keeping a good fit to cosmological data. Our goal here was only to introduce this methodology and apply it to the simplest cases while also pointing out the difficulties in resolving the tensions discussed. Using a smooth $H(z)$ deformation model and exploiting a parameter degeneracy like the one presented here, in order to elevate the value of H_0, has significant disadvantages. As we will show in the following chapters this approach manages to "solve" the Hubble tension only superficially.

CHAPTER 3

Proposing a w-M Transition at $z_t < 0.1$

As we have seen both in the previous chapter and generally in the literature [186, 187, 191, 198, 218–220], attempts to consider smooth deformations of $H(z)$ at $z \simeq O(1)$ have been successful in matching $r(z_{rec})$ with $r(z = 0)$ but have been unable to match the value of $r(z \simeq O(1))$ which is strongly constrained by BAO and SnIa data to be close to the form indicated by Planck18/ΛCDM.

In this chapter we consider the possibility of an abrupt deformation of $H(z)$ at $z \lesssim 0.1$ ($H(z)$ transition). However, even though this type of deformation has been considered for a long time in the literature [221–223] it has been constrained by both the comoving distance $r(z)$ at $z > 0.1$ as well as by the measured SnIa magnitudes which are not consistent with a large step-like discontinuity. Specifically, if this deformation were to occur below the redshift when Hubble flow begins, it would mean that it would be observationaly undetectable [222] and thus it would not have contributed to the measured decreased value of $r(z)$ at low z. In the event that this deformation occurred at $0.01 < z_t < 0.1$ with the proper amplitude to reduce $r(z)$ to the required level, it would have to produce a step-like feature in the SnIa Hubble diagram which would have an amplitude $\Delta m = 0.2$ and it would be inconsistent with the Pantheon data.

Our main goal in this chapter is to show that the latter problem can be avoided. The way to avoid it is by assuming a assuming a transition of the SnIa absolute magnitude M at $z_t \in [0.01, 0.1]$. By combining both a transition in the transition of the SnIa absolute magnitude accompanied and a transition of the equation dark energy of state parameter $w(z) \equiv p_{de}(z)/\rho_{de}(z)$ [224, 225] we show that it is possible to overcome the issue of the required step-like feature of the apparent magnitudes while being consistent with value of the absolute magnitude implied by local Cepheid calibrators.

In particular, we express these transitions as follows starting with the transition in the dark energy equation of state $w(z)$

$$w(z) = -1 + \Delta w\, \Theta(z_t - z) \tag{3.1}$$

and subsequently the transition in the SnIa absolute magnitude M with the form

$$M(z) = M_C + \Delta M\, \Theta(z - z_t) \tag{3.2}$$

where Θ is the Heaviside step function, $M_C = -19.24$ is the SnIa absolute magnitude calibrated by Cepheids [62, 226] at $z < 0.01$ and ΔM, Δw are parameters to be fit by the data. Therefore, we have defined the Late $w - M$ Transition ($LwMT$) model.

It is straightforward to show, using the energy momentum conservation $d(\rho_{de}a^3) = -p_{de}d(a^3)$, that the evolution of dark energy density ρ_{de} is obtained as

$$\rho_{de}(z) = \rho_{de}(z_p)\int_{z_p}^{z}\frac{dz'}{1+z'}(1+w(z')) = \rho_{de}(z_p)\left(\frac{1+z}{1+z_p}\right)^{3(1+w)} \tag{3.3}$$

where in the last equality a constant w was assumed and z_p is a pivot redshift which may be assumed equal to the present time or equal to the transition time z_t. Then, Eqs. (3.1) and (3.3) imply a continuous Hubble expansion rate $h(z) \equiv H(z)/100km/(sec\cdot Mpc)$ of the form

$$\begin{aligned} h_w(z)^2 &\equiv \omega_m(1+z)^3 + \omega_r(1+z)^4 + (h^2-\omega_m-\omega_r)\left(\frac{1+z}{1+z_t}\right)^{3\,\Delta w} && z < z_t \\ h_w(z)^2 &\equiv \omega_m(1+z)^3 + \omega_r(1+z)^4 + (h^2-\omega_m-\omega_r) && z > z_t \end{aligned} \tag{3.4}$$

where $\omega_m \equiv \Omega_{0m}h^2$, $\omega_r \equiv \Omega_{0r}h^2$ are the matter and radiation density parameters assumed fixed to their Planck18/ΛCDM values in the next section and h is a parameter distinct from the rescaled measurable Hubble parameter $h_w(z=0)$[1]. In what follows we define $h_{local} \equiv 0.74$ and $h_{CMB} \equiv 0.674$, by assuming $0.01 < z_t < 0.1$, which correspond to the Hubble constant values obtained with local standard candle measurements of $r(z)$ ($H_0 = H_0^{R19}$) and sound horizon standard ruler measurements ($H_0 = H_0^{P18}$ calibrated by Planck18/ΛCDM) respectively.

The questions we will occupy ourselves with in the next parts of this chapter are the following:

- What is the functional form of $\Delta w(z_t)$ so that $h_w(z=0) = h_{local}$ as implied by local measurements while maintaining the required Planck18/ΛCDM form of $r(z)$ for $z \gg z_t$?
- How closely does the $LwMT$ model reproduce the form of the Planck18/ΛCDM comoving distance $r(z)$ for $z > z_t$? How does this form of $r(z)$ compare with the corresponding form of the $H(z)$ transition?
- How does the quality of fit of the $LwMT$ model to cosmological data (CMB, SnIa, BAO and SH0ES) compare with the corresponding quality of fit of typical models that utilize smooth deformations of $H(z)$ to address the H_0 tension?
- What are the favored values of Δw, ΔM and what are the implications for general relativity and for the future evolution of the universe?

3.1 Introducing the $LwMT$ Model

Our first goal is to constrain the values of the ω_m, ω_r, h and Δw parameters that are present in the $LwMT$ ansatz (see Eqs. 3.4). In order to do that we impose two conditions. The first one is that the ansatz should reproduce the comoving distance corresponding to Planck18/ΛCDM r_Λ for $z \gg z_t$ where

$$r_\Lambda(z) \equiv \int_0^z \frac{dz'}{\omega_m(1+z')^3 + \omega_r(1+z')^4 + (h^2-\omega_m-\omega_r)} \tag{3.5}$$

[1]The parameter h would be equal to the measured rescaled Hubble parameter $h_w(z=0)$ in the limit $z_t \to 0$.

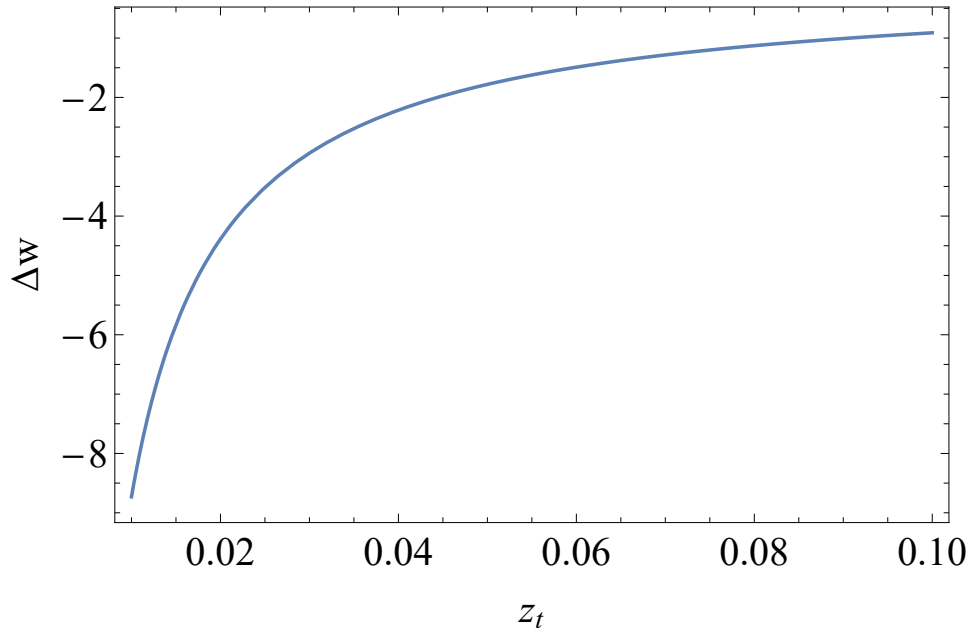

Figure 3.1: The equation of state shift Δw required for $h_w(z=0) = h_{local}$ as a function of the transition redshift z_t. Notice the strongly phantom behavior of the dark energy equation of state $w = -1 - \Delta w$ for $z < z_t$. Adopted from Ref. [227].

and $\omega_m \equiv \Omega_{0m}h^2 = 0.143$, $\omega_r \equiv \Omega_{0r}h^2 = 4.64 \times 10^{-5}$ and $h = h_{CMB} = 0.674$. This condition fixes the parameters ω_m, ω_r and h to their Planck18/ΛCDM best fit values. Since we consider $z_t < 0.1 \ll 1$ it is straightforward to obtain an upper bound for the relative difference

$$\frac{\Delta r}{r}(z) \equiv \frac{r_w(z) - r_\Lambda(z)}{r_\Lambda(z)} < \frac{h_{local} - h_{CMB}}{h_{CMB}} \simeq 0.1 \tag{3.6}$$

where $r_w(z) \equiv \int_0^z \frac{dz'}{h_w(z')}$ is the comoving distance corresponding to the $LwMT$ model (3.4). $\frac{\Delta r}{r}(z)$ is maximum at $z = 0$ and decreases rapidly as z increases as demonstrated below. The second constrain is that it should reproduce the local measurements of the Hubble parameter

$$h_w(z=0) = h_{local} = 0.74. \tag{3.7}$$

This means that we will have a relation between Δw and z_t of the form (here we neglect ω_r as it has practically no effect on Δw)

$$\Delta w = \frac{\log\left(h^2 - \omega_m\right) - \log\left(h_{local}^2 - \omega_m\right)}{3\log(1+z_t)} \tag{3.8}$$

where $h = h_{CMB} = 0.674$ and $\omega_m = \Omega_{0m}h^2 = 0.143$ as implied by the first condition and for consistency with the CMB anisotropy spectrum. These types of models imply a very strong phantom dark energy behaviour in the present, a fact that is shown also in Fig. 3.1 via a plot of $\Delta w(z_t)$.

In Fig. 3.2 we compare the forms of the comoving distance $r(z)$ of some of the proposed $H(z)$ deformations for the resolution of the Hubble tension, against the one predicted in the context of the $LwMT$ model $r_w(z)$. More specifically, we show a plot of the function $f(z) \equiv z/r(z)$ (whose $z \to 0$ limit is the Hubble constant) for the $LwMT$ model, the $H(z)$

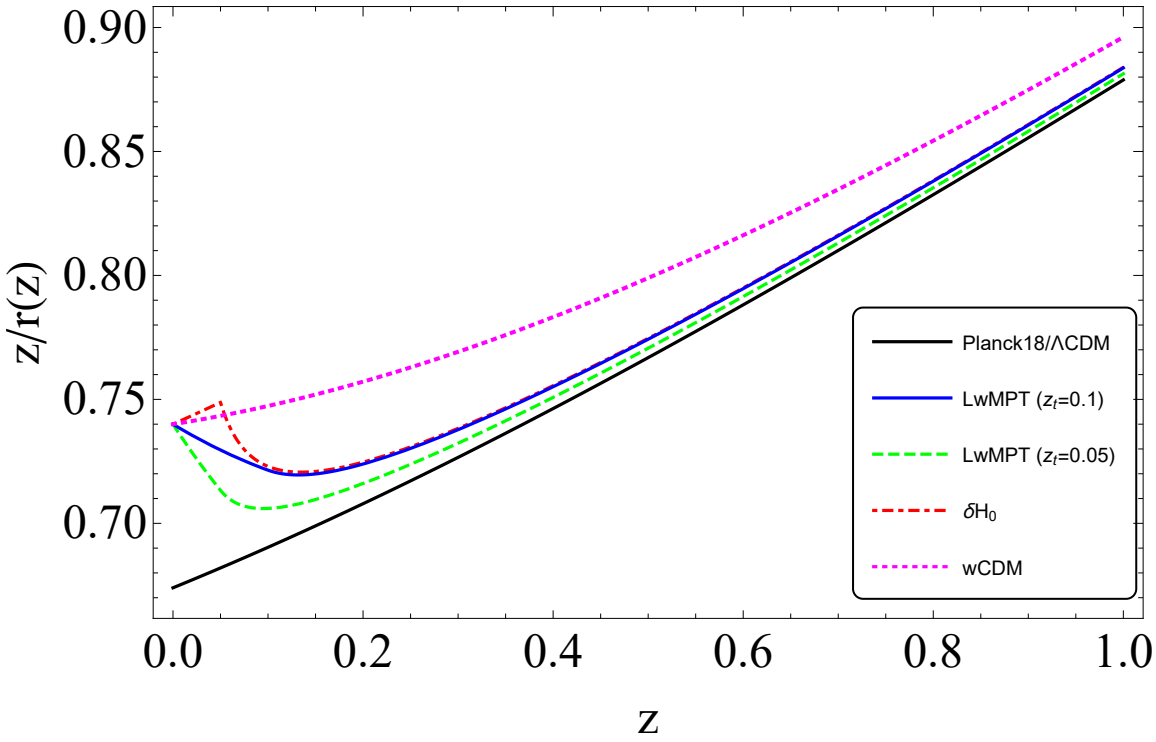

Figure 3.2: The function $f(z) = z/r(z)$ where $r(z)$ is the comoving distance to redshift z for the cosmological models Planck18/ΛCDM (black continuous line), wCDM with $w = -1.2$ (magenta dotted line), $H(z)$ transition (3.9) with $z_t = 0.05$ and $\frac{\delta h}{h} = (h_{local} - h_{CMB})/h_{CMB}$ (red dot-dashed line), $LwMT$ with $z_t = 0.05$ and $w(z < z_t) = -1 - \Delta w = -2.78$ as indicated by Eq. (3.8) (green dashed line) and $LwMT$ with $z_t = 0.1$ and $w(z < z_t) = -1 - \Delta w = -1.91$ as indicated by Eq. (3.8) (blue continuous line). Notice that even though all three models approach $r_\Lambda(z)$ asymptotically, the two $LwMT$ models remain closest to the Planck18/ΛCDM comoving distance $r_\Lambda(z)$ while at the same time they are consistent with the local measurement of the Hubble constant since $h_w(z = 0) = 0.74$. Adopted from Ref. [227].

transition model and the wCDM with fixed $w = -1.22$ model [186, 187, 198]. The $H(z)$ transition model is defined as

$$h_\delta(z)^2 \equiv (1 + \frac{\delta h}{h}\,\Theta(z_t - z))^2\left[\omega_m(1+z)^3 + \omega_r(1+z)^4 + (h^2 - \omega_m - \omega_r)\right] \tag{3.9}$$

where $\frac{\delta h}{h} = \frac{h_{local} - h_{CMB}}{h_{CMB}}$, $h = h_{CMB}$ and ω_m, ω_r are assumed fixed to their Planck18/ΛCDM best fit values. The fixed w (wCDM) smooth $H(z)$ deformation model is defined as

$$h_{wf}(z)^2 \equiv \omega_m(1+z)^3 + \omega_r(1+z)^4 + (h^2 - \omega_m - \omega_r)(1+z)^{3(1+w)} \tag{3.10}$$

where $w = -1.22$, $h = h_{local}$ and ω_m, ω_r are assumed fixed to their Planck18/ΛCDM best fit values [198]. All three models that address the H_0 tension shown in Fig. 3.2 satisfy by construction two necessary conditions

$$h(z = 0) = h_{local} \tag{3.11}$$

$$r(z) \to r_\Lambda(z) \quad for \quad z \gtrsim O(1). \tag{3.12}$$

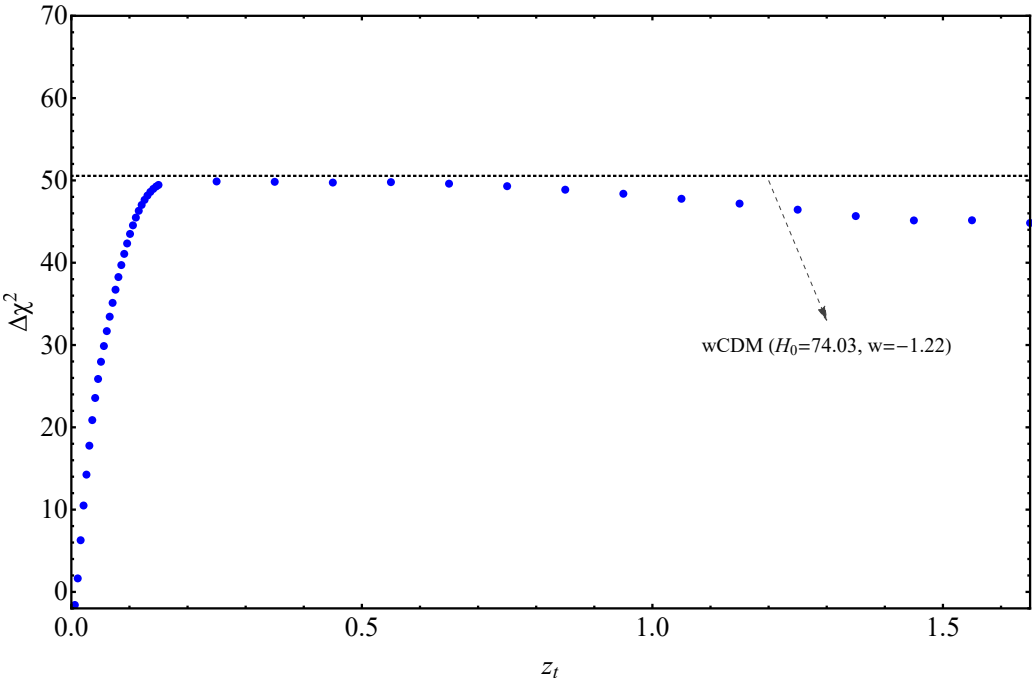

Figure 3.3: The residuals $\Delta\chi^2$ plotted against the values of the transition redshift z_t for the $LwMT$ (blue dots) and wCDM (black dotted line) with $w = -1.22$. The $LwMT$ model seems to achieve a significantly better fit for small z_t values. Adopted from Ref. [227].

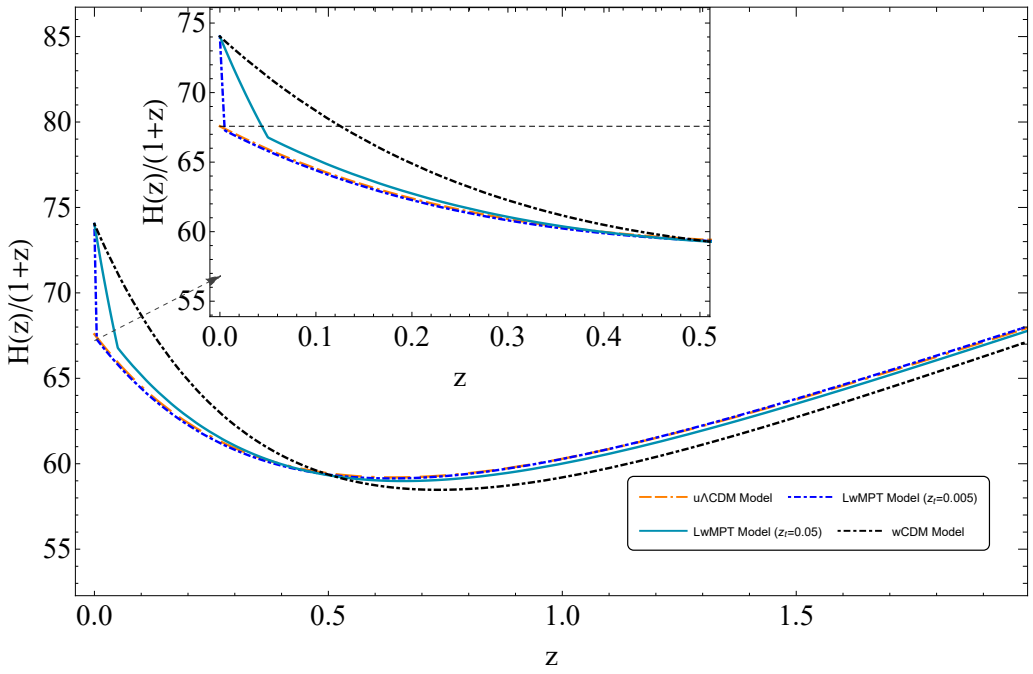

Figure 3.4: The forms of the comoving Hubble parameter $H(z)/(1+z)$ for two $LwMT$ models with $z_t < 0.1$, the best fit wCDM and uΛCDM. Adopted from Ref. [227].

These conditions along with the fact that we fix the parameters ω_m and ω_r to their best fit ΛCDM values secure the fact that all three models produce the same CMB anisotropy spectrum as Planck18/ΛCDM while at the same time they predict a Hubble parameter equal

to its locally measured value $h(z=0)=h_{local}$. However, the three models do not approach the Planck18/ΛCDM comoving distance $r_\Lambda(z)$ with the same efficiency as z increases. As is clearly seen in Fig. 3.2, the $LwMT$ model with both $z_t=0.1$ and $z_t=0.05$ approaches $r_\Lambda(z)$ faster than the other two models. Since Planck18/ΛCDM provides an excellent fit to most geometric cosmological probes at $z>0.1$ it is anticipated that $LwMT$ will produce a better fit to cosmological data than the smooth deformations of $H(z)$ like wCDM or the discontinuous $H(z)$ transition model which produces an unnatural step in $r(z)$ and moves away from $r_\Lambda(z)$ for $z<z_t$ as z increases. This improved quality of fit is also demonstrated in the next section.

A fact which lies at the heart of the Hubble tension is that a deformation of $H(z)$ model that claims to ease it should not only be preoccupied with being consistent with the locally measured value of the Hubble parameter H_0 and with the
Planck18/ΛCDM form of $H(z)$, but it should also be consistent with the value of the absolute magnitude of SnIa as determined by Cepheid calibrators M_C [62, 226]. This may be seen by considering the equation that connects the SnIa measured apparent magnitudes at redshift z_i with the Hubble free luminosity distance and the Hubble parameter which may be written as

$$m(z_i)=M-5\log_{10}\left[H_0\cdot \text{Mpc}/c\right]+5\log_{10}(D_L(z_i))+25 \tag{3.13}$$

where $D_L(z)=H_0\,d_L(z)/c$ is the Hubble free luminosity distance. Given the measured $m(z_i)$ datapoints the best fit Hubble parameter in the context of local measurements can decrease to become consistent with the sound horizon calibrator by either decreasing $D_L(z)$ (deforming $H(z)$) or by decreasing the absolute magnitude M. Such a decrease of M can be achieved either by discovering a systematic effect of the Cepheid calibrators or by assuming an M transition at $z\geq 0.01$ due to an abrupt change of fundamental physics. The deformation of $D_L(z)$ is severely constrained by the standard ruler constraints based on the sound horizon (CMB and BAO) and even though it is most efficient in the context of very late transitions as the one discussed in the present analysis it may still not be enough to compensate with the decrease of H_0 while keeping M fixed to its Cepheid calibrated value $M=M_C$. A common error made in late time approached of the Hubble tension is to either marginalize over M with a flat prior or allow it to vary along with the cosmological parameters in the context of the maximum likelihood method. This may lead to a best fit value of M that is inconsistent with the Cepheid measured value M_C thus invalidating the results of such analysis.

In order to overcome this issue, in the next section we allow the absolute magnitude M to vary along with the cosmological parameters and as we have already said we will hypothesize that both the M and w transitions happen simultaneously. However, let us not be oblivious to the fact that for $\Delta M=-5\log_{10}\left[\frac{H_0^{\rm R19}}{H_0^{\rm P18}}\right]\simeq -0.2$ the M transition may be sufficient for the resolution of the H_0 tension, meaning that there will no longer be a need for the simultaneous w transition.

3.2 Fitting $LwMT$ to Cosmological Data

It is now time to use a wide variety of robust cosmological data in order to estimate the quality of fit and the best fit parameter values of the $LwMT$ and two other classes of cosmological models. For the $LwMT$ model we remove the constraint $w_>=-1$ for $z>z_t$ as well as the constraint $\omega_m=0.143$. Thus the model is now allowed to have three free parameters for each

fixed value of z_t: $w_>$, $w_< \equiv w_> + \Delta w$ and ω_m. However, as discussed below, the additional free parameters end up constrained by the data very close to the values considered fixed in the previous section. The second model we use is wCDM (3.10) which possesses two free parameters, w and ω_m. For both these models the constraint $h(z=0) = h_{local}$ is imposed as a prior in the analysis. Lastly, we consider the well-known ΛCDM model. In order to maximize its quality of fit to the data no constraint for $h(z=0)$ is imposed on this model. This enables us to also use it as a benchmark in comparison to the other models that address the H_0 tension. Thus we use the term uΛCDM ("u" for "unconstrained") to denote it. We assume identical best fit parameter values ($\Omega_{0m} = 0.312 \pm 0.006, H_0 = 67.579 \pm 0.397$) to Planck18/$\Lambda$CDMand we therefore use it as a baseline to compute residuals of χ^2 to compare the other two representative models. We use the following data to identify the quality of fit of these models

- The Pantheon SnIa dataset [22] consisting of 1048 distance modulus datapoints in the redshift range $z \in [0.01, 2.3]$.
- A compilation of 9 BAO datapoints in the redshift range $z \in [0.1, 2.34]$. The compilation is shown in the Appendix.
- The latest Planck18/ΛCDM CMB distance prior data (shift parameter R [195] and the acoustic scale l_a [228]). These are highly constraining datapoints based on the observation of the sound horizon standard ruler at the last scattering surface $z \simeq 1100$. The covariance matrix of these datapoints and their values are shown in the Appendix.
- A compilation of 41 Cosmic Chronometer (CC) datapoints in the redshift range $z \in [0.1, 2.36]$. These datapoints are shown in the Appendix and have much less constraining power than the other data we use.

Taking that into account the total χ^2 is defined as

$$\chi^2 = \chi^2_{CMB} + \chi^2_{BAO} + \chi^2_{CC} + \chi^2_{Panth}. \tag{3.14}$$

As we have said above the residual $\Delta\chi^2$ of the $LwMT$ (as a function of z_t) and the wCDM models are calculated with respect to the uΛCDM model. Since the CMB data are the most constraining, for wCDM we have used the best fits $\omega_m \simeq 0.143$ and $w = -1.22$ [198] that were found using the methodology of Chapter 2.

These residuals $\Delta\chi^2$ for the best fit $LwMT$ models as a function of z_t (blue points) and the corresponding residual $\Delta\chi^2$ for the best fit wCDM model (horizontal black line) are shown in Fig. 3.3. It is obvious from the figure that the $LwMT$ models massively improve their fit as the z_t parameter decreases below $z_t \simeq 0.15$ in contrast to wCDM. The best fit parameter values for $w_<$ ($z < z_t$) and $w_>$ ($z > z_t$) are shown in Table 3.1. In parenthesis next to each $w_<$ best fit we show the predicted value in the context of the analysis of the previous section (Eq. (3.8)) which assumes $w_> = -1$.

In Fig. 3.4 by displaying the forms of the comoving Hubble parameter $H(z)/(1+z)$ for two $LwMT$ models with $z_t < 0.1$, the best fit wCDM and uΛCDM , we show the efficiency of the $LwMT$ of approaching the fit of the uΛCDM model. This is very important because the $LwMT$ model claims to address the Hubble tension by reaching $h(z=0) = h_{local}$ as well. This characteristic is not very easily achievable, a fact that is demonstrated by the failure of

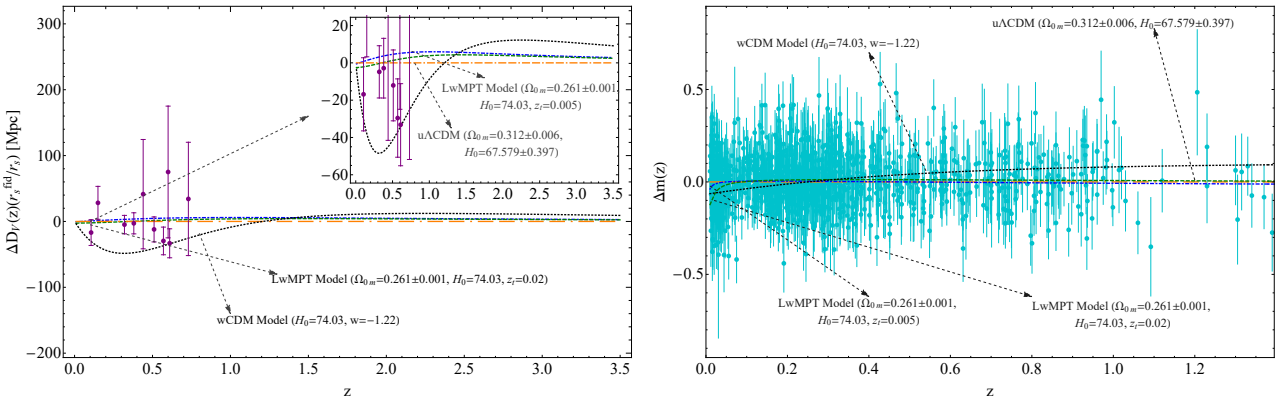

Figure 3.5: *Left panel:* BAO data residuals $\Delta D_V \times \frac{r_s^{fid}}{r_s}$ from the best fit uΛCDM (orange dashed line) superimposed with the best fit residual curves corresponding to wCDM (dotted black line), $LwMT$ with $z_t = 0.005$ (blue dot dashed line) and $LwMT$ with $z_t = 0.02$ (green dashed line). Notice the difficulty of smooth $H(z)$ deformation of wCDM to fit the data due to the constraint imposed by the local measurements of Hubble constant. *Right panel:* The Pantheon SnIa distance modulus residuals Δm from the best fit uΛCDM. The predicted distance modulus residual curves for wCDM (black dashed line), the $LwMT$ ($z_t = 0.005$) (blue dot dashed line) and the $LwMT$ ($z_t = 0.02$) (green dashed line) are also shown. Adopted from Ref. [227].

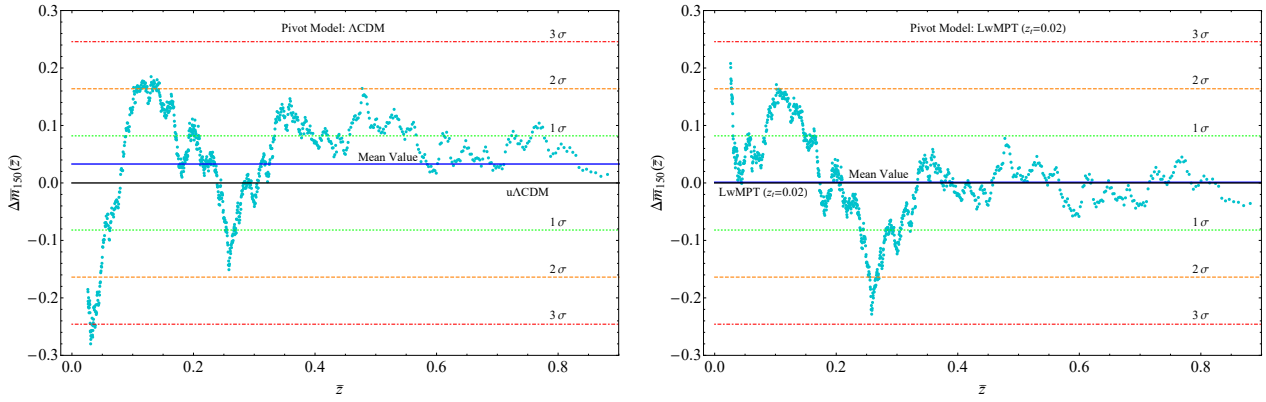

Figure 3.6: *Left panel:* The 150 point moving average of the Pantheon SnIa standardized residual absolute magnitudes with respect to the best fit ΛCDM ($\Delta\bar{m}_{150}(\bar{z})$ of eqs (3.16-3.17)). Notice the sharp and peculiar drop at $z \lesssim 0.1$ (unlikely at more than 3σ level). *Right panel:* The 150 point moving average of the Pantheon SnIa standardized residuals with respect to the best fit $LwMT$ ($z_t = 0.02$). The sharp drop shown in the left panel has disappeared while the mean and the standard deviation of the moving average points have dropped significantly indicating that the $LwMT$ is a more natural pivot model than Planck18/ΛCDM. Adopted from Ref. [227].

the wCDM, which employs a smoother approach and is therefore much less able to mimic the behaviour of Planck18/ΛCDM , this is also shown in in Fig. 3.3.

The difficulty of the smooth $H(z)$ deformation models that address the Hubble tension in fitting the BAO and SnIa data is also demonstrated in Fig. 3.5 where we show the BAO and SnIa data (residuals from the best fit uΛCDM) along with the best fit residuals for the

z_t	$\Delta\chi^2$	Ω_{0m}	$w_<$ $(z < z_t)$	$w_>$ $(z > z_t)$
0.005	-1.9	0.2609	$-18.44\,(-18.4)$	-1.005
0.01	0.8	0.2608	$-9.93\,(-9.7)$	-1.001
0.02	9.7	0.2607	$-5.28\,(-5.3)$	-1.011
0.04	23.1	0.2606	$-2.93\,(-3.2)$	-1.037
0.05	27.6	0.2607	$-2.48\,(-2.8)$	-1.049
0.06	31.3	0.2607	$-2.19\,(-2.5)$	-1.059
0.08	37.9	0.2608	$-1.81\,(-2.1)$	-1.085
0.1	43.3	0.2611	$-1.58\,(-1.9)$	-1.115
0.2	50.1	0.2622	$-1.22\,(-1.4)$	-1.230

Table 3.1: The values of the $LwMT$ model best fit parameters Ω_{0m}, $w_<$ $(z < z_t)$ and $w_>$ $(z > z_t)$ corresponding to different indicative values of the transition redshift z_t, along with each case's $\Delta\chi^2$ with respect to uΛCDM. In parenthesis we show the analytically predicted values of $w_<$ which were obtained from Eq. (3.8) (*i.e.* assuming $w_> = -1$ and imposing the constraint $h(z = 0) = h_{local}$ on the $LwMT$ ansatz (3.4)). Notice that the best fit values of Ω_{0m} are consistent with the CMB spectrum requirement of $\omega_m = 0.143$ in view of the constraint $h(z = 0) = h_{local}$ imposed in all cases.

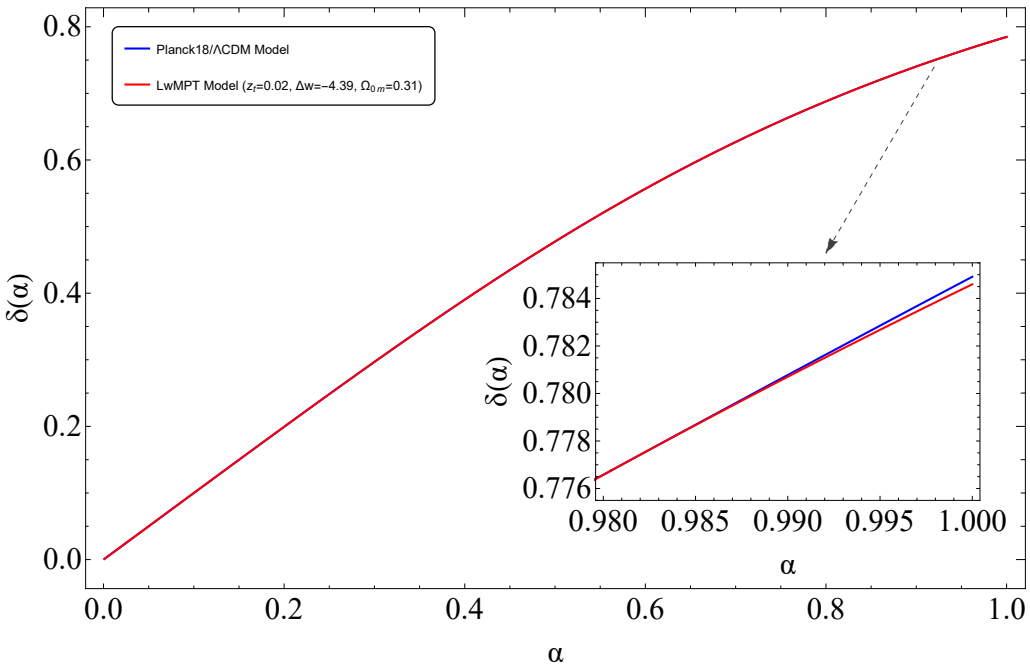

Figure 3.7: The growth factors $\delta(\alpha)$ of the linear perturbations, for both the $LwMT$, with $z_t = 0.02$ and $\Delta w = -4.39$ (red line), and Planck18/ΛCDM (blue line) models. Clearly, the effect of the w transition on the growth factor is negligible at it occurs at $a_t \simeq 0.98$. Adopted from Ref. [227].

wCDM and $LwMT$ models. The right panel of Fig. 3.5 indicates that the $LwMT$ model with $z_t = 0.02$ which can resolve the Hubble tension, closely mimics the apparent magnitudes of uΛCDM for $z > z_t$ but for $z < z_t$ it predicts a small reduction of the residual apparent magnitudes. The question therefore to address is the following: *Is there a hint for such a*

statistically significant reduction of the measured absolute magnitudes in redshifts close to the transition redshift $z_t \simeq 0.02$*?* Interestingly, this is indeed the case!

The left panel of Fig. 3.6 shows the $N = 150$ point moving average of the standardized residual absolute magnitudes with respect to the best fit ΛCDM model. The ΛCDM standardized residual apparent magnitudes are defined as

$$\Delta\bar{m}(z_i) \equiv \frac{m_{obs}(z_i) - m_{th\Lambda CDM}(z_i, M_{bf}, \Omega_{0mbf})}{\sigma_{i-tot}} \tag{3.15}$$

where σ_{i-tot} is the total error (statistical+systematic), $M_{bf} = -19.23$ and $\Omega_{0mbf} = 0.30$ are the best fit parameter values of ΛCDM in the context of the Pantheon data and $m_{th\Lambda CDM}$ are the corresponding theoretically predicted apparent magnitudes. The N point moving average corresponding to the residual standardized datapoint point j ($j \in [1, 1048 - N]$) is defined as

$$\Delta\bar{m}^j_N(\bar{z}) \equiv \frac{1}{N}\sum_{i=j}^{j+N} \Delta\bar{m}(z_i) \tag{3.16}$$

and the corresponding redshift is

$$\bar{z}^j_N \equiv \frac{1}{N}\sum_{i=j}^{j+N} z_i \tag{3.17}$$

For $N = 150$ the left panel of Fig. 3.6 shows the form of $\Delta\bar{m}_N(\bar{z})$. Since the points are standardized and ignoring their correlations, we expect that the 1σ region will approximately correspond to $\sigma \simeq 1/\sqrt{N} \simeq 0.08$ which is also indicated in Fig. 3.6 up to the 3σ level. Interesting features of the binned Pantheon data have been identified in previous studies [229, 230]. Related to such features is a clear abrupt drop of the moving average of the standardized residuals from the $+2\sigma$ region to the -3σ region and beyond clearly seen in the left panel of Fig. 3.6. The deepest part of this drop is at a redshift of about 0.02. This is precisely the type of signature anticipated in the context of the $LwMT$ model. Once we consider the residuals with respect not to the best fit ΛCDM but to the best fit $LwMT$ model with $z_t = 0.02$, this peculiar feature disappears (Fig. 3.6 right panel). In addition, the standard deviation of the points of the moving average of residuals decreases by about 20% (from 0.1 to 0.8) while their mean value shown in Fig. 3.6 drops sharply from 0.03 to 0.001. This is also a hint that the best fit $LwMT$ with $z_t = 0.02$ is a more natural pivot model than the best fit ΛCDM. This observation supports the consideration of a combined $w - M$ transition for the resolution of the Hubble tension instead of using simply an M transition.

In contrast to smooth $H(z)$ deformations that in general tend to worsen the growth tension by increasing the growth rate of cosmological perturbations at early times [231] the proposed ultra-late w transitions have negligible effect on the growth rate of cosmological perturbations. At $z_t = 0.02$ most structures have already gone nonlinear during the $w = -1$ era and have decoupled from the effects of the background expansion. Even those fluctuations that are still linear do not have the time to respond to the change of w since it occurs at very low z ($z \simeq 0.02$). In addition, the emerging strongly phantom background could only lead to a suppression of the growth due the super accelerating expansion which prevents the growth of perturbations. We demonstrate this minor suppressing effect on the growth in Fig. 3.7, where we have solved numerically the equation for the growth of linear perturbations for the $LwMT$ model for $z_t = 0.02$ and for the required $\Delta w = -4.39$ showing

that the effect on the growth factor is negligible compared to the Planck18/ΛCDM growth factor. If the effect of a possible gravitational transition inducing the change of M were to be taken into account, the decrease of the growth factor may be shown to be large enough to resolve also the growth tension [232].

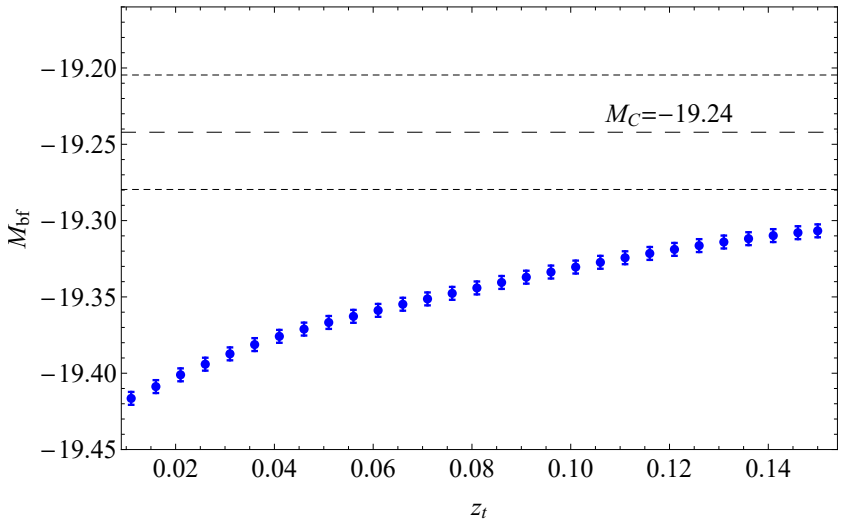

Figure 3.8: The best fit absolute magnitude M_{bf} (blue points) for various transitions z_t for the $LwMT$ model. The dashed line corresponds to the M_C value indicated by Refs. [62, 226], while the dot dashed lines correspond its 1σ error. Notice that if M_C is considered to be constant, the majority of the best fit values of M_{bf} are more than 2σ away from the M_C value. This difference reduces as z_t increases. Adopted from Ref. [227].

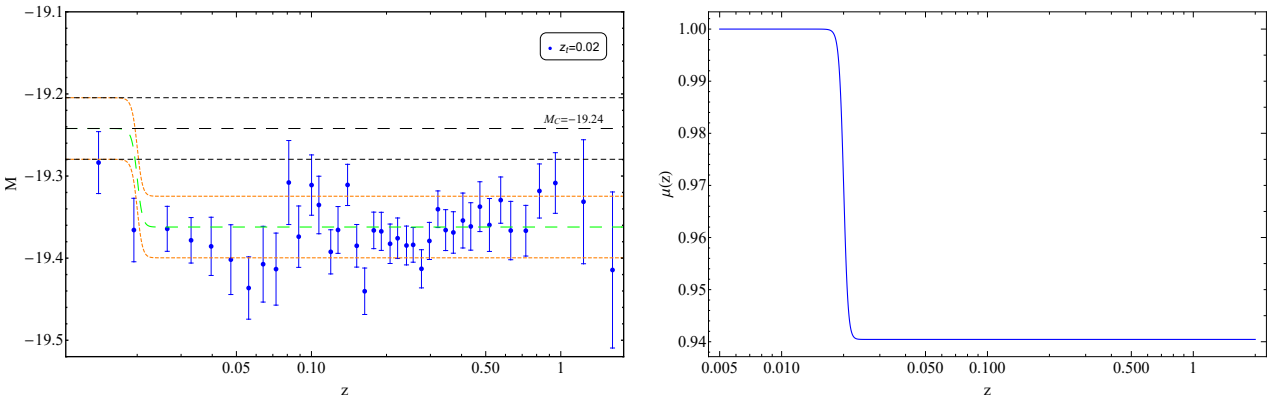

Figure 3.9: *Left panel:* The absolute magnitude M as a function of redshift z. The straight dashed line corresponds to the fixed M_C value [62, 226] from local Cepheid calibrators of SnIa while the dot dashed lines correspond to its 1σ error. Clearly Pantheon binned absolute magnitudes M_i (blue points) corresponding to the best fit $LwMT$ model ($z_t = 0.02$) are approximately 2σ away from M_C. However, in the context of an abrupt transition of M with $\Delta M \simeq -0.1$ at $z_t = 0.02$, the inconsistency disappears. *Right panel:* The form of $\mu = G_{\rm eff}/G_{\rm N}$ required to induce he M transition shown on the left panel. Clearly, for $z > 0.02$ $G_{\rm eff} < 1$ hinting towards weaker gravity [233–235] as indicated by other studies discussing the growth tension [71, 77, 94, 97, 208, 229]. Adopted from Ref. [227].

In order to identify the magnitude of the required M transition we evaluate the best fit value of the absolute magnitude $M_{bf}(z_t)$ for $z_t[0.01, 0.15]$ (Fig. 3.8). Notice that $\Delta M \equiv M_C - M_{bf}$ is maximum at $z_t = 0.01$ and approaches the 1σ distance from M_C at $z_t > 0.15$. For such high values of z_t however the BAO data are poorly fit and the value of χ^2 increases to the level of wCDM. The type of the required M transition for $z_t = 0.02$ is shown in the left panel of Fig. 3.9 where we also show the absolute magnitudes of the binned Pantheon datapoints obtained from Eq. (3.13) by solving with respect to M for each datapoint and using the best fit form of $D_L(z)$ for $z_t = 0.02$. Clearly, the derived absolute magnitudes are not consistent with the Cepheid calibrated value of M_C but in the context of an M transition with $\Delta M \simeq -0.1$ the inconsistency disappears. The right panel of Fig. 3.9 shows the required evolution of an effective Newton's constant that is required to produce the M transition obtained under the assumption that the SnIa absolute luminosity is proportional to the Chandrasekhar mass which varies as $L \sim G_{\rm eff}^b$ with $b = -3/2$.[2] This assumption leads to the variation of the SnIa absolute magnitude M with $\mu \equiv \frac{G_{\rm eff}}{G_{\rm N}}$ ($G_{\rm N}$ is the locally measured Newton's constant) as [77, 237, 238]

$$\Delta M = \frac{15}{4}\, log_{10}\, (\mu) \tag{3.18}$$

which implies that for $\Delta M \simeq -0.1$ we have a 6% reduction of μ.

Notice that if the SnIa data analysis assumes a fixed value of $M = M_C$ then the existing $m(z_i)$ data lead to a value of $H_0 = 74km/(sec \cdot Mpc)$ while if the transitions (3.1) and (3.2) are assumed with $z_t = 0.02$, $\Delta w = -4.3$ and $\Delta M = -0.1$ then the data analysis would lead to a value $H_0 = 67.5km/(sec \cdot Mpc)$ (consistent with CMB-BAO calibration) while the true value of H_0 would be $H_0 = 74km/(sec \cdot Mpc)$ due to the H_0 prior imposed on the w transition Δw.

3.3 In Brief

In this chapter we have demonstrated using both an analytical approach and a fit to cosmological data that a Late $w - M$ Transition ($LwMT$) can lead to a resolution of the Hubble tension in a more efficient manner than smooth deformations of the Hubble tension and other types of late time transitions (the Hubble expansion rate transition). The moving average statistic of the standardized residual Pantheon absolute magnitude SnIa data indicates the presence of a peculiar feature at $z < 0.1$ which is consistent with the anticipated signatures of the $LwMT$ model. Such a transition leads in general to a best fit value of the SnIa absolute magnitude that is not consistent with the value implied by local Cepheid calibrators of SnIa [62]. Therefore late time transitions can only constitute successful resolutions of the Hubble tension if they are accompanied by a transition of the SnIa absolute magnitude due to evolving fundamental constants. We have shown that a transition of the effective gravitational constant to a value lower by about 6% is sufficient to induce the required ΔM transition. This weakening of gravity may also justify the observed reduced growth of perturbations which is supported by Weak Lensing [71, 94, 97] and Redshift Space Distortion data [77, 208, 229] (growth tension). Therefore, this model simultaneously addresses both the Hubble and the growth tensions. Another basic advantage of such a late time model

[2] If $b \neq -3/2$ and especially if $b > 0$ as indicated in [236] under a wide range of assumptions, then the ability of the $LwMT$ model to resolve the growth tension could be negatively affected.

that can fully resolve the Hubble tension is that it can fit the local distance data (BAO and SnIa) in a very effective manner. This is due to the fact that by construction it has the same quality of fit to the BAO, SnIa and CMB data as Planck18/ΛCDM, in contrast to the usual late time smooth deformations of $H(z)$.

Moreover, there is a physical theoretical basis of the model since it can be realized in the context of modified gravity theory with a rapid gravitational transition. The rapid nature of the transition is a generic feature and can be made consistent with solar system tests with no need for screening as in other modified theories. Such models include the following:

- The most natural model that can induce a $LwMT$ involves a non-minimally coupled phantom scalar field initially frozen at $\phi = \phi_0$ due to cosmic friction close to the zero point of its potential which could be assumed to be of the form $V(\phi) = s\ \phi^n$. Such a field would initially have a dark energy equation of state $w = -1$ mimicking a cosmological constant. Once Hubble friction becomes smaller than the field dynamical (mass) scale, the field becomes free to roll up its potential (phantom fields move up their potential in contrast to quintessence fields [239, 240]) and develops a rapidly changing equation of state parameter $w < -1$ and shifted $G_{\rm eff}$. Thus the universe enters a ghost instability phase which will end in a Big Rip singularity in less than a Hubble time. Such a scenario for the simple (but also generic) case of linear potential ($n = 1$) has been investigated in Ref. [239]. For a general phantom potential we anticipate a redshift dependence of the equation of state $w_< = w_<(z)$ after the transition ($z < z_t$). In fact the phantom field potential could be reconstructed by demanding a form of $w_<(z)$ that further optimizes the quality of fit to the low z data or by simply demanding that $w_<$ is constant.

- A scalar-tensor modified gravity theory field initially frozen due to Hubble friction, mimicking general relativity and a cosmological constant. Once Hubble friction becomes smaller than the field mass scale, the field becomes free to roll down its potential inducing deviations from general relativity on cosmological scales and a phantom departure from the cosmological constant. Note that scalar tensor theories can induce phantom behavior without instabilities in contrast to a simple minimally coupled scalar field [183].

The detailed investigation of the above described dynamical scalar field evolution that can reproduce the $LwMT$ is an interesting extension of the analysis presented in this chapter.

If the phantom $LwMT$ is realized in Nature it would imply the existence of a rapidly approaching Big Rip singularity [241, 242] which may be avoided due to quantum effects [243]. Given the value of $w_<$ which emerges at approximately the present time t_0, it is straightforward to calculate the time t_* of the Big Rip singularity assuming that $w = w_< < -1$ at the present time t_0. The result is [242]

$$\frac{t_*}{t_0} = \frac{w_<}{1 + w_<} \tag{3.19}$$

For example for $z_t = 0.02$ we have $w_< \simeq -5$ which implies that the universe will end in a Big Rip singularity in less than 3.5 billion years (for $t_0 = 13.8 \times 10^9 yrs$). This implies that there may be observational effects of such coming singularity on the largest bound systems like the Virgo cluster, the Coma Cluster or the Virgo supercluster. A detailed investigation of

the observational effects on bound systems of the $LwMT$ is an interesting extension of the present analysis.

The detailed comparison of the quality of fit of the $LwMT$ (or similar) models with a variety of smooth $H(z)$ deformation models addressing the Hubble tension would also be a useful extension. The use of full CMB spectrum data and possibly other cosmological data sensitive to the dynamics of galaxies in clusters and superclusters could also be included.

The late time sudden deformation of the luminosity distance $D_L(z)$ induced through the w transition helps to decrease the required magnitude of the M transition from $\Delta M \simeq -0.2$ to $\Delta M \simeq -0.1$. In the absence of the w transition the Hubble tension could still be resolved via an M transition with $\Delta M \simeq -0.2$ and no deformation of $D_L(z)$. Even though this approach would be simpler it would require a larger amplitude of the ΔM transition at $z_t \simeq 0.01$ while it would not address the abrupt feature in the Pantheon data shown in Fig. 3.6. Nevertheless, the simplicity of such an approach in an attractive feature and thus this model deserves a detailed investigation by comparing its predictions with current and future data.

CHAPTER 4

Smooth Deformations of $H(z)$ and the S_8 Tension

Amongst the vast number of proposed late time solutions to the Hubble tension a great deal of them uses late time smooth deformations of the Hubble expansion rate $H(z)$ of the Planck18/ΛCDM best fit to match the locally measured value of H_0, while effectively keeping the comoving distance to the last scattering surface and $\Omega_{0m}h^2$ fixed to maintain consistency with Planck CMB measurements. Although this approach is common it suffers from a number of issues.

The most well-known problem of these models is that they worsen the fit to low z distance probes. In this chapter we show that another problem of these parametrizations is that they significantly worsen the level of the $\Omega_{0m} - \sigma_8$ growth tension. As we will discuss with greater in the following sections, we show this by using the paradigm of the generic CPL [199, 200] model. This parametrization corresponds to an evolving dark energy equation of state parameter of the form given by Eq. (2.13) with local measurements H_0 prior and we identify the pairs (w_0, w_1) that satisfy the condition mentioned above. The CPL parametrization is one of the most generic and well known classes of smooth deformations of $H(z)$ that are designed to address the Hubble tension. We show that for this type of models the growth tension between dynamical probe data and CMB constraints is worse than the corresponding tension of the standard Planck18/ΛCDM model. We justify this feature using a two-fold methodology, on one hand we explore an approximate analytic approach, and on the other hand we also provide a full numerical solution of the growth equation and subsequently fit to the data. However, it is very important to mention that this issue does not affect the proposed solution of the Hubble crisis involving a SnIa absolute magnitude transition at $z_t \simeq 0.01$ that is explored in Chapter 3. Therefore, in the context of this chapter we focus on the following question: *'Can this class of smooth deformation models improve the growth tension by decreasing the growth rate of cosmological perturbations compared to the Planck18/ΛCDM model?'*

The analytic part of our study is being done by considering a generic CPL parametrization which in redshift space is expressed via Eq. 2.13. We impose consistency with the Planck anisotropy spectrum and local measurements of $H(z)$ by using the methodology of Ref. [198] that is described in Chapter 2. More specifically, we fix $\omega_m \equiv \Omega_{0m}h^2$ ($h \equiv H_0/100km\,s^{-1}\,Mpc^{-1}$) to the Planck18/$\Lambda$CDM value $\omega_m = \bar{\omega}_m \equiv 0.143$. Then we fix the comoving distance to recombination (flat space) $r(z_{rec}) \equiv \int_0^{z_{rec}} \frac{dz}{H(z}$ to its Planck18/ΛCDM

value and, lastly, we fix the value of H_0 to its locally measured value H_0^{R20}.

These three conditions lead to the numerical evaluation of the function $w_{1h}(w_0)$ such that for any given value of w_0 we obtain the corresponding value of $w_1 = w_{1h}$ that can potentially address the Hubble problem by fitting local measurements of H_0 while being consistent with the CMB anisotropy spectrum [198]. We then focus on pairs $(w_0, w_{1h}(w_0))$, evaluate the predicted growth factor of perturbations in the context of general relativity $\frac{\delta(z=0)}{\delta(z_{rec})}$ and compare it with the corresponding growth factor predicted by the best fit Planck18/ΛCDM $H(z)$. We thus address the question: *Are there w_0, w_1 pairs that can potentially address the Hubble problem while having lower predicted growth of perturbations than the Planck18/ΛCDM form of $H(z)$ which is already in tension with RSD and weak lensing data?*

In Chapter 2 we showed that in the case of wCDM with $w_0 \simeq -1.22$, even though the model claims to address the Hubble tension (at least superficially), it fails to address the S_8 tension and at the same time does not fit well the low z distance data (BAO and SnIa) as it has been demonstrated in previous studies [189, 198, 219]. In fact, focusing on the growth tension, we see that it worsens it and as we will show by generalizing this analysis to more general cases of smooth deformations of $H(z)$, this constitutes a key characteristic for all of them. In order to do that, we calculate the growth factor for various values in the $w_0 - w_1$ parameter space that have the ability to superficially address the Hubble tension and we continue by constructing the $\sigma_8 - \Omega_{0m}$ likelihood contours for representative $(w_0, w_{1h}(w_0))$ pairs via the use of a robust RSD $f\sigma_8$ data compilation [76, 207]. By comparing these contours with the corresponding Planck likelihood ones, we are able to estimate the tension level for each case of $(w_0, w_{1h}(w_0))$ pairs.

The next part of this chapter revolves around the numerical confirmation of our results. To achieve that, we fitted these smooth deformations of $H(z)$ models to compilations of SnIa, BAO and CMB data and showed that the received fit in each case is much worse than that of the Planck18/ΛCDM model. We anticipated this issue since, as we mentioned before these models are expected to have a poor fit with respect to BAO and SnIa data. However, we will not occupy ourselves with this aspect of the study, since we are interested on their consistency with the growth $f\sigma_8$ data. Lastly, we will focus on the absolute magnitude M of the SnIa. Using the relevant Pantheon data we will identify the best fit values of M for these $H(z)$ deformations and we will compare these best fits with the corresponding range of M that is implied by the Cepheid calibrators. This approach could hint towards a new issue of the $H(z)$ deformation models, known as the M tension [62, 226] which is discussed also in Chapter 3.

4.1 Approximate Analytic Solutions to the Evolution of the Matter Density Perturbations

As mentioned with greater detail in Chapter 2, a deformation of the Hubble expansion rate from its Planck18/ΛCDM form may be expressed as

$$H(z, \omega_m, \omega_r, h, w(z)) = H_0 \sqrt{\Omega_{0m}(1+z)^3 + \Omega_{0r}(1+z)^4 + \Omega_{0de} e^{3\int_0^z dz' \, (1+w(z'))/(1+z')}} \tag{4.1}$$

where $w(z)$ is the dark energy equation of state parameter at redshift z, Ω_{0r}, Ω_{0m} are the present day radiation and matter density parameters and $\Omega_{0de} = 1 - \Omega_{0m} - \Omega_{0r}$ is the present

day value of the dark energy density parameter assuming spatial flatness. We also define $\omega_r \equiv \Omega_{0r}h^2$. This deformed Hubble expansion can become simultaneously consistent with local measurements of $H_0 = H_0^{R20}$ as well as with the CMB anisotropy spectrum. Reiterating the results displayed in Chapter 2 if we consider that [194, 195, 198]

- The matter and radiation density parameter combinations ω_m and ω_r are fixed to their Planck18/ΛCDM best fit value $\bar{\omega}_m = 0.1430 \pm 0.0011$ and $\bar{\omega}_r = (4.64 \pm 0.3)\ 10^{-5}$.

- The cosmological comoving distance to the recombination redshift

$$r(z_r, \omega_m, \omega_r, w(z)) = \int_0^{z_r} \frac{dz}{H(z)} = \int_{a_r}^{1} \frac{da'}{a'^2 H(a')} \tag{4.2}$$

  (a is the cosmic scale factor, $z_r \simeq 1091$ is the redshift of recombination) is fixed to the Planck18/ΛCDM best fit value $\bar{r} = (100\ km\ sec^{-1}\ Mpc^{-1})^{-1}(4.62 \pm 0.08)$.

- The Hubble parameter H_0 is fixed to its locally measured value H_0^{R20}.

then for the typical case of the CPL [see Eq. (2.13)] $H(z)$ deformation model we would have an $H(z)$ of the form

$$H(z) = H_0\sqrt{\Omega_{0m}(1+z)^3 + \Omega_{0r}(1+z)^4 + (1-\Omega_{0m}-\Omega_{0r})\,(1+z)^{3(1+w_0+w_1)}e^{-3\frac{w_1 z}{1+z}}} \tag{4.3}$$

while the corresponding constraint in the dark energy equation of state will be approximately expressed as [198]

$$w_{1h}(w_0) \simeq -4.17 w_0 - 5.08. \tag{4.4}$$

This equation defines a multitude of points in the $w_0 - w_{1h}$ parameter space that could claim to address the Hubble tension according to the theory described in Chapter 2. The above equation however is an approximation and as such more accurate values for the $w_{1h}(w_0)$ dependence could be found via the numerical solution of the equation $r(z_r, \bar{\omega}_m, \bar{\omega}_r, w(z)) = 4.62$. In the subsequent parts of this chapter, the latter will be the go to method of obtaining the $w_0 - w_1$ pairs we require, even though we will still refer to Eq. (4.4).

As we have mentioned in the start of this chapter the models that employ late deformations of $H(z)$ are susceptible to poor fits to local distance measurements at $z < 2$ by SnIa [22] and BAO [209–211] data. In the case that the asymptotic value of $w(z)$ at early times which in the CPL case is

$$w_\infty = w_0 + w_1 \tag{4.5}$$

increases to values $w_\infty > -0.5$ while the best possible fit to BAO-SnIa is obtained for $w_\infty \simeq -1.2$ the fit to these datasets becomes even worse. Far more worse than that of the Planck18/ΛCDM.

In the next parts we investigate the level of the S_8 tension and the growth of perturbations for the $H(z)$ deformations in questions, while assuming the validity of Eq. (4.4). In particular we compare the growth factor of these models with the corresponding growth factor of Planck18/ΛCDM and identify the tension level in the $\Omega_{0m} - \sigma_8$ parameter space between RSD growth data and Planck18/ΛCDM likelihoods contours.

4.1.1 Evolution of the Growth Factor of Cosmological Matter Perturbations

The evolution of the growth factor of cosmological matter perturbations $\delta(a) \equiv \frac{\delta\rho}{\rho}(a)$ in terms of the cosmic scale factor a is determined in sub-horizon scales by the equation [76, 155, 244–247]

$$\delta''(a) + \left(\frac{3}{a} + \frac{H'(a)}{H(a)}\right)\delta'(a) - \frac{3\Omega_{0m}}{2a^5 H(a)^2/H_0^2}\,\delta(a) = 0, \tag{4.6}$$

where the primes denote differentiation with respect to the scale factor a and $H(a) \equiv \frac{\dot{a}}{a}$ is the Hubble expansion rate. The initial conditions for the solution of Eq. (4.6) are usually taken deep in the matter era (*e.g.* for $a_i = 0.001$) where it is easy to show that $\delta(a_i) \sim a_i$. The growth factor $\delta(a)/\delta(a_i)$ indicated by this equation in the context of Planck18/ΛCDM best fit parameters is higher than the growth favored by dynamical probe data like weak lensing [85, 94, 248–253], cluster counts [32, 254–256] and redshift space distortions [75, 76, 111, 257, 258] at a $2-3\sigma$ level. This is known as the growth tension or $\Omega_{0m} - \sigma_8$ tension where σ_8 is defined as the matter density rms fluctuations within spheres of radius $8h^{-1}$ Mpc at the present time $z = 0$ and is connected with the amplitude of the primordial fluctuation spectrum. In particular the best fit value of the matter density parameter favored by Planck18/ΛCDM is higher than the value favored by the dynamical probes. This indicates that dynamical probes prefer a weaker growth of perturbations since the matter density parameter effectively 'drives' the growth of density perturbations.

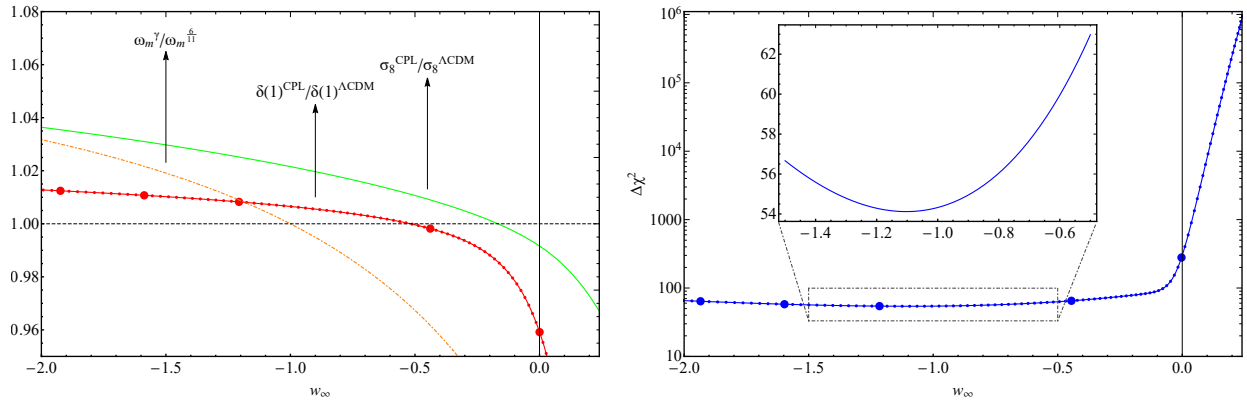

Figure 4.1: Left panel:The relative growth factor $\delta(1)^{CPL}/\delta(1)^{\Lambda CDM}$ (red line), the best fit ratio $\sigma_8^{CPL}/\sigma_8^{\Lambda CDM}$ (green line, fixed $\omega_m = 0.143$) and the ratio $\omega_m^\gamma/\omega_m^{\frac{6}{11}}$ (orange dot-dashed line) all have similar dependence on w_∞. The five thick dots correspond to the CPL parameter values (w_0, w_1) pairs, $(-1, -0.93)$, $(-1.1, -0.497)$, $(-1.22, 0)$, $(-1.5, 1.05)$ and $(-1.73, 1.72)$ of the five panels of Fig. 4.3 (the sixth corresponds to ΛCDM). Right panel: The quality of fit to the CMB shift parameters, Pantheon and BAO data compared to ΛCDM is significantly worse than ΛCDM for the CPL models that address the Hubble tension. In all cases $\Delta\chi^2 > 50$. The minimum ($\Delta\chi^2 \simeq 54$) occurs at about $w_\infty \simeq -1.2$ corresponding to wCDM. Adopted from Ref. [231].

A useful bias-free statistic probed by RSD data is the product $f\sigma_8$:

$$f\sigma_8(a) = \frac{\sigma_8}{\delta(a=1)}\; a\,\delta'(a, \Omega_{0m})\,, \tag{4.7}$$

where $f \equiv \frac{d\ln\delta}{d\ln a}$ is the growth rate of matter density perturbations. Notice that for a given measured value of $f\sigma_8(a)$, weaker growth (smaller $\delta(a=1)$) implies a lower value of σ_8 (assuming that $\delta'(a)$ does not change significantly for a given value of a). This is demonstrated in Fig. 4.1 where we show the properly normalized best fit value of σ_8 (green line) obtained by fitting the solution of Eq. (4.6) to the robust $f\sigma_8$ dataset of Ref. [76] [1] for various values of w_∞ under the assumption of $\omega_m = 0.143$, $h = 0.74$ and Eq. (4.4), conditions required for consistency of local measurements of H_0 and Planck18/ΛCDM anisotropy spectrum. Clearly $\sigma_8(w_\infty)/\sigma_8^{P18\Lambda}$ ($\sigma_8^{P18\Lambda}$ denotes the best fit value in the context of Planck18/ΛCDM) has the same monotonicity and differs by less than 2% from $\delta(1,w_\infty)/\delta(1)^{P18\Lambda}$ (red line) thus justifying that the best fit σ_8 and $\delta(a=1)$ are approximately proportional.

4.1.2 Approximate Analytic Solutions

An approximate solution to Eq. (4.6) can be found [259] by utilizing a growth index γ, which is used to parameterize the linear growing mode of models with time varying equations of state, such as Eq. (2.13). Using γ and ignoring the effects of radiation, the growth factor solution $\Delta(a) \equiv \frac{\delta(a=1)}{\delta(a_i)}$ of (4.6) may be approximated as [259, 260]

$$\Delta(a) = \exp\left[\int_{a_i}^{a} \frac{\Omega_m^\gamma(a')}{a'} da'\right] \tag{4.8}$$

where $\Delta(a)$ is the normalized growth factor $\delta(a)/\delta(a_i)$, $a_i = 0.001$ is an initial redshift deep in the matter era when $\delta(a) \sim a$ and

$$\Omega_m(a) \equiv \frac{\Omega_{0m} H_0^2 a^{-3}}{H(a)^2} = \frac{\omega_m\, a^{-3}}{h(a)^2} \tag{4.9}$$

with $h(a)^2 \equiv \omega_m a^{-3} + (h^2 - \omega_m) f_a(a)$ ($f_a(a)$ denotes the evolution of the dark energy density). The growth index is approximated by [259]

$$\gamma = \frac{6 - 3(1+w_\infty)}{11 - 6(1+w_\infty)}. \tag{4.10}$$

where w_∞ is defined in Eq. (4.5). For ΛCDM ($w = -1$) we have $\gamma = 6/11 \simeq 0.55$. From Eq. (4.8) it is easy to obtain the well known approximate expression for the growth rate $f(a)$ of density perturbations

$$f(a) \equiv \frac{d\ln\Delta}{d\ln a} \simeq \Omega_m(a)^\gamma \tag{4.11}$$

which may also be used as a definition of the growth index γ.

Using Eqs. (4.8), (4.9) it is easy to express the growth factor as

$$\Delta(a) = \frac{\delta(a)}{\delta(a_i)} = \exp\left[\omega_m^\gamma \int_{a_i}^{a} \frac{da'}{a'^{1+3\gamma}\, h(a')^{2\gamma}}\right] \tag{4.12}$$

Since $\gamma \in [0.45, 0.65]$ in most physically interesting cases, the integral in the exponential of Eq. (4.12) is very similar to the integral of the comoving distance (4.2) [260]. Since the dark

[1] This dataset is optimized for independence of datapoints but it involves significanty less datapoints than the more complete compilation of Ref. [208].

energy parameter values (*e.g.* pairs of $w_0 - w_1$ in the CPL case) that can address the Hubble tension have approximately fixed comoving distance to recombination they should also have approximately fixed growth integral in Eq. (4.12) for $a = 1$. Therefore, the growth factor $\Delta(a = 1)$ is expected to have approximately similar behavior as $\omega_m^{\gamma(w_\infty)}$. This is demonstrated in Fig. 4.1 where we show the growth factor $\delta(1)^{CPL}/\delta(1)^{P18\Lambda}$ as obtained by a numerical solution of Eq. (4.6) using the Planck18/ΛCDM best fit parameter values ($\delta(1)^{P18\Lambda}$) and the CPL parameter values (4.4) that address the Hubble problem ($\delta(1)^{CPL}$). In both case we fixed $\omega_m = 0.143$ for consistency with the CMB anisotropy spectrum while we set $h = 0.74$ for $\delta(1)^{CPL}$ and $h = 0.67$ for $\delta(1)^{P18\Lambda}$ in Eq. (4.6). Superimposed is the ratio $\omega_m^{\gamma(w_\infty)}/\omega_m^{\gamma(w_\infty=-1)}$ for $\omega_m = 0.143$ and $\gamma(w_\infty = -1) = \frac{6}{11}$ corresponding to the ΛCDM growth index. The two quantities ($\omega_m^{\gamma(w_\infty)}/\omega_m^{\gamma(w_\infty=-1)}$ and $\delta(1)^{CPL}/\delta(1)^{P18\Lambda}$) have similar monotonicities and differ by less than 4% in the range $w_\infty \in [-2, -0.5]$. This validates the approximation that the growth integral of Eq. (4.12) varies slowly with w_∞ when Eq. (4.4) is obeyed.

As shown in Fig. 4.1 (red curve) the $H(z)$ CPL deformations that can address the Hubble tension induce a growth factor that is larger than the one implied by a Planck18/ΛCDM background for all $w_\infty < -0.5$. This range of w_∞ includes all the values of parameters which are consistent with SnIa, BAO and CMB data. This is demonstrated in Fig. 4.1 (right panel) where we show the excess value of χ^2 with respect to Planck18/ΛCDM as a function of w_∞ using the Pantheon SnIa data along with a compilation of 9 BAO datapoints and two CMB effective distance/shift parameters [227]. Clearly, the best fit is obtained for $w_\infty \simeq -1.1 \pm 0.2$, while the value $w_\infty = -0.5$ is more than 3σ away from the best fit value.

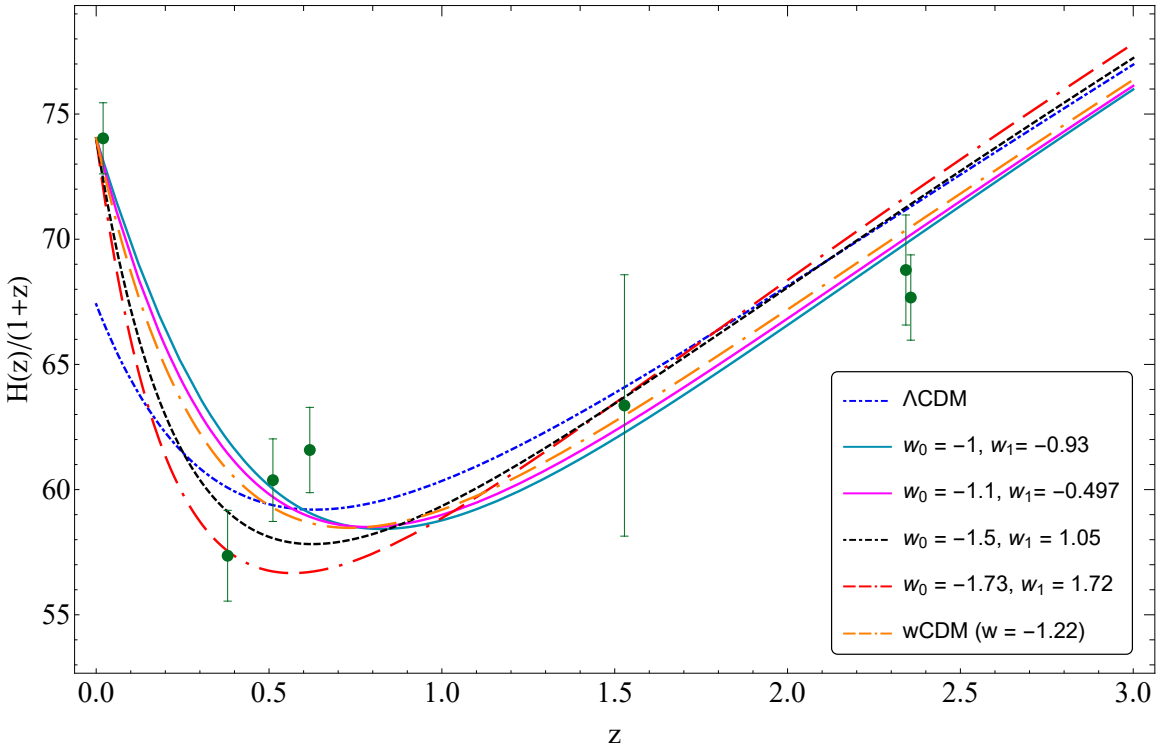

Figure 4.2: The Planck18/ΛCDM form of $H(z)/(1 + z)$ (blue dot-dashed line) is compared with the same function obtained with various pairs of CPL parameters that address the Hubble tension. Some BAO data are also shown. Adopted from Ref. [231].

The strong deformation of $H(z)$ implied by models with high values of w_∞ is also shown in

Fig. 4.2 where the Planck18/ΛCDM form of $H(z)/(1+z)$ (blue dot-dashed line) is compared with the same function obtained with various pairs of CPL parameters that address the Hubble tension. Clearly the strongest deformation at low z occurs for models with $w_\infty < -0.5$ which implies also inconsistency with BAO and SnIa data at redshifts of $O(1)$.

4.2 Numerical Fit Using $f\sigma_8$ Data

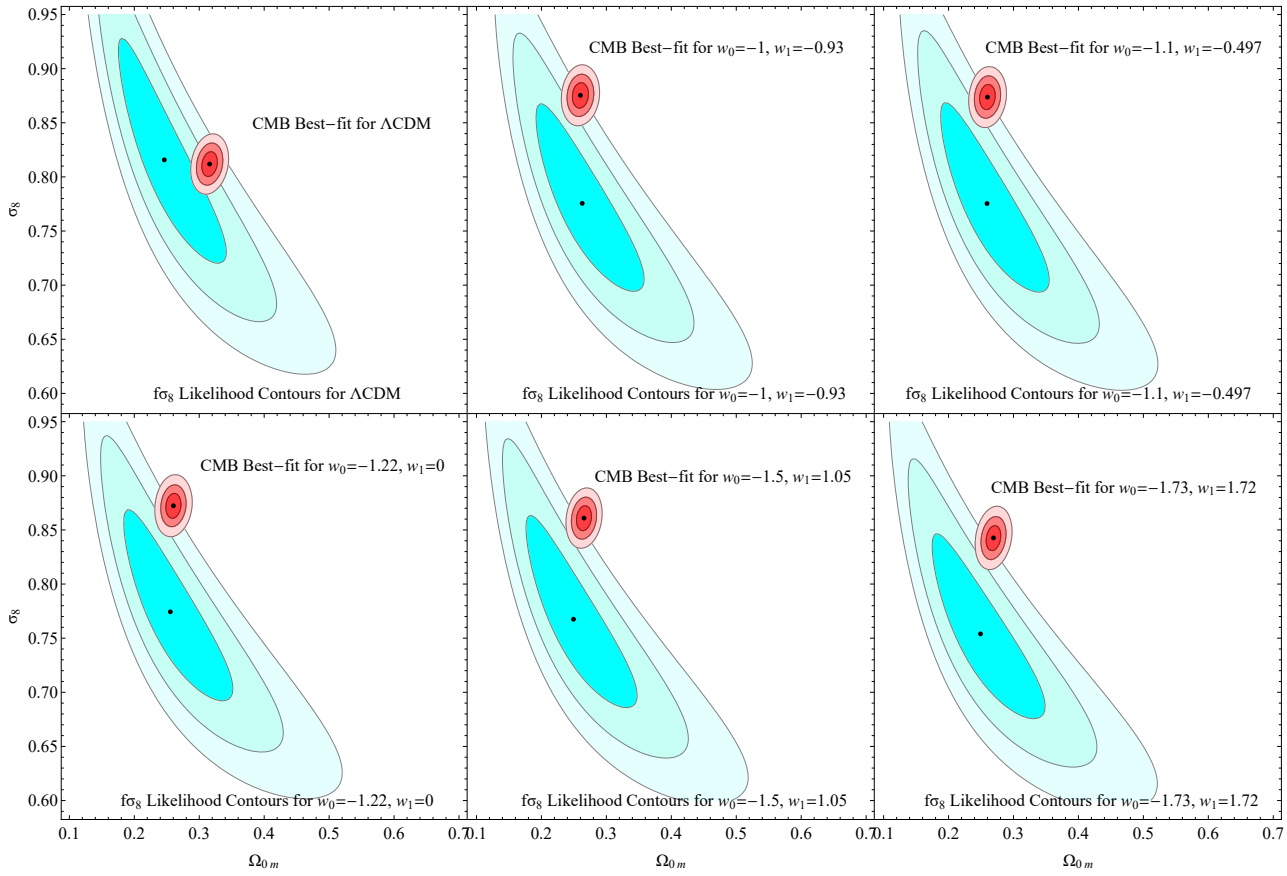

Figure 4.3: The cyan and the red contours correspond to the Growth and the Plank 18 CMB data respectively, for the ΛCDM and various (w_0, w_1) pairs of the CPL model. The $\Delta\sigma$ differences between the best fit values produced by the two contours in each case, are shown in Tab. 4.1. It is clear that the tension does not ease in the case of the CPL model despite the fact that it appears to solve the H_0 tension for the same w_0 and w_1 values used. Adopted from Ref. [231].

The increased tension level between CMB data and RSD growth data in the context of late time $H(z)$ deformations addressing the Hubble tension is demonstrated in Fig. 4.3 where we show the CMB data likelihood contours (Planck18 chains) in the parameter space $\Omega_{0m} - \sigma_8$ superimposed with the corresponding contours obtained from a robust compilation of RSD $f\sigma_8$ data [76, 207] for ΛCDM (upper left panel), and five CPL w_0, w_1 parameter pairs that can address the Hubble problem with $h = 0.74$. These five pairs (thick dots in Fig. 4.1) in addition to being disfavored by low z geometric probes (BAO and SnIa) by $\delta\chi^2 > 50$ (see Tab. 4.1), also lead to increased tension between CMB and growth data compared to ΛCDM as shown in

w_0	w_1	ΔM	$\Delta\chi^2$	$\Delta\sigma$
-1	0	-0.19	-	2
-1	-0.93	-0.02	63	2.9
-1.1	-0.50	-0.03	57	3.0
-1.22	0.0	-0.05	54	3.1
-1.50	1.05	-0.09	65	3.4
-1.73	1.72	-0.12	279	3.4

Table 4.1: The three problems of $H(z)$ deformations addressing the Hubble crisis (columns 1,2). Column 3: The deviation of the best fit value of the absolute magnitude M for each deformation, from the Cepheid calibrated value of Refs. [62, 226] shown in Fig. 4.4. Column 4: The $\Delta\chi^2$ differences with respect to Planck18/ΛCDM shown also in Fig. 4.1 (right panel) for each (w_0, w_1) pair that addresses the Hubble tension. Column 5: The $\Delta\sigma$ differences between the best fit values of the Growth and CMB data contours depicted in Fig. 4.3.

Fig. 4.3 and Tab. 4.1 even for parameter values where the growth factor is less than that of Planck18/ΛCDM (lower right panel corresponding to $w_\infty < -0.5$). In constructing Fig. 4.3 and Tab. 4.1 we have only fixed the parameters w_0, w_1 in each panel as indicated so that the Hubble tension is addressed (in the 5 panels) but have left free Ω_{0m} and σ_8 to be fitted by the data. Notice that in all panels the CMB data favor a value of $\omega_m \simeq 0.143$ as expected.

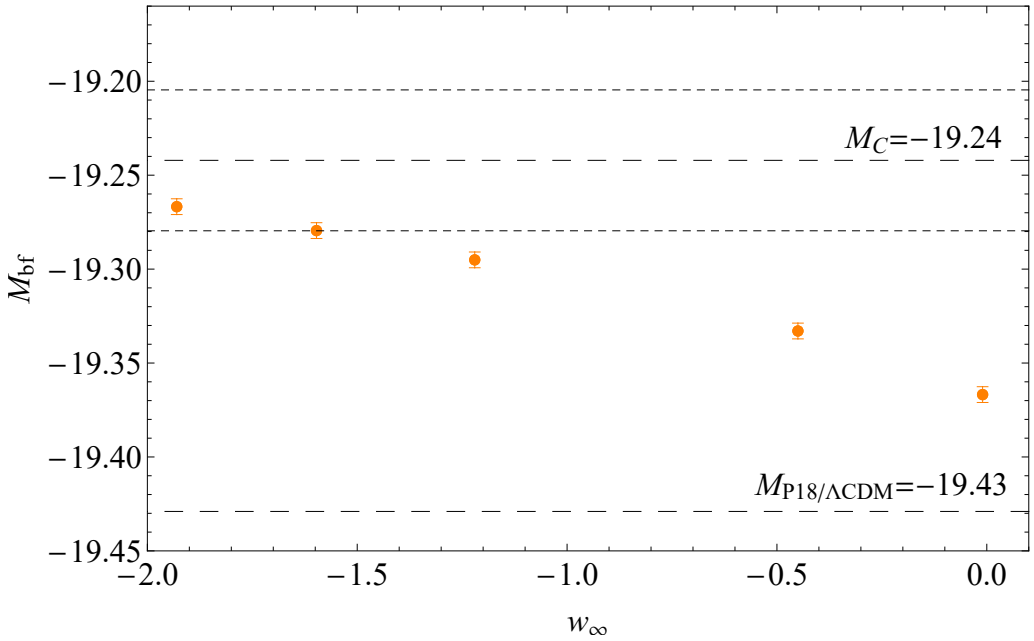

Figure 4.4: The best fit values of the absolute magnitude M, for the $(w_0, w1)$ pairs displayed in Tab. 4.1. These values are consistently lower than the corresponding value of M implied by local Cepheid calibrators (upper dashed line) even though this tension is not as large as for the best fit value of M obtained in the context of the standard Planck18/ΛCDM model (lower dashed line). Adopted from Ref. [231].

In addition to the reduced quality of fit to low z geometric probes and the increased growth tension, the $H(z)$ deformation models addressing the Hubble tension face another challenge:

They lead to a best fit value of the SnIa absolute magnitude M that is consistently lower than the corresponding value implied by the Cepheid calibrators at $z < 0.01$ $M = -19.24 \pm 0.04$. This difference is indicated in Fig. 4.4 and in Tab. 4.1. In Fig. 4.5 we show the values of the absolute magnitude in the context of a CPL model that attempts to address the H_0 tension with the use of an H_0 prior. It is clear that the mean value of these absolute magnitudes is in tension with the Cepheid calibrated M best fit (M_C), while the values themselves display a downwards evolution for $z > 0.1$ instead of being constant.

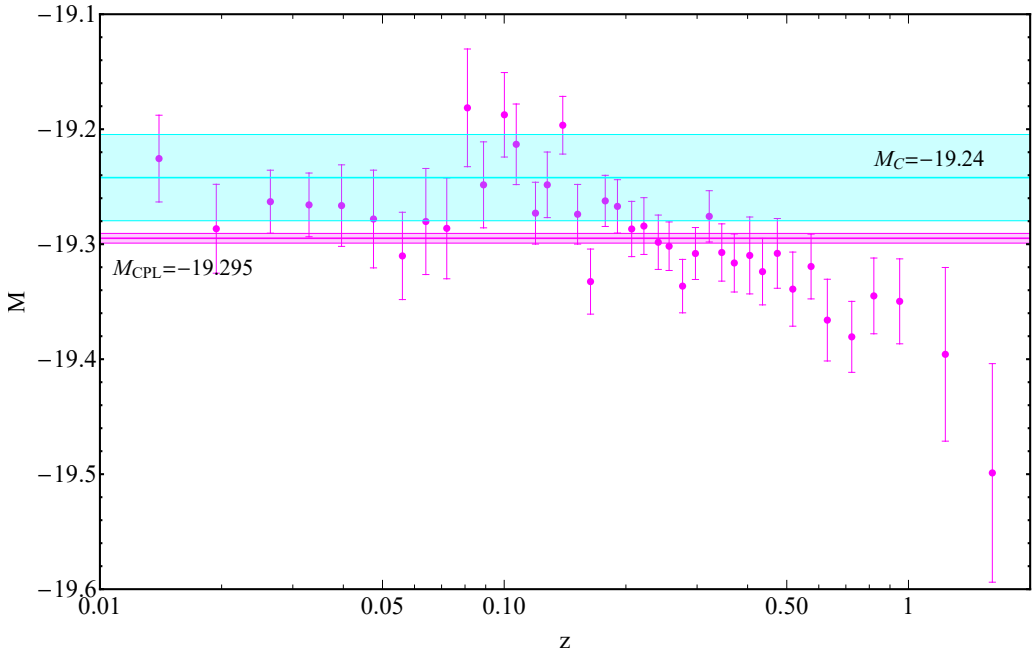

Figure 4.5: The values of the absolute magnitude corresponding to the binned SnIa data in the context of the CPL model $(w_0 = -1.22, w_1 = 0)$ that addresses the H_0 tension via an H_0 prior, shown to be in tension with the Cepheid calibrated M range. Adopted from Ref. [231].

4.3 In Brief

In this chapter we have demonstrated by analysing the typical CPL parameterization and subsequently generalizing our results to all the late time deformations of $H(z)$ that aim to superficially address the Hubble tension, that they consistently worsen the S_8 tension. This effect adds to the fact that they display a worse fit to low z geometric probes like SnIa and BAO data in comparison to Planck18/ΛCDM. Early time approaches to the Hubble tension also display similar issues as reported by Ref. [261]. Furthermore, we have considered the aspect of the M tension that is also discussed in the Chapter 3. To that end, we have shown that these models exhibit a tendency for lower best fit values of the SnIa absolute magnitude than the Cepheid calibrator one.

It may seem like a bold move to consider the CPL model as the quintessential paradigm in our study, and in fact this point has been made before in the literature [262, 263]. However, we still expect that the results presented in this chapter are general and generic for all similar parametrizations. That is because the issues of the generality of CPL become prevalent due to it being a linear expansion on w around the present and thus only being accurate around

the present as well. The aspect that ultimately makes the CPL a good representative of the smooth $H(z)$ deformation models is most eloquently shown in Fig. 5.3. With its help it is straightforward to see that the parameters that claim to solve the Hubble tension correspond to a wide range of shapes for $H(z)$.

In order to fully test our hypothesis we would need to consider a larger variety of cosmological data and a full MCMC analysis. That would mean the inclusion of the full CMB, the Pantheon and the growth data, as well as the BAO measurements. As we have said before, a similar analysis has been performed in [198] and described in Chapter 2. There we showed that the best-fit values of (w_0, w_1) that were produced, are approximately equal to those derived via the semi-analytic methodology. This was in the case where an an H_0 prior was implemented, alternatively we have demonstrated that the best fit values of (w_0, w_1) end up close to the Planck18/ΛCDM model. This effect most probably is due to the domination of the CMB - BAO data. Thus, such an MCMC extended analysis probably would require the inclusion of an H_0 prior along with the marginalization over other parameters demonstrating the growth tension level after such marginalization.

Concluding this chapter we are tempted to once again turn our attention to the $LwMT$ model that was proposed in the previous one. We remind the reader that this model is partially based on a rapid transition of SnIa absolute luminosity at $z \simeq 0.01$. This transition could be explained if one considers an equally rapid change of the value of the gravitational constant $G_{\rm eff}$ by about 10%. This type of ultra late time transition model has the advantages of fully resolving the Hubble tension while also simultaneously addressing the S_8 tension [227, 232] (two birds with one stone) and providing an equally good or even better fit to the low z data (BAO and SnIa) with the Planck18/ΛCDM model. Although this model is accompanied by w transition as well, it has been demonstrated that an M transition by itself (LMT model) would suffice. It is obvious that these models have very interesting theoretical implications with respect to fundamental physics and finally they are testable with the aid of upcoming data, especially those from standard sirens.

CHAPTER 5

Observational Hints for a Late M Transition

In this chapter we attempt to provide some observational support to the existence of a Late time $w - M$ transition $LwMT$ like the one postulated in Chapter 3. This type of model has the capabilities of resolving both the Hubble and S_8 tensions, while maintaining a quality of fit to the data equal to that of Planck18/ΛCDM. Therefore, we proceed by searching for observational indications of a sharp late transition in the SnIa absolute magnitude M, expressed in the form of an analogous gravitational constant transition.

Firstly, we have utilized an up-to-date compilation of galaxy data in order to probe for transitions in the evolution of the Baryonic Tully-Fisher (BTFR) relation [264]. As we will demonstrate in greater detail below, we find hints for a transition in the BTFR evolution at two citical distances, $D_c \simeq 9$ Mpc and $D_c \simeq 17$ Mpc, at an $\approx 3\sigma$ level of confidence. In brief this analysis was conducted by splitting the entire dataset in two subsets, according to the measured galaxy distance with respect to splitting distance D_c, and then proceeding to calculate the likelihood of the best-fit slope and intercept of one subset with respect to the best-fit corresponding values of the other subset. We have also demonstrated that these results are robust and not subject to major random systematic and statistical variations of the galactic distance data. The latter was shown with the help of a homogeneous mock dataset that was created using Monte Carlo simulations, and did not produce any discontinuities in the evolution of the BTFR.

Secondly, we attempted to impose constrains on the gravitational transition that would correspond to a transition in the Absolute Magnitude M [265]. To that effect we used two robust low-z redshift survey datasets ($z < 0.01$), taken from the Six-degree Field Galaxy Survey (6dFGS) as well as the 2MASS Redshift Survey (2MRS). Our goal was to observe and constrain a peak in the distribution of galaxies, as such an effect would be, among else, indicative of an ultra late-time gravitational transition. As we will demonstrate further on, we observed such a feature near a distance of approximately 20 Mpc, however this could be attributed to alternative causes such as the coherent peculiar velocities of galaxies or galactic density fluctuations. Thus a conclusion was reached that although a gravitational transition cannot be thoroughly constrained, it remains plausible and cannot be excluded by redshift survey data at $z < 0.01$.

5.1 Searching for Hints of a Gravitational Transition in Tully-Fisher Data

5.1.1 The Baryonic Tully-Fisher Relation as a Probe of Gravitational Dynamics

The classic Tully-Fisher relation (TFR) [266] is an empirical relation that has been proposed to serve as a connection between the observed maximum velocity v_{rot} of spiral galaxies in the rotation curve and their intrinsic optical luminosity L. It has the following form,

$$L = Av_{rot}^{s} \tag{5.1}$$

where $s \simeq 4$ is the slope in a logarithmic plot of (5.1), A is a constant and ($log(A)$ is the zero point or intercept). The constants s and A have a very weak dependence on galactic properties such as the mass to light ratio, the galactic profiles, the observed surface brightness, HI gas content, size, *etc.* [267]. They depend, however, on the fundamental properties of gravitational interactions.

The Baryonic Tully-Fisher relation (BTFR), on the other hand, is very similar to Eq. (5.1) but it differentiates by connecting the galaxies rotation velocity with their total baryonic mass (the sum of mass in stars and HI gas) M_B. This connection takes the form,

$$M_B = A_B v_{rot}^{s} \tag{5.2}$$

where $A_B \simeq 50 M_\odot$ km^{-4} s^4 [268]. This more generalized Tully-Fisher relation benefits significantly from including gas-rich dwarf galaxies that appear in groups and have stellar masses below $10^9 M_\odot$.

We can derive the the BTFR relation if we consider a star in a circular orbit of radius R around a galactic mass M rotating with velocity v [269]. Then, we can show that,

$$v^2 = G_{\text{eff}} M/R \implies v^4 = (G_{\text{eff}} M/R)^2 \sim M\ S\ G_{\text{eff}}^2 \tag{5.3}$$

where G_{eff} is the effective Newton's constant involved in gravitational interactions and S the surface density $S \equiv M/R^2$, which is expected to be constant [270]. Moving on, from Eqs. (5.2) and (5.3), the following is anticipated:

$$A_B \sim G_{\text{eff}}^{-2} S^{-1} \tag{5.4}$$

Therefore, the BTFR can, in principle, probe both galaxy formation dynamics (through, *e.g.* S) and possible fundamental constant dynamics (through G_{eff}). An interesting feature of the BTFR is that despite the above heuristic derivation, it appears to be robust, even in cases when the galaxy sample includes low S and/or varying S galaxies [271, 272]. In fact, no other parameter appears to be significant in the BTFR.

The BTFR has been shown to have lower scatter [267, 273, 274] than the classic stellar TFR and also to be applicable for galaxies with stellar masses lower than $10^9 M_\odot$. It is also more robust than the classic TFR [275–278] since the parameters A_B (intercept) and s (slope) are very weakly dependent on galactic properties, such as size and surface brightness [267]. The low scatter of the BTFR and its robustness make it useful as a distance indicator for

Method	$\left\|\frac{\Delta G_{\rm eff}}{G_{\rm eff}}\right\|_{max}$	$\left\|\frac{\dot{G}_{\rm eff}}{G_{\rm eff}}\right\|_{max}$ (yr^{-1})	time scale (yr)	References
Lunar ranging		1.47×10^{-13}	24	[280]
Solar system		4.6×10^{-14}	50	[281, 282]
Pulsar timing		3.1×10^{-12}	1.5	[283]
Strong Lensing		10^{-2}	0.6	[284]
Orbits of binary pulsar		1.0×10^{-12}	22	[285]
Ephemeris of Mercury		4×10^{-14}	7	[286]
Exoplanetary motion		10^{-6}	4	[287]
Hubble diagram SnIa	0.1	1×10^{-11}	$\sim 10^8$	[288]
Pulsating white-dwarfs		1.8×10^{-10}	0	[289]
Viking lander ranging		4×10^{-12}	6	[290]
Helioseismology		1.6×10^{-12}	4×10^9	[291]
Gravitational waves	8	5×10^{-8}	1.3×10^8	[292]
Paleontology	0.1	2×10^{-11}	4×10^9	[293]
Globular clusters		35×10^{-12}	$\sim 10^{10}$	[294]
Binary pulsar masses		4.8×10^{-12}	$\sim 10^{10}$	[295]
Gravitochemical heating		4×10^{-12}	$\sim 10^8$	[296]
Strong lensing		3×10^{-1}	$\sim 10^{10}$	[284]
Big Bang Nucleosynthesis *	0.05	4.5×10^{-12}	1.4×10^{10}	[297]
Anisotropies in CMB *	0.095	1.75×10^{-12}	1.4×10^{10}	[298]

Table 5.1: Solar system, astrophysical and cosmological constraints on the evolution of the gravitational constant. Methods with star (∗) constrain G_N while the rest constrain $G_{\rm eff}$. The latest and strongest constraints are shown for each method.

the measurement of the Hubble constant H_0. A calibration of the BTFR using Cepheid and TRGB distances leads to a value of $H_0 = 75 \pm 3.8$ km s^{-1} Mpc^{-1} [48].

The weak evolution and scatter of the BTFR can be used as a probe of galaxy formation models as well as a probe of possible transitions of fundamental properties of gravitational dynamics since the zero point constant A_B is inversely proportional to the square of the gravitational constant G. Previous studies investigating the evolution of the best-fit zero point $log\ A_B$ and slope s of the BTFR have found a mildly high z evolution of the zero point from $z \simeq 0.9$ to $z \simeq 2.3$ [279], which was attributed to the galactic evolution inducing a lower gas fraction at low redshifts after comparing with the corresponding evolution of the stellar TFR (STFR), which ignores the contribution of gas in the galactic masses.

Ref. [279] and other similar studies assumed a fixed strength of fundamental gravitational interactions and made no attempt to search for sharp features in the evolution of the zero point. In addition, they focused on the comparison of high redshift with low redshift effects without searching for possible transitions within the low z spiral galaxy data. Such transitions, if present, would be washed out and hidden from these studies, due to averaging effects. In the present analysis, we search for transition effects in the BTFR at $z \lesssim 0.01$ (distances $D \lesssim 40$ Mpc), which may be due to either astrophysical mechanisms or to a rapid transition in the strength of the gravitational interactions $G_{\rm eff}$, due to fundamental physics.

In many modified gravity theories, including scalar tensor theories, the strength of gravitational interactions $G_{\rm eff}$ measured in Cavendish-type experiments measuring force F be-

tween masses ($F = G_{\rm eff}\frac{m_1\, m_2}{r^2}$), is distinct from the Planck mass corresponding to G_N that determines the cosmological background expansion rate ($H^2 = \frac{8\pi G_N}{3}\rho_{tot}$).

For example, in scalar tensor theories involving a scalar field ϕ and a non-minimal coupling $F(\phi)$ of the scalar field to the Ricci scalar in the Lagrangian, the gravitational interaction strength is as follows [299]:

$$G_{\rm eff} = \frac{1}{F}\frac{2F + 4F_{,\phi}^2}{2F + 3F_{,\phi}^2} \tag{5.5}$$

while the Planck mass related G_N is as follows:

$$G_N = \frac{1}{F} \tag{5.6}$$

Most current astrophysical and cosmological constraints on Newton's constant constrain the time derivative of $G_{\rm eff}$ at specific times, assume a smooth power-law evolution of $G_{\rm eff}$, or constrain changes of the Planck mass–related G_N instead of $G_{\rm eff}$ (CMB and nucleosynthesis constraints [297]. Therefore, these studies are less sensitive in the detection of rapid transitions of $G_{\rm eff}$ at low z.

The current constraints on the evolution of $G_{\rm eff}$ and G_N are summarized in Table 5.1, where we review the experimental constraints from local and cosmological time scales on the time variation of the gravitational constant. The methods are based on very diverse physics, and the resulting upper bounds differ by several orders of magnitude. Most constraints are obtained from systems in which gravity is non-negligible, such as the motion of the bodies of the solar system, and the astrophysical and cosmological systems. They are mainly related in the comparison of a gravitational time scale, *e.g.* period of orbits, with a non-gravitational time scale. One can distinguish between two types of constraints, from observations on cosmological scales and on local (inner galactic or astrophysical) scales. The strongest constraints to date come from lunar ranging experiments.

In the first column of Table 5.1, we list the used method. The second column contains the upper bound $\left|\frac{\Delta G}{G}\right|_{max}$ of the fractional change of G during the corresponding timescale. Most of these bounds assume a smooth evolution of G. In the third column, we present the upper bound on the normalized time derivative $\left|\frac{\dot{G}}{G}\right|_{max}$. The fourth column is an approximate time scale over which each experiment is averaging each variation, and the fifth column refers to the corresponding study where the bound appears. Entries with a star ($*$) indicate constraints on G_N, while the rest of the constraints refer to the gravitational interaction constant $G_{\rm eff}$.

In this chapter, we will partially focus on the search for a transition of the BTFR best-fit parameter values (intercept and slope) between data subsamples at low and high distances. We consider sample dividing distances $D_c \in [2, 60]\,\mathrm{Mpc}$, using a robust BTFR dataset [277, 300–302], which consists of 118 carefully selected BTFR datapoints, providing distance, rotation velocity baryonic mass (D, V_f, M_B) as well as other observables with their 1σ errorbars. We focus on the gravitational strength Newton constant $G_{\rm eff}$ and address the following questions:

- Are there hints for a transition in the evolution of the BTFR?
- What constraints can be imposed on a possible $G_{\rm eff}$ transition, using BTFR data?
- Are these constraints consistent with the level of $G_{\rm eff}$ required to address the Hubble tension?

5.1.2 Transitions in the Evolution of the BTFR

The logarithmic form of the BTFR (Eq. (5.2)) is as follows:

$$y = \log M_B = s \log v_{rot} + \log A_B \equiv s\, x + b \tag{5.7}$$

and a similar form for the TFR. Due to Eq. (5.4), the intercept $b \equiv \log A_B$ depends on both the galaxy formation mechanisms through the surface density S and on the strength of gravitational interactions through $G_{\rm eff}$.

A controversial issue in the literature is the type of possible evolution of the slope and intercept of the TFR and the BTFR. Most studies have searched for possible evolution in high redshifts (redshift range $z \in [0, 3]$) with controversial results. For example, several studies found no statistically significant evolution of the intercept of the TFR up to redshifts of $z \sim 1.7$ [303–309], while other studies found a negative evolution of the intercept up to redshift $z \simeq 3$ [310–317]. Similar controversial results in high z appeared for the BTFR, where [311] found no significant evolution of the intercept since $z \simeq 0.6$, while [315] found a positive evolution of the intercept between low-z galaxies and a $z \simeq 2$ sample. In addition, cosmological simulations of disc galaxy formation based on cosmological N-body/hydrodynamical simulations have indicated no evolution of the TFR based on stellar masses in the range $z \in [0.1]$ [318], indicating also that any observed evolution of the TFR is an artifact of the luminosity evolution.

These studies have focused mainly on comparing high-z with low-z samples, making no attempt to scan low redshift samples for abrupt transitions of the intercept and slope. Such transitions would be hard to explain in the context of known galaxy formation mechanisms but are well motivated in the context of fundamental gravitational constant transitions, which may be used to address the Hubble tension [227, 232]. Thus, in this section, we attempt to fill this gap in the literature.

We consider the BTFR dataset shown in Appendix A.2 based on the data from [277, 300–302] of the flat rotation velocity of galaxies vs the baryonic mass (stars plus gas) consisting of 118 datapoints, shown in Table A.4. The sample is restricted to those objects for which both quantities are measured to better than 20% accuracy and includes galaxies in the approximate distance range $D \in [1, 130]\,{\rm Mpc}$. This is a robust low z dataset ($z < 0.1$) with low scatter showing no evolution of velocity residuals as a function of the central surface density of the stellar disks.

Our analysis is distinct from previous studies in two aspects:

- We use an exclusively low z sample to search for BTFR evolution.
- We focus on a particular type of evolution: *sharp transitions of the intercept and slope*.

In this context, we use the dataset shown in Table A.4 of Appendix A.2 [277, 300–302], consisting of the distance D, the logarithm of the baryonic mass $\log M_B$ and the logarithm of the asymptotically flat rotation velocity $\log v_{rot}$ of 118 galaxies along with 1σ errors. We fix a critical distance D_c and split this sample in two subsamples Σ_1 (galaxies with $D < D_c$) and Σ_2 (galaxies with $D > D_c$). For each subsample, we use the maximum likelihood method [319] and perform a linear fit to the data setting $y_i = \log(M_B)_i$, $x_i = \log(v_{rot})_i$, while the parameters to fit are the slope s and the intercept b of Eq. (5.7). Thus, for each sample j ($j = 0, 1, 2$ with

$j = 0$ corresponding to the full sample and $j = 1, 2$ corresponding to the two subsamples Σ_1 and Σ_2), we minimize the following:

$$\chi^2_j(s, b) = \sum_{i=1}^{N_j} \frac{[y_i - (s_j\ x_i + b_j)]^2}{s_j^2 \sigma_{xi}^2 + \sigma_{yi}^2 + \sigma_s^2} \tag{5.8}$$

with respect to the slope s_j and intercept b_j. We fix the scatter to $\sigma_s = 0.077$, obtained by demanding that $\frac{\chi^2_{0,min}}{N_0} = 1$, where $\chi^2_{0,min}$ is the minimized value of χ^2 for the full sample and N_0 is the number of datapoints of the full sample. We thus find the best fit values of the parameters s_j and b_j, ($j = 0, 1, 2$) and also construct the $1\sigma - 3\sigma$ likelihood contours in the $s - b$ parameter space for each sample (full, Σ_1 and Σ_2) for a given value of D_c. We then evaluate the $\Delta\chi^2_{kl}(D_c)$ of the best fit of each subsample k, best fit with respect to the likelihood contours of the other subsample l. Using these values, we also evaluate the σ-distances ($d_{\sigma,kl}(D_c)$ and $d_{\sigma,lk}(D_c)$) and conservatively define the minimum of these σ-distances as follows:

$$d_\sigma(D_c) \equiv Min\left[d_{\sigma,12}(D_c), d_{\sigma,21}(D_c)\right] \tag{5.9}$$

For example, for the σ-distance of the best fit of Σ_1 with respect to the likelihood contours of Σ_2, we have the following:

$$\Delta\chi^2_{12}(D_c) \equiv \chi^2_2(s_1, b_1)(D_c) - \chi^2_{2,min}(s_2, b_2)(D_c) \tag{5.10}$$

and $d_{\sigma,12}$ is obtained as a solution of the following equation [319]:

$$\Delta\chi^2_{12} = 2\ Q^{-1}\left[\frac{M}{2}, 1 - \mathrm{Erf}(\frac{d_{\sigma,12}}{\sqrt{2}})\right] \tag{5.11}$$

where Q^{-1} is the inverse regularized incomplete Gamma function, M is the number of parameters to fit ($M = 2$ in our case) and Erf is the error function.

Fig.5.1 shows the σ distance $d_\sigma(D_c)$ in the parameter space (b, s) as a function of the split sample distance D_c. There are two peaks indicating larger than 3σ difference between the two subsamples at $D_c = 9$ Mpc and $D_c = 17$ Mpc. In addition, a transition of the σ distance $d_\sigma(D_c)$ at $D_c \simeq 20$ Mpc is apparent. This Monte Carlo simulation is used to construct Fig. 5.2 (right panel green line range), where we show the mean and standard deviation range of the σ-distances obtained by the above-described 100 Monte Carlo samples. Clearly, the random variation in the galactic distances cannot change the qualitative features (high double peak at low D_c) of Fig. 5.1 corresponding to the real sample. The σ-distances obtained from such a typical Monte Carlo sample is shown in Fig. 5.2 (left panel green line).

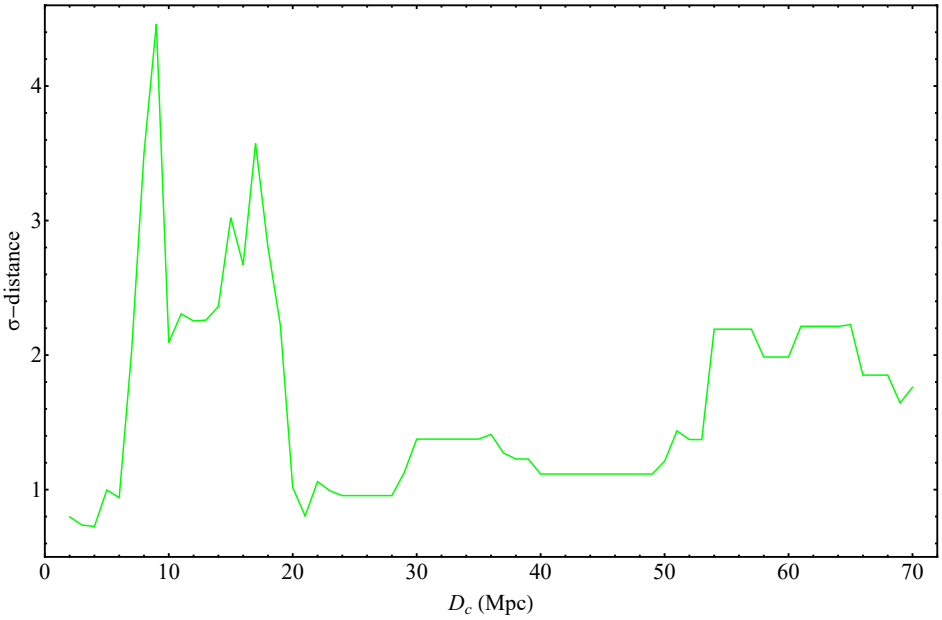

Figure 5.1: The σ-distance between the various Σ_1 and Σ_2 datasets as a function of the split distances D_c. There are 2 clear peaks at $D_c = 9$ Mpc and $D_c = 17$ Mpc and a transition seems to have been completed at $D_c \simeq 20\,\mathrm{Mpc}$. The anticipated plot would be a σ-distance that consistently varies in the range up to about 2σ for all values of D_c. The observed peaks indicate either the presence of systematics or the presence of interesting physics. Adopted from Ref. [264].

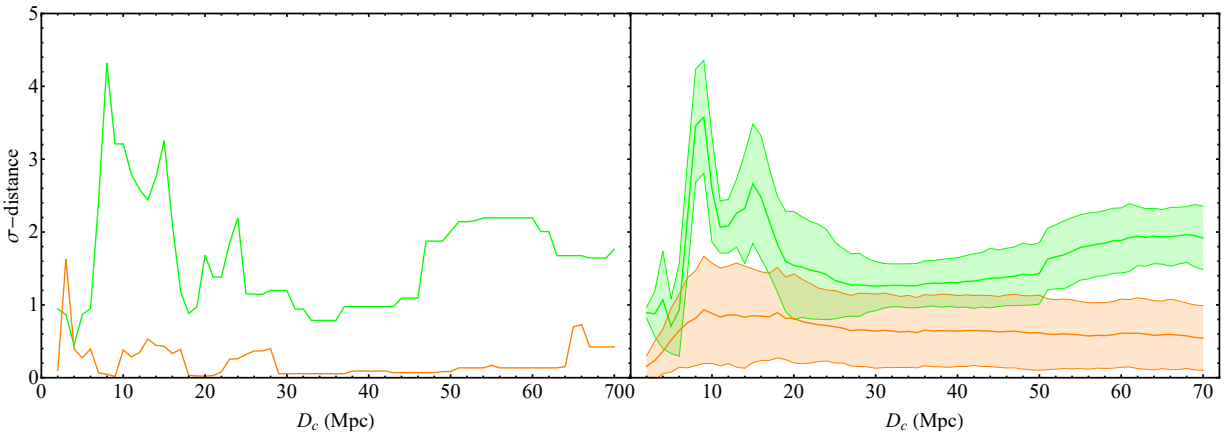

Figure 5.2: **Left panel**: The σ-distances as a function of the split distances D_c for a sample dataset with random distance values, normally distributed inside their individual $1-\sigma$ range (green line), versus the σ-distances as a function of the split distances D_c for a homogeneous Monte Carlo sample constructed using the best-fit BTFR (orange line). **Right panel**: The 68% range of the σ-distances versus the split distances D_c produced by a Monte Carlo simulation of 100 sample datasets obtained by randomly varying galaxy distance values with a Gaussian probability distribution (green band). Superimposed is the 68% range of the σ-distances versus the split distances D_c obtained from 100 homogeneous Monte Carlo samples constructed using the best-fit BTFR (orange band). Evidently, the characteristic two-peak form of the plot remains practically unchanged, even after the random variation in the distances (green band), whereas no significant tension is present in the case of the homogeneous Monte Carlo samples for any value of D_c (orange band). Adopted from Ref. [264].

D_c (Mpc)	intercept	slope	$\Delta\chi^2_{min}$
-	2.287 ± 0.18	3.7 ± 0.08	-
<9	2.461 ± 0.407	3.586 ± 0.216	$23.7\ (4.5\sigma)$
>9	2.854 ± 0.379	3.46 ± 0.204	$23.7\ (4.5\sigma)$
<17	2.467 ± 0.38	3.592 ± 0.17	$17.0\ (3.7\sigma)$
>17	2.677 ± 0.368	3.548 ± 0.166	$17.0\ (3.7\sigma)$
<40	2.327 ± 0.987	3.681 ± 0.419	$2.9\ (1.2\sigma)$
>40	3.318 ± 0.816	3.283 ± 0.349	$2.9\ (1.2\sigma)$

Table 5.2: The best-fit values of the intercept and slope parameters corresponding to the likelihood contours of Fig.5.3 alongside with their 1σ errors. The minimum $\Delta\chi^2$ between the best fits of the two samples is also shown. The corresponding σ-tension in parenthesis is obtained in the context of two free parameters from Eq. (5.11). Notice that, even though the parameter values appear to be consistent, the value of $\Delta\chi^2$ between the subsamples reveals the tension at $D_c = 9\,\mathrm{Mpc}$ and $D_c = 17$ Mpc.

The typical qualitative feature of $d_\sigma(D_c)$ corresponding to the real sample disappears if we homogenize the sample by randomizing both the velocities and the galactic masses, using the measured values of the velocities and the estimated values of the galactic masses in the context of the best-fit BTFR. In order to construct such a homogenized BTFR sample from the real sample, we use the following steps:

- We assign to each galaxy a randomly chosen distance obtained from a Gaussian distribution with mean equal to the measured distance and standard deviation equal to the 1σ error of the measured distance.
- We assign to each galaxy a randomly chosen $logv_{rot}$ obtained from a Gaussian distribution with mean equal to the measured $logv_{rot}$ and standard deviation equal to the 1σ error of the measured $logv_{rot}$.
- For each galaxy, we use the random $logv_{rot}$ obtained in the previous step to calculate the corresponding BTFR $logM_B$, using the best-fit slope and intercept of the real full dataset (first row of Table 5.2). We then obtain a random $logM_B$ for each galaxy from a Gaussian distribution with mean equal to the BTFR calculated $logM_B$ and standard deviation equal to the 1σ error of the measured $logM_B$.
- We repeat the above process 100 times, thereby generating 100 homogeneous Monte Carlo samples (HMCS) based on the SPARC dataset.
- For each HMCS, we find the σ distances $d_\sigma(D_c)$ and for each D_c, we find the mean σ distance and its standard deviation over the 100 HMCS. We thus construct the orange region in Fig. 5.2 (right panel). A typical form of $d_\sigma(D_c)$ is shown as the orange line of Fig. 5.2 (left panel) selected from the 100 HMCS.

Clearly, the forms of $d_\sigma(D_c)$ generated from the homogenized Monte Carlo samples have the expected property to be confined mainly between 0σ and 2σ in contrast to the real measured sample, where $d_\sigma(D_c)$ extends up to 4σ or more. Thus, the real dataset is statistically distinct from a homogeneous BTFR dataset.

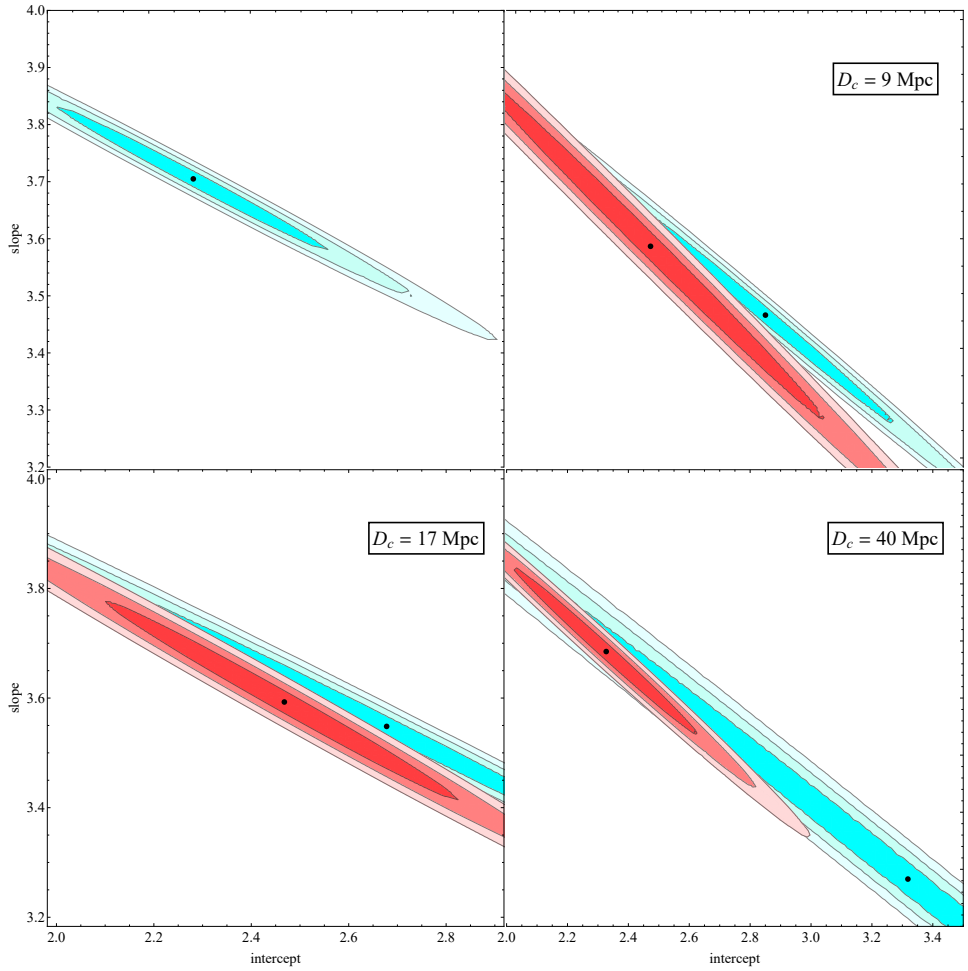

Figure 5.3: The best-fit contours of the slope and intercept for the entire dataset, as well for 3 different cases of split distance (D_c). The red contours correspond to the dataset with galaxies that have a distance below D_c, whereas the cyan contours correspond to galaxies with distances above D_c. Adopted from Ref. [264].

The two maxima of d_σ are more clearly illustrated in Fig. 5.3, where the likelihood contours are shown in the parameter space s (slope)-b (intercept) for the full sample (upper left panel) and for three pairs of subsamples Σ_i, including those corresponding to the peaks shown in Fig. 5.1 ($D_c = 17$ and $D_c = 9$). For both d_σ maxima, the tension between the two best-fit points is mainly due to the different intercepts, while the values of the slope are very similar for the two subsamples. In contrast, for $D_c = 40\,\mathrm{Mpc}$, where the σ distance is much lower (about 1σ, lower right panel), both the slope and the intercept differ significantly in magnitude but the statistical significance of this difference is low. Notice that the use of different statistics, such as the 1σ range of the best-fit intercept and slope shown in Table 5.2, or the level of likelihood contour overlap in Fig. 5.3 would not reveal the tension between far and nearby subsamples. In contrast, the σ-distance statistic demonstrates the effect and the Monte Carlo results of Fig. 5.2 verify the fact that such a large σ-distance would be rare in the context of a homogeneous sample.

The statistical significance of the different Tully-Fisher properties between near and far galaxies, which abruptly disappears for dividing distance $D_c \gtrsim 20$ Mpc, could be an unlikely

statistical fluctuation, a hint for systematics in the Tully-Fisher data[1], an indication for an abrupt change in the galaxy evolution or a hint for a transition in the values of fundamental constants and, in particular, the strength of gravitational interactions $G_{\rm eff}$. The best-fit values of the intercept and the slope for the cases shown in Fig. 5.3 are displayed in Table 5.2 along with their 1σ errors.

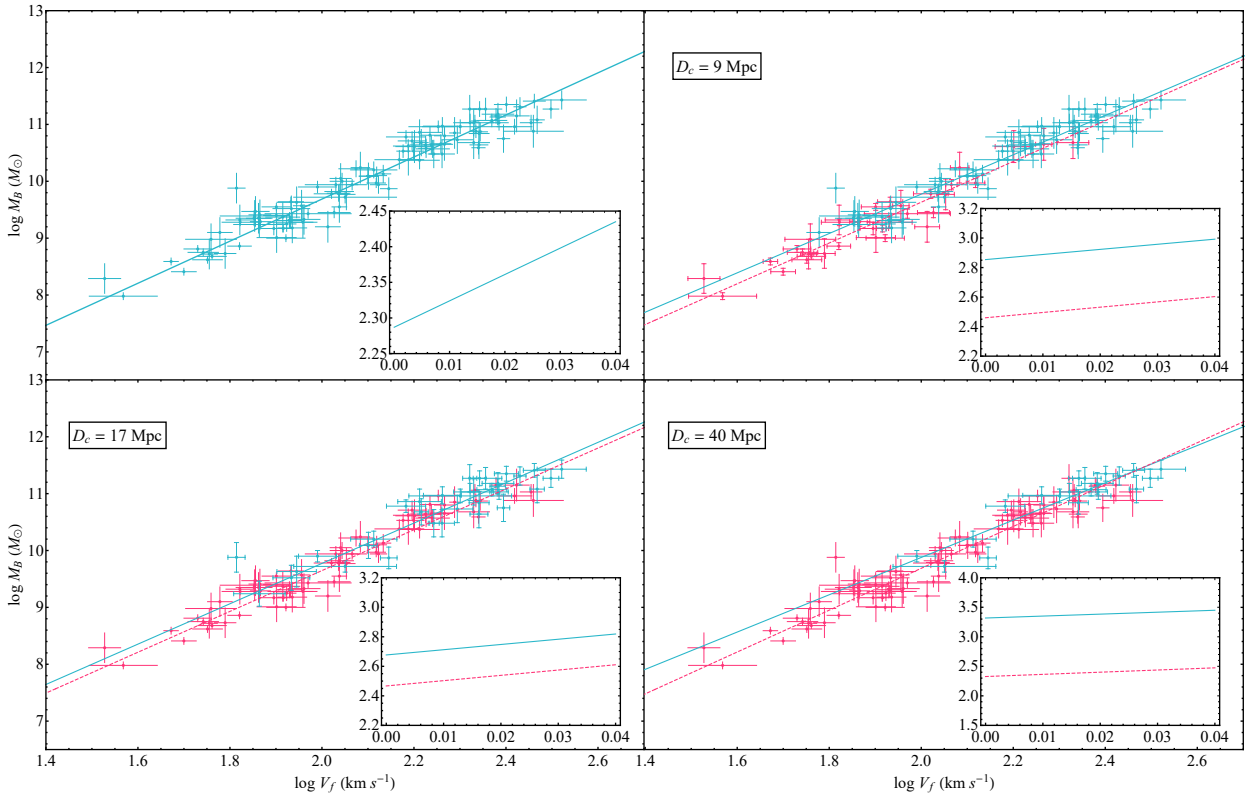

Figure 5.4: The best-fit lines corresponding to the best fit slope and intercept parameters of the whole galaxy dataset as well as each of the 2 datasets produced for 4 different split distances (D_c). The red dashed line and datapoints correspond to the data below D_c, and the cyan ones belong to the data over D_c for each case. Adopted from Ref. [264].

The best-fit $\log M_B - \log v_{rot}$ lines corresponding to Eq. (5.7) for the near–far galactic subsamples are shown in Fig. 5.4, superimposed with the datapoints (red/blue correspond to near/far galaxies). The full dataset corresponds to the upper-left panel. The difference between the two lines for $D_c = 9\,{\rm Mpc}$ and $D_c = 17\,{\rm Mpc}$ is evident, even though their slopes are very similar. The statistical significance of this difference disappears for larger values of the splitting distance (*e.g.* $D_c = 40\,{\rm Mpc}$), even though the slopes of the two lines become significantly different in this case.

The Hubble diagram of the considered dataset along with the best-fit line (black dot-dashed line) and the Hubble blue dashed line ($z \approx \frac{D}{c} H_0$) corresponding to $H_0 = 73\,{\rm km\ s^{-1}\ Mpc^{-1}}$ is shown in Fig.5.5. The distances to galaxies beyond 20 Mpc are determined using the Hubble flow with $H_0 = 73$ km/sec Mpc, and thus, there is no effect of their peculiar

[1]A possible source of systematics is the Malmquist bias, which would imply that the detected more distant galaxies are also more massive and may, therefore, display different slopes and intercepts in different mass bins [320, 321].

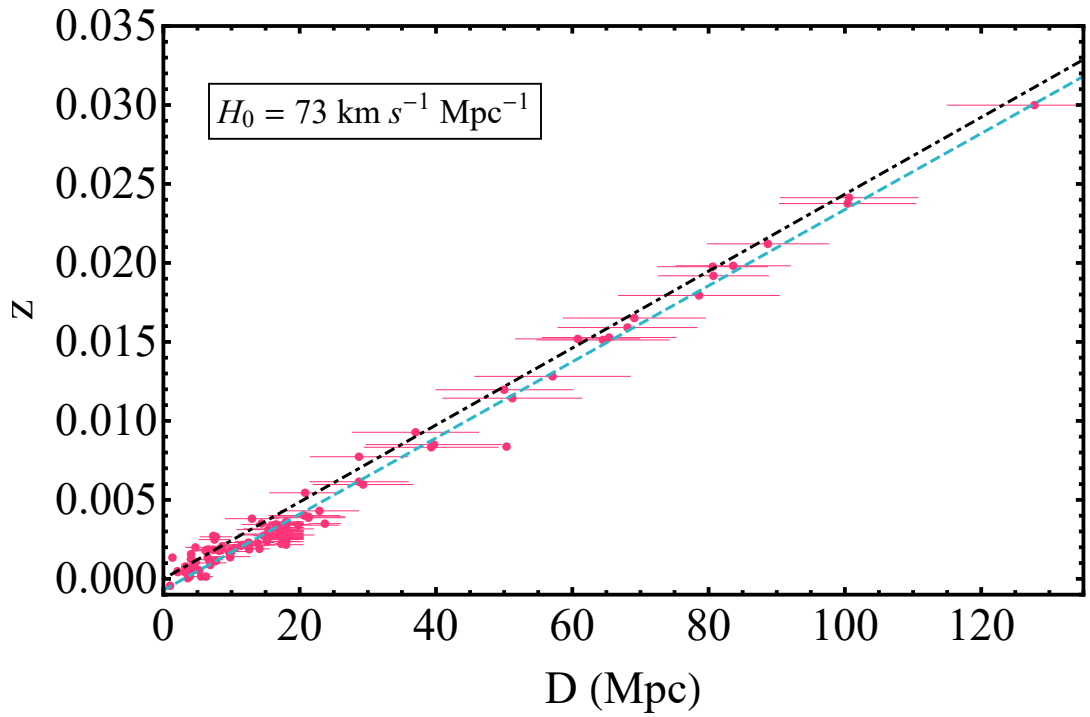

Figure 5.5: The distances alongside their errorbars versus the redshifts of each galaxy in our compilation. The blue dashed line corresponds to the best fit line, and the black dot-dashed one is produced by Eq. (5.1.2) for $H_0 = 73$ km s^{-1} Mpc^{-1}. Adopted from Ref. [264].

velocities. Galaxies closer than about $D \simeq 20\,\mathrm{Mpc}$ are clearly not in the Hubble flow and their redshift is affected significantly by their in-falling peculiar velocities, which tend to reduce their cosmological redshifts. The detected transitions at about 9 Mpc and 17 Mpc correspond to cosmological redshifts of $z \lesssim 0.005$, which is lower than the transition redshift required for the resolution of the Hubble tension ($z_t \simeq 0.07$ is the upper redshift of SnIa-Cepheid host galaxies).

In the context of the above-described analysis, we have ignored the possible systematic uncertainties induced on the estimated baryonic masses M_B, due to systematic uncertainties in the measurement of galactic distances. In particular, different sub-samples of galaxies in the SPARC database are affected by different systematic uncertainties. The SPARC sample includes galaxies with both direct and indirect distance measurements. Direct distance measurements are based on standard candles (Cepheids and Tip of Red Giant stars), while indirect measurements are based on the Hubble flow with Virgocentric infall correction. Systematic uncertainties of indirectly measured distances affecting mainly galaxies beyond 15 Mpc are due to uncertainties in the Hubble constant H_0 and in the a Virgocentric infall model. $H_0 = 73\,\mathrm{km/s/Mpc}$ is assumed in estimating the distances of the Hubble flow subsample of the SPARC sample along with the Virgocentric infall model used to correct the Hubble flow distances. The anticipated shift in $\log M_B$ due to an incorrect assumption of the H_0 value and/or the Virgocentric infall model is anticipated to be of the order of 0.1 dex, assuming a 5% change in H_0 and a scaling of the estimated value of M_B with distance D as $M_B\ D^{-2}$.

Thus, the identified mismatch of the Tully–Fisher parameters between low- and high-distance subsamples could, in principle, be due to such a systematic uncertainty of the

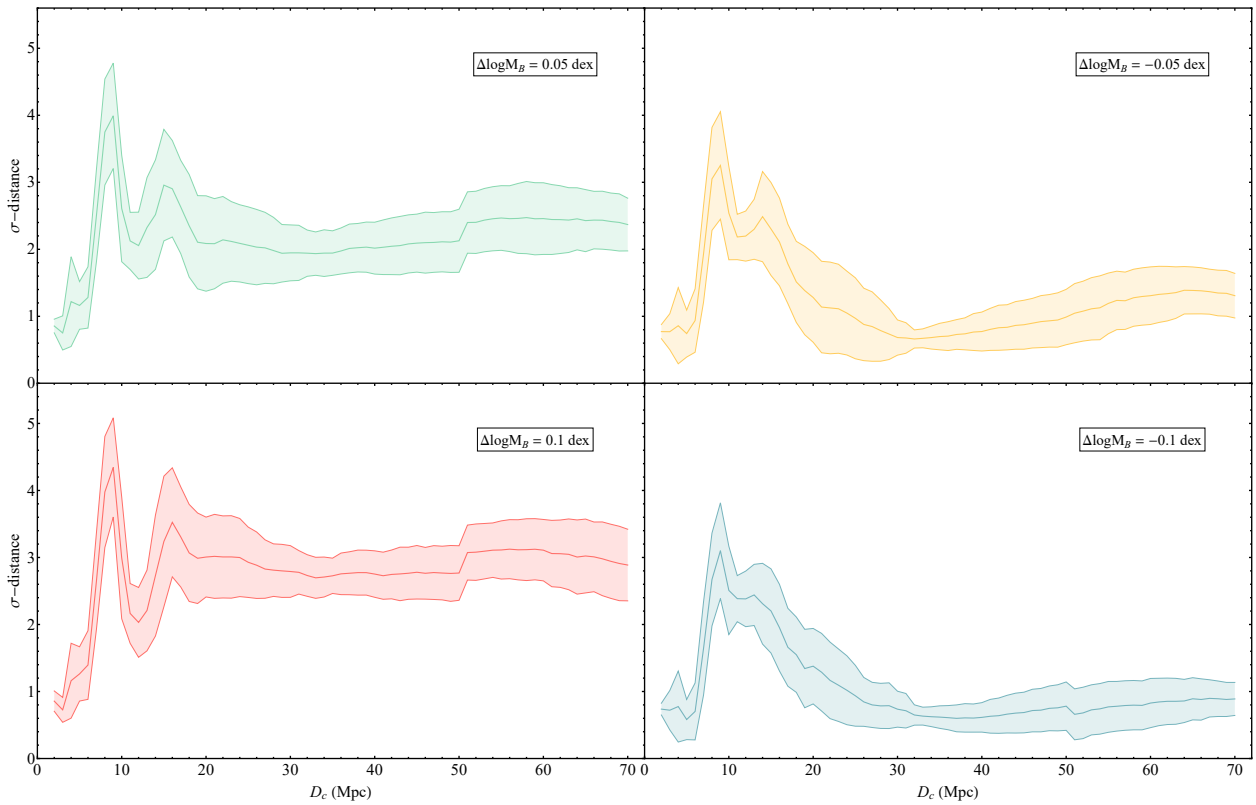

Figure 5.6: The 68% range of the σ-distances versus the split distances D_c produced by a Monte Carlo simulation of 100 sample datasets. The simulations are performed for different values of the shift $\Delta \log M_B$, which represents the possible systematic errors present in the datapoints whose distances are calculated using the Hubble flow, assuming $H_0 = 73\,\mathrm{km\,s^{-1}\,Mpc^{-1}}$, and correcting for Virgo-centric infall. The same characteristic two-peak structure remains for all shifts considered, indicating the robust nature of the identified effect. Adopted from Ref. [264].

galactic baryonic masses of Hubble flow galaxies. In order to examine this possibility, we have constructed new Monte Carlo samples where we not only vary randomly the distances but also add a fixed shift of $\Delta \log M_B$ along the vertical axis (mass) for all the datapoints where the mass is estimated using the Hubble flow with $H_0 = 73\,\mathrm{km\,s^{-1}\,Mpc^{-1}}$. The distances of these points are calculated using the Hubble flow, assuming $H_0 = 73\,\mathrm{km\,s^{-1}\,Mpc^{-1}}$, and correcting for Virgo-centric infall. We have considered four cases of systematic shifts (fixed values of $\Delta \log M_B$):-0.1 dex, -0.05 dex, $+0.05$ dex and $+0.1$ dex. The results for the σ-distance ranges in terms of the splitting distance D_c for each one of the above four cases are shown in Fig. 5.6. The corresponding likelihood contours for the subsamples corresponding to $D_c = 9\,\mathrm{Mpc}$ (maximum mismatch) are shown in Fig. 5.7. Clearly, the mismatch features at $D_c = 9\,\mathrm{Mpc}$ and $D_c = 17\,\mathrm{Mpc}$ remain in all four cases that explore this type of systematic uncertainty. In particular, the 9 Mpc peak height varies from about 4σ for $\Delta \log M_B = 0.1$ dex to about 3σ for $\Delta \log M_B = -0.1$ dex. We thus conclude that this type of systematic uncertainty is unable to wash out the mismatch effect we have identified.

If the intercepts' transitions are interpreted as being due to a transition in $G_{\rm eff}$, we can use Eq. (5.4) along with the observed intercept transition amplitude shown in Table 5.2 to identify the magnitude and sign of the corresponding $G_{\rm eff}$ transition. The intercept transition

at $D_c = 17\text{Mpc}$ indicated in Table 5.2 corresponds to the following:

$$\Delta\, log\, A_B \equiv log\, A_B^{>} - log\, A_B^{<} \simeq 0.2 \tag{5.12}$$

Since A_B is found to be higher at larger distances (early times), $G_{\rm eff}$ should be lower, due to Eq. (5.4). The corresponding fractional change in $G_{\rm eff}$ is easily obtained by differentiating the logarithmic form of Eq. (5.4) as follows:

$$\Delta\, log\, A_B = \frac{\Delta A_B}{A_B} = -2\frac{\Delta G_{\rm eff}}{G_{\rm eff}} \implies \frac{\Delta G_{\rm eff}}{G_{\rm eff}} \simeq -0.1 \tag{5.13}$$

This sign (weaker gravity at early times) and magnitude of the $G_{\rm eff}$ transition is consistent with the gravitational transition required for the resolution of the Hubble and growth tensions in the context of the mechanism of Ref. [232].

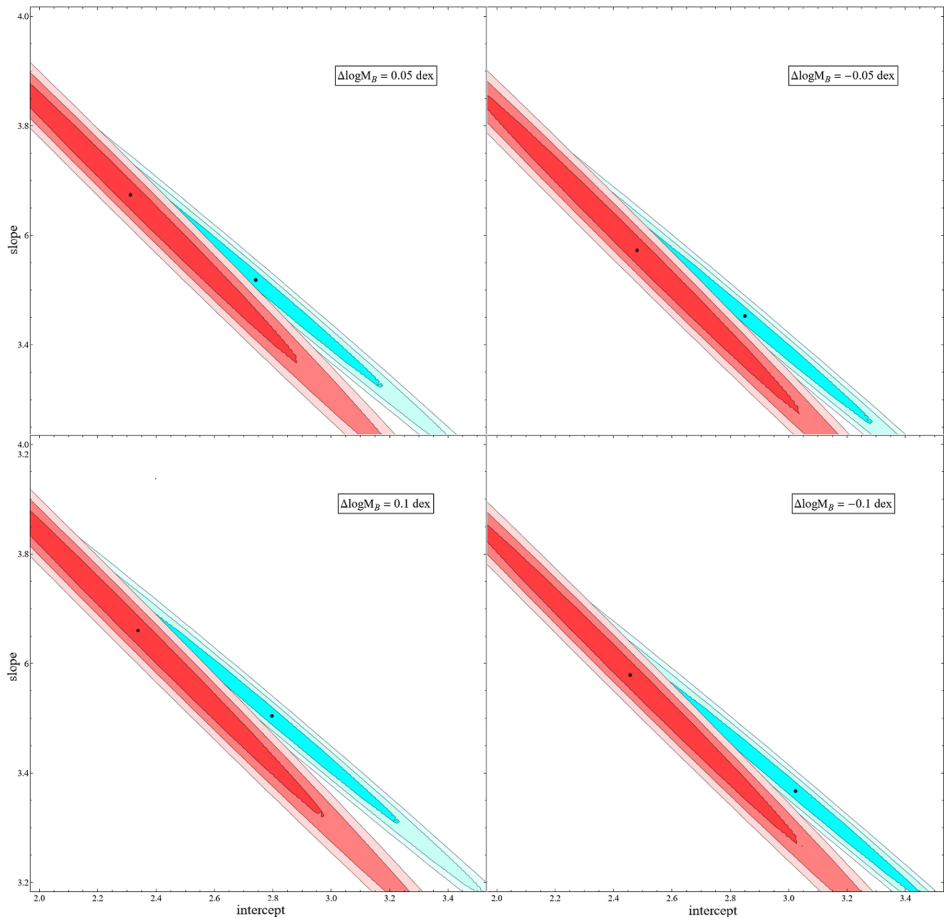

Figure 5.7: The likelihood contours of the slope and intercept for a sample splitting distance $D_c = 9$ Mpc corresponding to the different values of the systematic shift $\Delta \log M_B$ shown in Fig. 5.6. The red contours correspond to the dataset with galaxies that have distance below 9 Mpc, whereas the cyan contours correspond to galaxies with distances above 9 Mpc. The σ distance between the two best fits varies between 3σ and 4σ. Adopted from Ref. [264].

5.2 Constraining a Late Time Transition of $G_{\rm eff}$ Using Low-z Galaxy Survey Data

5.2.1 Effects of a gravitational transition on redshift survey data

As mentioned above, it is very likely that a transition of the $G_{\rm eff}$ at redshifts $z < 0.01$ would cause an analogous shift in the Hubble expansion rate. Although such a shift might be hard to detect directly considering how low the expected redshifts are, it could be detectable indirectly as a signal in the observed number of galaxies per redshift bin at $z < 0.01$. Therefore, we proceed by attempting to search for this gravitational transition in galaxy survey data, quantify and constrain it.

In the context of the scalar-tensor modified gravity theories the gravitational constant acquires dynamical properties and thus the Friedman equation in redshift space may be expressed as

$$H(z)^2 = \frac{8\pi G_{\rm eff}(z)}{3}\rho_{tot} \tag{5.14}$$

where ρ_{tot} refers to the total energy density including matter and an effective geometric dark energy component induced eg by the non-minimally coupled scalar field. Also, $G_{\rm eff}$ is the dynamical gravitational constant which is proportional to the inverse non-minimal coupling function $F(\Phi(z))$ of the scalar-tensor theory. The dynamical evolution of $G_{\rm eff}$ is severely constrained by a wide range of experiments and astronomical observations which constrain the time and redshift derivative of $G_{\rm eff}$ to $\frac{\dot{G}_{eff}}{G_{\rm eff}} < 10^{-12}$ at various specific time ranges [281, 293, 322] including the present time constrained mainly using solar system tests. Abrupt transitions of $G_{\rm eff}$ however can not be constrained by local constraints of the time derivative of $G_{\rm eff}$ since by definition, in the context of an abrupt transition $G_{\rm eff}$ would remain constant at (almost) all times. The overall change of $G_{\rm eff}$ between the present time and nucleosynthesis is weakly constrained to be less than about 10% [297].

Based on the generalized Friedman Eq. (5.14) an abrupt change of $G_{\rm eff}$ at $z = z_t$ would also lead to a corresponding abrupt change of $H(z)$ such that

$$\frac{\Delta G_{\rm eff}}{G_{\rm eff}} = 2\frac{\Delta H}{H} \tag{5.15}$$

In the Hubble flow $z_t > 0.01$ such a transition is well constrained by detailed Hubble diagram data based on Type Ia Supernovae (SnIa) [238]. For $z_t < 0.01$ the Hubble diagram involves significant contributions from galactic density inhomogeneities and peculiar velocity effects and thus similar constraints are expected to be significantly weaker.

Using galaxy redshift surveys at $z < 0.01$ it is possible to bin the observed galaxies in redshift bins of width Δz such that there are $\Delta N(z_i)$ galaxies in the i bin. In the presence of random peculiar velocities the measured redshift of a given galaxy may be written as

$$cz = H_0 s + c\Delta z_r \tag{5.16}$$

where H_0 is the Hubble expansion rate at the galactic distance s and $c\Delta z_r$ is a perturbation due to peculiar velocity effects and may be approximated to have random Gaussian distribution ($\mu = 0$, $\sigma = 300\,\mathrm{km\,s^{-1}}$). The number of galaxies that exist in a spherical shell with radius s is given by,

$$N(s) = \frac{4\pi}{3}s^3\rho(z) \tag{5.17}$$

where we approximate the density at the redshift $\rho(z) = \rho_0(1+z)^3 \approx \rho_0$ as homogeneous. The number of galaxies in the i redshift bin may be easily obtained from Eq. (5.17) as

$$\Delta N(z_i) = 4\pi\rho_0 \left(\frac{c}{H_0}\right)^3 (z_i - \Delta z_r)^2 \Delta z_i \tag{5.18}$$

where Δz_i is width of the i redshift bin assumed to be the same for all bins. Thus the predicted number of galaxies in the i bin $\Delta N(z_i)$ is related to the number of galaxies in the $j = 1$ bin as

$$\Delta N(z_i) = \Delta N(z_1) \left(\frac{cz_i - c\Delta z_r}{cz_1 - c\Delta z_r}\right)^2 \left(\frac{H_{01}}{H_{0i}}\right)^3 \tag{5.19}$$

Violation of Eq. (5.19) may be induced by either large density fluctuations of galaxies or coherent velocity flows. Eq. (5.19) however allows for a transition in the Hubble diagram slope H_0 at some redshift z_t. Such a transition could be expressed as

$$H_{0i} = H_{01} - \Delta H_0 \Theta(z_i - z_t) \tag{5.20}$$

In this case Eq. (5.19) takes the form

$$\Delta N(A, \delta, z_t, z_i) = A \left(\frac{cz_i - c\Delta z_r}{cz_1 - c\Delta z_r}\right)^2 [1 - \delta\ \Theta(z_i - z_t)]^{-3} \tag{5.21}$$

where $A \simeq \Delta N(z_1)$ and $\delta \equiv \frac{\Delta H_0}{H_0}$ are parameters to be fitted by survey data.

5.2.2 Analysis of the 6dF and 2MASS Galaxy Survey $z < 0.01$ Subsets

It is straightforward to implement the maximum likelihood method by minimizing χ^2 with respect to the parameters A, $\delta \equiv \frac{\Delta H_0}{H_0}$ and z_t. Thus we minimize

$$\chi^2(A, \delta, z_t) = \sum_{i=1}^{N_{tot}} \frac{[\Delta N(z_i)_{dat} - \Delta N(A, \delta, z_t, z_i)]^2}{\sigma_i^2 + \sigma_s^2} \tag{5.22}$$

where N_{tot} is the total number of bins, $\sigma_i^2 = N_{tot}/\Delta N(z_i)_{dat}$ is the Poisson distribution error for each bin and σ_s is the scatter error fixed such that the minimum χ^2_{min} per degree of freedom is equal to one. Also $\Delta N(z_i)_{dat}$ is the number of galaxies in each redshift bin after a random perturbation Δz_r is imposed on each measured galaxy redshift cz_i to account for the random component Δz_r in the parametrization (5.21).

We use the 6dFGS [209,323–329] focusing on the galaxies with $z < 0.01$ (≈ 2800 galaxies). The peculiar velocity sample consists of 8885 galaxies in the Southern Hemisphere with $z < 0.055$. The sky distribution of our low z galaxy subsample is shown in Fig. 5.8 split in 4 redshift bins of $\Delta z = 0.0025$ increments. The corresponding distribution of the galaxy sample in redshift space is shown in Fig. 5.9 where we split the sample in 25 redshift bins.

As shown in Fig. 5.9, there is a peak/dip feature in the redshift space number density of galaxies around $1500 - 2000\,\mathrm{km\,s^{-1}}$ ($21 - 28$ Mpc for a conservative value of $H_0 = 70\,\mathrm{km\,s^{-1}\,Mpc^{-1}}$). This abrupt break in the redshift density is most probably due to density fluctuations of galaxies and/or coherent peculiar velocity flows. However, it may also be induced by a step-like transition of the Newton's constant $G_{\rm eff}$ occurring for cz_t in the above

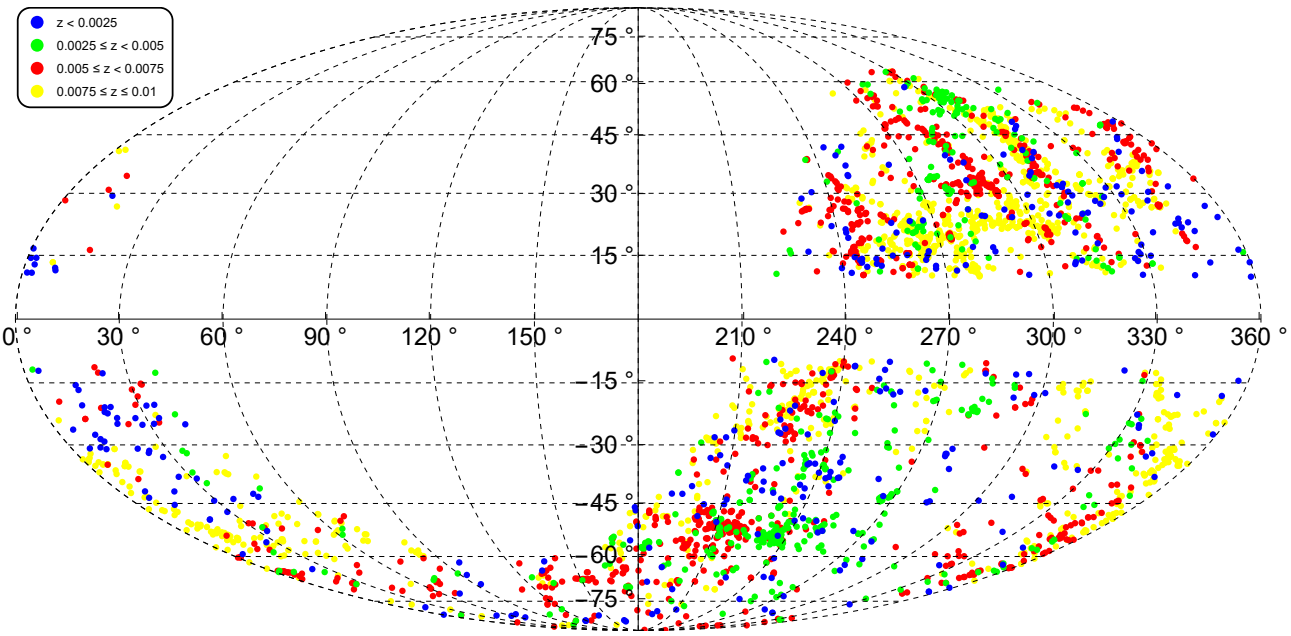

Figure 5.8: The sky coverage of our collection of low-z 6dF data ($z < 0.01$) plotted in a Mollweide projection, using galactic coordinates. The data is split in four bins, of $\Delta z = 0.0025$ increments. It is evident that data homogeneity is present when considering the different redshift increments. Adopted from Ref. [265].

range. Such gravitational transition would induce a similar transition in $H(z) \simeq H_0$ in accordance with eqs (5.14) and (5.15). This type of transition has been discussed in Chapter 3 with the introduction of the $LwMT$ model and could be expressed as [227],

$$\mu_G(z) \equiv \frac{G_{\rm eff}}{G_{\rm N}} = [1 + \Delta\mu_G\, \Theta(z - z_t)] \tag{5.23}$$

where $G_{\rm N}$ is the locally measured Newton's constant, and $\Theta(z)$ is the Heaviside step-function. This ansatz has been thoroughly explored in Refs. [232, 330], where it is proposed that it would have the dual effect of solving both the Hubble and growth tensions. There have also been observational hints for such a transition at ≈ 20 Mpc in Cepheid [331, 332] and Tully-Fisher data [264].

Assuming that the gravitational transition is the only cause of the observed dip in the $\Delta N(z)$ distribution we may use Eq. (5.21) to minimize χ^2 (Eq. (5.22)) and thus obtain the best fit parameters A, δ and z_t. Such a fit for $\delta \equiv \Delta H_0/H_0$ should be interpreted as an upper bound for the transition amplitude δ and therefore also for the gravitational transition amplitude as obtained from Eq. (5.15).

We thus obtain the best fit parameter values as $cz_t \approx 1810 \pm 150\,{\rm km\,s^{-1}}$, $A = 20.9 \pm 0.5$ and $\delta = \frac{\Delta H_0}{H_0} = -0.275 \pm 0.01$ for a fixed value of $\sigma_s \approx 3.7$. In the left panel of Fig. 5.10 we show the likelihood contours corresponding from inner to outer to the 68%, 95% and 99.7% confidence level (C.L.) intervals in the parameter space $A - \delta$, while in the right panel we show the best fit (blue curve) form of Eq. (5.21) (with its 68% C.L. error-band shown as cyan area) superposed with the $\Delta N(z_i)$ datapoints (red errorbars). In the context of the fit we have included the random gaussian perturbations of redshifts with $(\mu = 0,\, \sigma = 300\,{\rm km\,s^{-1}})$ due to the effects of peculiar velocities in the data and have set $\Delta z_r = 0$ in the ansatz (5.19),

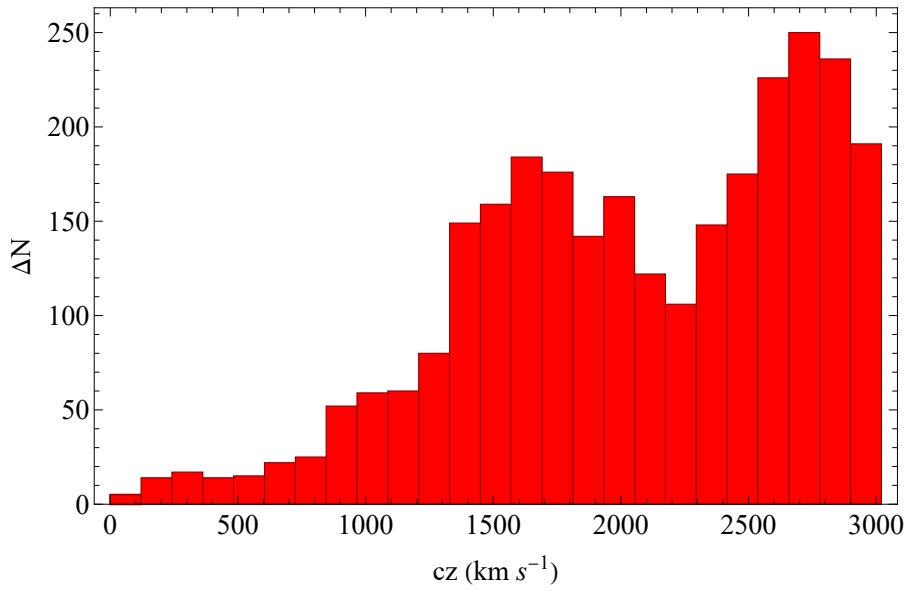

Figure 5.9: The $\Delta N - cz$ histogram plot corresponding to the data of the 6dFGS dataset. It is evident that a large peak in the distribution of galaxies exists at $cz = 1500 - 2000\,\mathrm{km\,s^{-1}}$. Adopted from Ref. [265].

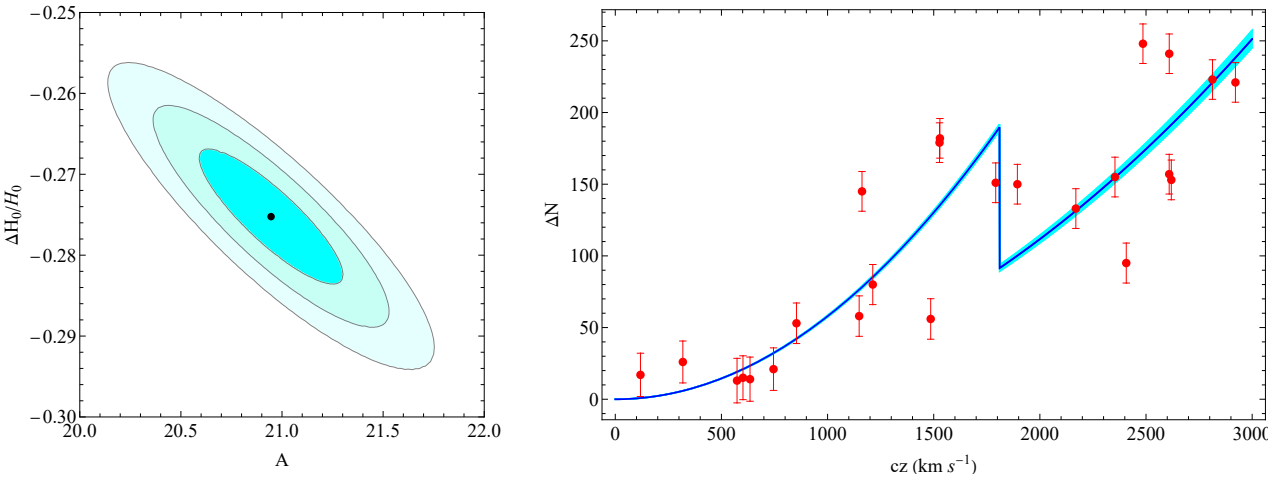

Figure 5.10: *Left panel:* The $\Delta H_0/H_0$ - A likelihood contours corresponding from inner to outer to the 68%, 95% and 99.7% C.L. intervals. The best-fit value is at the center (black bullet). The projected contours are taken at the best-fit value of the transition redshift z_t. *Right panel:* The ΔN - cz plot of the best-fit (blue curve) of Eq. (5.21) corresponding to the best-fit values of the parameters $\delta \equiv \Delta H_0/H_0$, A and z_t along with the 68% C.L. (cyan area). The binned numbers of galaxies in each redshift bin and their Poisson error are also shown (red errorbars). Adopted from Ref. [265].

(5.21). [2]

We may therefore conclude that a possible transition of the Hubble diagram slope H_0 has to be smaller than the best fit value $\delta = \frac{\Delta H_0}{H_0} \leq -0.275 \pm 0.01$. This upper bound for

[2]This approach is equivalent to keeping the galaxy redshifts in their original form while including the random redshift perturbation in the ansatz (5.19).

a Hubble diagram slope transition may be translated to an upper bound for an underlying gravitational transition using Eq. (5.15) which leads to $\frac{\Delta G_{\rm eff}}{G_{\rm eff}} \lesssim 0.6$. Such an upper bound can easily accommodate the gravitational transition amplitude $\frac{\Delta G_{\rm eff}}{G_{\rm eff}} \simeq 0.1$ which has been proposed for the resolution of the Hubble and growth tensions [232] which implies that this scenario remains viable in the context of the 6dFGS data.

We have repeated the analysis, in the same manner, using this time the larger and more recent 2MRS [333–337] dataset. This survey provides an almost full coverage of the sky (∼70%) including more data points than the 6dFGS peculiar velocity sample with a total number of 44599 spectroscopically observed sources at $z < 0.15$ (the subsample with $z < 0.01$ consists of ≈ 3200 galaxies). We simulate the peculiar velocities in the data as described previously, for the case of the 6dFGS dataset. The sky distribution of these galaxies are shown in Fig. 5.11 in four redshift bins up to $z = 0.01$.

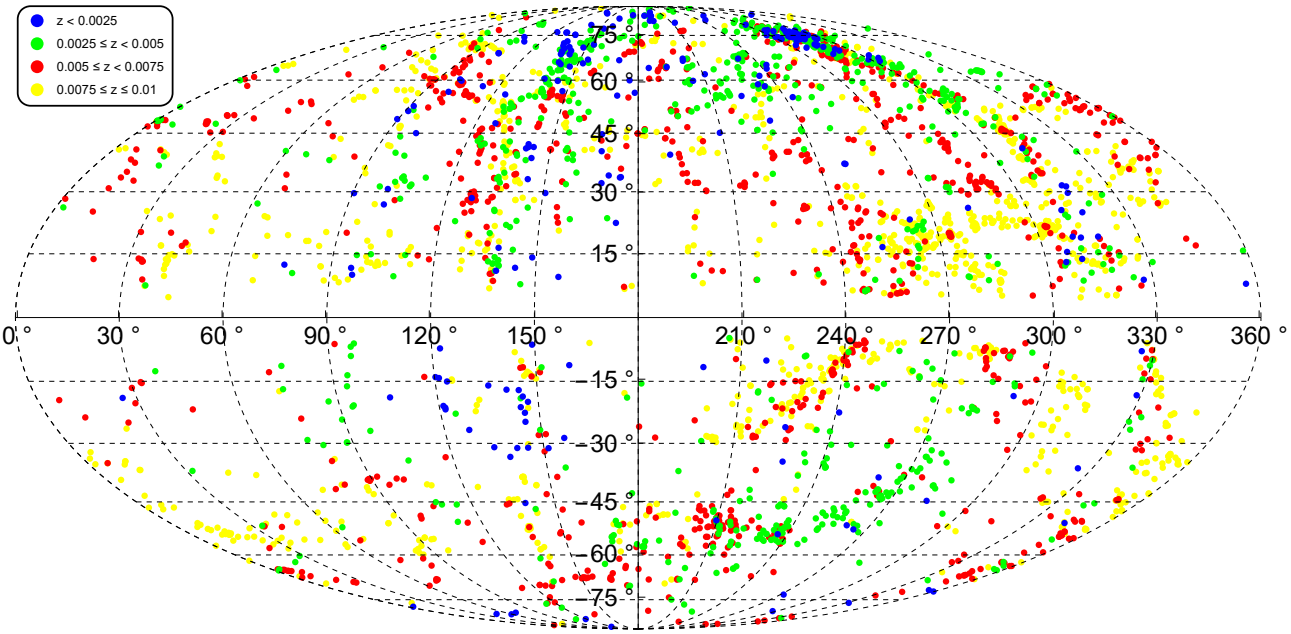

Figure 5.11: The sky coverage of our collection of low-z 2MRS data $(z < 0.01)$ plotted in a Mollweide projection, using galactic coordinates. The data is split into four bins, of $\Delta z = 0.0025$ increments. Adopted from Ref. [265].

The galaxy distribution in redshift space is shown in Fig. 5.12 where a similar dip may be seen at $cz \approx 1500\,{\rm km\,s^{-1}}$. As in the case of the 6dFGS dataset, this feature is most likely due to density variations of the galaxy distribution and to peculiar velocity flows. If however we assume that it is due to a gravitational transition of the form (5.23) leading to a transition of the Hubble parameter, then we can derive an upper bound on $\frac{\Delta G_{\rm eff}}{G_{\rm eff}}$.

In this case, the best fit parameter values are similar as in the 6dFGS and take the form $A = 17.5 \pm 0.5$, $\delta = \frac{\Delta H_0}{H_0} = -0.28 \pm 0.01$ and $cz_t \approx 1783 \pm 150$ km s^{-1} for $\sigma_s \approx 3.4$. We have plotted the confidence contours in the $A - \delta$ parameter subspace (left panel) as well as the best-fit form of $\Delta N(z)$ based on Eq. (5.21) (right panel), in Fig. 5.13.

In order to see how commonly, if at all, would the abrupt peak/dip in the galaxy distribution appear also in the simulated data based on a standard ΛCDM cosmology, we have used the Cosmological Lofty Realizations (CoLoRe) [338] software package that supports log-normal fields to generate synthetic realizations for the 2MRS galaxy survey. We opted to

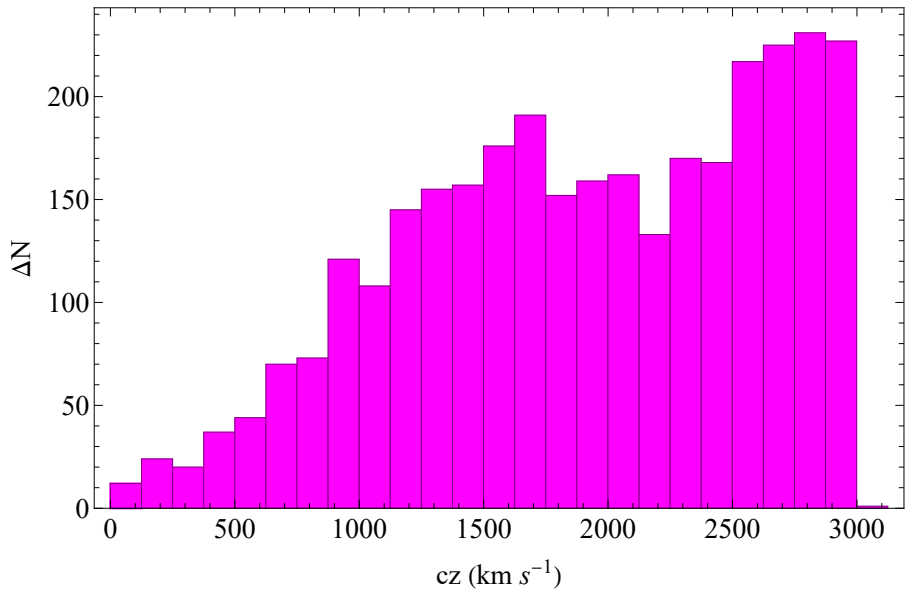

Figure 5.12: The $\Delta N - cz$ histogram plot corresponding to the data of the 2MRS dataset. The same peak/dip feature in the distribution of galaxies as in the 6dFGS dataset exists at $cz = 1500 - 2000\,\mathrm{km\,s^{-1}}$, albeit it is less prominent. Adopted from Ref. [265].

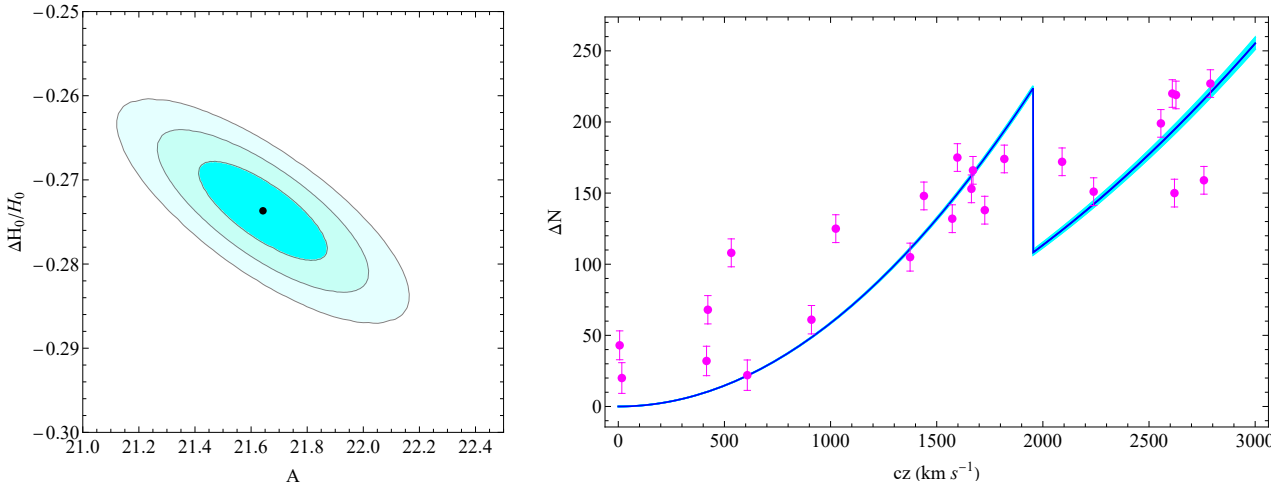

Figure 5.13: *Left panel:* Same as Left panel of FIG. 5.10 but for the 2MRS sample. *Right panel:* Same as Right panel of FIG. 5.10 but for the 2MRS sample. Adopted from Ref. [265].

generate mock catalogs for this survey since as we saw previously, it is more complete than the 6dFGS peculiar velocity sample. In particular, for the simulated catalogs on top of the assumed standard ΛCDM model for the input Gaussianised matter power spectrum $P(k)$ at $z = 0$, we also included a constant galaxy bias with redshift $b(z) = 1.3$ (a value found to be a good approximation at non-linear scales) and the approximated fitting function for the redshift distribution of the 2MRS found by [339] that reads:

$$\frac{dN}{dz} = \frac{N_g \beta}{z_0 \Gamma\left[(m+1)/\beta\right]} \left(\frac{z}{z_0}\right)^m \exp\left[-\left(\frac{z}{z_0}\right)^\beta\right] \tag{5.24}$$

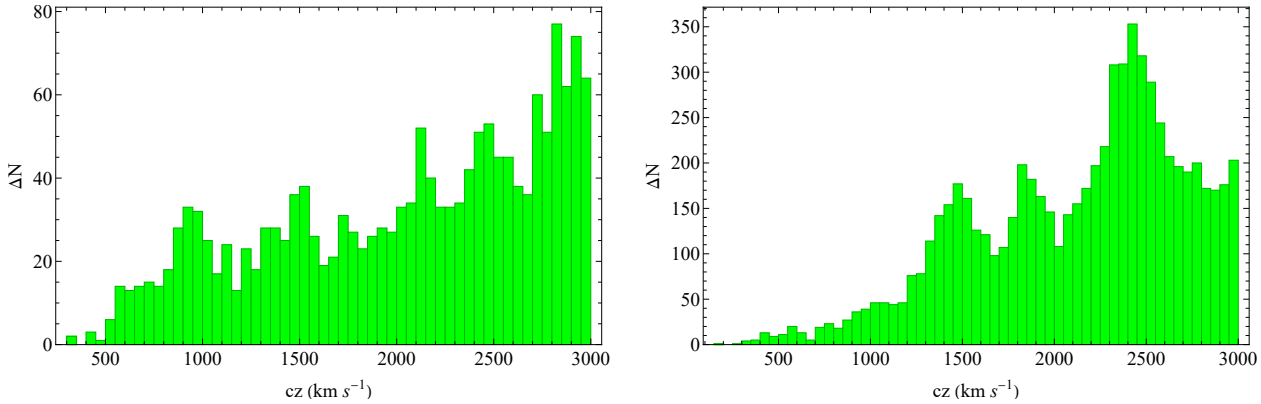

Figure 5.14: The $\Delta N - cz$ histogram plot corresponding to the data of two random simulated datasets based on ΛCDM . Features like the one shown in the real data appear to be common due to galactic number density inhomogeneities. Adopted from Ref. [265].

with $\beta = 1.64$, $z_0 = 0.0266$, $m = 1.31$ and the total number of sources $N_g = 44599$, see Fig. 5.15.

Then we set up 500 simulations with the aim to clarify if the peak/dip feature in $\Delta N(z)$ would occur naturally in them in the context of a standard ΛCDM cosmology. In this case the best fit value of δ derived in the context of our analysis can only be viewed as an upper bound.

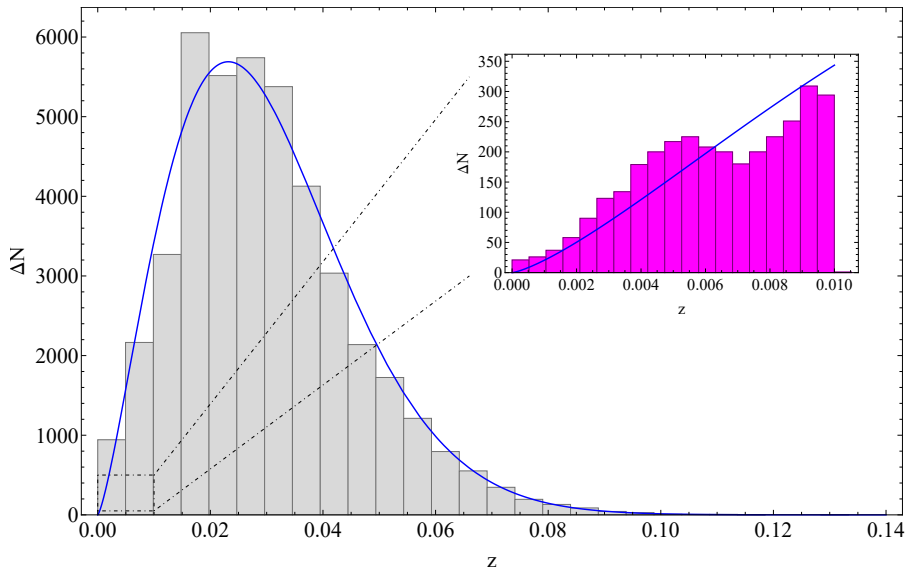

Figure 5.15: The number of galaxies in each redshift bin for the entire 2MRS sample (lightgray histogram), as well as for our subsample with $z < 0.01$ (magenta histogram), superimposed with the fitting function Eq. (5.24). Adopted from Ref. [265].

As expected, the simulated data indicate that peaks and dips like those found in the real data occur commonly in the corresponding simulated datasets based on standard ΛCDM cosmology due to density and peculiar velocity effects. This is demonstrated in the two simulated 2MRS datasets shown in Fig. 5.14 randomly chosen from the 500 mock catalogs to showcase here. The magnitude of these features overwhelms any possibility of interpreting

the observed peak/dip feature in the real $\Delta N(z)$ data as a signature of the presence of a $\Delta H_0/H_0$ transition and only allows the interpretation of the best fit value of $\Delta H_0/H_0$ as a bound on the magnitude of a possible corresponding Hubble and gravitational transition.

An assumption used in the analysis of the low-z galaxy survey data is that of uncorrelated Gaussian random peculiar velocity field which was superposed in the Hubble velocity flow. This assumption ignores the local bulk flows and the possible correlation among the redshift bins in estimating the uncertainties. The use of a diagonal covariance matrix, instead of using the full covariance matrix is a simplification which we had to implement, since the detailed form of the velocity flows on the considered scales is not precisely known and thus we do not have access to a reliable and detailed form of the full covariance matrix. However, it is clear that the use of the full covariance matrix would weaken the constraint on $G_{\rm eff}$ derived here. We have verified this result using toy covariance matrices that fully correlates only neighboring redshift bins. Following this approach, we have observed a very small (few percent) increase in the uncertainties of the best-fit parameters. This indicates that even after the inclusion of velocity correlations and the full covariance matrix, the constraint would remain consistent with a 10% gravitational transition at $z < 0.01$. Thus our approach can indeed lead to new constraints on a gravitational transition at redshifts $z < 0.01$ (last 150 Myrs) but these constraints are not powerful enough to rule out the gravitational transition class of models for the resolution to the Hubble tension.

5.3 In Brief

In this chapter we have used a two-sided approach in order to identify and constrain a possible late z gravitational transition. First of all, we employed a specific statistic on a robust dataset of 118 Tully-Fisher datapoints to demonstrate the existence of evidence for a transition in the evolution of BTFR. This evidence was verified by a wide range of Monte Carlo simulations that compare the real dataset with corresponding homogenized datasets constructed using the BTFR. It indicates a transition of the best-fit values of BTFR parameters, which is small in magnitude but appears at a level of statistical significance of more than 3σ. It corresponds to a transition of the intercept of the BTFR at a distance of $D_c \simeq 9\,\mathrm{Mpc}$ and/or at $D_c \simeq 17\,\mathrm{Mpc}$ (about 80 million years ago or less). Such a transition could be interpreted as a systematic effect or as a transition of the effective Newton constant with a 10% lower value at early times, with the transition taking place about 80 million years ago or less. The amplitude and sign of the gravitational transition are consistent with a recently proposed mechanism for the resolution of the Hubble and growth tensions [227, 232]. However, the time of the transition is about 60 million years later than the time suggested by the above mechanism (100-150 million years ago corresponding to $D_c \simeq$ 30-40 Mpc and $z \simeq$ 0.007-0.01).

The effect shown in our analysis could be attributed to causes other than a gravitational transition. One such possible cause would be the presence of systematic errors affecting the estimate of galactic masses or rotation velocities for particular distance ranges. Even if this is the case, it is important to point out these inhomogeneities, which may require further analysis to identify their origin. Alternatively, if the causes of the detected mismatch are physical, they could also be due to variation of conventional galaxy formation mechanisms, which may involve other types of modifications of gravitational physics (*e.g.* effects of MOND gravity). The BTFR is an observationally tight empirical correlation and has therefore been

used as a test of various modified gravity models (Refs. [156, 340, 341] offer comprehensive reviews on the cosmological implications of such models), including modified Newtonian dynamics (MOND) [342, 343] and Grumiller modified gravity [344].These models have been shown to be consistent with BTFR for specific values of their acceleration parameters. The BTFR has also been used as a test of the properties of Cold Dark Matter and galaxy formation mechanisms in the context of ΛCDM [345, 346].

An interesting effect in the direction of the one observed in the analysis described in this chapter was also reported in Ref. [332]. There, the authors found a transition of the Cepheid magnitude behavior in the range of 10–20 Mpc, which could explain the Hubble tension (see Fig.4 of Ref. [332]). The authors claimed that this transition is probably due to dust property variation, but there is currently a debate on the actual cause of this mismatch.

An important extension of this analysis is the search for similar transition signals and constraints in other types of astrophysical and geophysical-climatological data of Earth paleontology. For example, a wide range of solar system anomalies were discussed in Ref. [347], which could be revisited in the context of the gravitational transition hypothesis. Of particular interest, for example, is the 'Faint young Sun paradox' [348], which involves an inconsistency between geological findings and solar models about the temperature of the Earth about 4 billion years ago. Another interesting extension of this study would be the use of alternative methods for the identification of transition-like features in the data, *e.g.* the use of a Bayesian analysis tool, such as the internal robustness described in Refs. [349, 350].

Alternatively, other astrophysical relations that involve gravitational physics, such as the Faber–Jackson relation between intrinsic luminosity and velocity dispersion of elliptical galaxies or the Cepheid star period–luminosity relation, could also be screened for similar types of transitions as in the case of BTFR. For example, the question to address in the Cepheid case would be the following: 'What constraints can be imposed on a transition-type evolution of the absolute magnitude (M_v)-period (P) relation of Population I Cepheid stars?' This relation may be written as follows:

$$M_v = s\,(logP - 1) + b \tag{5.25}$$

where $s = -2.43 \pm 0.12$ and $b = -4.05 \pm 0.02$ [351, 352].

We also analysed the low z distribution ($z < 0.01$) of galaxies in the 6dFGS peculiar velocity sample and the complete 2MRS galaxy survey searching for a signal consistent with a gravitational abrupt transition. We have identified such a signal consistent with a gravitational transition $\frac{\Delta G_{\rm eff}}{G_{\rm eff}} \simeq 0.6$. Such a signal however is degenerate with corresponding expected features emerging due to density fluctuations in the number density of galaxies and peculiar velocity flows. This was demonstrated by simulating the expected redshift distribution of the galaxies for the more complete 2MRS catalog in the context of standard ΛCDM without gravitational transition. Thus the detected signal can only be interpreted as an upper bound on the magnitude of such a gravitational transition. Even though this bound is weaker than corresponding bounds obtained using nucleosynthesis and CMB power spectrum data implying $\frac{\Delta G_{\rm eff}}{G_{\rm eff}} \lesssim 0.1$ it remains interesting for two reasons:

- It is based on a novel method for constraining a gravitational transition.
- It focuses on a very specific ultra-late redshift range.

- It indicates that the proposed magnitude of a gravitational transition $\frac{\Delta G_{\rm eff}}{G_{\rm eff}} \simeq 0.1$ for the resolution of the Hubble and growth tension is consistent with current galaxy survey data.

Interesting extensions of the analysis presented in this chapter include the following:

- The identification of actual distances and peculiar velocities of the galaxies included in the surveys considered so that it can be estimated to what extend is the identified feature in $\Delta N(z)$ due to galactic density variations and/or peculiar velocity flows. If this feature can not be fully explained as a density and peculiar velocity effect then it is possible that at least part of it may be due to a gravitational transition.

- The identification of additional astrophysical datasets beyond galaxy surveys, Tully-Fisher data and solar system history which may lead to constraints on the magnitude of such a profound effect like an ultra-late gravitational transition.

- The simulation of the solar system evolution (and in particular of the Oort cloud) to identify the change of impactor rate in the context of a late gravitational transition. In this context, the solar system history could become a useful laboratory for the constraint of such a transition.

In conclusion, we can deduce that the hypothesis of a low z gravitational transition is weakly constrained in the context of current studies but it could lead to the resolution of important cosmological tensions of the standard ΛCDM model. We have, however, demonstrated that it is possible to extract hints for the existence of such a transition both in the evolution of the Tully-Fisher relation and in the low z ($z < 0.01$) distribution of galaxies.

CHAPTER 6

Final Remarks

We are currently living during an exciting era of modern Cosmology. That is because there is insurmountable evidence that the single most successful cosmological model in history is wrong. Never before since its formulation on 1998, when the observational discovery of the accelerated expansion of the Universe took place, has there been a more heated debate regarding the viability of the ΛCDM concordance model. Arguably the largest thorns on ΛCDM 's side are the so-called Hubble and S_8 tensions which have reached the 5 and $\approx 3\sigma$ levels respectively. The impact and possible resolution of these very significant tensions were the main focus of this dissertation.

In what follows we present a brief summary of the most crucial points that are discussed in each chapter. Furthermore, we comment on some unanswered questions and subsequent limitations of the work that this thesis is based on.

6.1 Summary

In order to fully understand the nature of the aforementioned tensions and the characteristics of the proposed solutions, we have dedicated the first chapter of this thesis to a quick review of the most basic aspects of modern Cosmology. We started by reviewing the General Relativity essentials for formulating the ΛCDM model, including the Friedmann-Lemaître-Roberson-Walker metric and the Friedmann-Lemaître equations. Subsequently, we discussed the current status of both the Hubble and growth tensions and offered a forecast in the future of the field.

In the second chapter, we demonstrated how the exploitation of a degeneracy between the equation of state parameter w and the Hubble parameter H_0 could enable us to construct a number of parametrizations that could serve as apparent solutions to the Hubble tension. More specifically we have shown that the relation of the w parameter best fit of the H_0 in the context of the CMB power spectrum follows the approximate linear equation

$$H_0 + 30.93w - 36.47 = 0. \tag{6.1}$$

Solving this equation we find that for $w = -1.22$ the best fit value of H_0 in the context of CMB is $74\ km\ sec^{-1}\ Mpc^{-1}$, while of course for $w = -1$ the predicted value of H_0 is consisted with the one given in the context of Planck18/ΛCDM. Fitting the wCDM model for various values of the w parameter with the Planck TT power spectrum we provide statistical evidence in the

form of the χ^2 quality of fit, that the $w = -1.22$ parametrization is not statistically inferior to ΛCDM. This is very important because this parametrization has the advantage of providing an apparent resolution to the Hubble tension.

However, we also demonstrated that if one includes the Pantheon SnIa, BAO or RSD data, the χ^2 quality of fit worsens as we cross the phantom divide. While this $w - H_0$ degeneracy can be generalized to the CPL parametrization, it is unfortunate that it only provides a superficial solution of the Hubble tension. That is because it does not take into account the Supernovae absolute magnitude aspect of the tension which is more accurately explained in Chapter 3.

The next three chapters were devoted to the formulation of a joint w - absolute magnitude M transition ($LwMT$) and its impact on resolving both the H_0 and S_8 tensions simultaneously, the study of the inability of smooth $H(z)$ deformations to resolve the growth tension and the observational hints in favour of $LwMT$, in this order. Therefore, the third chapter builds upon the idea of the $w - H_0$ degeneracy by introducing the $LwMT$ model which also deals with the problem of the difference in the values of the SnIa absolute magnitude predicted by the Planck18/ΛCDM and local Cepheid calibrators. As stated above this model consists of two parts, the first involves an abrupt transition of the dark energy equation of state parameter at an ultra-late transition redshift $z_t < 0.1$. This transition is capable of leading to a value of H_0 while mimicking a Planck18/ΛCDM form of the comoving distance $r(z) = \int_0^z H^{-1}(z')dz'$ for $z > z_t$. The second part of this model is what allows it to overcome the SnIa absolute magnitude aspect of the tension, since it involves a similarly abrupt transition of M.

We show that this type of M transition could be achieved by a reduction in the value of the effective Newton constant G_{eff}. This is made possible by the fact that the SnIa absolute luminosity is proportional to the Chandrasekhar mass which varies as $L \approx G^{-3/2}$. Furthermore, we provide a statistical analysis of the $LwMT$ model showing that it provides a better fit to cosmological data than the smooth late time deformations of $H(z)$ that also claim to solve the H_0 tension. It does so by also while also providing a satisfactory resolution of the growth tension, since it predicts a lower value of $\mu = G_{\text{eff}}/G_N$ for $z > z_t$.

Subsequently, we use the paradigm of the well-known CPL model in order to categorically show something that we have eluded to in the previous chapters. That any parametrization claiming to resolve the Hubble tension by using late time smooth deformations of the Hubble expansion rate $H(z)$ of the Planck18/ΛCDM best fit to match the locally measured value of H_0 while effectively keeping the comoving distance to the last scattering surface and $\Omega_{0m}h^2$ fixed to maintain consistency with Planck CMB measurements fails to address the S_8 tension. This is shown both by using an analytic approach and by using statistical analysis involving a numerical solution of the growth equation and then fitting to cosmological data.

Lastly, we search for observational hints of possible a gravitational transition and try to constrain its effect. We do so by, firstly, considering a compilation of galaxy data and probing for transitions in the evolution of the baryonic Tully-Fisher relation

$$M_B = A_B v_{rot}^s. \tag{6.2}$$

We indeed show that there are $\approx 3\sigma$ level hints for a gravitational transition at distances of 17 Mpc and 9 Mpc. Using Monte Carlo simulations to create homogeneous "mock" Tully-Fisher data, we show that our result is unaffected by random systematic and statistical variations of the galactic distances. Next, we consider the fact that a gravitational transition could lead

to a sharp change in the form of the Hubble diagram. This fact should theoretically enable us to search for such a transition and constrain it. In order to do that, use two low-z robust galaxy survey data compilations. Even though we observe a possible transition at a distance of 20 Mpc using both compilations, we report that this effect could also be attributed to either coherent peculiar galactic velocities or galactic density fluctuations. However, in any event the possibility of a gravitational transition can not be excluded by low-z galaxy survey data.

6.2 Open Questions and Limitations

Even though the $LwMT$ model presents us with an excellent fit to the data and is able to address both the Hubble and the S_8 tensions it remains an artificial solution. Artificial in the sense that it is not supported by a natural underpinning physical theory. The easiest way to interpret the proposed M transition is by considering it to be an equivalent gravitational one. This means that the proposed model must be accountable and consistent with solar system constraints in a similar fashion to other modified gravity theories. Due to its nature, the transition predicts a significant shift in the planet trajectories almost 100 Myrs. ago.

Such a trajectory modification would have a lot of observable impact, visible in the current solar system movements. No amount of echo of these type of monumental changes in the solar system have been observed thus far. Therefore, a study encompassing geological, astrophysical and solar system data could shed some more light in that direction categorically ruling out or in such a prospect. Another important open question of this study is whether it is possible to create a simple and intuitive modified gravity model, that could naturally induce the gravitational transition predicted by $LwMT$. This would, in all probability, resolve the fine-tuning issues that the model experiences.

Other than attributing the SnIa absolute magnitude transition to a gravitational transition and trying to deal with the plethora of issues this assumption creates, perhaps it would be a better idea to search for alternative mechanisms that could explain it. This approach could in principle lead to a more natural physical theory that will, ad principia, be free of the limitations imposed by the gravitational transition.

Despite its limitations, the ultimate goal of the $LwMT$ parametrization was to show that, in principle, the idea of a transition in the SnIa absolute magnitude is able to resolve the Hubble tension and at the same time ease the S_8 one as well. To that end it was successful and its approach is quite inviting since it is the simplest possible model of this type. Another aspect of this study was an effort to sort of "dislodge" the focus of the Hubble from the H_0 constant itself and shift it to the M parameter. The reasoning behind this, as it is discussed in more detail in Chapters 1 and 3, is that the SH0ES collaboration does not measure $H(z)$ at $z = 0$ directly, rather they infer its value by extrapolating from the value of H_0 they measure in the $0.023 < z < 0.15$ interval. This creates a blind-spot at $0.023 < z$ which is the very fact that enables us to conceive of a late M transition. If such a transition were to exist then it would imply that the value of H_0 reported by the SH0ES is not the "true" value, in the sense that the one given by the CMB is. Therefore, focusing on M would mean that we are focusing both on the mismatch that exists in the values of the SnIa absolute magnitude that one gets from the CMB+BAO measurements and the demarginalization method of Ref. [226], without the added issues that follow from the "recipe" of simply trying to raise the H_0 value.

Appendices

APPENDIX A

Data Used in the Analysis

A.1 The Cosmological Data Compilations of Chapter 3

The covariance matrix which corresponds to the latest Planck18/ΛCDM CMB distance prior data (shift parameter R and the acoustic scale l_a), for a flat universe has the following form [228]

$$C_{ij} = 10^{-8} \times \begin{pmatrix} 1598.9554 & 17112.007 \\ 17112.007 & 811208.45 \end{pmatrix}$$

where the corresponding Planck18/ΛCDM values for R and l_a are presented in Table A.1. Furthermore, we present the full dataset of the BAO and CC likelihoods used in the Mathematica analysis in Tables A.2 and A.3 respectively.

Table A.1: The CMB Distance Prior data for a flat Universe used in our analysis.

Index	CMB Observable	CMB Value	Reference
1	R	1.74963	[228]
2	l_a	301.80845	[228]

Table A.2: The BAO data that have been used in the analysis along with the corresponding references.

Index	z	D_A/r_s (Mpc)	$D_H/r_s(km/sec \cdot Mpc)$	D_V/r_s (Mpc)	Ref.
1	0.106	-	-	2.98 ± 0.13	[209]
2	0.44	-	-	13.69 ± 5.82	[353]
3	0.6	-	-	13.77 ± 3.11	[353]
4	0.73	-	-	16.89 ± 5.28	[353]
5	2.34	11.28 ± 0.65	-	-	[354]
6	2.34	-	9.18 ± 0.28	-	[354]
7	0.15	-	-	4.465 ± 0.168	[210]
8	0.32	-	-	8.62 ± 0.15	[355]
9	0.57	-	-	13.7 ± 0.12	[355]

Table A.3: The Cosmic Chronometer data that have been used in the analysis.

Index	z	$H(z)(km/sec \cdot Mpc)$	Ref.
1	0.09	69 ± 12	[356]
2	0.17	83 ± 8	[357]
3	0.179	75 ± 4	[358]
4	0.199	75 ± 5	[358]
5	0.27	77 ± 14	[357]
6	0.352	83 ± 14	[358]
7	0.3802	83 ± 13.5	[359]
8	0.4	95 ± 17	[357]
9	0.4004	77 ± 10.2	[359]
10	0.4247	87.1 ± 11.2	[359]
11	0.4497	92.8 ± 12.9	[359]
12	0.4783	80.9 ± 9	[359]
13	0.48	97 ± 62	[360]
14	0.593	104 ± 13	[358]
15	0.68	92 ± 8	[358]
16	0.781	105 ± 12	[358]
17	0.875	125 ± 17	[361]
18	0.88	90 ± 40	[360]
19	0.9	117 ± 23	[357]
20	1.037	154 ± 20	[358]
21	1.3	168 ± 17	[357]
22	1.363	160 ± 33.6	[362]
23	1.43	177 ± 18	[357]
24	1.53	140 ± 14	[357]
25	1.75	202 ± 40	[357]
26	1.965	186.5 ± 50.4	[362]
27	0.35	82.7 ± 8.4	[363]
28	0.44	82.6 ± 7.8	[364]
29	0.57	96.8 ± 3.4	[355]
30	0.6	87.9 ± 6.1	[364]
31	0.73	97.3 ± 7	[364]
32	2.34	222 ± 7	[365]
33	0.07	69 ± 19.6	[361]
34	0.12	68.6 ± 26.2	[361]
35	0.2	72.9 ± 29.6	[361]
36	0.24	79.69 ± 2.65	[288]
37	0.28	88.8 ± 36.6	[361]
38	0.43	86.45 ± 3.68	[288]
39	0.57	92.4 ± 4.5	[366]
40	2.3	224 ± 8	[367]
41	2.36	226 ± 8	[368]

A.2 The Tully-Fisher Data Compilation of Chapter 5

Table A.4: The robust compilation of galaxy data found in Refs. [277, 300–302].

Galaxy Name	$\log v_{rot}$ (km/s)	$\sigma_{\log v_{rot}}$ (km/s)	$\log M_B$ $(M_\odot)$	$\sigma_{\log M_B}$ $(M_\odot)$	D (Mpc)	σ_D (Mpc)
D631-7	1.76	0.03	8.68	0.05	7.72	0.39
DDO154	1.67	0.02	8.59	0.06	4.04	0.2
DDO161	1.82	0.03	9.32	0.26	7.5	2.25
DDO168	1.73	0.03	8.81	0.06	4.25	0.21
DDO170	1.78	0.03	9.1	0.26	15.4	4.62
ESO079-G014	2.24	0.01	10.48	0.24	28.7	7.17
ESO116-G012	2.04	0.02	9.55	0.27	13.	3.9
ESO563-G021	2.5	0.02	11.27	0.16	60.8	9.1
F568-V1	2.05	0.11	9.72	0.1	80.6	8.06
F571-8	2.15	0.02	9.87	0.19	53.3	10.7
F574-1	1.99	0.04	9.9	0.1	96.8	9.68
F583-1	1.93	0.04	9.52	0.22	35.4	8.85
IC2574	1.82	0.04	9.28	0.06	3.91	0.2
IC4202	2.38	0.02	11.03	0.13	100.4	10.
KK98-251	1.53	0.03	8.29	0.26	6.8	2.04
NGC0024	2.03	0.04	9.45	0.09	7.3	0.36
NGC0055	1.93	0.03	9.64	0.08	2.11	0.11
NGC0100	1.94	0.04	9.63	0.27	18.45	0.2
NGC0247	2.02	0.04	9.78	0.08	3.7	0.19
NGC0289	2.21	0.05	10.86	0.22	20.8	5.2
NGC0300	1.97	0.09	9.43	0.08	2.08	0.1
NGC0801	2.34	0.01	11.27	0.13	80.7	8.07
NGC0891	2.33	0.01	10.88	0.11	9.91	0.5
NGC1003	2.04	0.02	10.05	0.26	11.4	3.42
NGC1090	2.22	0.02	10.68	0.23	37.	9.25
NGC2403	2.12	0.02	9.97	0.08	3.16	0.16
NGC2683	2.19	0.03	10.62	0.11	9.81	0.49
NGC2841	2.45	0.02	11.03	0.13	14.1	1.4
NGC2903	2.27	0.02	10.65	0.28	6.6	1.98
NGC2915	1.92	0.04	9.	0.06	4.06	0.2
NGC2976	1.93	0.05	9.28	0.11	3.58	0.18
NGC2998	2.32	0.02	11.03	0.15	68.1	10.2
NGC3109	1.82	0.03	8.86	0.06	1.33	0.07
NGC3198	2.18	0.01	10.53	0.11	13.8	1.4
NGC3521	2.33	0.03	10.68	0.28	7.7	2.3
NGC3726	2.23	0.03	10.64	0.15	18.	2.5
NGC3741	1.7	0.03	8.41	0.06	3.21	0.17
NGC3769	2.07	0.04	10.22	0.14	18.	2.5
NGC3877	2.23	0.02	10.58	0.16	18.	2.5

NGC3893	2.25	0.04	10.57	0.15	18.	2.5
NGC3917	2.13	0.02	10.13	0.15	18.	2.5
NGC3949	2.21	0.04	10.37	0.15	18.	2.5
NGC3953	2.34	0.02	10.87	0.16	18.	2.5
NGC3972	2.12	0.02	9.94	0.15	18.	2.5
NGC3992	2.38	0.02	11.13	0.13	23.7	2.3
NGC4010	2.1	0.02	10.09	0.14	18.	2.5
NGC4013	2.24	0.02	10.64	0.16	18.	2.5
NGC4051	2.2	0.03	10.71	0.16	18.	2.5
NGC4085	2.12	0.02	10.1	0.15	18.	2.5
NGC4088	2.24	0.02	10.81	0.15	18.	2.5
NGC4100	2.2	0.02	10.53	0.15	18.	2.5
NGC4138	2.17	0.05	10.38	0.16	18.	2.5
NGC4157	2.27	0.02	10.8	0.15	18.	2.5
NGC4183	2.04	0.03	10.	0.14	18.	2.5
NGC4217	2.26	0.02	10.66	0.16	18.	2.5
NGC4559	2.08	0.02	10.24	0.27	7.31	0.2
NGC5005	2.42	0.04	10.96	0.13	16.9	1.5
NGC5033	2.29	0.01	10.85	0.27	15.7	4.7
NGC5055	2.26	0.03	10.96	0.1	9.9	0.5
NGC5371	2.32	0.02	11.27	0.24	39.7	9.92
NGC5585	1.96	0.02	9.57	0.27	7.06	2.12
NGC5907	2.33	0.01	11.06	0.1	17.3	0.9
NGC5985	2.47	0.02	11.08	0.24	50.35	0.2
NGC6015	2.19	0.02	10.38	0.27	17.	5.1
NGC6195	2.40	0.03	11.35	0.13	127.8	12.8
NGC6503	2.07	0.01	9.94	0.09	6.26	0.31
NGC6674	2.38	0.03	11.18	0.19	51.2	10.2
NGC6946	2.20	0.04	10.61	0.28	5.52	1.66
NGC7331	2.38	0.01	11.15	0.13	14.7	1.5
NGC7814	2.34	0.01	10.59	0.11	14.4	0.72
UGC00128	2.12	0.05	10.2	0.14	64.5	9.7
UGC00731	1.87	0.02	9.41	0.26	12.5	3.75
UGC01281	1.75	0.03	8.75	0.06	5.27	0.1
UGC02259	1.94	0.03	9.18	0.26	10.5	3.1
UGC02487	2.52	0.05	11.43	0.16	69.1	10.4
UGC02885	2.46	0.02	11.41	0.12	80.6	8.06
UGC02916	2.26	0.04	10.97	0.15	65.4	9.8
UGC02953	2.42	0.03	11.15	0.28	16.5	4.95
UGC03205	2.34	0.02	10.84	0.2	50.	10.
UGC03546	2.29	0.03	10.73	0.24	28.7	7.2
UGC03580	2.10	0.02	10.09	0.23	20.7	5.2
UGC04278	1.96	0.03	9.33	0.26	12.59	0.2
UGC04325	1.96	0.03	9.28	0.27	9.6	2.88
UGC04499	1.86	0.03	9.35	0.26	12.5	3.75
UGC05253	2.33	0.04	11.03	0.23	22.9	5.72

UGC05716	1.87	0.06	9.24	0.22	21.3	5.3
UGC05721	1.9	0.04	9.01	0.26	6.18	1.85
UGC05986	2.05	0.02	9.77	0.27	8.63	2.59
UGC06399	1.93	0.03	9.31	0.14	18.	2.5
UGC06446	1.92	0.04	9.37	0.26	12.	3.6
UGC06614	2.3	0.11	10.96	0.12	88.7	8.87
UGC06667	1.92	0.02	9.25	0.13	18.	2.5
UGC06786	2.34	0.02	10.64	0.24	29.3	7.32
UGC06787	2.4	0.01	10.75	0.24	21.3	5.32
UGC06818	1.85	0.04	9.35	0.13	18.	2.5
UGC06917	2.04	0.03	9.79	0.14	18.	2.5
UGC06923	1.90	0.03	9.4	0.14	18.	2.5
UGC06930	2.03	0.07	9.94	0.13	18.	2.5
UGC06983	2.04	0.03	9.82	0.13	18.	2.5
UGC07125	1.81	0.03	9.88	0.26	19.8	5.9
UGC07151	1.87	0.02	9.29	0.08	6.87	0.34
UGC07399	2.01	0.03	9.2	0.27	8.43	2.53
UGC07524	1.9	0.03	9.55	0.06	4.74	0.24
UGC07603	1.79	0.02	8.73	0.26	4.7	1.41
UGC07690	1.76	0.06	8.98	0.27	8.11	2.43
UGC08286	1.92	0.01	9.17	0.06	6.5	0.33
UGC08490	1.9	0.03	9.17	0.11	4.65	0.53
UGC08550	1.76	0.02	8.72	0.26	6.7	2.
UGC08699	2.26	0.03	10.48	0.24	39.3	9.82
UGC09037	2.18	0.04	10.78	0.11	83.6	8.4
UGC09133	2.36	0.04	11.27	0.19	57.1	11.4
UGC10310	1.85	0.08	9.39	0.27	15.2	4.6
UGC11455	2.43	0.01	11.31	0.16	78.6	11.8
UGC11914	2.46	0.07	10.88	0.28	16.9	5.1
UGC12506	2.37	0.03	11.07	0.11	100.6	10.1
UGC12632	1.86	0.03	9.47	0.26	9.77	2.93
UGCA442	1.75	0.03	8.62	0.06	4.35	0.22
UGCA444	1.57	0.07	7.98	0.06	0.98	0.05

APPENDIX B

Numerical Calculations

B.1 Maximum Likelihood Analysis

We present the Mathematica code that was used in the data analysis of cosmological models in the context of the CMB-shift, Cosmic Chronometers, BAO and Pantheon datasets. The code is written using the nCPL parametrization as an example. First we define some theoretical quantities and subsequently we calculate the χ^2 expressions in each case, before using them to define the total χ^2 for our example.

B.1.1 Essential Theoretical Expressions

```
(* nCPL Dark Energy Model *)
wcpl[a_, w0_, wa_, n_] := w0 + wa (1 - a)^n

fcpl[a_, w0_, wa_, n_] :=  a^(-3 (1 + w0 + wa)) E^(-3 wa
   HarmonicNumber[n] + 3 a n wa HypergeometricPFQ[{1, 1, 1 - n}, {2, 2},
   a])
Hcpl[a_?NumberQ, om_?NumberQ, w0_?NumberQ, wa_?NumberQ, n_?NumberQ,
   h_?NumberQ] := 100 h Sqrt[a^-3 om (1 + aeq[om, h]/a) + (1 - om (1 +
   aeq[om, h])) fcpl[a, w0, wa, n]]

(* Comoving sound horizon at drag redshift *)
rscpl[ze_, om_?NumberQ, obh2_?NumberQ, w0_?NumberQ, wa_?NumberQ,
  n_?NumberQ, h_?NumberQ] :=  NIntegrate[cs[x, obh2]/( x^2 Hcpl[x, om,
   w0, wa, n, h]), {x, 10^-11, 1/(1 + ze[om, obh2, h])}]

Clear[DLsolcpl, DLcpl, dLcpl]
DLsolcpl[om_?NumberQ, w0_?NumberQ, wa_?NumberQ, n_?NumberQ,
   h_?NumberQ]:= (DLsolcpl[om, w0, wa, n, h] =
   NDSolve[{D[dLcpl[zz]/(1 + zz), zz] == 1/(Hcpl[1/(1 + zz), om, w0, wa,
   n, h]/(100 h)), dLcpl[0] == 0}, dLcpl, {zz, 0, 1300}, MaxSteps ->
   Infinity])
DLcpl[z_?NumberQ, om_?NumberQ, w0_?NumberQ, wa_?NumberQ, n_?NumberQ,
   h_?NumberQ] := (c/(100 h) dLcpl[z] /. DLsolcpl[om, w0, wa, n,
   h])[[1]] // Chop
```

```
15
16 (* Angular diameter distance with curvature, see arxiv:0803.0547  *)
17 DAcpl[z_?NumberQ, om_?NumberQ, w0_?NumberQ, wa_?NumberQ, n_?NumberQ,
      h_?NumberQ] := 1/(1 + z)^2 DLcpl[z, om, w0, wa, n, h]
18
19 baodacpl[z_, om_, w0_, wa_, n_, h_] := DAcpl[z, om, w0, wa, n, h]
      (rscpl[zdrag, om0pl, obh2pl, -1, 0, 1, h0pl]/rscpl[zdrag, om, obh2pl,
      w0, wa, n, h]);
20
21 (* Dilation scale *)
22 Dvcpl[zbao_, om_?NumberQ, w0_?NumberQ, wa_?NumberQ, n_?NumberQ,
      h_?NumberQ] := ((DLcpl[zbao, om, w0, wa, n, h] /(1 + zbao))^2
      (c*zbao)/Hcpl[1/(1 + zbao), om, w0, wa, n, h])^(1/3)
23
24 (* BAO dz ratio *)
25 dzcpl[zbao_, om_, obh2_, w0_, wa_, n_, h_] := rscpl[zdrag, om, obh2, w0,
      wa, n, h]/Dvcpl[zbao, om, w0, wa, n, h]
26
27 (* DH "distance" *)
28 DHcpl[z_?NumberQ, om_?NumberQ, w0_?NumberQ, wa_?NumberQ, n_?NumberQ,
      h_?NumberQ] := c/Hcpl[1/(1 + z), om, w0, wa, n, h]
29
30 hzcpl[z_, om_, w0_, wa_, n_, h_] := Hcpl[1/(1 + z), om, w0, wa, n, h]
31 baodvcpl[z_, om_, w0_, wa_, n_, h_] := rscpl[zdrag, om0pl, obh2pl, -1,
      0, 1, h0pl]/ dzcpl[z, om, obh2pl, w0, wa, n, h];
32
33 (* Scaled distance at recombination *)
34 Rcpl[om_, obh2_, w0_, wa_, n_, h_] := Sqrt[om (100 h)^2] DAcpl[zcmb[om,
      obh2, h], om, w0, wa, n, h] (1 + zcmb[om, obh2, h])/c
35
36 (* Angular scale of sound horizon at recombination *)
37 lacpl[om_, obh2_, w0_, wa_, n_, h_] := \[Pi] (DAcpl[zcmb[om, obh2, h],
      om, w0, wa, n, h] (1 + zcmb[om, obh2, h]))/(rscpl[zcmb, om, obh2, w0,
      wa, n, h])
```

B.1.2 Calculation of χ^2 for CMB-shift Data

```
1 veccpl[om_, obh2_, w0_, wa_, n_, h_] := {Rcpl[om, obh2, w0, wa, n, h] -
      datacmb[[1]], lacpl[om, obh2, w0, wa, n, h] - datacmb[[2]], obh2 -
      datacmb[[3]]};
2 chi2Rcpl[om_, obh2_, w0_, wa_, n_, h_] := veccpl[om, obh2, w0, wa, n,
      h].invcovcmb.veccpl[om, obh2, w0, wa, n, h]
```

B.1.3 Calculation of χ^2 for Cosmic Chronometer Data

```
chi2cccpl[om_?NumberQ, w0_?NumberQ, wa_?NumberQ, n_?NumberQ, h_?NumberQ]
   :=  Sum[(1/dataHz[[i,3]] (dataHz[[i, 2]] - hzcpl[dataHz[[i, 1]], om,
   w0, wa, n, h]))^2, {i, 1, Length[dataHz]}];
```

B.1.4 Calculation of χ^2 for BAO Data

Here the covariance matrices are tailored to the specific data compilation mentioned in the comments.

```
(* 6dFGs and WiggleZ BAO data, see arxiv:1605.02702 *)
vecbaocpl[om_, obh2_, w0_, wa_, n_, h_] := Table[(databao[[i, 2]] -
   dzcpl[databao[[i, 1]], om, obh2, w0, wa, n, h]), {i, 1,
   Length[databao]}];

(* BAO measurements from Lya are {Da/rs, DH/rs} - arxiv:1904.03400 *)
vecLyacpl[om_, obh2_, w0_, wa_, n_, h_] := {dataLya[[1, 2]] -
   DAcpl[dataLya[[1, 1]], om, w0, wa, n, h]/rscpl[zdrag, om, obh2, w0,
   wa, n, h], dataLya[[2, 2]] - DHcpl[dataLya[[2, 1]], om, w0, wa, n,
   h]/rscpl[zdrag, om, obh2, w0, wa, n, h]};

(* Total BAO chi^2 *)
chi2baocpl[om_, obh2_, w0_, wa_, n_, h_] := vecbaocpl[om, obh2, w0, wa,
   n, h].Cijbaoinv.vecbaocpl[om, obh2, w0, wa, n, h] + Sum[(dataSDSS[[i,
   2]] - 1/dzcpl[dataSDSS[[i, 1]], om, obh2, w0, wa, n, h])^2/
   dataSDSS[[i, 3]]^2, {i, 1, Length[dataSDSS]}] + vecLyacpl[om, obh2,
   w0, wa, n, h].CijLyainv.vecLyacpl[om, obh2, w0, wa, n, h]
```

B.1.5 Calculation of χ^2 for SnIa (Pantheon) Data

```
chi2Panthcpl[M_?NumberQ, om_?NumberQ, w0_?NumberQ, wa_?NumberQ,
   n_?NumberQ] := Module[{Dm}, Dm = Table[dataPanth[[1 + i, 5]] - (M + 5
   Log10[(1 + dataPanth[[1 + i, 3]])/(1 + dataPanth[[1 + i, 2]])
   DLcpl[dataPanth[[1 + i, 2]], om, w0, wa, n, h0]] + 25), {i, 1,
   ndatPanth}]; Dm.InvCovTotal.Dm]
```

B.1.6 Total χ^2

```
(* The total chi^2 is the sum of the individuals calculated above*)
chi2totalcpl[M_?NumberQ, om_?NumberQ, w0_?NumberQ, wa_?NumberQ,
   h_?NumberQ] := chi2Rcpl[om, obh2, w0, wa, 1, h] + chi2baocpl[om,
   obh2, w0, wa, 1, h] + chi2cccpl[om, w0, wa, 1, h] + chi2Panthcpl[M,
   om, w0, wa, 1]
```

B.2 Modifications in MGCAMB: Analysis of Chapter 2

We present, as an example, the modifications done in the MGCAMB core files *params_MG.ini and params.ini for the case of the wCDM model with $w = -1.2$.*

B.2.1 Modified params_MG.ini File

```
###### Part 1. Choose the Modified Growth flag
# MG_flag = 0 :  default GR
# MG_flag = 1 :  pure MG models
# MG_flag = 2 :  alternative MG models
# MG_flag = 3 :  QSA models

MG_flag = 1

# Choose at which time to turn on MG
GRtrans = 0.001d0

###### Part 2.1 - Pure MG models
# pure_MG_flag = 1 : mu, gamma parametrization
# pure_MG_flag = 2 : mu, sigma parametrization
# pure_MG_flag = 3 : Q, R  parametrization

pure_MG_flag = 1


###### Part 2.2 - Alternative MG models
# alt_MG_flag = 1 : Linder Gamma parametrization ( introduced in
   arXiv:0507263 )

alt_MG_flag = 1


###### Part 2.3 - QSA models
# QSA_flag = 1 : f(R)
# QSA_flag = 2 : Symmetron
# QSA_flag = 3 : Dilaton
# QSA_flag = 4 : Hu-Sawicki f(R)

QSA_flag = 4


###### Part 3.1.1. - mu, gamma functions
# mugamma_par = 1 : BZ parametrization    ( introduced in
   arXiv:0809.3791 )
# mugamma_par = 2 : Planck parametrization
# mugamma_par = 3 : Effective Newton's constant

```

```
mugamma_par = 3

#BZ parameters:
B1        = 1.333
lambda1_2   = 1000
B2        = 0.5
lambda2_2   = 1000
ss        = 4

#Planck parameters
E11 = 1
E22 = 1

# Effective Newtons constant
ga = 0
nn = 1


###### Part 3.1.2. - mu, Sigma functions
# musigma_par = 1 : DES parametrization

musigma_par = 1

mu0 = -1
sigma0 = 0


###### Part 3.1.3. - Q,R functions
# QR_par = 1 : (Q,R)        ( introduced in arXiv:1002.4197 )
# QR_par = 2 : (Q0,R0,s)    ( introduced in arXiv:1002.4197 )

QR_par = 1

#Bean parameters :
#(Q,R)
MGQfix=1
MGRfix=1

#(Q0,R0,s)
Qnot=1.
Rnot=1.
sss=0


##### Part 3.2.1 - Linder Gamma
# Linder's gamma :
Linder_gamma = 0.545


```

```
##### Part 3.3.1 - QSA f(R) model
B0 = 1.d-3


##### Part 3.3.2 - QSA Symmetron model
beta_star = 1.0d0
a_star = 0.5d0
xi_star = 0.001d0


##### Part 3.3.3 - QSA Dilaton model
beta0 = 1.d0
xi0 = 0.0001
DilS = 0.24d0
DilR = 1.d0
A2 = 1e3


##### Part 3.3.4 - QSA Hu-Sawicki f(R)
F_R0 = 0.0001d0
FRn = 1.d0


##### Part 4. Parameters for the DE model
# Note that the modification of the background works only for pure MG
   models.
#
# DE_model = 0 : LCDM
# DE_model = 1 : wCDM
# DE_model = 2 : (w0,wa)CDM
# DE_model = 3 : user defined

DE_model = 1

# DE model 1 (choose w0DE) 2 (choose both)
w0DE = -1.2d0
waDE = 0.d0
```

B.2.2 Modified params.ini File

This is the MGCAMB model selection file.

```
DEFAULT(params_MG.ini)

#Parameters for CAMB

#output_root is prefixed to output file names
output_root = mg_wneg12
```

```
7
8  #What to do
9  get_scalar_cls = T
10 get_vector_cls = F
11 get_tensor_cls = F
12 get_transfer   = F
13
14 #if do_lensing then lens_potential_output_file contains the unlensed CMB
       and lensing potential power spectra
15 #and lensed CMB Cls (without tensors) are in lensed_output_file, total
       in lensed_total_output_file.
16 do_lensing     = T
17
18 # 0: linear, 1: non-linear matter power (HALOFIT), 2: non-linear CMB
       lensing (HALOFIT),
19 # 3: both non-linear matter power and CMB lensing (HALOFIT)
20 do_nonlinear = 1
21
22 #Maximum multipole and k*eta.
23 #  Note that C_ls near l_max are inaccurate (about 5%), go to 50 more
       than you need
24 #  Lensed power spectra are computed to l_max_scalar-100
25 #  To get accurate lensed BB need to have l_max_scalar>2000,
       k_eta_max_scalar > 10000
26 #  To get accurate lensing potential you also need k_eta_max_scalar >
       10000
27 #  Otherwise k_eta_max_scalar=2*l_max_scalar usually suffices, or don't
       set to use default
28 l_max_scalar      = 2600
29 k_eta_max_scalar  = 5000
30
31 #  Tensor settings should be less than or equal to the above
32 l_max_tensor      = 1500
33 k_eta_max_tensor  = 3000
34
35 #Main cosmological parameters, neutrino masses are assumed degenerate
36 # If use_phyical set physical densities in baryons, CDM and neutrinos +
       Omega_k
37 use_physical   = T
38 ombh2          = 0.02226
39 omch2          = 0.1195
40 omnuh2         = 0.00064
41 omk            = 0
42 hubble         = 73.6
43
44 #effective equation of state parameter for dark energy
45 w              = -1
46 #constant comoving sound speed of the dark energy (1=quintessence)
47 cs2_lam        = 1
```

```
48
49 #varying w is not supported by default, compile with
      EQUATIONS=equations_ppf to use crossing PPF w-wa model:
50 #wa              = 0
51 ##if use_tabulated_w read (a,w) from the following user-supplied file
      instead of above
52 #use_tabulated_w = F
53 #wafile = wa.dat
54
55 #if use_physical = F set parameters as here
56 #omega_baryon   = 0.0462
57 #omega_cdm      = 0.2538
58 #omega_lambda   = 0.7
59 #omega_neutrino = 0
60
61 temp_cmb           = 2.7255
62 helium_fraction    = 0.24
63
64 #for share_delta_neff = T, the fractional part of massless_neutrinos
      gives the change in the effective number
65 #(for QED + non-instantaneous decoupling)  i.e. the increase in neutrino
      temperature,
66 #so Neff = massless_neutrinos + sum(massive_neutrinos)
67 #For full neutrino parameter details see
      http://cosmologist.info/notes/CAMB.pdf
68 massless_neutrinos = 2.046
69
70 #number of distinct mass eigenstates
71 nu_mass_eigenstates = 1
72 #array of the integer number of physical neutrinos per eigenstate, e.g.
      massive_neutrinos = 2 1
73 massive_neutrinos  = 1
74 #specify whether all neutrinos should have the same temperature,
      specified from fractional part of massless_neutrinos
75 share_delta_neff = T
76 #nu_mass_fractions specifies how Omeganu_h2 is shared between the
      eigenstates
77 #i.e. to indirectly specify the mass of each state; e.g.
      nu_mass_factions= 0.75 0.25
78 nu_mass_fractions = 1
79 #if share_delta_neff = F, specify explicitly the degeneracy for each
      state (e.g. for sterile with different temperature to active)
80 #(massless_neutrinos must be set to degeneracy for massless, i.e.
      massless_neutrinos does then not include Deleta_Neff from massive)
81 #if share_delta_neff=T then degeneracies is not given and set internally
82 #e.g. for massive_neutrinos = 2 1, this gives equal temperature to 4
      neutrinos: nu_mass_degeneracies = 2.030 1.015, massless_neutrinos =
      1.015
83 nu_mass_degeneracies =
```

```
84
85  #Initial power spectrum, amplitude, spectral index and running. Pivot k
       in Mpc^{-1}.
86  initial_power_num         = 1
87  pivot_scalar              = 0.05
88  pivot_tensor              = 0.05
89  scalar_amp(1)             = 2.1e-9
90  scalar_spectral_index(1)  = 0.9626
91  scalar_nrun(1)            = 0
92  scalar_nrunrun(1)         = 0
93  tensor_spectral_index(1)  = 0
94  tensor_nrun(1)            = 0
95  #Three parameterizations (1,2,3) for tensors, see
       http://cosmologist.info/notes/CAMB.pdf
96  tensor_parameterization   = 1
97  #ratio is that of the initial tens/scal power spectrum amplitudes,
       depending on parameterization
98  #for tensor_parameterization == 1, P_T =
       initial_ratio*scalar_amp*(k/pivot_tensor)^tensor_spectral_index
99  #for tensor_parameterization == 2, P_T =
       initial_ratio*P_s(pivot_tensor)*(k/pivot_tensor)^tensor_spectral_index
100 #Note that for general pivot scales and indices,
       tensor_parameterization==2 has P_T depending on n_s
101 initial_ratio(1)          = 1
102 #tensor_amp is used instead if tensor_parameterization == 3, P_T =
       tensor_amp *(k/pivot_tensor)^tensor_spectral_index
103 #tensor_amp(1)             = 4e-10
104
105 #note vector modes use the scalar settings above
106
107
108 #Reionization, ignored unless reionization = T, re_redshift measures
       where x_e=0.5
109 reionization         = T
110
111 re_use_optical_depth = F
112 re_optical_depth     = 0.09
113 #If re_use_optical_depth = F then use following, otherwise ignored
114 re_redshift          = 7.5
115 #width of reionization transition. CMBFAST model was similar to
       re_delta_redshift0.5.
116 re_delta_redshift    = 1.5
117 #re_ionization_frac=-1 sets it to become fully ionized using Yhe to get
       helium contribution
118 #Otherwise x_e varies from 0 to re_ionization_frac
119 re_ionization_frac   = -1
120
121 #Parameters for second reionization of helium
122 re_helium_redshift = 3.5
```

```
re_helium_delta_redshift = 0.5

#RECFAST 1.5.x recombination parameters;
RECFAST_fudge = 1.14
RECFAST_fudge_He = 0.86
RECFAST_Heswitch = 6
RECFAST_Hswitch  = T

# CosmoMC parameters - compile with RECOMBINATION=cosmorec and link to CosmoMC to use these
#
# cosmorec_runmode== 0: CosmoMC run with diffusion
#                    1: CosmoMC run without diffusion
#                    2: RECFAST++ run (equivalent of the original RECFAST version)
#                    3: RECFAST++ run with correction function of Calumba & Thomas, 2010
#
# For 'cosmorec_accuracy' and 'cosmorec_fdm' see CosmoMC for explanation
#-----------------------------------------------------------------------
#cosmorec_runmode        = 0
#cosmorec_accuracy       = 0
#cosmorec_fdm            = 0

#Initial scalar perturbation mode (adiabatic=1, CDM iso=2, Baryon iso=3,
# neutrino density iso =4, neutrino velocity iso = 5)
initial_condition   = 1
#If above is zero, use modes in the following (totally correlated) proportions
#Note: we assume all modes have the same initial power spectrum
initial_vector = -1 0 0 0 0

#For vector modes: 0 for regular (neutrino vorticity mode), 1 for magnetic
vector_mode = 0

#Normalization
COBE_normalize = F
##CMB_outputscale scales the output Culs
#To get MuK^2 set realistic initial amplitude (e.g. scalar_amp(1) = 2.3e-9 above) and
#otherwise for dimensionless transfer functions set scalar_amp(1)=1 and use
#CMB_outputscale = 1
CMB_outputscale = 7.42835025e12

#Transfer function settings, transfer_kmax=0.5 is enough for sigma_8
#transfer_k_per_logint=0 sets sensible non-even sampling;
#transfer_k_per_logint=5 samples fixed spacing in log-k
```

```
#transfer_interp_matterpower =T produces matter power in regular interpolated grid in log k;
# use transfer_interp_matterpower =F to output calculated values (e.g. for later interpolation)
transfer_high_precision = F
transfer_kmax           = 2
transfer_k_per_logint   = 0
transfer_num_redshifts  = 1
transfer_interp_matterpower = T
transfer_redshift(1)    = 0
transfer_filename(1)    = transfer_out.dat
#Matter power spectrum output against k/h in units of h^{-3} Mpc^3
transfer_matterpower(1) = matterpower.dat

#which variable to use for defining the matter power spectrum and sigma8
#main choices are 2: CDM, 7: CDM+baryon+neutrino, 8: CDM+baryon, 9: CDM+baryon+neutrino+de perts
transfer_power_var = 7

#Output files not produced if blank. make camb_fits to use the FITS setting.
scalar_output_file = scalCls.dat
vector_output_file = vecCls.dat
tensor_output_file = tensCls.dat
total_output_file  = totCls.dat
lensed_output_file = lensedCls.dat
lensed_total_output_file  =lensedtotCls.dat
lens_potential_output_file = lenspotentialCls.dat
FITS_filename      = scalCls.fits

#Bispectrum parameters if required; primordial is currently only local model (fnl=1)
#lensing is fairly quick, primordial takes several minutes on quad core
do_lensing_bispectrum = F
do_primordial_bispectrum = F

#1 for just temperature, 2 with E
bispectrum_nfields = 1
#set slice non-zero to output slice b_{bispectrum_slice_base_L L L+delta}
bispectrum_slice_base_L = 0
bispectrum_ndelta=3
bispectrum_delta(1)=0
bispectrum_delta(2)=2
bispectrum_delta(3)=4
#bispectrum_do_fisher estimates errors and correlations between bispectra
#note you need to compile with LAPACK and FISHER defined to use get the Fisher info
bispectrum_do_fisher= F
#Noise is in muK^2, e.g. 2e-4 roughly for Planck temperature
```

```
bispectrum_fisher_noise=0
bispectrum_fisher_noise_pol=0
bispectrum_fisher_fwhm_arcmin=7
#Filename if you want to write full reduced bispectrum (at sampled
   values of l_1)
bispectrum_full_output_file=
bispectrum_full_output_sparse=F
#Export alpha_l(r), beta_l(r) for local non-Gaussianity
bispectrum_export_alpha_beta=F

##Optional parameters to control the computation speed,accuracy and
   feedback

#If feedback_level > 0 print out useful information computed about the
   model
feedback_level = 1

#whether to start output files with comment describing columns
output_file_headers = T

#write out various derived parameters
derived_parameters = T

# 1: curved correlation function, 2: flat correlation function, 3:
   inaccurate harmonic method
lensing_method = 1
accurate_BB = F


#massive_nu_approx: 0 - integrate distribution function
#                   1 - switch to series in velocity weight once
   non-relativistic
massive_nu_approx = 1

#Whether you are bothered about polarization.
accurate_polarization   = T

#Whether you are bothered about percent accuracy on EE from reionization
accurate_reionization   = T

#whether or not to include neutrinos in the tensor evolution equations
do_tensor_neutrinos     = T

#whether you care about accuracy of the neutrino transfers themselves
accurate_massive_neutrino_transfers = F

#Whether to turn off small-scale late time radiation hierarchies (save
   time,v. accurate)
do_late_rad_truncation   = T
```

```
251
252 #Which version of Halofit approximation to use (default currently
       Takahashi):
253 #1. Original Smith et al. (2003; arXiv:astro-ph/0207664) HALOFIT
254 #2. Bird et al. (arXiv:1109.4416) updated HALOFIT
255 #3. Original plus fudge from http://www.roe.ac.uk/jap/haloes/,
256 #4. Takahashi (2012; arXiv:1208.2701) HALOFIT update
257 #5. HMcode (Mead et al. 2016; arXiv 1602.02154)
258 #6. A standard (inaccurate) halo model power spectrum calcultion
259 #7. PKequal (Casarini et al. arXiv:0810.0190, arXiv:1601.07230)
260 #8. HMcode (Mead et al. 2015; arXiv 1505.07833)
261 halofit_version=
262
263 #Computation parameters
264 #if number_of_threads=0 assigned automatically
265 number_of_threads       = 0
266
267 #Default scalar accuracy is about 0.3% (except lensed BB) if
       high_accuracy_default=F
268 #If high_accuracy_default=T the default target accuracy is 0.1% at L>600
       (with boost parameter=1 below)
269 #Try accuracy_boost=2, l_accuracy_boost=2 if you want to check
       stability/even higher accuracy
270 #Note increasing accuracy_boost parameters is very inefficient if you
       want higher accuracy,
271 #but high_accuracy_default is efficient
272
273 high_accuracy_default=T
274
275 #Increase accuracy_boost to decrease time steps, use more k values, etc.
276 #Decrease to speed up at cost of worse accuracy. Suggest 0.8 to 3.
277 accuracy_boost          = 1
278
279 #Larger to keep more terms in the hierarchy evolution.
280 l_accuracy_boost        = 1
281
282 #Increase to use more C_l values for interpolation.
283 #Increasing a bit will improve the polarization accuracy at l up to 200 -
284 #interpolation errors may be up to 3%
285 #Decrease to speed up non-flat models a bit
286 l_sample_boost          = 1
```

Bibliography

[1] A. Einstein, "The Foundation of the General Theory of Relativity," Annalen Phys. **49** no. 7, (1916) 769-822. 1

[2] I. Newton, Philosophiæ Naturalis Principia Mathematica. England, 1687. 1

[3] J. C. Maxwell, "A dynamical theory of the electromagnetic field," Phil. Trans. Roy. Soc. Lond. **155** (1865) 459-512. 1

[4] M. P. Hobson, G. P. Efstathiou, and A. N. Lasenby, General Relativity: An Introduction for Physicists. Cambridge University Press, 2006. 3, 4, 5, 7, 8, 9

[5] C. W. Misner, K. S. Thorne, and J. A. Wheeler, Gravitation. W. H. Freeman, San Francisco, 1973. 3, 4, 7, 8

[6] E. Hubble, "A relation between distance and radial velocity among extra-galactic nebulae," Proceedings of the National Academy of Sciences **15** no. 3, (1929) 168-173. https://www.pnas.org/doi/abs/10.1073/pnas.15.3.168. 4

[7] R. B. Tully, "Origin of the Hubble constant controversy," Nature **334** no. 6179, (July, 1988) 209-212. 5

[8] S. Weinberg, Gravitation and Cosmology: Principles and Applications of the General Theory of Relativity. John Wiley and Sons, New York, 1972. 5

[9] **Supernova Search Team** Collaboration, A. G. Riess et al., "Observational evidence from supernovae for an accelerating universe and a cosmological constant," Astron. J. **116** (1998) 1009-1038, arXiv:astro-ph/9805201. 9

[10] J. F. Navarro, C. S. Frenk, and S. D. White, "The Structure of cold dark matter halos," Astrophys. J. **462** (1996) 563-575, arXiv:astro-ph/9508025. 9

[11] A. R. Liddle and D. H. Lyth, "The Cold dark matter density perturbation," Phys. Rept. **231** (1993) 1-105, arXiv:astro-ph/9303019. 9

[12] B. Moore, F. Governato, T. R. Quinn, J. Stadel, and G. Lake, "Resolving the structure of cold dark matter halos," Astrophys. J. Lett. **499** (1998) L5, arXiv:astro-ph/9709051. 9

[13] A. A. Starobinsky, "A New Type of Isotropic Cosmological Models Without Singularity," Phys. Lett. B **91** (1980) 99–102. 9

[14] A. H. Guth, "The Inflationary Universe: A Possible Solution to the Horizon and Flatness Problems," Phys. Rev. D **23** (1981) 347–356. 9

[15] D. Kazanas, "Dynamics of the Universe and Spontaneous Symmetry Breaking," Astrophys. J. Lett. **241** (1980) L59–L63. 9

[16] A. D. Linde, "A New Inflationary Universe Scenario: A Possible Solution of the Horizon, Flatness, Homogeneity, Isotropy and Primordial Monopole Problems," Phys. Lett. B **108** (1982) 389–393. 9

[17] A. Albrecht and P. J. Steinhardt, "Cosmology for Grand Unified Theories with Radiatively Induced Symmetry Breaking," Phys. Rev. Lett. **48** (1982) 1220–1223. 9

[18] **WMAP** Collaboration, G. Hinshaw et al., "Nine-Year Wilkinson Microwave Anisotropy Probe (WMAP) Observations: Cosmological Parameter Results," Astrophys. J. Suppl. **208** (2013) 19, arXiv:1212.5226 [astro-ph.CO]. 9

[19] **Planck** Collaboration, P. A. R. Ade et al., "Planck 2015 results. XIII. Cosmological parameters," Astron. Astrophys. **594** (2016) A13, arXiv:1502.01589 [astro-ph.CO]. 9

[20] **Planck** Collaboration, N. Aghanim et al., "Planck 2018 results. VI. Cosmological parameters," Astron. Astrophys. **641** (2020) A6, arXiv:1807.06209 [astro-ph.CO]. 9, 15

[21] **SDSS** Collaboration, M. Betoule et al., "Improved cosmological constraints from a joint analysis of the SDSS-II and SNLS supernova samples," Astron. Astrophys. **568** (2014) A22, arXiv:1401.4064 [astro-ph.CO]. 9

[22] D. M. Scolnic et al., "The Complete Light-curve Sample of Spectroscopically Confirmed SNe Ia from Pan-STARRS1 and Cosmological Constraints from the Combined Pantheon Sample," Astrophys. J. **859** no. 2, (2018) 101, arXiv:1710.00845 [astro-ph.CO]. 9, 26, 27, 36, 46

[23] D. Stern, R. Jimenez, L. Verde, M. Kamionkowski, and S. A. Stanford, "Cosmic Chronometers: Constraining the Equation of State of Dark Energy. I: H(z) Measurements," JCAP **02** (2010) 008, arXiv:0907.3149 [astro-ph.CO]. 9

[24] M. Moresco et al., "Improved constraints on the expansion rate of the Universe up to z˜1.1 from the spectroscopic evolution of cosmic chronometers," JCAP **08** (2012) 006, arXiv:1201.3609 [astro-ph.CO]. 9

[25] A. Gómez-Valent and L. Amendola, "H_0 from cosmic chronometers and Type Ia supernovae, with Gaussian Processes and the novel Weighted Polynomial Regression method," JCAP **04** (2018) 051, arXiv:1802.01505 [astro-ph.CO]. 9

[26] **BOSS** Collaboration, S. Alam et al., "The clustering of galaxies in the completed SDSS-III Baryon Oscillation Spectroscopic Survey: cosmological analysis of the DR12 galaxy sample," Mon. Not. Roy. Astron. Soc. **470** no. 3, (2017) 2617-2652, arXiv:1607.03155 [astro-ph.CO]. 9

[27] E. Aubourg et al., "Cosmological implications of baryon acoustic oscillation measurements," Phys. Rev. D **92** no. 12, (2015) 123516, arXiv:1411.1074 [astro-ph.CO]. 9

[28] S. Basilakos and S. Nesseris, "Testing Einstein's gravity and dark energy with growth of matter perturbations: Indications for new physics?," Phys. Rev. D **94** no. 12, (2016) 123525, arXiv:1610.00160 [astro-ph.CO]. 9

[29] A. Quelle and A. L. Maroto, "On the tension between growth rate and CMB data," Eur. Phys. J. C **80** no. 5, (2020) 369, arXiv:1908.00900 [astro-ph.CO]. 9

[30] E. Baxter et al., "Joint measurement of lensing{galaxy correlations using SPT and DES SV data," Mon. Not. Roy. Astron. Soc. **461** no. 4, (2016) 4099-4114, arXiv:1602.07384 [astro-ph.CO]. 9

[31] G. Efstathiou and P. Lemos, "Statistical inconsistencies in the KiDS-450 data set," Mon. Not. Roy. Astron. Soc. **476** no. 1, (2018) 151-157, arXiv:1707.00483 [astro-ph.CO]. 9

[32] D. Rapetti, S. W. Allen, A. Mantz, and H. Ebeling, "Constraints on modified gravity from the observed X-ray luminosity function of galaxy clusters," Mon. Not. Roy. Astron. Soc. **400** (2009) 699, arXiv:0812.2259 [astro-ph]. 9, 47

[33] **DSDD** Collaboration, E. Rozo et al., "Cosmological Constraints from the SDSS maxBCG Cluster Catalog," Astrophys. J. **708** (2010) 645-660, arXiv:0902.3702 [astro-ph.CO]. 9

[34] **Planck** Collaboration, P. A. R. Ade et al., "Planck 2015 results. XXIV. Cosmology from Sunyaev-Zeldovich cluster counts," Astron. Astrophys. **594** (2016) A24, arXiv:1502.01597 [astro-ph.CO]. 9, 15

[35] L. Salvati, M. Douspis, and N. Aghanim, "Constraints from thermal Sunyaev-Zel'dovich cluster counts and power spectrum combined with CMB," Astron. Astrophys. **614** (2018) A13, arXiv:1708.00697 [astro-ph.CO]. 9, 15

[36] **DES** Collaboration, M. Costanzi et al., "Methods for cluster cosmology and application to the SDSS in preparation for DES Year 1 release," Mon. Not. Roy. Astron. Soc. **488** no. 4, (2019) 4779-4800, arXiv:1810.09456 [astro-ph.CO]. 9, 15, 16

[37] E. Di Valentino, O. Mena, S. Pan, L. Visinelli, W. Yang, A. Melchiorri, D. F. Mota, A. G. Riess, and J. Silk, "In the realm of the Hubble tension|a review of solutions," Class. Quant. Grav. **38** no. 15, (2021) 153001, arXiv:2103.01183 [astro-ph.CO]. 10

[38] L. Perivolaropoulos and F. Skara, "Challenges for ΛCDM: An update," arXiv:2105.05208 [astro-ph.CO]. 10, 15

[39] E. Abdalla et al., "Cosmology intertwined: A review of the particle physics, astrophysics, and cosmology associated with the cosmological tensions and anomalies," JHEAp **34** (2022) 49–211, arXiv:2203.06142 [astro-ph.CO]. 10

[40] **Planck** Collaboration, N. Aghanim et al., "Planck 2018 results. VI. Cosmological parameters," Astron. Astrophys. **641** (2020) A6, arXiv:1807.06209 [astro-ph.CO]. 11, 20

[41] A. G. Riess et al., "A Comprehensive Measurement of the Local Value of the Hubble Constant with 1 km/s/Mpc Uncertainty from the Hubble Space Telescope and the SH0ES Team," arXiv:2112.04510 [astro-ph.CO]. 11, 12

[42] **SPT-3G** Collaboration, L. Balkenhol et al., "Constraints on ΛCDM extensions from the SPT-3G 2018 EE and TE power spectra," Phys. Rev. D **104** no. 8, (2021) 083509, arXiv:2103.13618 [astro-ph.CO]. 11

[43] **LIGO Scientific, VIRGO, KAGRA** Collaboration, R. Abbott et al., "GWTC-3: Compact Binary Coalescences Observed by LIGO and Virgo During the Second Part of the Third Observing Run," arXiv:2111.03606 [gr-qc]. 11

[44] **ACT** Collaboration, S. Aiola et al., "The Atacama Cosmology Telescope: DR4 Maps and Cosmological Parameters," JCAP **12** (2020) 047, arXiv:2007.07288 [astro-ph.CO]. 11, 13, 14, 15, 16

[45] M. Moresco et al., "Unveiling the Universe with Emerging Cosmological Probes," arXiv:2201.07241 [astro-ph.CO]. 11

[46] S. Mukherjee, G. Lavaux, F. R. Bouchet, J. Jasche, B. D. Wandelt, S. M. Nissanke, F. Leclercq, and K. Hotokezaka, "Velocity correction for Hubble constant measurements from standard sirens," Astron. Astrophys. **646** (2021) A65, arXiv:1909.08627 [astro-ph.CO]. 11

[47] A. Palmese, C. R. Bom, S. Mucesh, and W. G. Hartley, "A standard siren measurement of the Hubble constant using gravitational wave events from the first three LIGO/Virgo observing runs and the DESI Legacy Survey," arXiv:2111.06445 [astro-ph.CO]. 11

[48] J. Schombert, S. McGaugh, and F. Lelli, "Using the Baryonic Tully{Fisher Relation to Measure H o," Astron. J. **160** no. 2, (2020) 71, arXiv:2006.08615 [astro-ph.CO]. 11, 56

[49] D. Pesce et al., "The Megamaser Cosmology Project. XIII. Combined Hubble constant constraints," Astrophys. J. Lett. **891** no. 1, (2020) L1, arXiv:2001.09213 [astro-ph.CO]. 11, 14

[50] T. de Jaeger, L. Galbany, A. G. Riess, B. E. Stahl, B. J. Shappee, A. V. Filippenko, and W. Zheng, "A 5% measurement of the Hubble constant from Type II supernovae," arXiv:2203.08974 [astro-ph.CO]. 11

[51] J. P. Blakeslee, J. B. Jensen, C.-P. Ma, P. A. Milne, and J. E. Greene, "The Hubble Constant from Infrared Surface Brightness Fluctuation Distances," Astrophys. J. **911** no. 1, (2021) 65, arXiv:2101.02221 [astro-ph.CO]. 11, 14

[52] W. L. Freedman, B. F. Madore, T. Hoyt, I. S. Jang, R. Beaton, M. G. Lee, A. Monson, J. Neeley, and J. Rich, "Calibration of the Tip of the Red Giant Branch (TRGB)," arXiv:2002.01550 [astro-ph.GA]. 11

[53] C. D. Huang, A. G. Riess, W. Yuan, L. M. Macri, N. L. Zakamska, S. Casertano, P. A. Whitelock, S. L. Hoffmann, A. V. Filippenko, and D. Scolnic, "Hubble Space Telescope Observations of Mira Variables in the Type Ia Supernova Host NGC 1559: An Alternative Candle to Measure the Hubble Constant," arXiv:1908.10883 [astro-ph.CO]. 11

[54] **SPT-3G** Collaboration, D. Dutcher et al., "Measurements of the E-mode polarization and temperature-E-mode correlation of the CMB from SPT-3G 2018 data," Phys. Rev. D **104** no. 2, (2021) 022003, arXiv:2101.01684 [astro-ph.CO]. 11, 13

[55] B. F. Madore, "The period-luminosity relation. IV. Intrinsic relations and reddenings for the Large Magellanic Cloud Cepheids.," Astroph. J. **253** (Feb., 1982) 575-579. 12

[56] D. Scolnic et al., "SUPERCAL: CROSS-CALIBRATION OF MULTIPLE PHOTOMETRIC SYSTEMS TO IMPROVE COSMOLOGICAL MEASUREMENTS WITH TYPE ia SUPERNOVAE," The Astrophysical Journal **815** no. 2, (Dec, 2015) 117. https://doi.org/10.1088/0004-637x/815/2/117. 12

[57] A. G. Riess et al., "A 2.4% Determination of the Local Value of the Hubble Constant," Astrophys. J. **826** no. 1, (2016) 56, arXiv:1604.01424 [astro-ph.CO]. 12

[58] J. P. Gardner et al., "The James Webb Space Telescope," Space Sci. Rev. **123** (2006) 485, arXiv:astro-ph/0606175. 13

[59] **eBOSS** Collaboration, S. Alam et al., "Completed SDSS-IV extended Baryon Oscillation Spectroscopic Survey: Cosmological implications from two decades of spectroscopic surveys at the Apache Point Observatory," Phys. Rev. D **103** no. 8, (2021) 083533, arXiv:2007.08991 [astro-ph.CO]. 13

[60] M. M. Ivanov, M. Simonović, and M. Zaldarriaga, "Cosmological Parameters from the BOSS Galaxy Power Spectrum," JCAP **05** (2020) 042, arXiv:1909.05277 [astro-ph.CO]. 13, 15

[61] W. Cardona, M. Kunz, and V. Pettorino, "Determining H_0 with Bayesian hyper-parameters," JCAP **03** (2017) 056, arXiv:1611.06088 [astro-ph.CO]. 14

[62] D. Camarena and V. Marra, "On the use of the local prior on the absolute magnitude of Type Ia supernovae in cosmological inference," Mon. Not. Roy. Astron. Soc. **504** (2021) 5164-5171, arXiv:2101.08641 [astro-ph.CO]. 14, 30, 35, 40, 41, 45, 51

[63] S. Dhawan, S. W. Jha, and B. Leibundgut, "Measuring the Hubble constant with Type Ia supernovae as near-infrared standard candles," Astron. Astrophys. **609** (2018) A72, arXiv:1707.00715 [astro-ph.CO]. 14

[64] S. M. Feeney, D. J. Mortlock, and N. Dalmasso, "Clarifying the Hubble constant tension with a Bayesian hierarchical model of the local distance ladder," Mon. Not. Roy. Astron. Soc. **476** no. 3, (2018) 3861-3882, arXiv:1707.00007 [astro-ph.CO]. 14

[65] L. Breuval et al., "The Milky Way Cepheid Leavitt law based on Gaia DR2 parallaxes of companion stars and host open cluster populations," Astron. Astrophys. **643** (2020) A115, arXiv:2006.08763 [astro-ph.SR]. 14

[66] M. Cantiello et al., "A Precise Distance to the Host Galaxy of the Binary Neutron Star Merger GW170817 Using Surface Brightness Fluctuations," Astrophys. J. Lett. **854** no. 2, (2018) L31, arXiv:1801.06080 [astro-ph.GA]. 14

[67] W. L. Freedman, "Measurements of the Hubble Constant: Tensions in Perspective," Astrophys. J. **919** no. 1, (2021) 16, arXiv:2106.15656 [astro-ph.CO]. 14

[68] G. S. Anand, R. B. Tully, L. Rizzi, A. G. Riess, and W. Yuan, "Comparing Tip of the Red Giant Branch Distance Scales: An Independent Reduction of the Carnegie-Chicago Hubble Program and the Value of the Hubble Constant," arXiv:2108.00007 [astro-ph.CO]. 14

[69] M. J. Reid, J. A. Braatz, J. J. Condon, L. J. Greenhill, C. Henkel, and K. Y. Lo, "The Megamaser Cosmology Project: I. VLBI observations of UGC 3789," Astrophys. J. **695** (2009) 287-291, arXiv:0811.4345 [astro-ph]. 14

[70] **KiDS** Collaboration, M. Asgari et al., "KiDS-1000 Cosmology: Cosmic shear constraints and comparison between two point statistics," 7, 2020. arXiv:2007.15633 [astro-ph.CO]. 14, 15

[71] H. Hildebrandt et al., "KiDS-450: Cosmological parameter constraints from tomographic weak gravitational lensing," Mon. Not. Roy. Astron. Soc. **465** (2017) 1454, arXiv:1606.05338 [astro-ph.CO]. 14, 15, 40, 41

[72] **Planck** Collaboration, P. Ade et al., "Planck 2015 results. XIII. Cosmological parameters," Astron. Astrophys. **594** (2016) A13, arXiv:1502.01589 [astro-ph.CO]. 14, 25, 26, 27

[73] S. Joudaki et al., "KiDS+VIKING-450 and DES-Y1 combined: Cosmology with cosmic shear," Astron. Astrophys. **638** (2020) L1, arXiv:1906.09262 [astro-ph.CO]. 14, 15

[74] R. Arjona, J. García-Bellido, and S. Nesseris, "Cosmological constraints on nonadiabatic dark energy perturbations," Phys. Rev. D **102** no. 10, (2020) 103526, arXiv:2006.01762 [astro-ph.CO]. 14

[75] E. Macaulay, I. K. Wehus, and H. K. Eriksen, "Lower Growth Rate from Recent Redshift Space Distortion Measurements than Expected from Planck," Phys. Rev. Lett. **111** no. 16, (2013) 161301, arXiv:1303.6583 [astro-ph.CO]. 14, 47

[76] S. Nesseris, G. Pantazis, and L. Perivolaropoulos, "Tension and constraints on modified gravity parametrizations of $G_{eff}(z)$ from growth rate and Planck data," Phys. Rev. D **96** no. 2, (2017) 023542, arXiv:1703.10538 [astro-ph.CO]. 14, 45, 47, 48, 50

[77] L. Kazantzidis and L. Perivolaropoulos, "Is gravity getting weaker at low z? Observational evidence and theoretical implications," preprint (arXiv:1907.03176) (2019) , arXiv:1907.03176 [astro-ph.CO]. 14, 40, 41

[78] **Planck** Collaboration, N. Aghanim et al., "Planck 2018 results. V. CMB power spectra and likelihoods," arXiv:1907.12875 [astro-ph.CO]. 14, 16

[79] M. Asgari et al., "KiDS+VIKING-450 and DES-Y1 combined: Mitigating baryon feedback uncertainty with COSEBIs," Astron. Astrophys. **634** (2020) A127, arXiv:1910.05336 [astro-ph.CO]. 15

[80] A. H. Wright, H. Hildebrandt, J. L. van den Busch, C. Heymans, B. Joachimi, A. Kannawadi, and K. Kuijken, "KiDS+VIKING-450: Improved cosmological parameter constraints from redshift calibration with self-organising maps," Astron. Astrophys. **640** (2020) L14, arXiv:2005.04207 [astro-ph.CO]. 15

[81] H. Hildebrandt et al., "KiDS+VIKING-450: Cosmic shear tomography with optical and infrared data," Astron. Astrophys. **633** (2020) A69, arXiv:1812.06076 [astro-ph.CO]. 15

[82] F. Köhlinger et al., "KiDS-450: The tomographic weak lensing power spectrum and constraints on cosmological parameters," Mon. Not. Roy. Astron. Soc. **471** no. 4, (2017) 4412-4435, arXiv:1706.02892 [astro-ph.CO]. 15

[83] **DES** Collaboration, A. Amon et al., "Dark Energy Survey Year 3 results: Cosmology from cosmic shear and robustness to data calibration," Phys. Rev. D **105** no. 2, (2022) 023514, arXiv:2105.13543 [astro-ph.CO]. 15

[84] **DES** Collaboration, L. F. Secco et al., "Dark Energy Survey Year 3 results: Cosmology from cosmic shear and robustness to modeling uncertainty," Phys. Rev. D **105** no. 2, (2022) 023515, arXiv:2105.13544 [astro-ph.CO]. 15

[85] **DES** Collaboration, M. A. Troxel et al., "Dark Energy Survey Year 1 results: Cosmological constraints from cosmic shear," Phys. Rev. D **98** no. 4, (2018) 043528, arXiv:1708.01538 [astro-ph.CO]. 15, 47

[86] T. Hamana et al., "Cosmological constraints from cosmic shear two-point correlation functions with HSC survey first-year data," Publ. Astron. Soc. Jap. **72** no. 1, (2020) Publications of the Astronomical Society of Japan, Volume 72, Issue 1, February 2020, 16, https://doi.org/10.1093/pasj/psz138, arXiv:1906.06041 [astro-ph.CO]. 15

[87] **KiDS, Euclid** Collaboration, A. Loureiro et al., "KiDS & Euclid: Cosmological implications of a pseudo angular power spectrum analysis of KiDS-1000 cosmic shear tomography," arXiv:2110.06947 [astro-ph.CO]. 15, 16

[88] **HSC** Collaboration, C. Hikage et al., "Cosmology from cosmic shear power spectra with Subaru Hyper Suprime-Cam first-year data," Publ. Astron. Soc. Jap. **71** no. 2, (2019) 43, arXiv:1809.09148 [astro-ph.CO]. 15, 16

[89] S. Joudaki et al., "CFHTLenS revisited: assessing concordance with Planck including astrophysical systematics," Mon. Not. Roy. Astron. Soc. **465** no. 2, (2017) 2033-2052, arXiv:1601.05786 [astro-ph.CO]. 15

[90] **DES, SPT** Collaboration, C. Chang et al., "Joint analysis of DES Year 3 data and CMB lensing from SPT and Planck II: Cross-correlation measurements and cosmological constraints," arXiv:2203.12440 [astro-ph.CO]. 15

[91] H. Miyatake et al., "Cosmological inference from the emulator based halo model II: Joint analysis of galaxy-galaxy weak lensing and galaxy clustering from HSC-Y1 and SDSS," arXiv:2111.02419 [astro-ph.CO]. 15

[92] C. García-García, J. R. Zapatero, D. Alonso, E. Bellini, P. G. Ferreira, E.-M. Mueller, A. Nicola, and P. Ruiz-Lapuente, "The growth of density perturbations in the last ∼10 billion years from tomographic large-scale structure data," JCAP **10** (2021) 030, arXiv:2105.12108 [astro-ph.CO]. 15

[93] C. Heymans et al., "KiDS-1000 Cosmology: Multi-probe weak gravitational lensing and spectroscopic galaxy clustering constraints," Astron. Astrophys. **646** (2021) A140, arXiv:2007.15632 [astro-ph.CO]. 15

[94] S. Joudaki et al., "KiDS-450 + 2dFLenS: Cosmological parameter constraints from weak gravitational lensing tomography and overlapping redshift-space galaxy clustering," Mon. Not. Roy. Astron. Soc. **474** no. 4, (2018) 4894-4924, arXiv:1707.06627 [astro-ph.CO]. 15, 40, 41, 47

[95] E. van Uitert et al., "KiDS+GAMA: cosmology constraints from a joint analysis of cosmic shear, galaxy{galaxy lensing, and angular clustering," Mon. Not. Roy. Astron. Soc. **476** no. 4, (2018) 4662-4689, arXiv:1706.05004 [astro-ph.CO]. 15

[96] **DES** Collaboration, T. M. C. Abbott et al., "Dark Energy Survey Year 3 results: Cosmological constraints from galaxy clustering and weak lensing," Phys. Rev. D **105** no. 2, (2022) 023520, arXiv:2105.13549 [astro-ph.CO]. 15

[97] **DES** Collaboration, T. Abbott et al., "Dark Energy Survey year 1 results: Cosmological constraints from galaxy clustering and weak lensing," Phys. Rev. D **98** no. 4, (2018) 043526, arXiv:1708.01530 [astro-ph.CO]. 15, 40, 41

[98] T. Tröster et al., "Cosmology from large-scale structure: Constraining ΛCDM with BOSS," Astron. Astrophys. **633** (2020) L10, arXiv:1909.11006 [astro-ph.CO]. 15

[99] O. H. E. Philcox and M. M. Ivanov, "BOSS DR12 full-shape cosmology: ΛCDM constraints from the large-scale galaxy power spectrum and bispectrum monopole," Phys. Rev. D **105** no. 4, (2022) 043517, arXiv:2112.04515 [astro-ph.CO]. 15

[100] M. M. Ivanov, "Cosmological constraints from the power spectrum of eBOSS emission line galaxies," Phys. Rev. D **104** no. 10, (2021) 103514, arXiv:2106.12580 [astro-ph.CO]. 15

[101] S.-F. Chen, Z. Vlah, and M. White, "A new analysis of galaxy 2-point functions in the BOSS survey, including full-shape information and post-reconstruction BAO," JCAP **02** no. 02, (2022) 008, arXiv:2110.05530 [astro-ph.CO]. 15

[102] M. White et al., "Cosmological constraints from the tomographic cross-correlation of DESI Luminous Red Galaxies and Planck CMB lensing," JCAP **02** no. 02, (2022) 007, arXiv:2111.09898 [astro-ph.CO]. 15

[103] A. Krolewski, S. Ferraro, and M. White, "Cosmological constraints from unWISE and Planck CMB lensing tomography," JCAP **12** no. 12, (2021) 028, arXiv:2105.03421 [astro-ph.CO]. 15

[104] G. F. Lesci et al., "AMICO galaxy clusters in KiDS-DR3: Cosmological constraints from counts and stacked weak lensing," Astron. Astrophys. **659** (2022) A88, arXiv:2012.12273 [astro-ph.CO]. 15

[105] A. B. Mantz et al., "Weighing the giants { IV. Cosmology and neutrino mass," Mon. Not. Roy. Astron. Soc. **446** (2015) 2205-2225, arXiv:1407.4516 [astro-ph.CO]. 15

[106] **DES** Collaboration, T. M. C. Abbott et al., "Dark Energy Survey Year 1 Results: Cosmological constraints from cluster abundances and weak lensing," Phys. Rev. D **102** no. 2, (2020) 023509, arXiv:2002.11124 [astro-ph.CO]. 15

[107] **XXL** Collaboration, F. Pacaud et al., "The XXL Survey: XXV. Cosmological analysis of the C1 cluster number counts," Astron. Astrophys. **620** (2018) A10, arXiv:1810.01624 [astro-ph.CO]. 15

[108] **SPT** Collaboration, S. Bocquet et al., "Cluster Cosmology Constraints from the 2500 deg^2 SPT-SZ Survey: Inclusion of Weak Gravitational Lensing Data from Magellan and the Hubble Space Telescope," Astrophys. J. **878** no. 1, (2019) 55, arXiv:1812.01679 [astro-ph.CO]. 15

[109] R. C. Nunes and S. Vagnozzi, "Arbitrating the S8 discrepancy with growth rate measurements from redshift-space distortions," Mon. Not. Roy. Astron. Soc. **505** no. 4, (2021) 5427-5437, arXiv:2106.01208 [astro-ph.CO]. 15

[110] D. Benisty, "Quantifying the S_8 tension with the Redshift Space Distortion data set," Phys. Dark Univ. **31** (2021) 100766, arXiv:2005.03751 [astro-ph.CO]. 15

[111] L. Kazantzidis and L. Perivolaropoulos, "Evolution of the $f\sigma_8$ tension with the Planck15/ΛCDM determination and implications for modified gravity theories," Phys. Rev. D **97** no. 10, (2018) 103503, arXiv:1803.01337 [astro-ph.CO]. 15, 47

[112] E. Di Valentino and S. Bridle, "Exploring the Tension between Current Cosmic Microwave Background and Cosmic Shear Data," Symmetry **10** no. 11, (2018) 585. 16

[113] C. Heymans et al., "CFHTLenS tomographic weak lensing cosmological parameter constraints: Mitigating the impact of intrinsic galaxy alignments," Mon. Not. Roy. Astron. Soc. **432** (2013) 2433, arXiv:1303.1808 [astro-ph.CO]. 16

[114] A. Edge, W. Sutherland, K. Kuijken, S. Driver, R. McMahon, S. Eales, and J. P. Emerson, "The VISTA Kilo-degree Infrared Galaxy (VIKING) Survey: Bridging the Gap between Low and High Redshift," The Messenger **154** (Dec., 2013) 32-34. 16

[115] M. Zaldarriaga and U. Seljak, "Gravitational lensing effect on cosmic microwave background polarization," Phys. Rev. D **58** (1998) 023003, arXiv:astro-ph/9803150. 16

[116] E. Calabrese, A. Slosar, A. Melchiorri, G. F. Smoot, and O. Zahn, "Cosmic Microwave Weak lensing data as a test for the dark universe," Phys. Rev. D **77** (2008) 123531, arXiv:0803.2309 [astro-ph]. 16

[117] A. de Oliveira-Costa, M. Tegmark, M. Zaldarriaga, and A. Hamilton, "The Significance of the largest scale CMB fluctuations in WMAP," Phys. Rev. D **69** (2004) 063516, arXiv:astro-ph/0307282. 16

[118] D. J. Schwarz, G. D. Starkman, D. Huterer, and C. J. Copi, "Is the low-l microwave background cosmic?," Phys. Rev. Lett. **93** (2004) 221301, arXiv:astro-ph/0403353. 16

[119] C. J. Copi, D. Huterer, D. J. Schwarz, and G. D. Starkman, "On the large-angle anomalies of the microwave sky," Mon. Not. Roy. Astron. Soc. **367** (2006) 79-102, arXiv:astro-ph/0508047. 16

[120] C. Copi, D. Huterer, D. Schwarz, and G. Starkman, "The Uncorrelated Universe: Statistical Anisotropy and the Vanishing Angular Correlation Function in WMAP Years 1-3," Phys. Rev. D **75** (2007) 023507, arXiv:astro-ph/0605135. 16

[121] C. J. Copi, D. Huterer, D. J. Schwarz, and G. D. Starkman, "Large angle anomalies in the CMB," Adv. Astron. **2010** (2010) 847541, arXiv:1004.5602 [astro-ph.CO]. 16

[122] C. J. Copi, D. Huterer, D. J. Schwarz, and G. D. Starkman, "Large-scale alignments from WMAP and Planck," Mon. Not. Roy. Astron. Soc. **449** no. 4, (2015) 3458-3470, arXiv:1311.4562 [astro-ph.CO]. 16

[123] P. Vielva, E. Martinez-Gonzalez, R. B. Barreiro, J. L. Sanz, and L. Cayon, "Detection of non-Gaussianity in the WMAP 1 - year data using spherical wavelets," Astrophys. J. **609** (2004) 22-34, arXiv:astro-ph/0310273. 16

[124] **Planck** Collaboration, P. A. R. Ade et al., "Planck 2013 results. XXIII. Isotropy and statistics of the CMB," Astron. Astrophys. **571** (2014) A23, arXiv:1303.5083 [astro-ph.CO]. 16

[125] **Planck** Collaboration, P. A. R. Ade et al., "Planck 2015 results. XVI. Isotropy and statistics of the CMB," Astron. Astrophys. **594** (2016) A16, arXiv:1506.07135 [astro-ph.CO]. 16

[126] **Planck** Collaboration, Y. Akrami et al., "Planck 2018 results. VII. Isotropy and Statistics of the CMB," Astron. Astrophys. **641** (2020) A7, arXiv:1906.02552 [astro-ph.CO]. 16

[127] E. Di Valentino et al., "Snowmass2021 - Letter of interest cosmology intertwined IV: The age of the universe and its curvature," Astropart. Phys. **131** (2021) 102607, arXiv:2008.11286 [astro-ph.CO]. 17

[128] E. Di Valentino, A. Melchiorri, and J. Silk, "Planck evidence for a closed Universe and a possible crisis for cosmology," Nature Astron. **4** no. 2, (2019) 196-203, arXiv:1911.02087 [astro-ph.CO]. 17

[129] W. Handley, "Curvature tension: evidence for a closed universe," Phys. Rev. D **103** no. 4, (2021) L041301, arXiv:1908.09139 [astro-ph.CO]. 17

[130] R. H. Cyburt, B. D. Fields, and K. A. Olive, "Primordial nucleosynthesis in light of WMAP," Phys. Lett. B **567** (2003) 227-234, arXiv:astro-ph/0302431. 17

[131] M. Asplund, D. L. Lambert, P. E. Nissen, F. Primas, and V. V. Smith, "Lithium isotopic abundances in metal-poor halo stars," Astrophys. J. **644** (2006) 229-259, arXiv:astro-ph/0510636. 17

[132] R. H. Cyburt, B. D. Fields, and K. A. Olive, "An Update on the big bang nucleosynthesis prediction for Li-7: The problem worsens," JCAP **11** (2008) 012, arXiv:0808.2818 [astro-ph]. 17

[133] **LISA Cosmology Working Group** Collaboration, E. Belgacem et al., "Testing modified gravity at cosmological distances with LISA standard sirens," JCAP **07** (2019) 024, arXiv:1906.01593 [astro-ph.CO]. 17

[134] P. Amaro-Seoane et al., "Laser Interferometer Space Antenna," arXiv e-prints (Feb., 2017) arXiv:1702.00786, arXiv:1702.00786 [astro-ph.IM]. 17

[135] M. Maggiore et al., "Science Case for the Einstein Telescope," JCAP **03** (2020) 050, arXiv:1912.02622 [astro-ph.CO]. 17

[136] D. Reitze et al., "Cosmic Explorer: The U.S. Contribution to Gravitational-Wave Astronomy beyond LIGO," Bull. Am. Astron. Soc. **51** no. 7, (2019) 035, arXiv:1907.04833 [astro-ph.IM]. 17

[137] **Euclid Theory Working Group** Collaboration, L. Amendola et al., "Cosmology and fundamental physics with the Euclid satellite," Living Rev. Rel. **16** (2013) 6, arXiv:1206.1225 [astro-ph.CO]. 17

[138] R. Laureijs et al., "Euclid Definition Study Report," arXiv e-prints (Oct., 2011) arXiv:1110.3193, arXiv:1110.3193 [astro-ph.CO]. 17

[139] S. Capozziello, "Curvature quintessence," Int. J. Mod. Phys. D **11** (2002) 483-492, arXiv:gr-qc/0201033. 17

[140] S. M. Carroll, V. Duvvuri, M. Trodden, and M. S. Turner, "Is cosmic speed - up due to new gravitational physics?," Phys. Rev. D **70** (2004) 043528, arXiv:astro-ph/0306438. 17

[141] S. Capozziello, V. F. Cardone, S. Carloni, and A. Troisi, "Curvature quintessence matched with observational data," Int. J. Mod. Phys. D **12** (2003) 1969-1982, arXiv:astro-ph/0307018. 17

[142] G. Allemandi, A. Borowiec, and M. Francaviglia, "Accelerated cosmological models in Ricci squared gravity," Phys. Rev. D **70** (2004) 103503, arXiv:hep-th/0407090. 17

[143] S. Carloni, P. K. S. Dunsby, S. Capozziello, and A. Troisi, "Cosmological dynamics of R**n gravity," Class. Quant. Grav. **22** (2005) 4839-4868, arXiv:gr-qc/0410046. 17

[144] S. Nojiri and S. D. Odintsov, "Introduction to modified gravity and gravitational alternative for dark energy," eConf **C0602061** (2006) 06, arXiv:hep-th/0601213. 17

[145] L. Amendola, D. Polarski, and S. Tsujikawa, "Are f(R) dark energy models cosmologically viable ?," Phys. Rev. Lett. **98** (2007) 131302, arXiv:astro-ph/0603703. 17

[146] S. Capozziello, S. Nojiri, S. D. Odintsov, and A. Troisi, "Cosmological viability of f(R)-gravity as an ideal fluid and its compatibility with a matter dominated phase," Phys. Lett. B **639** (2006) 135-143, arXiv:astro-ph/0604431. 17

[147] V. Faraoni, "Solar System experiments do not yet veto modified gravity models," Phys. Rev. D **74** (2006) 023529, arXiv:gr-qc/0607016. 17

[148] S. Nojiri and S. D. Odintsov, "Modified f(R) gravity consistent with realistic cosmology: From matter dominated epoch to dark energy universe," Phys. Rev. D **74** (2006) 086005, arXiv:hep-th/0608008. 17

[149] L. Amendola, R. Gannouji, D. Polarski, and S. Tsujikawa, "Conditions for the cosmological viability of f(R) dark energy models," Phys. Rev. D **75** (2007) 083504, arXiv:gr-qc/0612180. 17

[150] S. Fay, S. Nesseris, and L. Perivolaropoulos, "Can f(R) Modified Gravity Theories Mimic a LCDM Cosmology?," Phys. Rev. D **76** (2007) 063504, arXiv:gr-qc/0703006. 17

[151] W. Hu and I. Sawicki, "Models of f(R) Cosmic Acceleration that Evade Solar-System Tests," Phys. Rev. D **76** (2007) 064004, arXiv:0705.1158 [astro-ph]. 17

[152] A. A. Starobinsky, "Disappearing cosmological constant in f(R) gravity," JETP Lett. **86** (2007) 157-163, arXiv:0706.2041 [astro-ph]. 17

[153] T. P. Sotiriou and V. Faraoni, "f(R) Theories Of Gravity," Rev. Mod. Phys. **82** (2010) 451-497, arXiv:0805.1726 [gr-qc]. 17

[154] S. Nojiri and S. D. Odintsov, "Dark energy, inflation and dark matter from modified F(R) gravity," TSPU Bulletin **N8(110)** (2011) 7-19, arXiv:0807.0685 [hep-th]. 17

[155] A. De Felice and S. Tsujikawa, "f(R) theories," Living Rev. Rel. **13** (2010) 3, arXiv:1002.4928 [gr-qc]. 17, 47

[156] S. Nojiri and S. D. Odintsov, "Unified cosmic history in modified gravity: from F(R) theory to Lorentz non-invariant models," Phys. Rept. **505** (2011) 59-144, arXiv:1011.0544 [gr-qc]. 17, 75

[157] E. Elizalde, S. Nojiri, S. D. Odintsov, L. Sebastiani, and S. Zerbini, "Non-singular exponential gravity: a simple theory for early- and late-time accelerated expansion," Phys. Rev. D **83** (2011) 086006, arXiv:1012.2280 [hep-th]. 17

[158] A. Aviles, A. Bravetti, S. Capozziello, and O. Luongo, "Updated constraints on f(R) gravity from cosmography," Phys. Rev. D **87** no. 4, (2013) 044012, arXiv:1210.5149 [gr-qc]. 17

[159] S. Basilakos, S. Nesseris, and L. Perivolaropoulos, "Observational constraints on viable f(R) parametrizations with geometrical and dynamical probes," Phys. Rev. **D87** no. 12, (2013) 123529, arXiv:1302.6051 [astro-ph.CO]. 17

[160] M. O'Dwyer, S. E. Joras, and I. Waga, "γ gravity: Steepness control," Phys. Rev. D **88** no. 6, (2013) 063520, arXiv:1305.4654 [astro-ph.CO]. 17

[161] S. D. Odintsov, V. K. Oikonomou, and L. Sebastiani, "Unification of Constant-roll Inflation and Dark Energy with Logarithmic R^2-corrected and Exponential $F(R)$ Gravity," Nucl. Phys. B **923** (2017) 608-632, arXiv:1708.08346 [gr-qc]. 17

[162] A. de la Cruz-Dombriz, P. K. S. Dunsby, S. Kandhai, and D. Sáez-Gómez, "Theoretical and observational constraints of viable f(R) theories of gravity," Phys. Rev. D **93** no. 8, (2016) 084016, arXiv:1511.00102 [gr-qc]. 17

[163] C. Álvarez Luna, S. Basilakos, and S. Nesseris, "Cosmological constraints on γ-gravity models," Phys. Rev. D **98** no. 2, (2018) 023516, arXiv:1805.02926 [astro-ph.CO]. 17

[164] R. Ferraro and F. Fiorini, "Modified teleparallel gravity: Inflation without inflaton," Phys. Rev. D **75** (2007) 084031, arXiv:gr-qc/0610067. 17

[165] G. R. Bengochea and R. Ferraro, "Dark torsion as the cosmic speed-up," Phys. Rev. D **79** (2009) 124019, arXiv:0812.1205 [astro-ph]. 17

[166] E. V. Linder, "Einstein's Other Gravity and the Acceleration of the Universe," Phys. Rev. D **81** (2010) 127301, arXiv:1005.3039 [astro-ph.CO]. [Erratum: Phys.Rev.D 82, 109902 (2010)]. 17

[167] S.-H. Chen, J. B. Dent, S. Dutta, and E. N. Saridakis, "Cosmological perturbations in f(T) gravity," Phys. Rev. D **83** (2011) 023508, arXiv:1008.1250 [astro-ph.CO]. 17

[168] S. Nesseris, S. Basilakos, E. N. Saridakis, and L. Perivolaropoulos, "Viable $f(T)$ models are practically indistinguishable from ΛCDM," Phys. Rev. D **88** (2013) 103010, arXiv:1308.6142 [astro-ph.CO]. 17

[169] Y.-F. Cai, S. Capozziello, M. De Laurentis, and E. N. Saridakis, "f(T) teleparallel gravity and cosmology," Rept. Prog. Phys. **79** no. 10, (2016) 106901, arXiv:1511.07586 [gr-qc]. 17

[170] S. Basilakos, S. Nesseris, F. K. Anagnostopoulos, and E. N. Saridakis, "Updated constraints on $f(T)$ models using direct and indirect measurements of the Hubble parameter," JCAP **08** (2018) 008, arXiv:1803.09278 [astro-ph.CO]. 17

[171] S.-F. Yan, P. Zhang, J.-W. Chen, X.-Z. Zhang, Y.-F. Cai, and E. N. Saridakis, "Interpreting cosmological tensions from the effective field theory of torsional gravity," arXiv:1909.06388 [astro-ph.CO]. 17

[172] C. Escamilla-Rivera and J. Levi Said, "Cosmological viable models in $f(T, B)$ theory as solutions to the H_0 tension," Class. Quant. Grav. **37** no. 16, (2020) 165002, arXiv:1909.10328 [gr-qc]. 17

[173] S. Bahamonde, K. F. Dialektopoulos, C. Escamilla-Rivera, G. Farrugia, V. Gakis, M. Hendry, M. Hohmann, J. L. Said, J. Mifsud, and E. Di Valentino, "Teleparallel Gravity: From Theory to Cosmology," arXiv:2106.13793 [gr-qc]. 17

[174] S. Capozziello, R. de Ritis, and A. A. Marino, "Recovering the effective cosmological constant in extended gravity theories," Gen. Rel. Grav. **30** (1998) 1247-1272, arXiv:gr-qc/9804053. 17

[175] J.-P. Uzan, "Cosmological scaling solutions of nonminimally coupled scalar fields," Phys. Rev. D **59** (1999) 123510, arXiv:gr-qc/9903004. 17

[176] T. Chiba, "Quintessence, the gravitational constant, and gravity," Phys. Rev. D **60** (1999) 083508, arXiv:gr-qc/9903094. 17

[177] L. Amendola, "Scaling solutions in general nonminimal coupling theories," Phys. Rev. D **60** (1999) 043501, arXiv:astro-ph/9904120. 17

[178] F. Perrotta, C. Baccigalupi, and S. Matarrese, "Extended quintessence," Phys. Rev. D **61** (1999) 023507, arXiv:astro-ph/9906066. 17

[179] N. Bartolo and M. Pietroni, "Scalar tensor gravity and quintessence," Phys. Rev. D **61** (2000) 023518, arXiv:hep-ph/9908521. 17

[180] Y. Fujii, "Quintessence, scalar tensor theories and nonNewtonian gravity," Phys. Rev. D **62** (2000) 044011, arXiv:gr-qc/9911064. 17

[181] B. Boisseau, G. Esposito-Farese, D. Polarski, and A. A. Starobinsky, "Reconstruction of a scalar tensor theory of gravity in an accelerating universe," Phys. Rev. Lett. **85** (2000) 2236, arXiv:gr-qc/0001066. 17

[182] G. Esposito-Farese and D. Polarski, "Scalar tensor gravity in an accelerating universe," Phys. Rev. D **63** (2001) 063504, arXiv:gr-qc/0009034. 17

[183] L. Perivolaropoulos, "Crossing the phantom divide barrier with scalar tensor theories," JCAP **10** (2005) 001, arXiv:astro-ph/0504582. 17, 28, 42

[184] A. Coc, K. A. Olive, J.-P. Uzan, and E. Vangioni, "Big bang nucleosynthesis constraints on scalar-tensor theories of gravity," Phys. Rev. D **73** (2006) 083525, arXiv:astro-ph/0601299. 17

[185] S. Nesseris and L. Perivolaropoulos, "The Limits of Extended Quintessence," Phys. Rev. D **75** (2007) 023517, arXiv:astro-ph/0611238. 17

[186] S. Vagnozzi, "New physics in light of the H_0 tension: An alternative view," Phys. Rev. D **102** no. 2, (2020) 023518, arXiv:1907.07569 [astro-ph.CO]. 18, 21, 30, 33

[187] E. Di Valentino, A. Melchiorri, and J. Silk, "Reconciling Planck with the local value of H_0 in extended parameter space," Phys. Lett. B **761** (2016) 242-246, arXiv:1606.00634 [astro-ph.CO]. 18, 21, 27, 30, 33

[188] Q.-G. Huang and K. Wang, "How the dark energy can reconcile Planck with local determination of the Hubble constant," Eur. Phys. J. C **76** no. 9, (2016) 506, arXiv:1606.05965 [astro-ph.CO]. 18

[189] E. Di Valentino, A. Melchiorri, E. V. Linder, and J. Silk, "Constraining Dark Energy Dynamics in Extended Parameter Space," Phys. Rev. D **96** no. 2, (2017) 023523, arXiv:1704.00762 [astro-ph.CO]. 18, 45

[190] W. Yang, S. Pan, E. Di Valentino, E. N. Saridakis, and S. Chakraborty, "Observational constraints on one-parameter dynamical dark-energy parametrizations and the H_0 tension," Phys. Rev. D **99** no. 4, (2019) 043543, arXiv:1810.05141 [astro-ph.CO]. 18

[191] X. Li and A. Shafieloo, "A Simple Phenomenological Emergent Dark Energy Model can Resolve the Hubble Tension," Astrophys. J. Lett. **883** (2019) L3, arXiv:1906.08275 [astro-ph.CO]. 18, 23, 30

[192] X. Li and A. Shafieloo, "Evidence for Emergent Dark Energy," Astrophys. J. **902** no. 1, (2020) 58, arXiv:2001.05103 [astro-ph.CO]. 18

[193] M. Rezaei, T. Naderi, M. Malekjani, and A. Mehrabi, "A Bayesian comparison between ΛCDM and phenomenologically emergent dark energy models," Eur. Phys. J. C **80** no. 5, (2020) 374, arXiv:2004.08168 [astro-ph.CO]. 18

[194] G. Efstathiou and J. Bond, "Cosmic confusion: Degeneracies among cosmological parameters derived from measurements of microwave background anisotropies," Mon. Not. Roy. Astron. Soc. **304** (1999) 75-97, arXiv:astro-ph/9807103. 19, 46

[195] O. Elgaroy and T. Multamaki, "On using the CMB shift parameter in tests of models of dark energy," Astron. Astrophys. **471** (2007) 65, arXiv:astro-ph/0702343. 19, 36, 46

[196] W. Hu and N. Sugiyama, "Small scale cosmological perturbations: An Analytic approach," Astrophys. J. **471** (1996) 542-570, arXiv:astro-ph/9510117. 19

[197] Y. Wang and P. Mukherjee, "Robust dark energy constraints from supernovae, galaxy clustering, and three-year wilkinson microwave anisotropy probe observations," Astrophys. J. **650** (2006) 1-6, arXiv:astro-ph/0604051. 19

[198] G. Alestas, L. Kazantzidis, and L. Perivolaropoulos, "H_0 tension, phantom dark energy, and cosmological parameter degeneracies," Phys. Rev. D **101** no. 12, (2020) 123516, arXiv:2004.08363 [astro-ph.CO]. 20, 21, 22, 23, 25, 26, 27, 30, 33, 36, 44, 45, 46, 53

[199] M. Chevallier and D. Polarski, "Accelerating universes with scaling dark matter," Int. J. Mod. Phys. D **10** (2001) 213-224, arXiv:gr-qc/0009008. 22, 44

[200] E. V. Linder, "Exploring the expansion history of the universe," Phys. Rev. Lett. **90** (2003) 091301, arXiv:astro-ph/0208512. 22, 44

[201] A. G. Riess, S. Casertano, W. Yuan, L. M. Macri, and D. Scolnic, "Large Magellanic Cloud Cepheid Standards Provide a 1% Foundation for the Determination of the Hubble Constant and Stronger Evidence for Physics beyond ΛCDM," Astrophys. J. **876** no. 1, (2019) 85, arXiv:1903.07603 [astro-ph.CO]. 22, 25, 26, 27

[202] L. Kazantzidis, L. Perivolaropoulos, and F. Skara, "Constraining power of cosmological observables: blind redshift spots and optimal ranges," Phys. Rev. D **99** no. 6, (2019) 063537, arXiv:1812.05356 [astro-ph.CO]. 23

[203] G. Benevento, W. Hu, and M. Raveri, "Can Late Dark Energy Transitions Raise the Hubble constant?," ArXiv e-prints (Feb, 2020) , 2002.11707. 23

[204] G.-B. Zhao, L. Pogosian, A. Silvestri, and J. Zylberberg, "Searching for modified growth patterns with tomographic surveys," Phys. Rev. D **79** (2009) 083513, arXiv:0809.3791 [astro-ph]. 24

[205] A. Hojjati, L. Pogosian, and G.-B. Zhao, "Testing gravity with CAMB and CosmoMC," JCAP **08** (2011) 005, arXiv:1106.4543 [astro-ph.CO]. 24

[206] A. Zucca, L. Pogosian, A. Silvestri, and G.-B. Zhao, "MGCAMB with massive neutrinos and dynamical dark energy," JCAP **05** (2019) 001, arXiv:1901.05956 [astro-ph.CO]. 24

[207] B. Sagredo, S. Nesseris, and D. Sapone, "Internal Robustness of Growth Rate data," Phys. Rev. D **98** no. 8, (2018) 083543, arXiv:1806.10822 [astro-ph.CO]. 26, 45, 50

[208] F. Skara and L. Perivolaropoulos, "Tension of the E_G statistic and redshift space distortion data with the Planck - ΛCDM model and implications for weakening gravity," Phys. Rev. D **101** no. 6, (2020) 063521, arXiv:1911.10609 [astro-ph.CO]. 26, 40, 41, 48

[209] F. Beutler, C. Blake, M. Colless, D. Jones, L. Staveley-Smith, L. Campbell, Q. Parker, W. Saunders, and F. Watson, "The 6dF Galaxy Survey: Baryon Acoustic Oscillations and the Local Hubble Constant," Mon. Not. Roy. Astron. Soc. **416** (2011) 3017-3032, arXiv:1106.3366 [astro-ph.CO]. 26, 27, 46, 68, 81

[210] A. J. Ross, L. Samushia, C. Howlett, W. J. Percival, A. Burden, and M. Manera, "The clustering of the SDSS DR7 main Galaxy sample - I. A 4 per cent distance measure at $z = 0.15$," Mon. Not. Roy. Astron. Soc. **449** no. 1, (2015) 835-847, arXiv:1409.3242 [astro-ph.CO]. 26, 27, 46, 81

[211] **BOSS** Collaboration, S. Alam et al., "The clustering of galaxies in the completed SDSS-III Baryon Oscillation Spectroscopic Survey: cosmological analysis of the DR12 galaxy sample," Mon. Not. Roy. Astron. Soc. **470** no. 3, (2017) 2617-2652, arXiv:1607.03155 [astro-ph.CO]. 26, 27, 46

[212] N. Arendse et al., "Cosmic dissonance: new physics or systematics behind a short sound horizon?," arXiv:1909.07986 [astro-ph.CO]. 26

[213] C.-G. Park and B. Ratra, "Measuring the Hubble constant and spatial curvature from supernova apparent magnitude, baryon acoustic oscillation, and Hubble parameter data," Astrophys. Space Sci. **364** no. 8, (2019) 134, arXiv:1809.03598 [astro-ph.CO]. 27

[214] P. Peebles and B. Ratra, "Cosmology with a Time Variable Cosmological Constant," Astrophys. J. Lett. **325** (1988) L17. 28

[215] B. Ratra and P. Peebles, "Cosmological Consequences of a Rolling Homogeneous Scalar Field," Phys. Rev. D **37** (1988) 3406. 28

[216] I. Zlatev, L.-M. Wang, and P. J. Steinhardt, "Quintessence, cosmic coincidence, and the cosmological constant," Phys. Rev. Lett. **82** (1999) 896-899, arXiv:astro-ph/9807002. 28

[217] T. Chiba, T. Okabe, and M. Yamaguchi, "Kinetically driven quintessence," Phys. Rev. D **62** (2000) 023511, arXiv:astro-ph/9912463. 28

[218] T. L. Smith, V. Poulin, and M. A. Amin, "Oscillating scalar fields and the Hubble tension: a resolution with novel signatures," Phys. Rev. D **101** no. 6, (2020) 063523, arXiv:1908.06995 [astro-ph.CO]. 30

[219] E. Di Valentino, A. Mukherjee, and A. A. Sen, "Dark Energy with Phantom Crossing and the H_0 Tension," Entropy **23** no. 4, (2021) 404, arXiv:2005.12587 [astro-ph.CO]. 30, 45

[220] C. Krishnan, E. O. Colgain, M. Sheikh-Jabbari, and T. Yang, "Running Hubble Tension and a H0 Diagnostic," arXiv:2011.02858 [astro-ph.CO]. 30

[221] M. J. Mortonson, W. Hu, and D. Huterer, "Hiding dark energy transitions at low redshift," Phys. Rev. D **80** (2009) 067301, arXiv:0908.1408 [astro-ph.CO]. 30

[222] G. Benevento, W. Hu, and M. Raveri, "Can Late Dark Energy Transitions Raise the Hubble constant?," Phys. Rev. D **101** no. 10, (2020) 103517, arXiv:2002.11707 [astro-ph.CO]. 30

[223] S. Dhawan, D. Brout, D. Scolnic, A. Goobar, A. Riess, and V. Miranda, "Cosmological Model Insensitivity of Local H_0 from the Cepheid Distance Ladder," Astrophys. J. **894** no. 1, (2020) 54, arXiv:2001.09260 [astro-ph.CO]. 30

[224] R. E. Keeley, S. Joudaki, M. Kaplinghat, and D. Kirkby, "Implications of a transition in the dark energy equation of state for the H_0 and σ_8 tensions," JCAP **12** (2019) 035, arXiv:1905.10198 [astro-ph.CO]. 30

[225] B. A. Bassett, M. Kunz, J. Silk, and C. Ungarelli, "A Late time transition in the cosmic dark energy?," Mon. Not. Roy. Astron. Soc. **336** (2002) 1217-1222, arXiv:astro-ph/0203383. 30

[226] D. Camarena and V. Marra, "Local determination of the Hubble constant and the deceleration parameter," Phys. Rev. Res. **2** no. 1, (2020) 013028, arXiv:1906.11814 [astro-ph.CO]. 30, 35, 40, 45, 51, 79

[227] G. Alestas, L. Kazantzidis, and L. Perivolaropoulos, "$w - M$ phantom transition at z_t $<$0.1 as a resolution of the Hubble tension," Phys. Rev. D **103** no. 8, (2021) 083517, arXiv:2012.13932 [astro-ph.CO]. 32, 33, 34, 37, 38, 40, 49, 53, 58, 69, 74

[228] Z. Zhai and Y. Wang, "Robust and model-independent cosmological constraints from distance measurements," JCAP **07** (2019) 005, arXiv:1811.07425 [astro-ph.CO]. 36, 81

[229] L. Kazantzidis, H. Koo, S. Nesseris, L. Perivolaropoulos, and A. Shafieloo, "Hints for possible low redshift oscillation around the best-fitting ΛCDM model in the expansion history of the Universe," Mon. Not. Roy. Astron. Soc. **501** no. 3, (2021) 3421-3426, arXiv:2010.03491 [astro-ph.CO]. 39, 40, 41

[230] L. Kazantzidis and L. Perivolaropoulos, "Hints of a Local Matter Underdensity or Modified Gravity in the Low z Pantheon data," Phys. Rev. D **102** no. 2, (2020) 023520, arXiv:2004.02155 [astro-ph.CO]. 39

[231] G. Alestas and L. Perivolaropoulos, "Late-time approaches to the Hubble tension deforming H(z), worsen the growth tension," Mon. Not. Roy. Astron. Soc. **504** no. 3, (2021) 3956, arXiv:2103.04045 [astro-ph.CO]. 39, 47, 49, 50, 51, 52

[232] V. Marra and L. Perivolaropoulos, "Rapid transition of Geff at zt$\simeq$0.01 as a possible solution of the Hubble and growth tensions," Phys. Rev. D **104** no. 2, (2021) L021303, arXiv:2102.06012 [astro-ph.CO]. 40, 53, 58, 66, 69, 71, 74

[233] R. Gannouji, L. Kazantzidis, L. Perivolaropoulos, and D. Polarski, "Consistency of modified gravity with a decreasing $G_{\rm eff}(z)$ in a ΛCDM background," Phys. Rev. D **98** no. 10, (2018) 104044, arXiv:1809.07034 [gr-qc]. 40

[234] R. Gannouji, L. Perivolaropoulos, D. Polarski, and F. Skara, "Weak gravity on a ΛCDM background," Phys. Rev. D **103** no. 6, (2021) 063509, arXiv:2011.01517 [gr-qc]. 40

[235] L. Amendola, M. Kunz, I. D. Saltas, and I. Sawicki, "Fate of Large-Scale Structure in Modified Gravity After GW170817 and GRB170817A," Phys. Rev. Lett. **120** no. 13, (2018) 131101, arXiv:1711.04825 [astro-ph.CO]. 40

[236] B. S. Wright and B. Li, "Type Ia supernovae, standardizable candles, and gravity," Phys. Rev. D **97** no. 8, (2018) 083505, arXiv:1710.07018 [astro-ph.CO]. 41

[237] L. Amendola, P. S. Corasaniti, and F. Occhionero, "Time variability of the gravitational constant and type Ia supernovae," arXiv:astro-ph/9907222. 41

[238] E. Gaztanaga, E. Garcia-Berro, J. Isern, E. Bravo, and I. Dominguez, "Bounds on the possible evolution of the gravitational constant from cosmological type Ia supernovae," Phys. Rev. D **65** (2002) 023506, arXiv:astro-ph/0109299. 41, 67

[239] L. Perivolaropoulos, "Constraints on linear negative potentials in quintessence and phantom models from recent supernova data," Phys. Rev. D **71** (2005) 063503, arXiv:astro-ph/0412308. 42

[240] S. Nesseris and L. Perivolaropoulos, "Crossing the Phantom Divide: Theoretical Implications and Observational Status," JCAP **01** (2007) 018, arXiv:astro-ph/0610092. 42

[241] R. R. Caldwell, M. Kamionkowski, and N. N. Weinberg, "Phantom energy and cosmic doomsday," Phys. Rev. Lett. **91** (2003) 071301, arXiv:astro-ph/0302506. 42

[242] S. Nesseris and L. Perivolaropoulos, "The Fate of bound systems in phantom and quintessence cosmologies," Phys. Rev. D **70** (2004) 123529, arXiv:astro-ph/0410309. 42

[243] E. Elizalde, S. Nojiri, and S. D. Odintsov, "Late-time cosmology in (phantom) scalar-tensor theory: Dark energy and the cosmic speed-up," Phys. Rev. D **70** (2004) 043539, arXiv:hep-th/0405034. 42

[244] A. De Felice, S. Mukohyama, and S. Tsujikawa, "Density perturbations in general modified gravitational theories," Phys. Rev. D **82** (2010) 023524, arXiv:1006.0281 [astro-ph.CO]. 47

[245] S. Tsujikawa, "Matter density perturbations and effective gravitational constant in modified gravity models of dark energy," Phys. Rev. D **76** (2007) 023514, arXiv:0705.1032 [astro-ph]. 47

[246] S. Nesseris and A. Mazumdar, "Newton's constant in f(R,R_{\mu\nu}R^{\mu\nu},\Box R) theories of gravity and constraints from BBN," Phys. Rev. D **79** (2009) 104006, arXiv:0902.1185 [astro-ph.CO]. 47

[247] E. V. Linder and A. Jenkins, "Cosmic structure and dark energy," Mon. Not. Roy. Astron. Soc. **346** (2003) 573, arXiv:astro-ph/0305286. 47

[248] F. Schmidt, "Weak Lensing Probes of Modified Gravity," Phys. Rev. **D78** (2008) 043002, arXiv:0805.4812 [astro-ph]. 47

[249] H. Hildebrandt et al., "KiDS-450: Cosmological parameter constraints from tomographic weak gravitational lensing," Mon. Not. Roy. Astron. Soc. **465** (2017) 1454, arXiv:1606.05338 [astro-ph.CO]. 47

[250] C. Heymans et al., "CFHTLenS: The Canada-France-Hawaii Telescope Lensing Survey," Mon. Not. Roy. Astron. Soc. **427** (2012) 146, arXiv:1210.0032 [astro-ph.CO]. 47

[251] F. Köhlinger et al., "KiDS-450: The tomographic weak lensing power spectrum and constraints on cosmological parameters," Mon. Not. Roy. Astron. Soc. **471** no. 4, (2017) 4412-4435, arXiv:1706.02892 [astro-ph.CO]. 47

[252] **DES** Collaboration, T. M. C. Abbott et al., "Dark Energy Survey year 1 results: Cosmological constraints from galaxy clustering and weak lensing," Phys. Rev. **D98** no. 4, (2018) 043526, arXiv:1708.01530 [astro-ph.CO]. 47

[253] **DES** Collaboration, T. M. C. Abbott et al., "Dark Energy Survey Year 1 Results: Constraints on Extended Cosmological Models from Galaxy Clustering and Weak Lensing," Phys. Rev. **D99** no. 12, (2019) 123505, arXiv:1810.02499 [astro-ph.CO]. 47

[254] **DSDD** Collaboration, E. Rozo et al., "Cosmological Constraints from the SDSS maxBCG Cluster Catalog," Astrophys. J. **708** (2010) 645-660, arXiv:0902.3702 [astro-ph.CO]. 47

[255] **SPT** Collaboration, S. Bocquet et al., "Mass Calibration and Cosmological Analysis of the SPT-SZ Galaxy Cluster Sample Using Velocity Dispersion σ_v and X-ray Y_X Measurements," Astrophys. J. **799** no. 2, (2015) 214, arXiv:1407.2942 [astro-ph.CO]. 47

[256] E. J. Ruiz and D. Huterer, "Testing the dark energy consistency with geometry and growth," Phys. Rev. D **91** (2015) 063009, arXiv:1410.5832 [astro-ph.CO]. 47

[257] L. Samushia et al., "The Clustering of Galaxies in the SDSS-III DR9 Baryon Oscillation Spectroscopic Survey: Testing Deviations from Λ and General Relativity using anisotropic clustering of galaxies," Mon. Not. Roy. Astron. Soc. **429** (2013) 1514-1528, arXiv:1206.5309 [astro-ph.CO]. 47

[258] A. Johnson, C. Blake, J. Dossett, J. Koda, D. Parkinson, and S. Joudaki, "Searching for Modified Gravity: Scale and Redshift Dependent Constraints from Galaxy Peculiar Velocities," Mon. Not. Roy. Astron. Soc. **458** no. 3, (2016) 2725-2744, arXiv:1504.06885 [astro-ph.CO]. 47

[259] E. V. Linder and R. N. Cahn, "Parameterized Beyond-Einstein Growth," Astropart. Phys. **28** (2007) 481-488, arXiv:astro-ph/0701317. 48

[260] S. Basilakos, S. Nesseris, and L. Perivolaropoulos, "Is the CMB shift parameter connected with the growth of cosmological perturbations?," Mon. Not. Roy. Astron. Soc. **387** (2008) 1126-1130, arXiv:0804.1631 [astro-ph]. 48

[261] K. Jedamzik, L. Pogosian, and G.-B. Zhao, "Why reducing the cosmic sound horizon alone can not fully resolve the Hubble tension," Commun. in Phys. **4** (2021) 123, arXiv:2010.04158 [astro-ph.CO]. 52

[262] R. J. Scherrer, "Mapping the Chevallier-Polarski-Linder parametrization onto Physical Dark Energy Models," Phys. Rev. D **92** no. 4, (2015) 043001, arXiv:1505.05781 [astro-ph.CO]. 52

[263] V. C. Busti, A. de la Cruz-Dombriz, P. K. S. Dunsby, and D. Sáez-Gómez, "Is cosmography a useful tool for testing cosmology?," Phys. Rev. D **92** no. 12, (2015) 123512, arXiv:1505.05503 [astro-ph.CO]. 52

[264] G. Alestas, I. Antoniou, and L. Perivolaropoulos, "Hints for a Gravitational Transition in Tully{Fisher Data," Universe **7** no. 10, (2021) 366, arXiv:2104.14481 [astro-ph.CO]. 54, 60, 62, 63, 64, 65, 66, 69

[265] G. Alestas, L. Perivolaropoulos, and K. Tanidis, "Constraining a late time transition of G_{eff} using low-z galaxy survey data," arXiv:2201.05846 [astro-ph.CO]. 54, 69, 70, 71, 72, 73

[266] R. B. Tully and J. R. Fisher, "A New method of determining distances to galaxies," Astron. Astrophys. **54** (1977) 661-673. 55

[267] den Heijer, Milan, Oosterloo, Tom A., Serra, Paolo, Józsa, Gyula I. G., Kerp, Jürgen, Morganti, Raffaella, Cappellari, Michele, Davis, Timothy A., Duc, Pierre-Alain, Emsellem, Eric, Krajnovi´c, Davor, McDermid, Richard M., Naab, Torsten, Weijmans, Anne-Marie, and Tim de Zeeuw, P., "The hully-fisher relation of early-type galaxies," A&A **581** (2015) A98. https://doi.org/10.1051/0004-6361/201526879. 55

[268] S. S. McGaugh, "The baryonic tully-fisher relation of galaxies with extended rotation curves and the stellar mass of rotating galaxies," The Astrophysical Journal **632** no. 2, (Oct, 2005) 859-871. https://doi.org/10.1086/432968. 55

[269] M. Aaronson, J. Huchra, and J. Mould, "The infrared luminosity/H I velocity-width relation and its application to the distance scale.," Astroph. J. **229** (Apr., 1979) 1-13. 55

[270] K. C. Freeman, "On the Disks of Spiral and S0 Galaxies," Astroph. J. **160** (June, 1970) 811. 55

[271] M. A. Zwaan, J. M. van der Hulst, W. J. G. de Blok, and S. S. McGaugh, "The Tully-Fisher relation for low surface brightness galaxies - Implications for galaxy evolution," Mon. Not. Roy. Astron. Soc. **273** (1995) L35, arXiv:astro-ph/9501102. 55

[272] S. S. McGaugh and W. J. G. de Blok, "Testing the dark matter hypothesis with low surface brightness galaxies and other evidence," Astrophys. J. **499** (1998) 41, arXiv:astro-ph/9801123. 55

[273] A. A. Dutton, "The baryonic Tully{Fisher relation and galactic outflows," Monthly Notices of the Royal Astronomical Society **424** no. 4, (08, 2012) 3123-3128. https://doi.org/10.1111/j.1365-2966.2012.21469.x. 55

[274] L. V. Sales, J. F. Navarro, K. Oman, A. Fattahi, I. Ferrero, M. Abadi, R. Bower, R. A. Crain, C. S. Frenk, T. Sawala, M. Schaller, J. Schaye, T. Theuns, and S. D. M. White, "The low-mass end of the baryonic Tully{Fisher relation," Monthly Notices of the Royal Astronomical Society **464** no. 2, (09, 2016) 2419-2428. https://doi.org/10.1093/mnras/stw2461. 55

[275] K. C. Freeman, "On the Origin of the Hubble Sequence," Astroph. & Space Science **269** (Dec., 1999) 119-137. 55

[276] S. S. McGaugh, J. M. Schombert, G. D. Bothun, and W. J. G. de Blok, "The Baryonic Tully-Fisher Relation," Astroph. J. Lett. **533** no. 2, (Apr., 2000) L99-L102, arXiv:astro-ph/0003001 [astro-ph]. 55

[277] M. A. W. Verheijen, "The Ursa Major Cluster of Galaxies. V. H I Rotation Curve Shapes and the Tully-Fisher Relations," Astroph. J. **563** no. 2, (Dec., 2001) 694-715, arXiv:astro-ph/0108225 [astro-ph]. 55, 57, 58, 83

[278] D. Zaritsky et al., "The Baryonic Tully-Fisher Relationship for S^4G Galaxies and the "Condensed" Baryon Fraction of Galaxies," Astron. J. **147** (2014) 134, arXiv:1402.6315 [astro-ph.GA]. 55

[279] H. Übler, N. M. Förster Schreiber, R. Genzel, E. Wisnioski, S. Wuyts, P. Lang, T. Naab, A. Burkert, P. G. van Dokkum, L. J. Tacconi, D. J. Wilman, M. Fossati, J. T. Mendel, A. Beifiori, S. Belli, R. Bender, G. B. Brammer, J. Chan, R. Davies, M. Fabricius, A. Galametz, D. Lutz, I. G. Momcheva, E. J. Nelson, R. P. Saglia, S. Seitz, and K. Tadaki, "The Evolution of the Tully-Fisher Relation between z ˜ 2.3 and z ˜ 0.9 with $KMOS^{3D}$," Astroph. J. **842** no. 2, (June, 2017) 121, arXiv:1703.04321 [astro-ph.GA]. 56

[280] F. Hofmann and J. Müller, "Relativistic tests with lunar laser ranging," Class. Quant. Grav. **35** no. 3, (2018) 035015. 56

[281] E. V. Pitjeva, N. P. Pitjev, D. A. Pavlov, and C. C. Turygin, "Estimates of the change rate of solar mass and gravitational constant based on the dynamics of the Solar System," Astron. Astrophys. **647** (2021) A141. 56, 67

[282] E. V. Pitjeva and N. P. Pitjev, "Relativistic effects and dark matter in the Solar system from observations of planets and spacecraft," Mon. Not. Roy. Astron. Soc. **432** (2013) 3431, arXiv:1306.3043 [astro-ph.EP]. 56

[283] A. T. Deller, J. P. W. Verbiest, S. J. Tingay, and M. Bailes, "Extremely high precision VLBI astrometry of PSR J0437-4715 and implications for theories of gravity," Astrophys. J. Lett. **685** (2008) L67, arXiv:0808.1594 [astro-ph]. 56

[284] L. Giani and E. Frion, "Testing the Equivalence Principle with Strong Lensing Time Delay Variations," JCAP **09** (2020) 008, arXiv:2005.07533 [astro-ph.CO]. 56

[285] W. W. Zhu et al., "Tests of Gravitational Symmetries with Pulsar Binary J1713+0747," Mon. Not. Roy. Astron. Soc. **482** no. 3, (2019) 3249-3260, arXiv:1802.09206 [astro-ph.HE]. 56

[286] A. Genova, E. Mazarico, S. Goossens, F. G. Lemoine, G. A. Neumann, D. E. Smith, and M. T. Zuber, "Solar system expansion and strong equivalence principle as seen by the nasa messenger mission," Nature communications **9** no. 1, (January, 2018) 289. https://europepmc.org/articles/PMC5773540. 56

[287] K. Masuda and Y. Suto, "Transiting planets as a precision clock to constrain the time variation of the gravitational constant," Publ. Astron. Soc. Jap. **68** no. 3, (2016) L5, arXiv:1602.02513 [gr-qc]. 56

[288] E. Gaztañaga, A. Cabré, and L. Hui, "Clustering of luminous red galaxies - iv. baryon acoustic peak in the line-of-sight direction and a direct measurement of h(z)," Monthly Notices of the Royal Astronomical Society **399** no. 3, (Nov, 2009) 1663{1680. http://dx.doi.org/10.1111/j.1365-2966.2009.15405.x. 56, 82

[289] A. H. Córsico, L. G. Althaus, E. García-Berro, and A. D. Romero, "An independent constraint on the secular rate of variation of the gravitational constant from pulsating white dwarfs," JCAP **06** (2013) 032, arXiv:1306.1864 [astro-ph.SR]. 56

[290] R. W. Hellings, P. J. Adams, J. D. Anderson, M. S. Keesey, E. L. Lau, E. M. Standish, V. M. Canuto, and I. Goldman, "Experimental test of the variability of $\dot{G}$ using viking lander ranging data," Phys. Rev. Lett. **51** (Oct, 1983) 1609-1612. https://link.aps.org/doi/10.1103/PhysRevLett.51.1609. 56

[291] D. B. Guenther, L. M. Krauss, and P. Demarque, "Testing the constancy of the gravitational constant using helioseismology," The Astrophysical Journal **498** no. 2, (May, 1998) 871-876. https://doi.org/10.1086/305567. 56

[292] A. Vijaykumar, S. J. Kapadia, and P. Ajith, "Constraints on the time variation of the gravitational constant using gravitational wave observations of binary neutron stars," preprint (arXiv:2003.12832) (3, 2020) , arXiv:2003.12832 [gr-qc]. 56

[293] J.-P. Uzan, "The Fundamental Constants and Their Variation: Observational Status and Theoretical Motivations," Rev. Mod. Phys. **75** (2003) 403, arXiv:hep-ph/0205340. 56, 67

[294] S. Degl'Innocenti, G. Fiorentini, G. G. Raffelt, B. Ricci, and A. Weiss, "Time variation of Newton's constant and the age of globular clusters," Astron. Astrophys. **312** (1996) 345-352, arXiv:astro-ph/9509090. 56

[295] S. E. Thorsett, "The Gravitational constant, the Chandrasekhar limit, and neutron star masses," Phys. Rev. Lett. **77** (1996) 1432-1435, arXiv:astro-ph/9607003. 56

[296] P. Jofre, A. Reisenegger, and R. Fernandez, "Constraining a possible time-variation of the gravitational constant through gravitochemical heating of neutron stars," Phys. Rev. Lett. **97** (2006) 131102, arXiv:astro-ph/0606708. 56

[297] J. Alvey, N. Sabti, M. Escudero, and M. Fairbairn, "Improved BBN Constraints on the Variation of the Gravitational Constant," Eur. Phys. J. C **80** no. 2, (2020) 148, arXiv:1910.10730 [astro-ph.CO]. 56, 57, 67

[298] F. Wu and X. Chen, "Cosmic microwave background with Brans-Dicke gravity II: constraints with the WMAP and SDSS data," Phys. Rev. D **82** (2010) 083003, arXiv:0903.0385 [astro-ph.CO]. 56

[299] G. Esposito-Farese and D. Polarski, "Scalar tensor gravity in an accelerating universe," Phys. Rev. D **63** (2001) 063504, arXiv:gr-qc/0009034. 57

[300] F. Walter, E. Brinks, W. J. G. de Blok, F. Bigiel, R. C. Kennicutt, M. D. Thornley, and A. Leroy, "THINGS: THE h i NEARBY GALAXY SURVEY," The Astronomical Journal **136** no. 6, (Nov, 2008) 2563-2647. https://doi.org/10.1088/0004-6256/136/6/2563. 57, 58, 83

[301] F. Lelli, S. S. McGaugh, J. M. Schombert, H. Desmond, and H. Katz, "The baryonic Tully-Fisher relation for different velocity definitions and implications for galaxy angular momentum," Mon. Not. R. Ast. Soc. **484** no. 3, (Apr., 2019) 3267-3278, arXiv:1901.05966 [astro-ph.GA]. 57, 58, 83

[302] F. Lelli, S. S. McGaugh, and J. M. Schombert, "The Small Scatter of the Baryonic Tully-Fisher Relation," Astroph. J. Lett. **816** no. 1, (Jan., 2016) L14, arXiv:1512.04543 [astro-ph.GA]. 57, 58, 83

[303] C. J. Conselice, K. Bundy, R. S. Ellis, J. Brichmann, N. P. Vogt, and A. C. Phillips, "Evolution of the near-infrared Tully-Fisher relation: Constraints on the relationship between the stellar and total masses of disk galaxies since z=1," Astrophys. J. **628** (2005) 160-168, arXiv:astro-ph/0503597. 58

[304] S. A. Kassin et al., "The Stellar Mass Tully-Fisher Relation to z=1.2 from AEGIS," Astrophys. J. Lett. **660** (2007) L35-L38, arXiv:astro-ph/0702643. 58

[305] S. H. Miller, K. Bundy, M. Sullivan, R. S. Ellis, and T. Treu, "The Assembly History of Disk Galaxies: I - The Tully-Fisher Relation to z˜1.3 from Deep Exposures with DEIMOS," Astrophys. J. **741** (2011) 115, arXiv:1102.3911 [astro-ph.CO]. 58

[306] Contini, T., Epinat, B., Bouché, N., Brinchmann, J., Boogaard, L. A., Ventou, E., Bacon, R., Richard, J., Weilbacher, P. M., Wisotzki, L., Krajnovi´c, D., Vielfaure, J-B., Emsellem, E., Finley, H., Inami, H., Schaye, J., Swinbank, M., Guérou, A., Martinsson, T., Michel-Dansac, L., Schroetter, I., Shirazi, M., and Soucail, G., "Deep muse observations in the hdfs - morpho-kinematics of distant star-forming galaxies down to 108m," A&A **591** (2016) A49. https://doi.org/10.1051/0004-6361/201527866. 58

[307] Di Teodoro, E. M., Fraternali, F., and Miller, S. H., "Flat rotation curves and low velocity dispersions in kmos star-forming galaxies at z 1," A&A **594** (2016) A77. https://doi.org/10.1051/0004-6361/201628315. 58

[308] J. Molina, E. Ibar, A. M. Swinbank, D. Sobral, P. N. Best, I. Smail, A. Escala, and M. Cirasuolo, "SINFONI-HiZELS: the dynamics, merger rates and metallicity gradients

of 'typical' star-forming galaxies at z = 0.8-2.2" Mon. Not. R. Ast. Soc. **466** no. 1, (Apr., 2017) 892-905, arXiv:1612.00447 [astro-ph.GA]. 58

[309] Pelliccia, D., Tresse, L., Epinat, B., Ilbert, O., Scoville, N., Amram, P., Lemaux, B. C., and Zamorani, G., "Hr-cosmos: Kinematics of star-forming galaxies at z 0.9," A&A **599** (2017) A25. https://doi.org/10.1051/0004-6361/201629064. 58

[310] Puech, M., Flores, H., Hammer, F., Yang, Y., Neichel, B., Lehnert, M., Chemin, L., Nesvadba, N., Epinat, B., Amram, P., Balkowski, C., Cesarsky, C., Dannerbauer, H., di Serego Alighieri, S., Fuentes-Carrera, I., Guiderdoni, B., Kembhavi, A., Liang, Y. C., Östlin, G., Pozzetti, L., Ravikumar, C. D., Rawat, A., Vergani, D., Vernet, J., and Wozniak, H., "Images* - iii. the evolution of the near-infrared tully-fisher relation over the last 6 gyr," A&A **484** no. 1, (2008) 173-187. https://doi.org/10.1051/0004-6361:20079313. 58

[311] Puech, M., Hammer, F., Flores, H., Delgado-Serrano, R., Rodrigues, M., and Yang, Y., "The baryonic content and tully-fisher relation at z 0.6," A&A **510** (2010) A68. https://doi.org/10.1051/0004-6361/200912081. 58

[312] G. Cresci, E. K. S. Hicks, R. Genzel, N. M. F. Schreiber, R. Davies, N. Bouché, P. Buschkamp, S. Genel, K. Shapiro, L. Tacconi, et al., "THE SINS SURVEY: MODELING THE DYNAMICS OF z ∼ 2 GALAXIES AND THE HIGH-z TULLY{FISHER RELATION∗," Astrophysical Journal **697** no. 1, (Apr, 2009) 115. 58

[313] Gnerucci, A., Marconi, A., Cresci, G., Maiolino, R., Mannucci, F., Calura, F., Cimatti, A., Cocchia, F., Grazian, A., Matteucci, F., Nagao, T., Pozzetti, L., and Troncoso, P., "Dynamical properties of amaze and lsd galaxies from gas kinematics and the tully-fisher relation at z ," A&A **528** (2011) A88. https://doi.org/10.1051/0004-6361/201015465. 58

[314] M. Swinbank, D. Sobral, I. Smail, J. Geach, P. Best, I. McCarthy, R. Crain, and T. Theuns, "The Properties of the Star-Forming Interstellar Medium at z=0.84-2.23 from HiZELS - I: Mapping the Internal Dynamics and Metallicity Gradients in High-Redshift Disk Galaxies," Mon. Not. Roy. Astron. Soc. **426** (2012) 935, arXiv:1209.1395 [astro-ph.CO]. 58

[315] S. H. Price, M. Kriek, A. E. Shapley, N. A. Reddy, W. R. Freeman, A. L. Coil, L. de Groot, I. Shivaei, B. Siana, M. Azadi, G. Barro, B. Mobasher, R. L. Sanders, and T. Zick, "THE MOSDEF SURVEY: DYNAMICAL AND BARYONIC MASSES AND KINEMATIC STRUCTURES OF STAR-FORMING GALAXIES AT 1.4 ≤z≤ 2.6," The Astrophysical Journal **819** no. 1, (Mar, 2016) 80. https://doi.org/10.3847/0004-637x/819/1/80. 58

[316] A. L. Tiley, J. P. Stott, A. M. Swinbank, M. Bureau, C. M. Harrison, R. Bower, H. L. Johnson, A. J. Bunker, M. J. Jarvis, G. Magdis, R. Sharples, I. Smail, D. Sobral, and P. Best, "The KMOS Redshift One Spectroscopic Survey (KROSS): the Tully{Fisher relation at z ∼ 1," Monthly Notices of the Royal Astronomical Society **460** no. 1, (04, 2016) 103-129. https://doi.org/10.1093/mnras/stw936. 58

[317] C. M. S. Straatman, K. Glazebrook, G. G. Kacprzak, I. Labbé, T. Nanayakkara, L. Alcorn, M. Cowley, L. J. Kewley, L. R. Spitler, K.-V. H. Tran, and T. Yuan, "ZFIRE: The evolution of the stellar mass tully{fisher relation to redshift $\sim$2.2," The Astrophysical Journal **839** no. 1, (Apr, 2017) 57. https://doi.org/10.3847/1538-4357/aa643e. 58

[318] L. Portinari and J. Sommer-Larsen, "The Tully-Fisher relation and its evolution with redshift in cosmological simulations of disc galaxy formation," Mon. Not. Roy. Astron. Soc. **375** (2007) 913-924, arXiv:astro-ph/0606531. 58

[319] W. H. Press, S. A. Teukolsky, W. T. Vetterling, and B. P. Flannery, Numerical Recipes 3rd Edition: The Art of Scientific Computing. Cambridge University Press, USA, 3 ed., 2007. 58, 59

[320] A. A. Dutton, A. Obreja, L. Wang, T. A. Gutcke, T. Buck, S. M. Udrescu, J. Frings, G. S. Stinson, X. Kang, and A. V. Macciò, "NIHAO XII: galactic uniformity in a ΛCDM universe," Monthly Notices of the Royal Astronomical Society **467** no. 4, (02, 2017) 4937-4950. https://doi.org/10.1093/mnras/stx458. 63

[321] H. Desmond, "The scatter, residual correlations and curvature of the sparc baryonic Tully-Fisher relation," Monthly Notices of the Royal Astronomical Society: Letters **472** no. 1, (08, 2017) L35-L39. https://doi.org/10.1093/mnrasl/slx134. 63

[322] C. M. Will, "The Confrontation between general relativity and experiment," Living Rev. Rel. **9** (2006) 3, arXiv:gr-qc/0510072. 67

[323] D. H. Jones, M. A. Read, W. Saunders, M. Colless, T. Jarrett, Q. A. Parker, A. P. Fairall, T. Mauch, E. M. Sadler, F. G. Watson, D. Burton, L. A. Campbell, P. Cass, S. M. Croom, J. Dawe, K. Fiegert, L. Frankcombe, M. Hartley, J. Huchra, D. James, E. Kirby, O. Lahav, J. Lucey, G. A. Mamon, L. Moore, B. A. Peterson, S. Prior, D. Proust, K. Russell, V. Safouris, K.-I. Wakamatsu, E. Westra, and M. Williams, "The 6dF Galaxy Survey: final redshift release (DR3) and southern large-scale structures," Mon. Not. R. Ast. Soc. **399** no. 2, (Oct., 2009) 683-698, arXiv:0903.5451 [astro-ph.CO]. 68

[324] D. H. Jones, W. Saunders, M. Read, and M. Colless, "Second data release of the 6dF Galaxy Survey," Publ. Astron. Soc. Austral. **22** (2005) 277, arXiv:astro-ph/0505068. 68

[325] D. H. Jones et al., "The 6dF Galaxy Survey: Samples, observational techniques and the first data release," Mon. Not. Roy. Astron. Soc. **355** (2004) 747-763, arXiv:astro-ph/0403501. 68

[326] F. Beutler, C. Blake, M. Colless, D. Jones, L. Staveley-Smith, G. B. Poole, L. Campbell, Q. Parker, W. Saunders, and F. Watson, "The 6dF Galaxy Survey: $z \approx 0$ measurement of the growth rate and σ_8," Mon. Not. Roy. Astron. Soc. **423** (2012) 3430-3444, arXiv:1204.4725 [astro-ph.CO]. 68

[327] C. M. Springob, C. Magoulas, M. Colless, J. Mould, P. Erdogdu, D. H. Jones, J. R. Lucey, L. Campbell, and C. J. Fluke, "The 6dF Galaxy Survey: Peculiar Velocity Field

and Cosmography," Mon. Not. Roy. Astron. Soc. **445** no. 3, (2014) 2677-2697, arXiv:1409.6161 [astro-ph.CO]. 68

[328] A. Johnson et al., "The 6dF Galaxy Survey: cosmological constraints from the velocity power spectrum," Mon. Not. Roy. Astron. Soc. **444** no. 4, (2014) 3926-3947, arXiv:1404.3799 [astro-ph.CO]. 68

[329] M. I. Scrimgeour et al., "The 6dF Galaxy Survey: Bulk Flows on $50 - 70h^{-1}$ Mpc scales," Mon. Not. Roy. Astron. Soc. **455** no. 1, (2016) 386-401, arXiv:1511.06930 [astro-ph.CO]. 68

[330] G. Alestas, D. Camarena, E. Di Valentino, L. Kazantzidis, V. Marra, S. Nesseris, and L. Perivolaropoulos, "Late-transition versus smooth H(z)-deformation models for the resolution of the Hubble crisis," Phys. Rev. D **105** no. 6, (2022) 063538, arXiv:2110.04336 [astro-ph.CO]. 69

[331] L. Perivolaropoulos and F. Skara, "Hubble tension or a transition of the Cepheid SnIa calibrator parameters?," Phys. Rev. D **104** no. 12, (2021) 123511, arXiv:2109.04406 [astro-ph.CO]. 69

[332] E. Mortsell, A. Goobar, J. Johansson, and S. Dhawan, "The Hubble Tension Bites the Dust: Sensitivity of the Hubble Constant Determination to Cepheid Color Calibration," arXiv:2105.11461 [astro-ph.CO]. 69, 75

[333] J. P. Huchra, L. M. Macri, K. L. Masters, T. H. Jarrett, P. Berlind, M. Calkins, A. C. Crook, R. Cutri, P. Erdoğdu, E. Falco, T. George, C. M. Hutcheson, O. Lahav, J. Mader, J. D. Mink, N. Martimbeau, S. Schneider, M. Skrutskie, S. Tokarz, and M. Westover, "The 2MASS Redshift Survey | Description and Data Release," Astroph. J. Suppl. **199** no. 2, (Apr., 2012) 26, arXiv:1108.0669 [astro-ph.CO]. 71

[334] M. Bilicki, T. H. Jarrett, J. A. Peacock, M. E. Cluver, and L. Steward, "2MASS Photometric Redshift catalog: a comprehensive three-dimensional census of the whole sky," Astrophys. J. Suppl. **210** (2014) 9, arXiv:1311.5246 [astro-ph.CO]. 71

[335] D. Alonso, A. I. Salvador, F. J. Sánchez, M. Bilicki, J. García-Bellido, and E. Sánchez, "Homogeneity and isotropy in the Two Micron All Sky Survey Photometric Redshift catalogue," Mon. Not. Roy. Astron. Soc. **449** no. 1, (2015) 670-684, arXiv:1412.5151 [astro-ph.CO]. 71

[336] **Pierre Auger** Collaboration, A. Aab et al., "Searches for Anisotropies in the Arrival Directions of the Highest Energy Cosmic Rays Detected by the Pierre Auger Observatory," Astrophys. J. **804** no. 1, (2015) 15, arXiv:1411.6111 [astro-ph.HE]. 71

[337] R. B. Tully, "Galaxy Groups: A 2MASS Catalog," Astron. J. **149** (2015) 171, arXiv:1503.03134 [astro-ph.CO]. 71

[338] C. Ramírez-Pérez, J. Sanchez, D. Alonso, and A. Font-Ribera, "CoLoRe: fast cosmological realisations over large volumes with multiple tracers," arXiv:2111.05069 [astro-ph.CO]. 71

[339] S. Ando, A. Benoit-Lévy, and E. Komatsu, "Angular power spectrum of galaxies in the 2MASS Redshift Survey," Monthly Notices of the Royal Astronomical Society **473** no. 4, (10, 2017) 4318–4325, arXiv:1706.05422. https://doi.org/10.1093/mnras/stx2634. 72

[340] S. Nojiri, S. D. Odintsov, and V. K. Oikonomou, "Modified Gravity Theories on a Nutshell: Inflation, Bounce and Late-time Evolution," Phys. Rept. **692** (2017) 1–104, arXiv:1705.11098 [gr-qc]. 75

[341] T. Clifton, P. G. Ferreira, A. Padilla, and C. Skordis, "Modified Gravity and Cosmology," Phys. Rept. **513** (2012) 1–189, arXiv:1106.2476 [astro-ph.CO]. 75

[342] M. Milgrom, "A modification of the Newtonian dynamics - Implications for galaxies.," Astroph. J. **270** (July, 1983) 371–383. 75

[343] S. S. McGaugh, "THE BARYONIC TULLY{FISHER RELATION OF GAS-RICH GALAXIES AS a TEST OF λCDM AND MOND," The Astronomical Journal **143** no. 2, (Jan, 2012) 40. https://doi.org/10.1088/0004-6256/143/2/40. 75

[344] S. Ghosh, A. Bhadra, A. Mukhopadhyay, and K. Sarkar, "Baryonic Tully{Fisher Test of Grumiller's Modified Gravity Model," Grav. Cosmol. **27** no. 2, (2021) 157–162, arXiv:2101.08721 [gr-qc]. 75

[345] M. R. Blanton, M. Geha, and A. A. West, "Testing Cold Dark Matter with the Low-Mass Tully-Fisher Relation," Astroph. J. **682** no. 2, (Aug., 2008) 861–873, arXiv:0707.3813 [astro-ph]. 75

[346] F. Governato, C. Brook, L. Mayer, A. Brooks, G. Rhee, J. Wadsley, P. Jonsson, B. Willman, G. Stinson, T. Quinn, and P. Madau, "Bulgeless dwarf galaxies and dark matter cores from supernova-driven outflows," Nature **463** no. 7278, (Jan., 2010) 203–206, arXiv:0911.2237 [astro-ph.CO]. 75

[347] L. Iorio, "Gravitational Anomalies in the Solar System?," Int. J. Mod. Phys. D **24** no. 06, (2015) 1530015, arXiv:1412.7673 [gr-qc]. 75

[348] G. Feulner, "The faint young Sun problem," Rev. Geophys. **50** (May, 2012) RG2006. 75

[349] L. Amendola, V. Marra, and M. Quartin, "Internal robustness: systematic search for systematic bias in SN Ia data," Mon. Not. R. Ast. Soc. **430** no. 3, (Apr., 2013) 1867–1879, arXiv:1209.1897 [astro-ph.CO]. 75

[350] C. Heneka, V. Marra, and L. Amendola, "Extensive search for systematic bias in supernova Ia data," Mon. Not. Roy. Astron. Soc. **439** no. 2, (2014) 1855–1864, arXiv:1310.8435 [astro-ph.CO]. 75

[351] G. F. Benedict, B. E. McArthur, M. W. Feast, T. G. Barnes, T. E. Harrison, R. J. Patterson, J. W. Menzies, J. L. Bean, and W. L. Freedman, "Hubble Space Telescope Fine Guidance Sensor Parallaxes of Galactic Cepheid Variable Stars: Period-Luminosity Relations," Astron. J. **133** (2007) 1810–1827, arXiv:astro-ph/0612465. [Erratum: Astron.J. 133, 2980 (2007)]. 75

[352] G. F. Benedict et al., "Astrometry with hubble space telescope: a parallax of the fundamental distance calibrator delta cephei," Astron. J. **124** (2002) 1695-1705, arXiv:astro-ph/0206214. 75

[353] C. Blake et al., "The WiggleZ Dark Energy Survey: Joint measurements of the expansion and growth history at $z < 1$," Mon. Not. Roy. Astron. Soc. **425** (2012) 405-414, arXiv:1204.3674 [astro-ph.CO]. 81

[354] V. de Sainte Agathe et al., "Baryon acoustic oscillations at $z = 2.34$ from the correlations of Lyα absorption in eBOSS DR14," Astron. Astrophys. **629** (2019) A85, arXiv:1904.03400 [astro-ph.CO]. 81

[355] **BOSS** Collaboration, L. Anderson et al., "The clustering of galaxies in the SDSS-III Baryon Oscillation Spectroscopic Survey: baryon acoustic oscillations in the Data Releases 10 and 11 Galaxy samples," Mon. Not. Roy. Astron. Soc. **441** no. 1, (2014) 24-62, arXiv:1312.4877 [astro-ph.CO]. 81, 82

[356] R. Jimenez, L. Verde, T. Treu, and D. Stern, "Constraints on the equation of state of dark energy and the Hubble constant from stellar ages and the CMB," ArXiv e-prints (Feb, 2003) , astro-ph/0302560. 82

[357] J. Simon, L. Verde, and R. Jimenez, "Constraints on the redshift dependence of the dark energy potential," Phys. Rev. D **71** (Jun, 2005) 123001. https://link.aps.org/doi/10.1103/PhysRevD.71.123001. 82

[358] M. Moresco, A. Cimatti, R. Jimenez, L. Pozzetti, G. Zamorani, M. Bolzonella, J. Dunlop, F. Lamareille, M. Mignoli, H. Pearce, and et al., "Improved constraints on the expansion rate of the universe up to $z \sim 1.1$ from the spectroscopic evolution of cosmic chronometers," Journal of Cosmology and Astroparticle Physics **2012** no. 08, (Aug, 2012) 006{006. http://dx.doi.org/10.1088/1475-7516/2012/08/006. 82

[359] M. Moresco, L. Pozzetti, A. Cimatti, R. Jimenez, C. Maraston, L. Verde, D. Thomas, A. Citro, R. Tojeiro, and D. Wilkinson, "A 6% measurement of the Hubble parameter at z$\sim$0.45: direct evidence of the epoch of cosmic re-acceleration," Journal of Cosmology and Astroparticle Physics **2016** no. 05, (May, 2016) 014. 82

[360] D. Stern, R. Jimenez, L. Verde, M. Kamionkowski, and S. A. Stanford, "Cosmic chronometers: constraining the equation of state of dark energy. I: H(z) measurements," Journal of Cosmology and Astroparticle Physics **2010** no. 02, (Feb, 2010) 008. 82

[361] C. Zhang, H. Zhang, S. Yuan, S. Liu, T.-J. Zhang, and Y.-C. Sun, "Four New Observational $H(z)$ Data From Luminous Red Galaxies of Sloan Digital Sky Survey Data Release Seven," ArXiv e-prints (Jul, 2012) , 1207.4541. 82

[362] M. Moresco, "Raising the bar: new constraints on the Hubble parameter with cosmic chronometers at $z \sim 2$," Monthly Notices of the Royal Astronomical Society: Letters **450** no. 1, (Jun, 2015) L16-L20. 82

[363] C.-H. Chuang and Y. Wang, "Modelling the anisotropic two-point galaxy correlation function on small scales and single-probe measurements of H(z), DA(z) and f(z)σ8(z)

from the Sloan Digital Sky Survey DR7 luminous red galaxies," Monthly Notices of the Royal Astronomical Society **435** no. 1, (Oct, 2013) 255-262. 82

[364] C. Blake et al., *"The WiggleZ Dark Energy Survey: joint measurements of the expansion and growth history at $z < 1$,"* Monthly Notices of the Royal Astronomical Society **425** no. 1, (Sep, 2012) 405-414. 82

[365] T. Delubac et al., *"Baryon acoustic oscillations in the Lyα forest of BOSS DR11 quasars,"* Astronomy & Astrophysics **574** (Feb, 2015) A59. 82

[366] L. Samushia et al., *"The clustering of galaxies in the SDSS-III DR9 Baryon Oscillation Spectroscopic Survey: testing deviations from Λ and general relativity using anisotropic clustering of galaxies,"* Monthly Notices of the Royal Astronomical Society **429** no. 2, (Feb, 2013) 1514-1528. 82

[367] N. G. Busca et al., *"Baryon acoustic oscillations in the Lyα forest of BOSS quasars,"* Astronomy & Astrophysics **552** (Apr, 2013) A96. 82

[368] A. F.-R. et al., *"Quasar-lyman α forest cross-correlation from boss dr11: Baryon acoustic oscillations,"* Journal of Cosmology and Astroparticle Physics **2014** no. 05, (May, 2014) 027{027. http://dx.doi.org/10.1088/1475-7516/2014/05/027. 82